Design and Synthesis of BODIPY based Donor-Acceptor Chromophores

Ph.D. Thesis

By

INDRESH SINGH YADAV

DEPARTMENT OF CHEMISTRY

INDIAN INSTITUTE OF TECHNOLOGY INDORE

June 2023

Design and Synthesis of BODIPY based Donor-Acceptor Chromophores

A THESIS

Submitted in partial fulfillment of the requirements for the award of the degree

of

DOCTOR OF PHILOSOPHY

by

INDRESH SINGH YADAV

DEPARTMENT OF CHEMISTRY
INDIAN INSTITUTE OF TECHNOLOGY INDORE

June 2023

INDIAN INSTITUTE OF TECHNOLOGY INDORE

CANDIDATE'S DECLARATION

I hereby certify that the work which is being presented in the thesis entitled **"Design and Synthesis of BODIPY based Donor-Acceptor Chromophores"** in the partial fulfillment of the requirements for the award of the degree of **DOCTOR OF PHILOSOPHY** and submitted in the **Department of Chemistry, Indian Institute of Technology Indore**, is an authentic record of my own work carried out during the time period from **July 2017** to **June 2023** under the supervision of **Dr. Rajneesh Misra, Professor, Department of Chemistry, IIT Indore**.

I have not submitted the matter presented in this thesis for the award of any other degree of this or any other institute.

27-03-2024

Signature of the Student with date

(INDRESH SINGH YADAV)

This is to certify that the above statement made by the candidate is correct to the best of my knowledge.

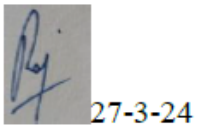

Signature of Thesis Supervisor with date

(Dr. RAJNEESH MISRA)

INDRESH SINGH YADAV has successfully given his Ph.D. Oral Examination held on …27-03-2024…

Signature of Chairperson (OEB)
Date:

Signature of External Examiner
Date:

Signature(s) of Thesis Supervisor(s)
Date:

Signature of PSPC Member #1
Date:

Signature of PSPC Member #2
Date:

ACKNOWLEDGEMENTS

The work in this thesis could not have been done without the help of many people who were always there for me when I needed them the most. This is my time to thank them sincerely for their assistance in making it possible for me to complete this long journey of Ph.D. First and foremost, I would like to offer my sincere gratitude to my supervisor, Dr. Rajneesh Misra, for the wonderful opportunity to pursue research in the colorful chemistry world and for believing in my research work abilities. His constant guidance, support, and careful monitoring throughout the journey are so excellent that even my most profound gratitude is not enough. I dedicate this thesis to him as it would not have been possible without his excellent leadership, persistent help, support and kindness.

I extend my profound thanks to my PSPC members Dr. Satya S. Bulusu and Dr. Niraj Kumar Shukla, for their guidance, valuable suggestions, and counsel during my journey of Ph.D. as a supervisor.

With great respect, I would like to express my special thanks of gratitude to Prof. Suhas S. Joshi [Director, Indian Institute of Technology Indore] for providing and accessing all the facilities at Indian Institute of Technology Indore.

I would like to express my thanks to IIT Indore for its infrastructure and Council of Scientific & Industrial Research (CSIR), New Delhi, for financial help through Fellowship.

I am grateful to Prof. Tushar Kanti Mukherjee (Head, Department of Chemistry, Indian Institute of Technology Indore) for his suggestions and guidance in various aspects. I am also grateful to Prof. Sanjay Singh, Prof. Sampak Samanta, Prof. Suman Mukhopadhyay, Prof. Biswarup Pathak, Prof. Apurba K. Das, Dr. Tridib K. Sarma, Dr. Anjan Chakraborty, Dr. Satya S. Bulusu, Dr. Chelvam Venkatesh, Dr.

Amrendra Kumar Singh, Dr. Abhinav Raghuvanshi, Dr. Dipak Kumar Roy, Dr. Umesh A. Kshirsagar, Dr. Debayan Sarkar, Dr. Pravarthana Dhanapal and Dr. Selvakumar Sermadurai for their guidance and help during various activities. I am thankful to the technical staff of Sophisticated Instrumentation Centre (SIC), IIT Indore, Mr. Kinney Pandey, Mr. Ghansyam Bhavsar and Mr. Manish Kushwaha and Mrs. Vinita Kothari for their technical help and support.

I would like to acknowledge all my teachers who have taught me in some or the other way since my school time. I would have never achieved anything without their guidance, blessing, and support. I would also like to express my special thanks to Mr. Anand Prakash (Assistant professor Delhi University) for their guidance. I would like to extend my deepest gratitude to Dr. Sheila Srivastava (Associate professor, Feroze Gandhi College, Raebareli) and Dr. Shaifali Srivastava (Assistant professor, Feroze Gandhi College, Raebareli), who guided me during graduation and post-graduation studies and inspired me to pursue a career in research. I am thankful to Dr. Ramendra Pratap Singh (Associate Professor Delhi University) for his guidance and support.

I personally extend my heartiest gratitude to my Ph.D. mentors Mr. Jivan Shinde, Dr. Yuvraj Patil and Dr. Yogajivan Rout for their constant guidance, help and support in all my ups and downs and during my initial days of the Ph.D. program. I take this opportunity to express a deep sense of gratitude to my group members, Dr. Rekha Sharma, Dr. Gangala Sivakumar, Dr. Shubhra Bikash Maity, Dr. Madhurima Poddar, Dr. Anupama Ekbote, Dr. S. Bijesh, Mr. Faizal Khan, Mrs. Manju, Mrs. Charu Popli, Dilip Pinjari Patil, Mohd. Wazid, Pankaj Kumar Gupta, Nikhil ji Tiwari, Ramakant Gawale, Amiy Krishna, Nitin Rajesh, Kusum Yadav, Renuka Soni, Sudhanshu Kumar and Nitish Kumar for their kind cooperation and cheerful support.

I would like to express my thanks to Mr. Vishal Chaurasia, Mr. Monty Kohli, Mr. Vibhau Shukla, Mr. Rahul Kumar Singh, Mr. Rishi Ranjan, Mr. Chandan Shah, Mr. Abhishek Agrahari, Dr. Dibya Yadav, and Mrs. Reeshu Yadav for their wonderful support in my hard time. My deepest gratitude and heartfelt thanks to my lovable grandfather late Mr. Ram Sewak Yadav, father Mr. Shyam Lal Yadav and mother Mrs. Rakesh Kumari and my dear sisters Mrs. Malti Yadav, Mrs. Chhaya Yadav and Mrs. Pooja Yadav, the other family members Ms. Rakshita Yadav, Ms. Saloni Yadav, Mr. Yogendra Yadav and Mr. Manvendra Yadav, Mr. Prabhakar Yadav, Mr. Saurabh Yadav whose indefinite love, support and guidance kept me motivated and confident. My heart-felt thanks to my splendid juniors and seniors at IIT Indore for their generous co-operation and help. My Ph.D. journey at IIT Indore was exciting, fulfilling, and rewarding. I am taking a bagful of experiences and memories from here and would like to acknowledge each one who was a part of this beautiful journey.

Thank You…

Indresh

DEDICATED TO

MY BELOVED PARENTS, TEACHERS, FRIENDS AND MY MOTHERLAND INDIA

-Indresh

SYNOPSIS

In recent years, the development of donor-acceptor molecular systems with low HOMO–LUMO gap has gained significant attention considering their utilization in applications such as organic photovoltaics, organic field-effect transistors, photodynamic therapy, sensing, nonlinear optics and bioimaging. The BODIPY (4,4-difluoro-4-bora-3a,4a-diaza-*s*-indacene) is a highly conjugated molecule that consist of pyrrole, azafulvene and diazaborinin-type ring (Figure 1). The BODIPY dye exhibits excellent properties such as a high absorption coefficient, strong fluorescence, high thermal and chemical stability, high solubility and resistance towards self-aggregation, these properties are useful for various optoelectronic and biological applications. The BODIPY core can be functionalized at the α, β, *meso*-positions and the B(III) center. The photophysical, electrochemical and energy gap between HOMO and LUMO of the BODIPY can be tuned by incorporating appropriate electron donor and acceptor units and altering the conjugation length by properly using π-linker or spacer unit. The BODIPY is an electron-deficient molecule; therefore, incorporating an electron-donating group promotes a donor-acceptor interaction. The donor-acceptor BODIPYs exhibit a strong absorption band in the visible to NIR region with a low HOMO–LUMO gap, which makes them a good candidate for dye-sensitized solar cells (DSSCs), fluorescent switches, bulk heterojunction organic solar cells (BHJOSCs), nonlinear optics, bioimaging and photodynamic therapy.

4,4-difluoro-4-borata-3a-azonia-4a-aza-*s*-indacene (BODIPY)

Figure 1. The molecular structure of the BODIPY core.

A variety of electron donors (phenothiazine, carbazole, *N*,*N*-dimethylaniline, triphenylamine *etc*.) and acceptors (1,1,2,2-tetracyanoethylene (TCNE) and 7,7,8,8-tetracyanoquinodimethane (TCNQ)) were incorporated at the *β*-pyrrolic and *meso*-positions of the BODIPY core to tune the photophysical, redox properties and HOMO–LUMO gap (Figure 2). The photophysical, redox and thermal properties of these donor–acceptor BODIPYs were explored, which reveals their application in optoelectronics.

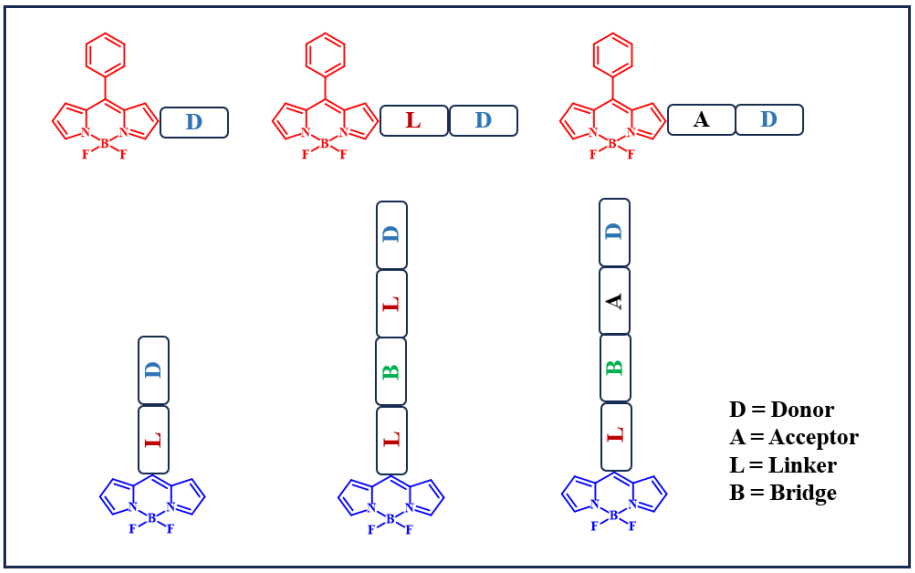

Figure 2. General representation of donor-bridge-acceptor functionalized BODIPYs in this work.

The main objectives of the present study are:

1. To design and synthesize the donor-acceptor BODIPYs for optoelectronic applications.
2. To synthesize BODIPY dyes by altering the donor and acceptor moieties at the *β*-pyrrolic and *meso*-positions and to investigate their photophysical, electrochemical and thermal properties.
3. To investigate the effect of incorporating various donors, acceptor units and the incorporation of oxygen atoms in the thiazine ring on their photophysical, redox properties and energy gap between HOMO and LUMO energy levels.

4. To fine-tune the HOMO–LUMO gap by introducing an electron donor/acceptor unit or π-linker group at the *β*-pyrrolic and *meso*-position of the BODIPY core.
5. To understand the electronic structure, photophysical properties and to investigate the distribution of electron density in HOMO and LUMO of the donor-acceptor BODIPYs *via* density functional theory (DFT) and time-dependent density functional theory (TD-DFT) calculations and correlated with the experimental data.

Chapter 1: Introduction

Chapter 1 describes the design, synthesis, and functionalization of the BODIPY dyes and their applications in different fields.

Chapter 2: Materials and experimental techniques

Chapter 2 summarizes the general experimental methods, characterization techniques and details of the instruments used for molecular structure characterization.

Chapter 3: Phenothiazine and Carbazole Substituted Push–Pull Boron-Dipyrromethenes: Synthesis, Photophysical, Electrochemical and Computational Studies

In chapter 3, *β*-pyrrole functionalized unsymmetrical push–pull BODIPYs **1**–**10** were synthesized by the Pd-catalyzed Suzuki, Heck, Sonogashira cross-coupling and [2+2] CA-RE reactions. The photophysical, redox properties of the push–pull BODIPYs **1**–**10** were explored. The push–pull BODIPY **5** shows a red-shifted intramolecular charge transfer (ICT) band compared to BODIPY **10** due to strong donor-acceptor interaction. The push–pull BODIPYs **4**, **5**, **9** and **10**, exhibit multiple reduction waves due to redox-active TCBD, cyclohexa-2,5-diene-1,4-ylidene-expanded TCBD and BODIPY unit.

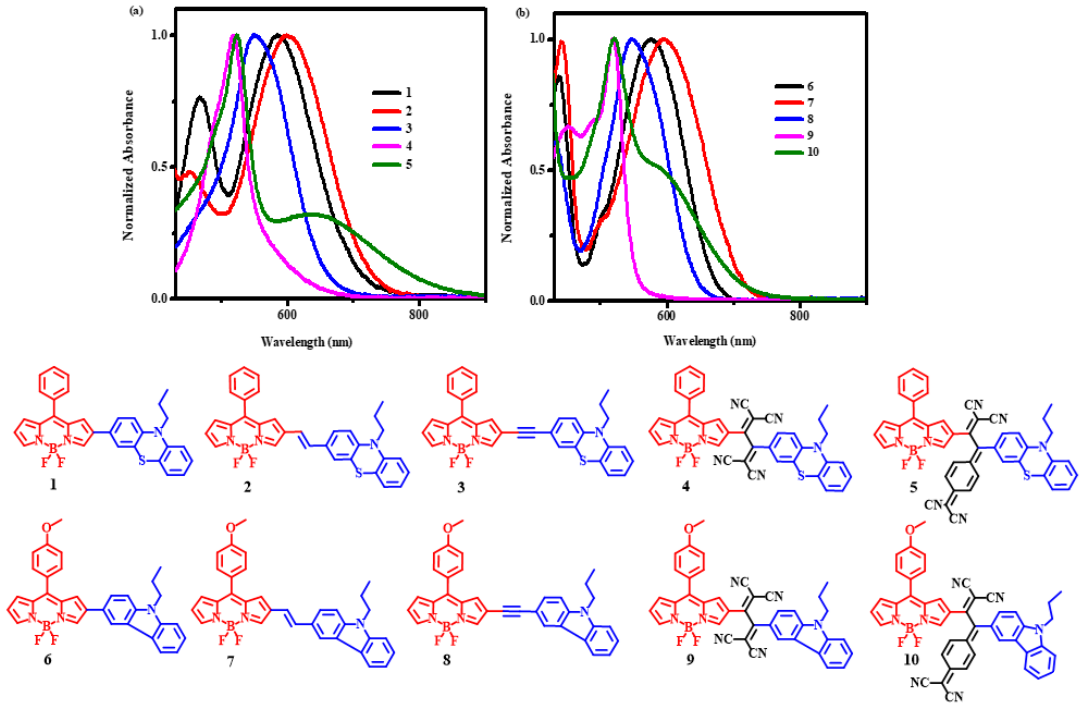

The computational studies of the BODIPYs **1**–**10**, show that the HOMOs are localized over phenothiazine and carbazole units, whereas LUMOs are delocalized over the acceptor BODIPY, TCBD and expanded TCBD units. The push–pull BODIPYs **1–5** exhibit a low HOMO–LUMO gap compared to BODIPYs **6–10** due to strong donor–acceptor interaction.

Chapter 4: *β*-Functionalized Donor-Acceptor BODIPYs: Design, Synthesis and Properties

In Chapter 4, donor-acceptor BODIPYs **3–5** and **7–9** were synthesized *via* Palladium-catalyzed Sonogashira cross-coupling and [2+2] CA-RE reactions in good yields. The photophysical, redox and thermal properties of the donor–acceptor BODIPYs **3–5** and **7–9** were explored. The dono-acceptor BODIPYs **5** and **9** show bathochromic shift compared to the BODIPYs **4** and **8** due to strong donor-acceptor interaction. The redox properties of the donor-acceptor BODIPYs **4**, **5**, **7,** and **9** exhibit multiple reduction waves due to redox-active BODIPY, TCBD and expanded TCBD units. The BODIPY **3** shows high thermal decomposition temperature compared to BODIPYs **4, 5, 7, 8,** and **9**.

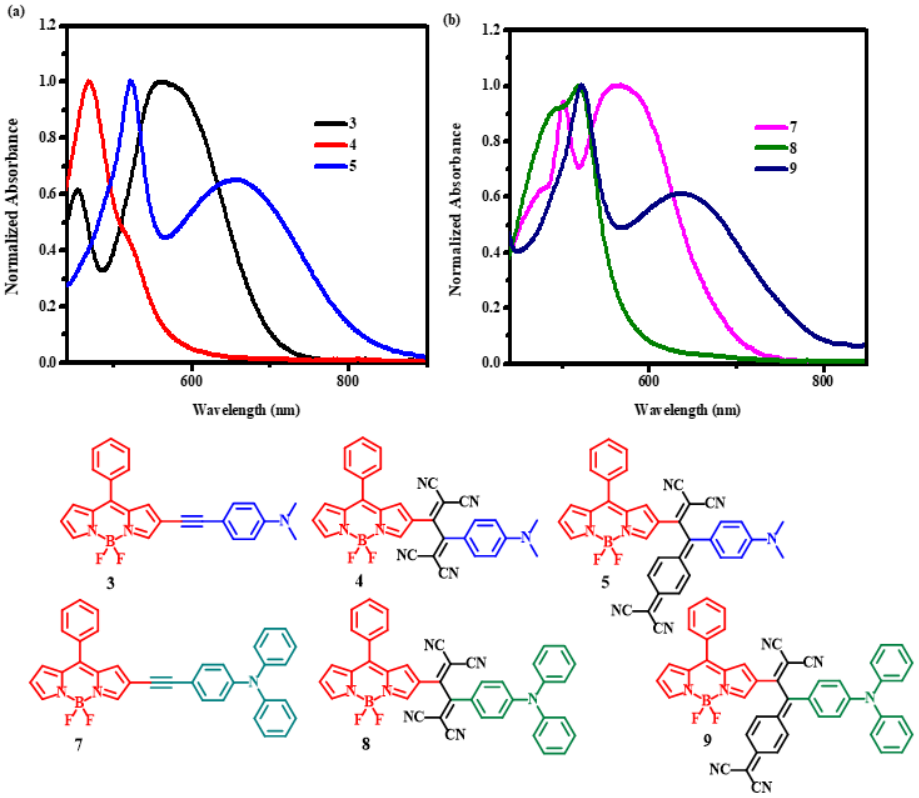

The computational studies of the donor-acceptor BODIPYs **4**, **5**, **8** and **9** suggest that the HOMOs are presented over the donor unit, whereas LUMOs are delocalized over acceptor BODIPY, TCBD and expanded TCBD units. The donor-acceptor BODIPYs **5** and **9** exhibits strong donor–acceptor interaction and low HOMO–LUMO gap compared to the BODIPYs **4** and **8**.

Chapter 5: *Meso*-Donor *N,N*-dimethylaniline Functionalized BODIPYs: Synthesis, Photophysical, Electrochemical, Thermal and Theoretical Studies

In chapter 5, the donor-acceptor **BODIPYs 1–4** were synthesized by the Palladium-catalyzed Sonogashira cross-coupling and [2+2] CA-RE reactions. The effect of donor and acceptor groups on the photophysical, redox and thermal properties of the donor-acceptor **BODIPYs 1–4** were explored. The **BODIPY 4** exhibits a strong donor–acceptor interaction, low HOMO–LUMO gap compared to the **BODIPY 3**.

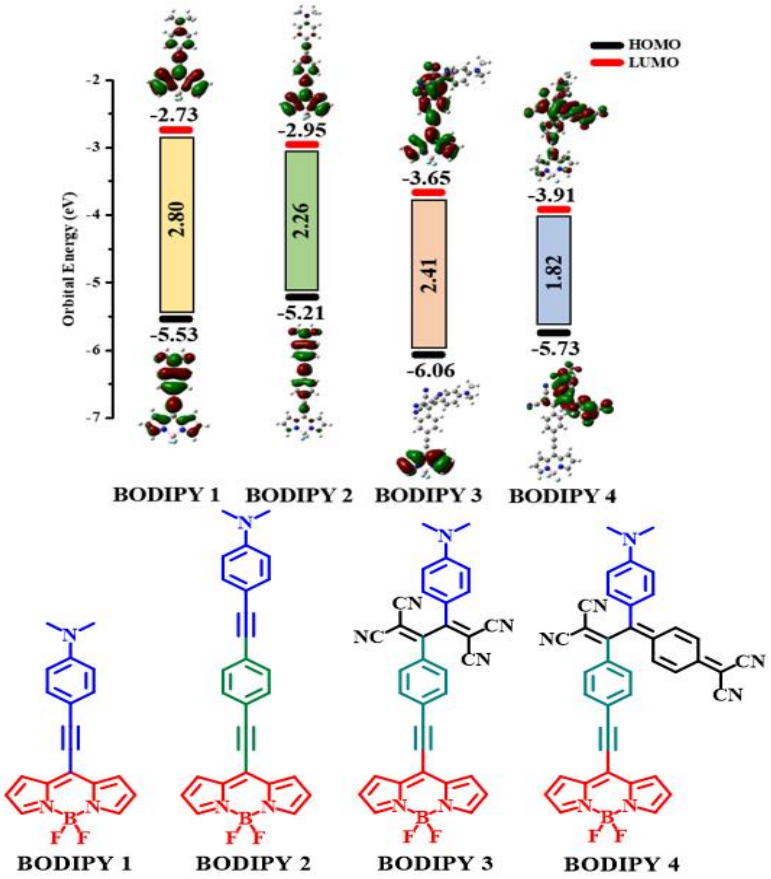

The electrochemical properties of the **BODIPYs 1–4** exhibit multiple-redox waves which corresponds to redox-active donor and acceptor BODIPY, TCBD and expanded TCBD units. The **BODIPY 2** shows better thermal stability compared to **BODIPYs 1, 3** and **4**. The computational studies on the **BODIPYs 1−4** show that the HOMOs are localized over NND and BODIPY unit, whereas the LUMO is delocalized over the BODIPY, TCBD and expanded TCBD units. The strong donor-acceptor interaction in **BODIPY 4** minimizes the HOMO-LUMO gap to a greater extent compared to **BODIPY 3**.

Chapter 6: Phenothiazine and Phenothiazine-5,5-dioxide Based BODIPYs: Synthesis, Photophysical, Electrochemical and Theoretical Studies

In chapter 6, a set of phenothiazine and phenothiazine-5,5-dioxide functionalized push–pull BODIPYs **BPTZ 1–8** were synthesized *via* Pd-catalyzed Suzuki cross-coupling reaction and followed by incorporating the oxygen atoms in the thiazine ring. We

explored the photophysical and redox features of the BODIPYs **BPTZ 1–8**.

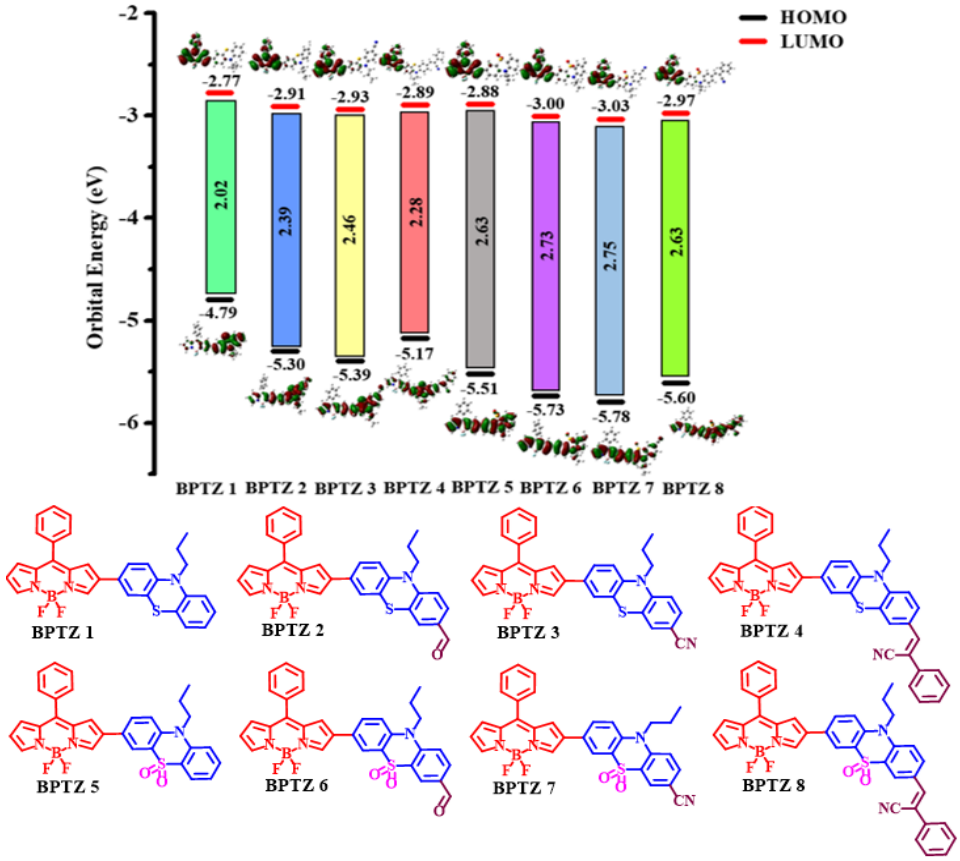

The **BPTZ 1–4** shows the red shifted absorption band compared to the **BPTZ 5–8** due to the strong electron donating nature of the phenothiazine unit. The multi-redox waves were observed due to redox-active phenothiazine, BODIPY and phenothiazine-5,5-dioxide unit. Theoretical investigations demonstrate that the phenothiazine functionalized **BPTZ 1–4** exhibits low HOMO-LUMO gap compared to phenothiazine-5,5-dioxide functionalized **BPTZ 5–8** due to strong donor-acceptor interaction.

Chapter 7: *β*-Pyrrole Functionalized Push–Pull BODIPYs: Synthesis, Photophysical, Electrochemical, Thermal and Computational Studies

In chapter 7, a series of *β*-pyrrole functionalized push–pull BODIPYs **BDP 1–6** were synthesized *via* Palladium-catalyzed Suzuki cross-coupling reaction and incorporating the oxygen atom in the

thiazine ring. The photophysical, redox and thermal properties of the push–pull BODIPYs **BDP 1–6** were studied.

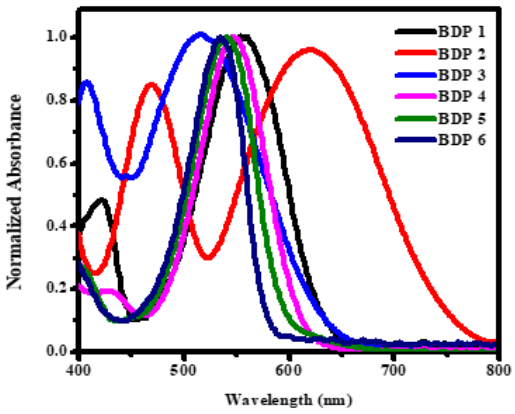

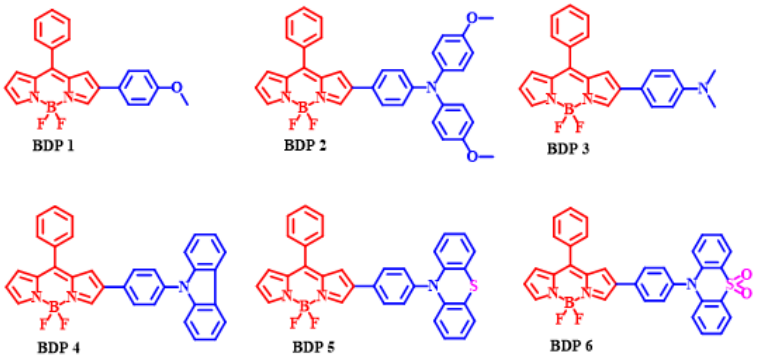

The BODIPY **BDP 6** exhibits a blue-shifted absorption band compared to the phenothiazine substituted BODIPY **BDP 5** due to the low electron donating power of the phenothiazine-5,5-dioxide unit. The **BDP 5** shows easier oxidation compared to the **BDP 6** due to the high donor ability of phenothiazine unit. The BODIPY **BDP 2** shows better thermal stability compared to the **BDP 1, 3, 4, 5,** and **6**. The computational results of the push–pull BODIPYs **BDP 1–4** show that the highest molecular orbitals (HOMOs) are delocalized over donor and BODIPY units, whereas in BODIPYs **BDP 5** and **BDP 6** the HOMOs are localized on phenothiazine and phenothiazine 5,5-dioxide unit. The lowest occupied molecular orbitals (LUMOs) of the push–pull BODIPYs **BDP 1–6** are centered on the acceptor BODIPY unit. The phenothiazine 5,5-dioxide-substituted **BDP 6** exhibits a large HOMO–LUMO gap compared to phenothiazine substituted **BDP 5** due to weak donor-acceptor interaction.

Chapter 8: Conclusions and Future scope

Chapter 8 summarizes the salient features of the work and future prospectives for developing new donor-acceptor materials for optoelectronic applications.

List of Publications

1. Dhokale, Bhausaheb., **Yadav, I. S.,** Mobin, M. S., & Misra, R., (2021). Thioether linked *meso* functionalized BODIPY DYEmer. *Journal of Porphyrins and Phthalocyanines, 25*, 428–435. https://doi.org/10.1142/S1088424621500176 (Impact Factor = 1.91)
2. **Yadav, I. S.**, Alsaleh, A. Z., Misra, R., & D'Souza, F., (2021). Charge stabilization via electron exchange: excited charge separation in symmetric, central triphenylamine derived, dimethylaminophenyl–tetracyanobutadiene donor–acceptor conjugates. *Chemical Science*, *12*(3), 1109–1120. https://doi.org/10.1039/D0SC04648E (Impact Factor = 9.96)
3. **Yadav, I. S.**, Jang, Y., Rout, Y., Thomas, M. B., Misra, R., & D'Souza, F., (2022). Near-IR Intramolecular Charge Transfer in Strongly Interacting Diphenothiazene-TCBD and Diphenothiazene-DCNQ Push-Pull Triads. *Chemistry – A European Journal*, *28*(25). https://doi.org/10.1002/chem.202200348 (Impact Factor = 5.02)
4. **Yadav, I. S.**, Alsaleh, A. Z., Martin, B., Misra, R., & D'Souza, F., (2022). Star-Shaped Triphenylamine–Tetracyanobutadiene–Phenothiazine Push–Pull Systems: Role of Terminal Phenothiazine in Improving Charge Transfer. *The Journal of Physical Chemistry C*, *126*(31), 13300–13310. https://doi.org/10.1021/acs.jpcc.2c03495 (Impact Factor = 4.12)
5. **Yadav, I. S.**, & Misra, R., (2022). Phenothiazine and phenothiazine-5,5-dioxide-based push–pull derivatives: synthesis, photophysical, electrochemical and computational studies. *New Journal of Chemistry*, *46*(33), 15999–16006. https://doi.org/10.1039/D2NJ03089F (Impact Factor = 3.92)

6. **Yadav, I. S.**, & Misra, R., (2023). Design, Synthesis and Functionalization of BODIPY dyes: Applications in Dye-Sensitized Solar Cell (DSSC) and Photodynamic Therapy (PDT). *Journal of Materials Chemistry C*, 11**,** 8688–8723. https://doi.org/10.1039/D3TC00171G (Impact Factor = 8.06) †
7. **Yadav, I. S.**, & Misra, R., (2023). *β*-Pyrrole Functionalized Push–Pull BODIPYs: Synthesis, Photophysical, Electrochemical, Thermal and Computational Studies. *Journal of Porphyrins and Phthalocyanines*, 27, 887–895. https://doi.org/10.1142/S1088424623501018 (Impact Factor = 1.91) †
8. **Yadav, I. S.**, & Misra, R., Phenothiazine and Carbazole Substituted Push–Pull Boron-Dipyrromethenes: Synthesis, Photophysical, Electrochemical and Computational Studies (Manuscript under preparation) †
9. **Yadav, I. S.**, & Misra, R., *β*-Functionalized Donor-Acceptor BODIPYs: Design, Synthesis and Properties (Manuscript under preparation) †
10. **Yadav, I. S.**, Kaswan, R. R., Liyanage A., Misra, R., & D'Souza, F., (2024). Dimethylaniline-tetracyanobutadiene and dimethylaniline-extended-tetracyanobutadiene functionalized BODIPYs witnessing ultrafast charge transfer. *The Journal of Physical Chemistry C*, https://doi.org/10.1021/acs.jpcc.4c00072 (Impact Factor = 4.12) †
11. **Yadav, I. S.**, & Misra, R., Phenothiazine and Phenothiazine-5,5-dioxide Based BODIPYs: Synthesis, Photophysical, Electrochemical and Theoretical studies (Manuscript under preparation) †
12. Shinde J., **Yadav, I. S.**, & Misra, R., Effect of Secondary Acceptors on Photophysical and Electrochemical Properties of Ferrocenyl based *α*-BODIPYs (Manuscript under preparation)

†Papers pertaining to the thesis.

TABLE OF CONTENTS

LIST OF FIGURES

LIST OF SCHEMES

LIST OF TABLES

LIST OF CHARTS

ACRONYMS

D–A	Donor–acceptor
PPh_3	Triphenylphosphine
DMF	Dimethylformamide
DCM	Dichloromethane
PTZ	Phenothiazine
CBZ	Carbazole
TPA	Triphenylamine
BDP	BODIPY
TCNE	1,1,2,2-tetracyanoethylene
TCNQ	7,7,8,8-tetracyanoquinodimethane
EtOH	Ethanol
MeOH	Methanol
THF	Tetrahydrofuran
TLC	Thin Layer Chromatography
TEA	Triethylamine
DIPEA	*N*,*N*-Di-isopropyl-ethylamine
Ph	Phenyl
IR	Infrared
UV-Vis	UV-Visible Spectroscopy
ICT	Intramolecular Charge Transfer
Calcd.	Calculated
$CDCl_3$	Chloroform-d
ESI-MS	Electrospray Ionization-Mass Spectrometry

HRMS	High-Resolution Mass Spectrometry
NMR	Nuclear Magnetic Resonance
DFT	Density Functional Theory
TD-DFT	Time-dependent Density Functional Theory
HOMO	Highest Occupied Molecular Orbital
LUMO	Lowest Unoccupied Molecular Orbital

NOMENCLATURE

λ	Wavelength
ε	Extinction coefficient
α	Alfa
β	Beta
γ	Gamma
π	Pi
ϕ	Fluorescence quantum yield
σ	Sigma
Å	Angstrom
nm	Nanometer
cm	Centimeter
°	Degree
°C	Degree Centigrade
mmol	Millimole
mL	Milliliter
μL	Microliter
a. u.	Arbitrary Unit

Chapter 1

Introduction

1.1. Donor–Acceptor Systems

The design and synthesis of novel multi-modular π-conjugated donor–acceptor (D–A) chromophores have attracted much attention in the scientific community due to their wide range of applications in organic solar cells (OSCs), organic light-emitting diodes (OLEDs), organic photovoltaics (OPVs), thermally activated delayed fluorescence (TADF) as well as in biological studies.[1–10] The D–A based chromophores which exhibit a high photochemical and thermal stability, broad absorption in the UV-vis region and low HOMO–LUMO gap are the potential candidate for optoelectronic applications.[11] The donor-acceptor technique is one of the useful method for developing NIR absorbing/emitting materials with narrow HOMO–LUMO gap.[12] The optoelectronic properties of the D–A molecules are controlled by the HOMO–LUMO gap, which may be easily tuned by (a) adjusting the π-bridge between donor and acceptor units or (b) choosing the appropriate donor/acceptor unit in the molecular system.[13–16] The donor–acceptor molecular systems consist of an electron-rich donor unit and an electron-poor acceptor unit linked by an appropriate spacer. Using a suitable π-linker (such as a double or triple bond or an aromatic ring), the hybridization of donor and acceptor moieties significantly perturbs the HOMO–LUMO energy levels.[17, 18] The strength of the D–A interaction depends on the donor group, acceptor group, as well as the type of π-linker/spacer unit which play a significant role in the D–A systems.[19] The donor–acceptor chromophores with low HOMO–LUMO gap exhibit potential applications in dye sensitized solar cells (DSSCs) [20], bulk heterojunction organic solar cells (BHJOSCs) [21], non-linear optics (NLOs) [22], organic field effect transistors (OFETs) [23], bioimaging [24] and photodynamic therapy [25].

The donor–acceptor (D–A) system is made up of an electron-rich donor and an electron-deficient acceptor unit connected by an appropriate spacer (Figure 1.1).

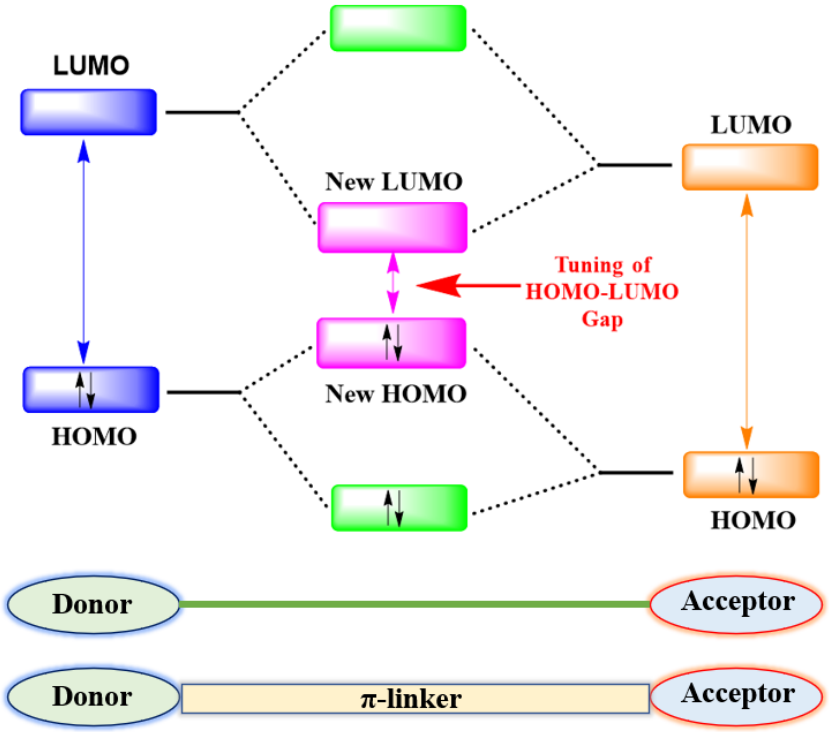

Figure 1.1. HOMO–LUMO energy level diagram of the D–A system.

The D–A system's LUMO is more stable than the LUMO of individual donor and acceptor units, but the HOMO is less stable than the HOMO of individual donor and acceptor units (Figure 1.1).[26] The hybridization of the donor and acceptor units increases HOMO energy levels and decreases the LUMO energy levels *via* using appropriate π-linker, such as a double or triple bond or an aromatic ring.[17] This makes the absorption spectrum shifts towards NIR region and the HOMO–LUMO gap gets smaller.

The electron-rich moiety in D–A molecules that provides an electron to another moiety is referred to as the donor, and the electron-deficient moiety that accepts the electron from the donor is referred to as the acceptor. In Chart 1, there are numerous examples of donor and acceptor moieties. The [2+2] cycloaddition-retroelectrocyclization reaction is generally a rapid, high-yielding, and catalyst-free

reaction.[27] The electron-rich alkynes react with cyano group containing strong electron acceptor tetracyanoethylene (TCNE) and 7,7,8,8-tetracyanoquinodimethane (TCNQ) *via* [2+2] cycloaddition retroelectrocyclic ring-opening reaction, resulted in D–A based π-conjugated chromophores in excellent yield.[28] The incorporation of the 1,1,4,4-tetracyanobuta-1,3-diene (TCBD) and cyclohexa-2,5-diene-1,4-diylidene-expanded TCBD, provides a variable charge transfer, low HOMO–LUMO gap, longer absorption, and enhances the electron accepting ability of the chromophores.[29–31]

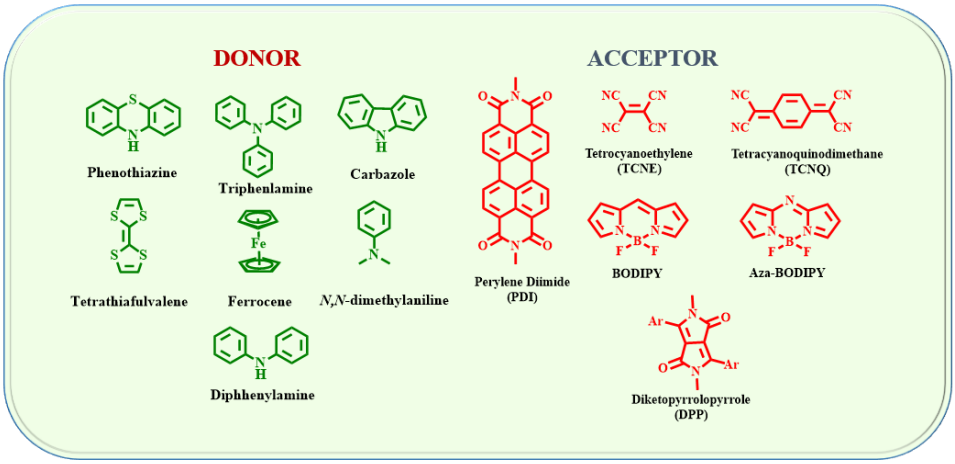

Chart 1. Molecular structures of the donor and acceptor units.

1.2. BODIPY

Dipyrromethene is a bidentate ligand that exists in both *cis* and *trans* isomeric forms and is involved in a wide range of metal complexes. The synthesis of a complex with BF_2 constricts the BODIPY framework and limits *cis-trans* isomerization. The BODIPY is highly planar, however the boron atom is slightly distorted from the normal plane in some cases.[32] The BF_2-chelated dipyrromethenes have received considerable interest in the scientific community as a building component for artificial photosynthetic systems, light-harvesting arrays, fluorescent switches, tunable laser dyes, and molecular probes and many more.[33–38] The BODIPY is an electron-deficient (acceptor) molecule; therefore, incorporating an electron-donating (donor) group induces a donor–acceptor interaction in the molecule. In 1968, Treibs & Kreuzer synthesized BODIPY which exhibit a pyrrole, azafulvene and

diazaborinin-type ring in the π-conjugated systems.[39] The IUPAC numbering method for 4,4-Difluoro-4-bora-3a,4a-diaza-*s*-indacene (BODIPY) dye differs from that of dipyrromethene (Figure 1.2). These approaches of naming are broadly accepted across the world and are frequently used in the current literature. The BODIPY fluorophores exhibit remarkable optical and redox properties.[40–44] These properties make them useful candidate for organic electronics, chemosensors, photodynamic therapy and bioimaging applications.[45–51]

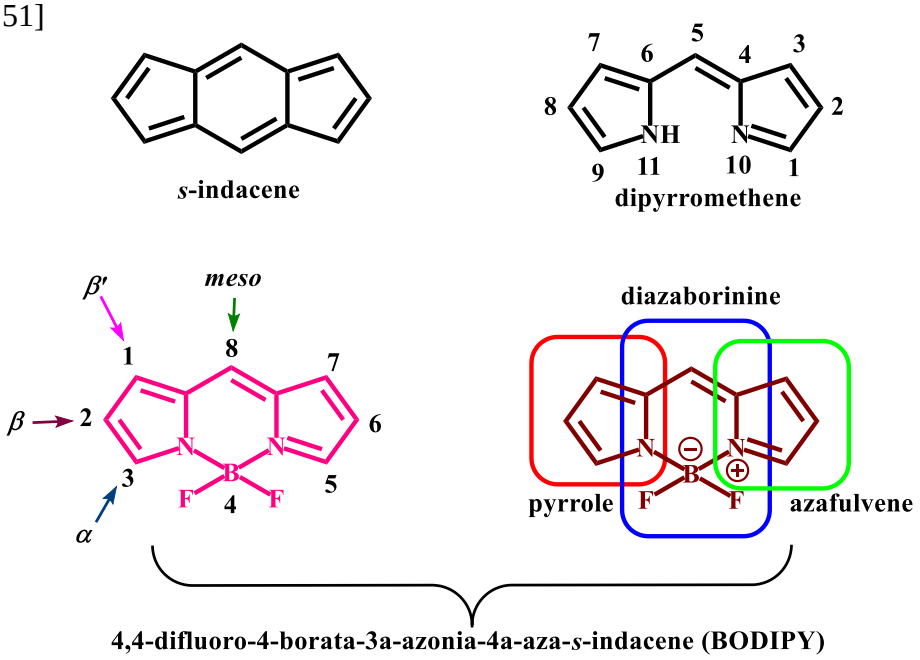

Figure 1.2. Nomenclature of *s*-indacene, dipyrromethene and BODIPY core. [32–51]

The BODIPYs generally exhibit a strong absorption band around 500–550 nm (ε = 40000–80000 $M^{-1}.cm^{-1}$) corresponding to $S_0 \rightarrow S_1$ (π–π^*) transition and a shoulder peak at lower wavelength region due to a vibrational transition.[52, 53] The BODIPY also has a weak absorption band around 350–380 nm, which corresponds to the $S_0 \rightarrow S_2$ (π–π^*) transition and emit a narrow spectrum between 530–560 nm.[54, 55] The BODIPY derivatives exhibit a good photochemical stability and excellent solubility in common organic solvents.[56] The BODIPY

fluorophore exhibits a high electron affinity, making it an excellent acceptor in the donor–acceptor type molecular systems.[57]

The BODIPY dyes exhibit excellent photonic properties such as absorption with high molar extinction coefficient, excellent fluorescent quantum yield, high electron affinity, high photochemical and thermal stability. These properties can be perturbed by incorporating suitable substituent at the α, β-pyrrolic and *meso*-positions of the BODIPY core.[58] The properties and easy synthetic modification of the BODIPYs make them most studied fluorophore and used as a potential candidate for dye-sensitized solar cells (DSSCs), sensors, photosensitizers, fluorescent switches, nonlinear optics, photodynamic therapy (PDT), laser dyes, light harvesters and bioimaging applications.[59–66]

In this work, the classifications of the donor–acceptor BODIPYs have been done based on attachment of substituents at the β-pyrrolic and *meso*-position of the BODIPY core (Figure 1.3).

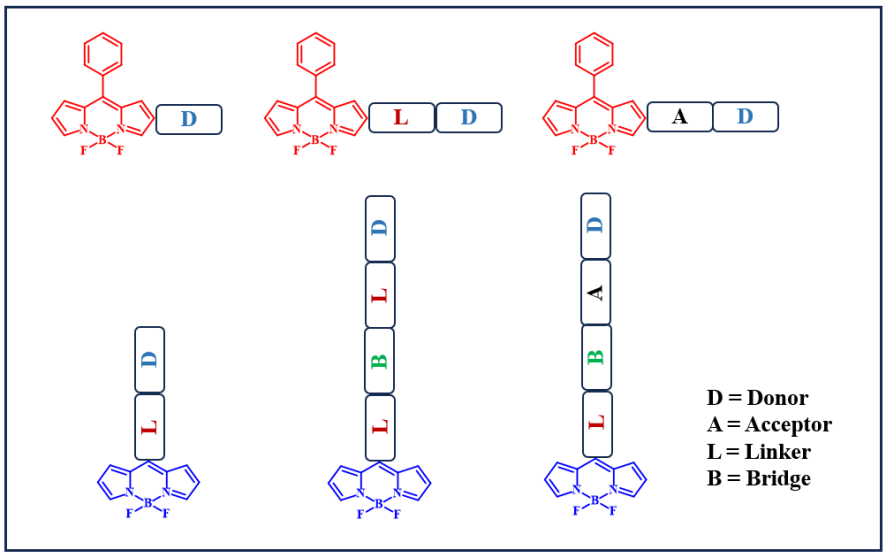

Figure 1.3. General classification of BODIPY based donor-bridge-acceptor derivatives in this work.

The β-mono and *meso* substituted BODIPYs were synthesized by the incorporation of donor/acceptor units at the β-pyrrolic and *meso*

position of the BODIPY. The donor/acceptor units were added to the BODIPY core *via* spacer (π-linker) or phenyl group.

1.2.1. Synthesis of BODIPY core

The methodologies of synthesizing the BODIPY is mentioned in the following sections. In 1968, Treibs and Kreuzer accidentally found the typically strong fluorescent F-BODIPY framework, while attempting to acylate 2,4-dimethylpyrrole with excess acetic anhydride and $BF_3.OEt_2$ (Lewis acid as catalyst). The two brightly colored mono and di-substituted BODIPYs **1** and **2** were isolated in <10% yield respectively. The chelation of dipyrrin with BF_2 facilitates tetrahedral geometry at the boron center (Scheme 1).[67]

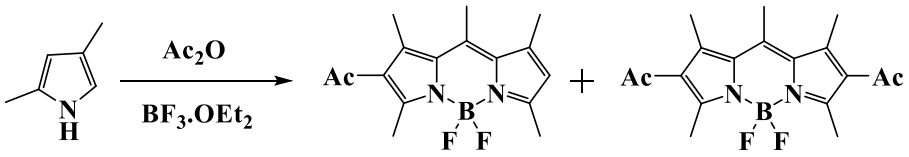

Scheme 1. Synthesis of the BODIPYs **1** and **2** from the 2,4-dimethylpyrrole.

1.2.2. From Aldehyde and pyrrole

The BODIPYs were synthesized by Lindsey method. This approach is based on the acid-catalyzed condensation reaction of pyrrole with benzaldehyde. The final product was obtained by using DDQ and $BF_3.OEt_2$ in 22% yield (Scheme 2). The BODIPY **3** exhibits an absorption band at 503 nm in toluene.[68]

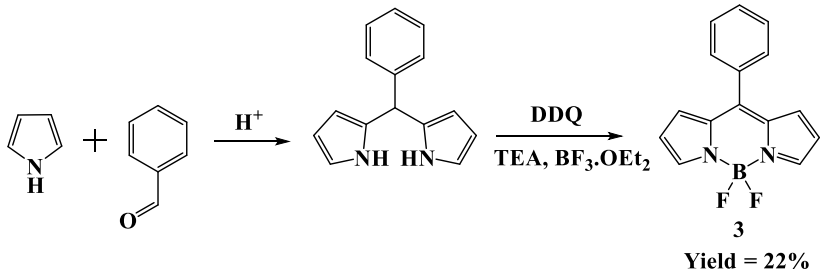

Scheme 2. Lindsey method for the synthesis of BODIPY **3**.

1.2.3. From pyrrole and acid chloride

In 2012, Zhang *et al.* reported a facile one-pot synthesis of BODIPY **4** by the reaction of pyrrole and acid chloride followed by the complexation reaction with $BF_3.OEt_2$ in 21% yield (Scheme 3). The BODIPY **4** shows absorption band at 494 and emission band at 512 nm. The BODIPY **4** exhibits high fluorescence quantum yield (0.87) and longer fluorescence lifetime in dichloromethane (DCM) solvent.[69, 70]

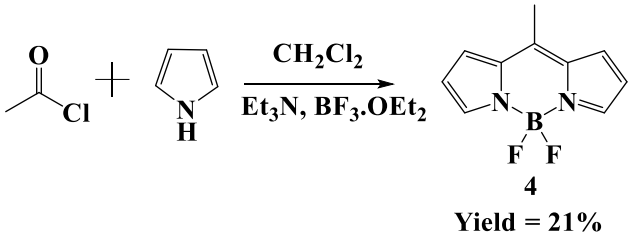

4

Yield = 21%

Scheme 3. Synthesis of BODIPY **4** from pyrrole and acid chloride.

1.2.4. From substituted pyrrole-2-carbaldehyde

The BODIPY dyes were synthesized from the self-condensation reaction with pyrrole-2-carbaldehyde and $POCl_3$ followed by TEA and $BF_3.OEt_2$. The *5-tert*-butyl-pyrrole-2-carbaldehyde was used to synthesize BODIPY **5** in a 15% yield (Scheme 4). The BODIPY **5** exhibits a narrow absorption band at a higher wavelength (492–500 nm) assigned to the $S_0 \rightarrow S_1$ transition and at shorter wavelength assigned to the $S_0 \rightarrow S_2$ transition.[71]

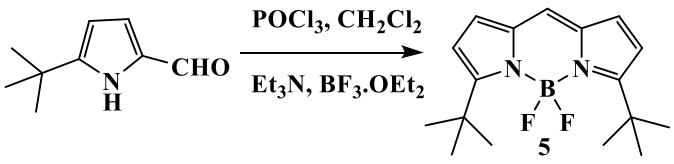

5

Yield = 15%

Scheme 4. Synthesis of BODIPY **5** from *5-tert*-butyl-pyrrole-2-carbaldehyde.

1.2.5. From pyrrole and triethyl orthoformate

In 2014, Kolemen *et al.* reported BODIPY **6** by using 2,4-dimethylpyrrole, triethyl orthoformate, $POCl_3$ and complexation reaction with $BF_3.OEt_2$ at 40 ^oC which resulted in a 40% yield (Scheme 5).[72]

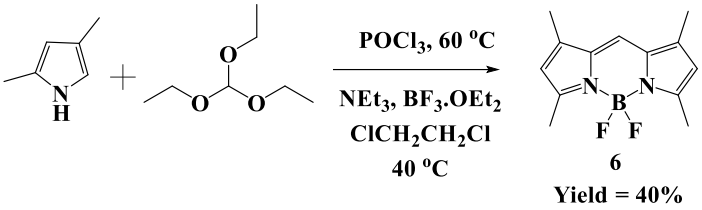

Scheme 5. Synthesis of BODIPY **6** from the 2,4-dimethylpyrrole and triethyl orthoformate.

1.2.6. From pyrrole and thiophosgene

In 2012, Kim *et al.* reported the synthesis of BODIPY **7** and used this as an intermediate to form BODIPY **8** for ratiometric fluorescence sensing of Hg^{2+} ion. The BODIPY **8** undergoes Hg^{2+} promoted hydrolysis to produce the 8-hydroxy-BODIPY with a large emission.[73] In 2019, Chai *et al.* synthesized BODIPY **8** by using pyrrole and thiophosgene. The pyrrole reacts with $CSCl_2$ in the presence of DCM or toluene solvent, which results in an intermediate bis-(1*H*-pyrrol-2-yl)-methanethione. The bis-(1*H*-pyrrol-2-yl)-methanethione was further reacted with methyl iodide followed by triethylamine and $BF_3.OEt_2$ which resulted BODIPY **8** in 26% yield (Scheme 6). The BODIPY **8** exhibits an absorption band at 485 nm and emission band at 525 nm. Bright green fluorescence can be seen in a solution of BODIPY **8**, however after being exposed to $HgCl_2$, blue fluorescence was produced.[74] Recently, Dehaen and co-workers also reported the procedure for the design and synthesis of *meso*-halo BODIPYs *via* dipyrryl thione (**7)** as shown in Scheme 10.[75]

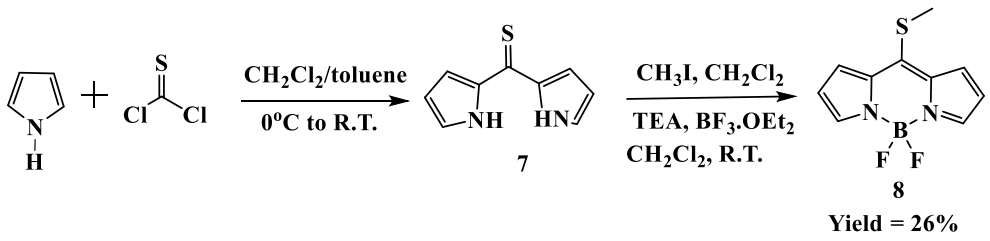

Scheme 6. Synthesis of BODIPY **7** and **8** from pyrrole and $CSCl_2$.

1.2.7. From substituted pyrroles

In 2012, Boens *et al.* reported BODIPY **9** by using substituted pyrroles followed by complexation with TEA and $BF_3.OEt_2$ (Scheme 7). The BODIPY **9** consist of two cyclohexane rings fused at the 2,3- and 5,6-position. The BODIPY **9** exhibits absorption at 534–543 nm and emission band at 543–551 nm with high fluorescence quantum yield between 0.76–0.89.[76]

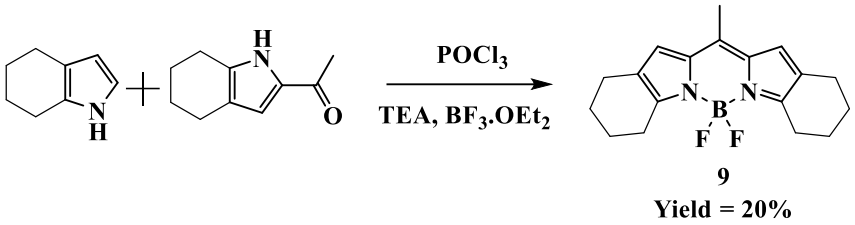

9

Yield = 20%

Scheme 7. Synthesis of BODIPY **9** from substituted pyrrole.

1.3. Functionalization of BODIPY core

The spectroscopic and photophysical properties can be fine-tuned by adding appropriate groups to the BODIPY core at the right positions. Boron dipyrrin dyes can be easily functionalized at the pyrrole C-ring positions, *meso*-position and the boron atom.[77]

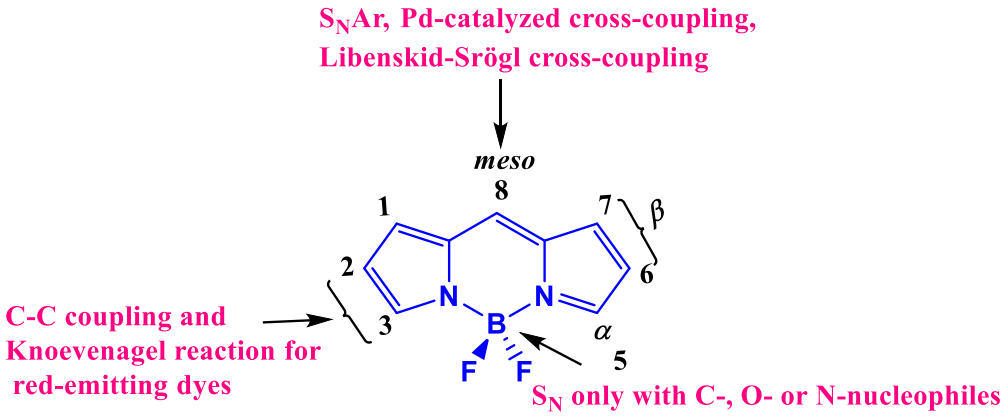

4,4-difluoro-4-bora-3a,4a-diaza-*s*-indacene (BODIPY)

Figure 1.4. Schematic representation of the structural modifications and chemical reactions of the BODIPY dye. [77]

There are many different functionalization methods that can be utilized in order to derivatize the BODIPY framework. Significant progress has been made in functionalizing the BODIPY dyes at different

pyrrolic positions by nucleophilic substitution, Knoevenagel-type condensation reactions, substitution of the fluorine atoms on boron, direct styrylation, nucleophilic substitution at the *meso*-position, Libenskid cross-coupling and metal-catalyzed C-C coupling reactions (Figure 1.4.).[78] All these methods can be used to synthesize BODIPY derivatives to tune the optoelectronic properties. The design and synthesis of donor-acceptor based BODIPYs are widely used for developing NIR absorbing materials for PDT with a low band gap value and improved power conversion efficiency of the DSSCs. The expansion of the π-conjugation is a primary method to enhance the absorption band from visible to NIR region and improving J_{SC} value for DSSCs.[79] Nagano *et al.* reported D-A BODIPY dyes, which exhibit low fluorescence quantum yield due to photoinduced electron transfer (PeT) from donor trimethoxy benzene to acceptor BODIPY.[80]

1.3.1. Halogenation

1.3.1.1. Halogenation reaction at α-position of the BODIPY

In 2005, Rohand *et al.* reported α-chloro functionalized BODIPYs **10** and **11**. The benzaldehyde reacts with pyrrole and catalytic amount of trifluoroacetic acid to form dipyrromethane. Chlorination occurs selectively at the α-position of the dipyrromethane by varying the equivalents of *N*-chlorosuccinimide (NCS).

The halogenated dipyrromethane was treated with DDQ or *p*-chloranil for oxidation, followed by complexation with TEA and $BF_3.OEt_2$ which resulted in α-chloro or α-bromo substituted BODIPYs in good yields.[81, 82] The BODIPYs **10** and **11** were synthesized using 2 and 14 equivalents of *N*-chlorosuccinimide in the presence THF solvent followed by complexation reaction with $BF_3.Et_2O$, in 20% and 22% yields respectively (Scheme 8). The α-brominated BODIPYs **12–17** were synthesized by reacting dipyrromethane with 1–10 equivalents of *N*-bromo succinimide (NBS) resulting in 16–40% yields (Scheme 8).

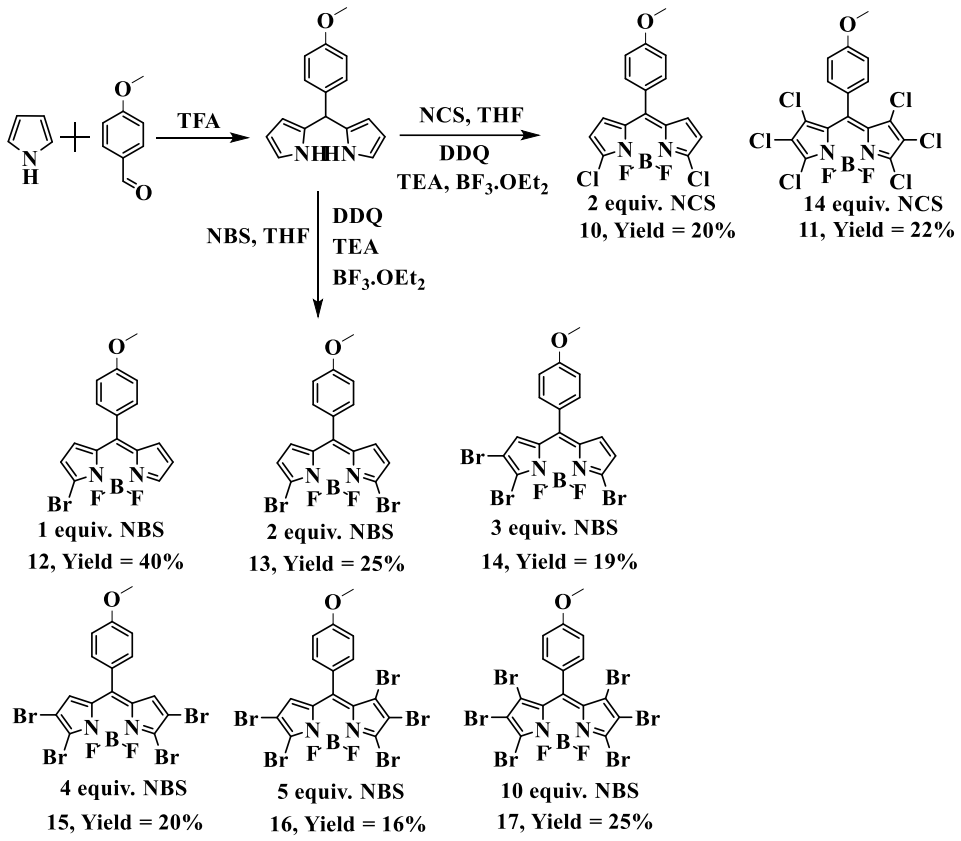

Scheme 8. Synthesis of halogenated BODIPYs **10–17**.

1.3.1.2. Halogenation reaction at *β*-position of the BODIPY

The BODIPY exhibits electrophilic substitution reaction at the *β*-pyrrolic positions of the BODIPY. Different procedures are reported in the literature in which the BODIPY can be chlorinated, brominated and iodinated to get *β*-halogenated BODIPYs in good yields. The halogenating reagents such as NCS (2–10 equivalents), I_2:HIO_3 (from 0.8 to excess equiv.) and Br_2 (from 0.8 to excess equivalents) were used for the synthesis of the *β*-halogenated BODIPYs **18–29** in 8–98% yields (Scheme 9). The methyl-substituted BODIPY reacts with 0.8 to excess equivalents of bromine resulting in *β*-mono and di-brominated BODIPYs **30–31** in 76% and 67% yields. The methyl-substituted BODIPY was used to avoid excess bromination.[83, 84]

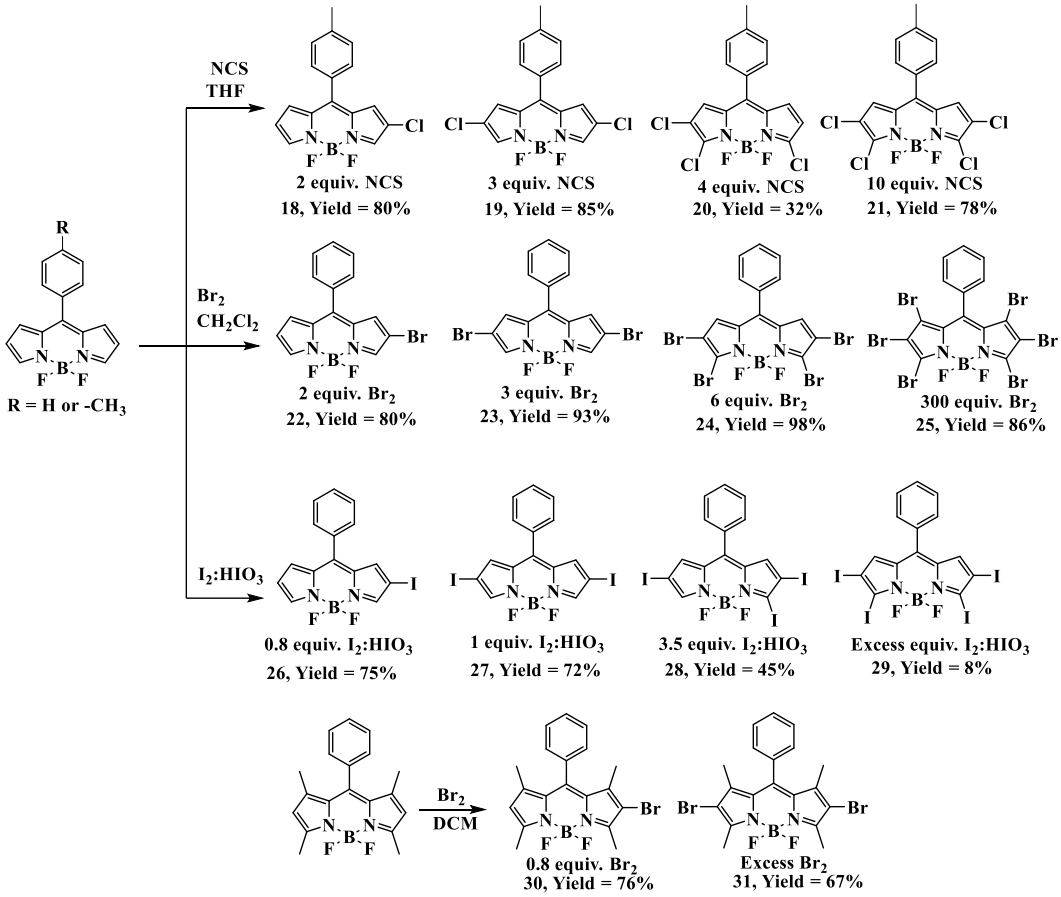

Scheme 9. Synthesis of chloro/bromo and iodo substituted BODIPYs **18–31**.

1.3.1.3. Halogenation reaction at *meso*-position of the BODIPY

Dehaen *et al.* reported the synthesis of 8-chloro/ 8-bromo BODIPYs by using phosphorus oxychloride ($POCl_3$)/ phosphoryl bromide ($POBr_3$) respectively and followed by complexation with $BF_3.OEt_2$. The 8-chloro group can be replaced by 8-iodo group by the sodium iodide (NaI) which resulted in 8-iodo-BODIPY **32c** in 66% yield (Scheme 10). The 8-chloro-BODIPY was synthesized from dipyrryl ketone. The dipyrryl ketone was obtained from the reaction of pyrrole and triphosgene or thiophosgene.[85] The dipyrryl thione, on further reaction with H_2O_2, gives dipyrryl ketone. The dipyrryl ketone on further treatment with POX_3 (X = Cl or Br) followed by a complexation

reaction with TEA and $BF_3.OEt_2$ resulted in 8-halo-BODIPY **32a–32b** in 59% and 68% yields respectively (Scheme 10).[52, 86]

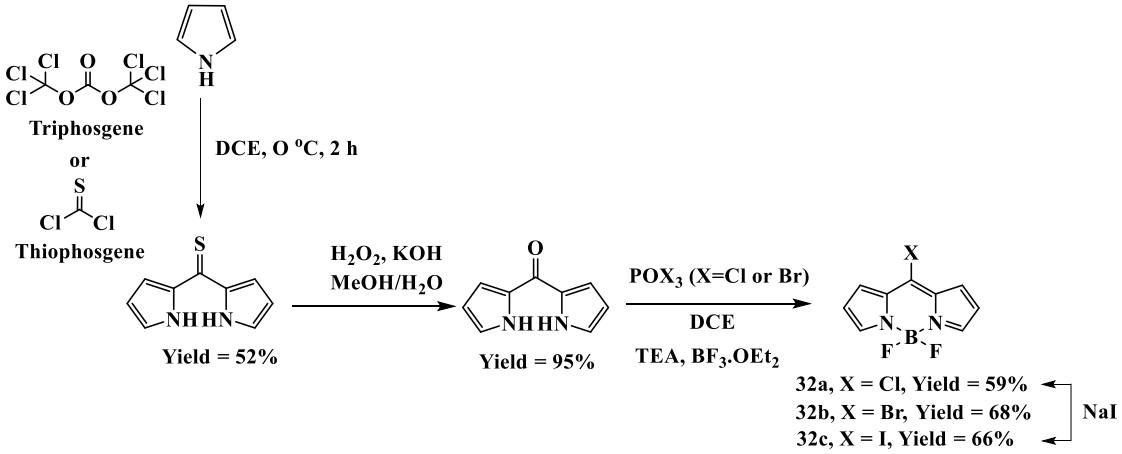

Scheme 10. Synthetic route for the 8-halo BODIPY **32a–32c**.

1.3.2. Incorporation of S, N and O at *meso*-position of the BODIPY

The 8-halo BODIPYs are highly fluorescent and have been used as the starting material for synthesizing BODIPYs **33–41** *via* aromatic nucleophilic substitution reaction (Scheme 11). The chloride substituent is an excellent leaving group in the S_NAr reaction and exhibit high reactivity compared to Br and I group. The 8-chloro-BODIPY undergoes S_NAr reaction to introduce S, N and O atoms at the *meso*-position through suitable nucleophile and base (Scheme 11). The BODIPYs **34**, **35** and **37** show absorption bands at 413 nm, 456 nm and 443 nm and emission bands at 420 nm, 495 nm and 486 nm respectively. The BODIPYs **35** and **37** exhibit high fluorescence quantum yield, whereas 8-N- and 8-S-substituted BODIPYs **33**, **34** and **36** are nonfluorescent. The BODIPY dye with 8-Nitrogen or 8-Oxygen substituents exhibited a blue shift of absorption and emission band compared to unsubstituted BODIPY.[86]

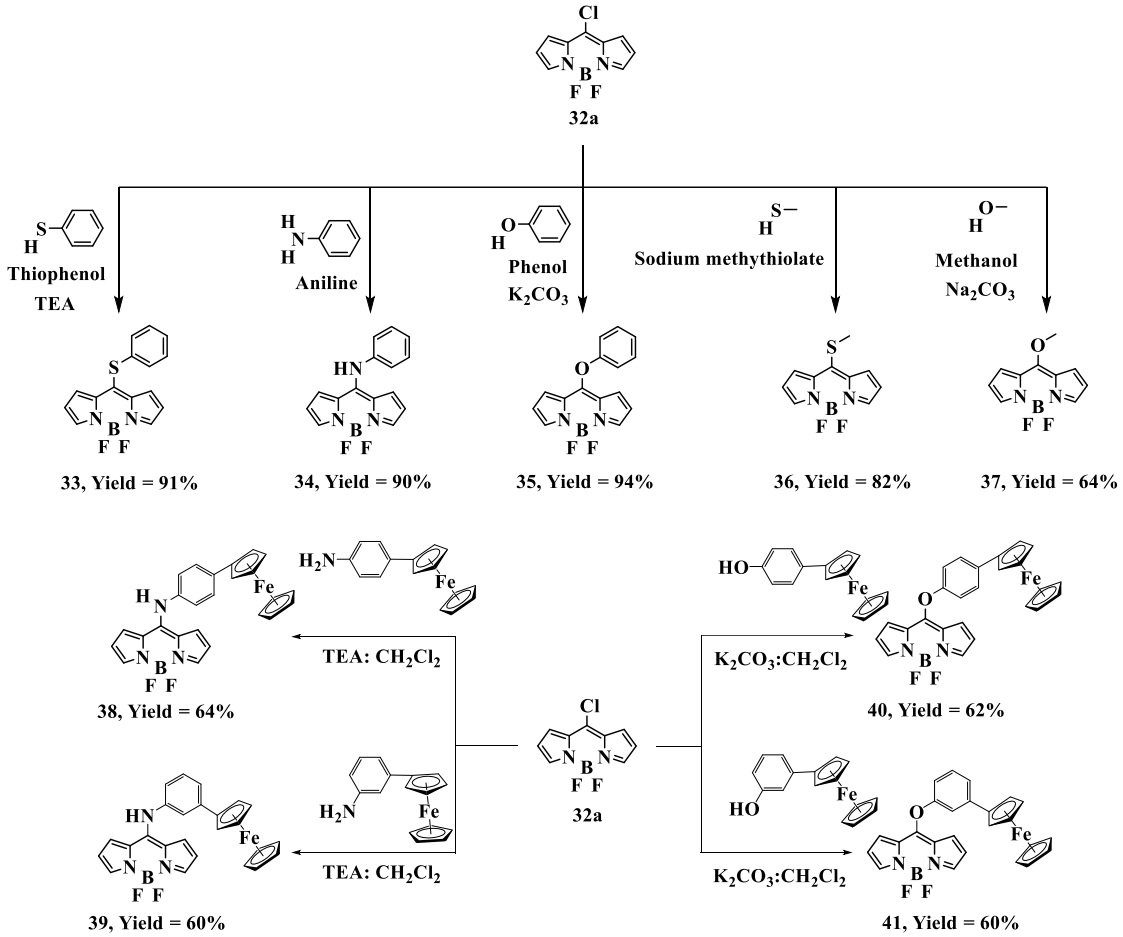

Scheme 11. Synthesis of *meso*-heteroatom substituted BODIPYs **33–41**.

Misra *et al.* investigated a series of O and N-connected ferrocenyl BODIPYs **38–41** through nucleophilic aromatic substitution (S_NAr) reaction using 8-chloro BODIPY and ferrocenyl phenols/anilines (Scheme 11). The BODIPYs **38** and **39** were synthesized by reacting 8-chloro BODIPY with para- and meta-ferrocenyl aniline whereas the BODIPYs **40** and **41** were synthesized by reacting 8-chloro BODIPY with para- and meta-ferrocenyl phenols. The absorption spectra of nitrogen atom-linked BODIPYs **38** and **39** exhibit 80 nm blue shift. The 8-chloro BODIPY exhibits a strong ($S_0 \rightarrow S_1$) absorption band at 503 nm. The oxygen atom linked BODIPYs **40** and **41** exhibit a 50 nm blue shift compared to 8-chloro BODIPY. The BODIPYs **38–41** exhibit absorption bands at 418 nm, 419 nm, 455

nm and 455 nm respectively. The donor-acceptor BODIPYs **38–41** have oxidation potentials of 0.06 V, 1.06 V; 0.03 V, 1.12 V; 0.06 V, 1.07 V; 0.10 V, 1.12 V and reduction potentials of –1.19 V, –1.39 V; –1.21 V, –1.39 V; –1.14 V, –1.25 V; and –1.24 V, –1.28 V respectively. The ferrocenyl BODIPYs **38–41** show two reduction potential that are attributed to the BODIPY unit and two oxidation potential that correspond to the oxidation of the ferrocenyl and BODIPY unit. The BODIPYs **38–41** exhibited high thermal stability with the decomposition temperature at 300 ℃, 309 ℃, 264 ℃ and 254 ℃ respectively.[41]

1.3.3. Vilsmeier-Haack formylation reaction of BODIPY

The α-mono and di-formylated BODIPYs were prepared by using phosphorus oxychloride ($POCl_3$), dimethylformamide (DMF) followed by DDQ for oxidation of dipyrromethane intermediate (Scheme 12).

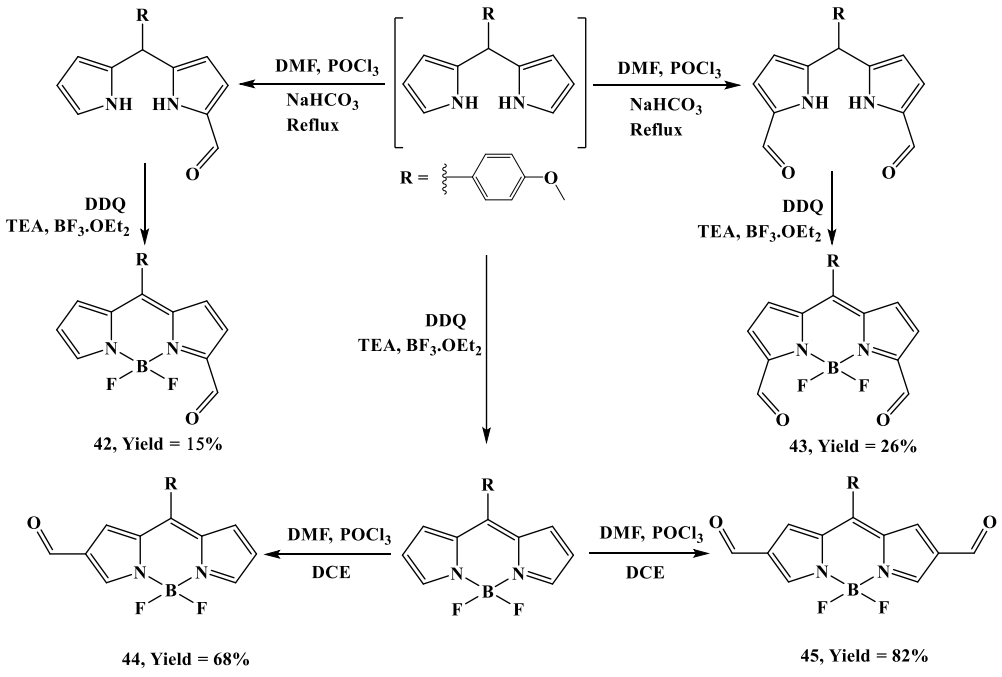

Scheme 12. Synthesis of α- and β-mono and di-formylated BODIPYs **42–45**.

After complete oxidation, the mixture was treated with TEA and $BF_3.OEt_2$ for complexation which results in α-mono and di-formylated BODIPYs **42** and **43** in 15% and 26% yields respectively. The β-mono and di-formylated BODIPYs **44** (yield = 68%) and **45** (yield = 82%) were synthesized after the formation of BODIPY using Vilsmeier reagent (Scheme 12). The BODIPYs **42–45** showed a characteristic absorption $S_0 \rightarrow S_1$ (π–π^*) transition at 540–550 nm. The formylated BODIPYs **42–45** showed weak fluorescence because of the electron-rich *meso*-aryl group which is associated with photoinduced electron transfer with the BODIPY.[87, 88]

1.3.4. Knoevenagel condensation reaction of BODIPY

Zang *et al.* reported the design and synthesis of carbazole-based BODIPY derivatives through Knoevenagel condensation reaction for solar cell application. The methyl-substituted BODIPYs reacts with aldehyde groups in the presence of piperidine, acetic acid and toluene at reflux condition (Dean-stark apparatus). The mono-, di- and tetra-vinyl substituted BODIPYs **46–48** were synthesized by using 1.0, 3.0 and 6 equivalents of carbazole-aldehyde (Ar), which resulted in 37%, 79%, and 13% yields respectively (Scheme 13). The BODIPYs **46–48** show absorption band at 590 nm, 674 nm, 728 nm and emission band at 609 nm, 692 nm and 755 nm respectively. The fluorescence quantum yield of BODIPYs **46–48** exhibit 0.69, 0.98 and 0.42 respectively. The frontier molecular orbitals calculated from cyclic voltammetry of BODIPYs **46–48** are HOMO energy levels at -5.36 eV, -5.34 eV, -5.34 eV and LUMO energy levels at -3.47 eV, -3.52 eV and -3.66 eV respectively. The electrochemical band gap for BODIPYs **46–48** estimated from HOMMO/LUMO values are 1.89, 1.82 and 1.68 eV respectively. The decomposition temperatures for the BODIPYs **46–48** were found to be at 346 ℃, 372 ℃ and 305 ℃ respectively. The Knoevenagel condensation reaction can be used to synthesize highly conjugated BODIPY dyes.[89] Obondi *et al.* reported a set of donor-acceptor based BODIPYs **49–51** in which the BODIPY unit was connected to two vinyl linkers that carry phenyl, triphenylamine and

phenothiazine units (Scheme 13). The fulleropyrrolidine group act as an electron acceptor at the *meso*-position of the BODIPYs **49–51**. The BODIPYs **49–51** exhibit absorption and emission in 300–850 nm region. The absorption spectra of the BODIPYs **49–51** show a characteristic sharp peak of fulleropyrrolidine at 432 nm.

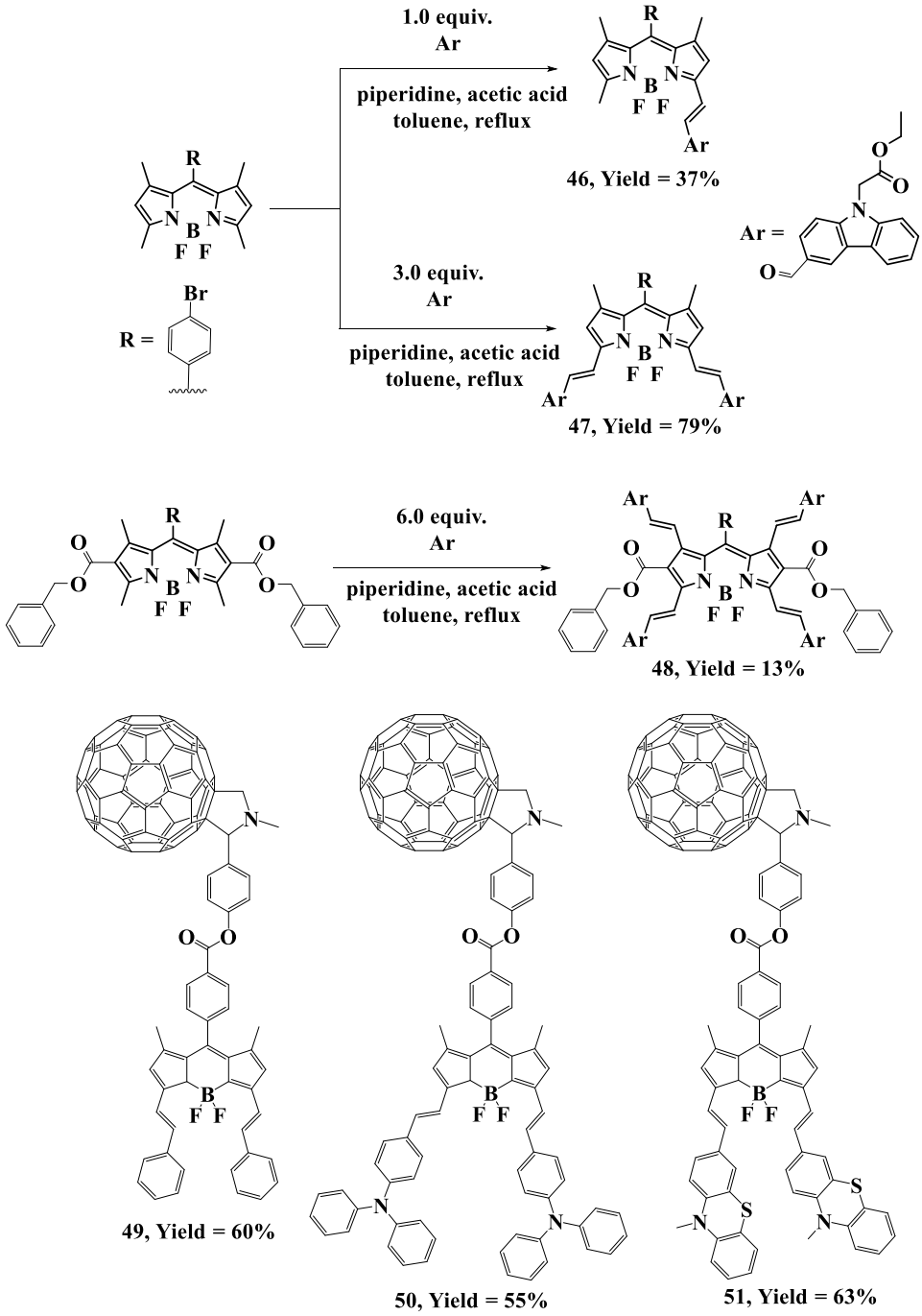

Scheme 13. Synthesis and molecular structures of the BODIPYs **46–48** and **49–51** respectively.

The BODIPYs **49–51** exhibit absorption peaks at 634 nm, 676 nm, 702 nm and fluorescence peak at 652 nm, 763 nm, and 709 nm respectively. The BODIPYs **49–51** show fluorescence quantum yield of 0.114, 0.07, < 0.01 respectively. The BODIPYs **49–51** exhibit oxidation potentials at 0.52 eV, 0.20 eV, 0.39 eV and reduction potentials at -1.00 eV, -1.27 eV; -1.01 eV, -1.36 eV; and -1.00 eV, -1.31 eV respectively. The triphenylamine and phenothiazine substituted BODIPYs **50** and **51** covers the spectrum range from 300–780 nm.[90]

1.3.5. Cross-coupling Reactions of BODIPYs

Generally, the cross-coupling reactions are used to synthesize BODIPY based donor–acceptor chromophores. The halogen substituted BODIPYs shows Pd-catalyzed cross-coupling reactions such as Sonogashira, Suzuki, Heck and Stille cross-coupling reactions.

1.3.5.1. Sonogashira Cross-Coupling Reactions

Shinde *et al.* reported the donor–acceptor BODIPYs which were synthesized by the Palladium-catalyzed Sonogashira cross-coupling reaction and investigated their photophysical and redox properties. The precursors α-bromo, β-iodo and 8-chloro BODIPY react with 1-ethynyl-4-(ethynylferrocene) benzene (1.0 equiv.) in the presence of Pd-catalyst which gives α, β and *meso*-ferrocenyl-substituted BODIPYs **52–54** in 80–85% yield (Scheme 14). The BODIPYs **52–54** shows an absorption maxima at 568 nm, 545 nm and 550 nm and emission maxima at 580 nm, 608 nm and 568 nm respectively. The highest bathochromic shift was observed for BODIPY **52** compared to BODIPYs **53** and **54**. The electrochemical studies show that the BODIPYs **52–54** exhibit oxidation waves at 1.13 V, 0.97 V; 0.11 V, 1.03 V and 0.14 V, 1.04 V, whereas the reduction wave at –1.16 V, –1.09 V and –0.97 V, respectively. Incorporating the ferrocene unit in BODIPYs **52–54** revealed that the oxidation values anodically shifted by 0.11–0.14 V compared to pristine ferrocene oxidation.[91] Ravikanth and co-workers have reported the BODIPY-ferrocene derivatives **55–57** in which one or two ferrocenyl units were linked through the ethynyl group at the α- and *meso*-position

of the BODIPY unit (Scheme 14). The BODIPYs **55–57** exhibit absorption bands at 531 nm, 631 nm; 558 nm, 680 nm, and 505 nm respectively. The absorption studies reveal that the BODIPYs **55** and **56** show ICT band in the UV-visible region due to strong conjugation between donor ferrocene and BODIPY. The CT band was not observed for BODIPY **57** in which the ferrocene unit is the *meso*-phenyl group of BODIPY which shows less effective conjugation between ferrocene and BODIPY as compared to the BODIPYs **55** and **56**.

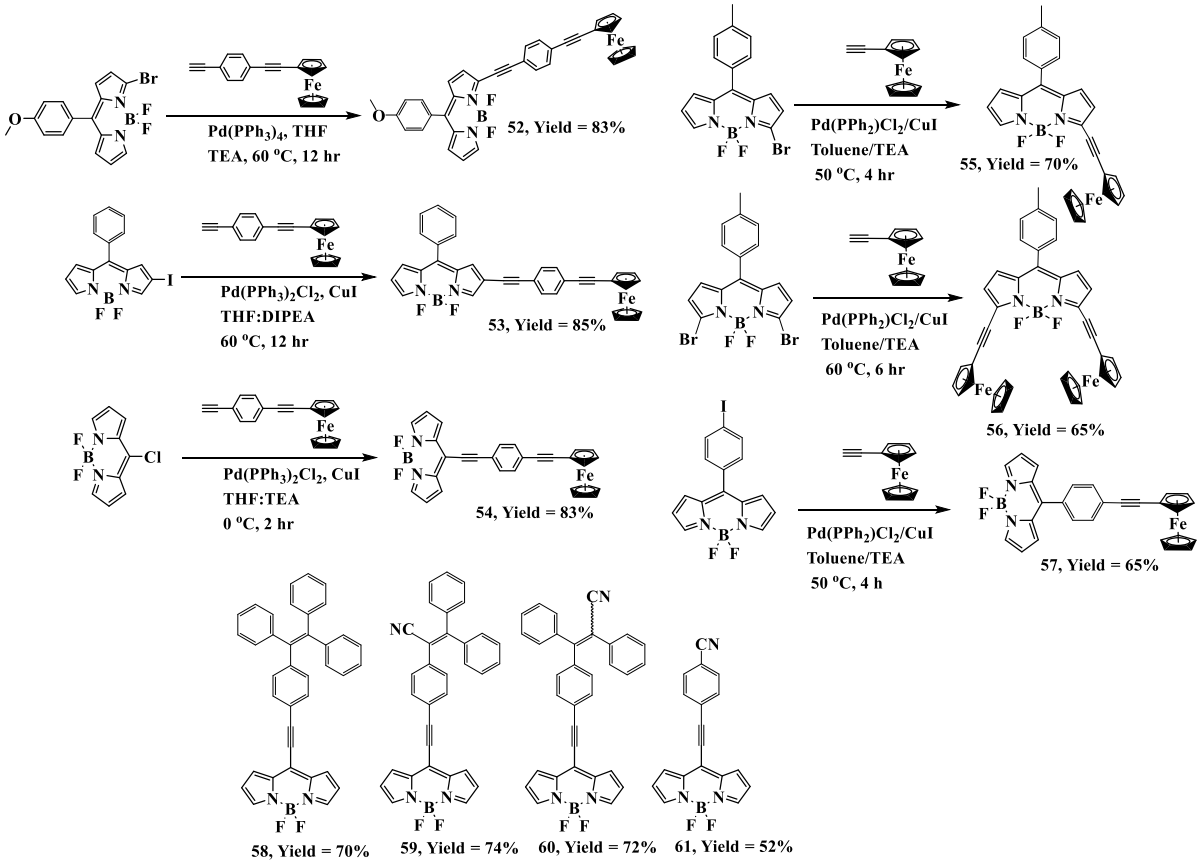

Scheme 14. Synthesis and molecular structures of the α, β and *meso*-substituted BODIPYs **52–61**.

The BODIPYs **55–57** are non-fluorescent in nature due to fast photo-induced electron transfer from donor ferrocene to acceptor BODIPY. Generally, BODIPY exhibits single oxidation and single reduction wave due to the formation of mono-cation and mono-anion respectively. In BODIPYs **55–57** the BODIPY exhibits a single irreversible oxidation wave in the range of 1.30–1.50 V and a single reversible reduction wave in the –0.70 V to –0.80 V region whereas the

BODIPY **57** shows only one reduction. The BODIPYs **55–57** show reversible oxidation in 0.64–0.74 V region attributed to formation of ferrocene to ferrocenium ion.[92] Dhokale *et al.* reported the synthesis of BODIPYs **58–61** by using Palladium-catalyzed Sonogashira cross-coupling reaction (Scheme 14). The BODIPYs **59** and **60** exhibit red-shifted absorption and emission as well as high fluorescence quantum yield compared to the BODIPY **58**. The BODIPYs **58–61** exhibit absorption bands at 468 nm, 543 nm; 435 nm, 546 nm; 428 nm, 546 nm; and 552 nm whereas the emission bands were observed at 561 nm, 731 nm; 564 nm; 564 nm; and 571 nm respectively. The presence of electron-withdrawing group at the *meso*-position of the BODIPY shows a blue shifts in absorption and emission spectra and lowers the quantum yield.[58]

1.3.5.2. Suzuki Cross-Coupling Reactions

Ravikanth *et al.* synthesized a set of mono, and di phenyl substituted BODIPYs **62** and **63** through Pd-catalyzed Suzuki cross-coupling reaction and investigated their optical and redox properties. The α and β-bromo BODIPYs reacted with the phenyl boronic acid in controlled equivalents in the presence of Pd-catalyst, Na_2CO_3, Toluene: THF: H_2O (6:3:1) under reflux condition resulting in mono and di phenyl substituted BODIPYs **62** and **63** in 85% and 87% yield respectively (Scheme 15). The phenyl-substituted BODIPYs **62** and **63** exhibit absorption bands in 500–600 nm region corresponding to $S_0 \rightarrow S_1$ transition and a vibronic transition at about 400 nm corresponding $S_0 \rightarrow S_2$ transition. The BODIPYs **62** and **63** exhibit oxidation potential at 1.46 V and 1.33 V and reduction potential at –0.83 V, –0.84 V respectively.[93] Recently, Wanwong *et al.* have reported a series of donor–acceptor BODIPYs **64–67** by using Pd-catalyzed Suzuki cross-coupling reaction in which the triphenylamine and carbazole act as donor groups and BODIPY as an acceptor (Scheme 15). The BODIPYs **64–67** exhibited two strong absorption band in the range of 269–307 nm and 511–531 nm with high extinction coefficients (10^4 M^{-1} cm^{-1}). The absorption maxima of the BODIPYs **66** and **67** show red-shift by 25 nm

and 20 nm compared to the BODIPYs **64** and **65** respectively. The optical bandgap of BODIPYs **64–67** were 2.05 eV, 2.07 eV, 1.98 eV and 2.00 eV respectively. Triphenylamine and carbazole were used as donor groups because they easily undergo oxidation into radical cations which can be employed in various optoelectronic applications. The redox properties of the BODIPYs **64–67** exhibit oxidation wave at 0.39 V, 0.45 V, 0.23 V and 0.37 V and these are attributed to the HOMO energy levels of –5.03 eV, –5.10 eV, –4.92 eV and –5.06 eV respectively.[94]

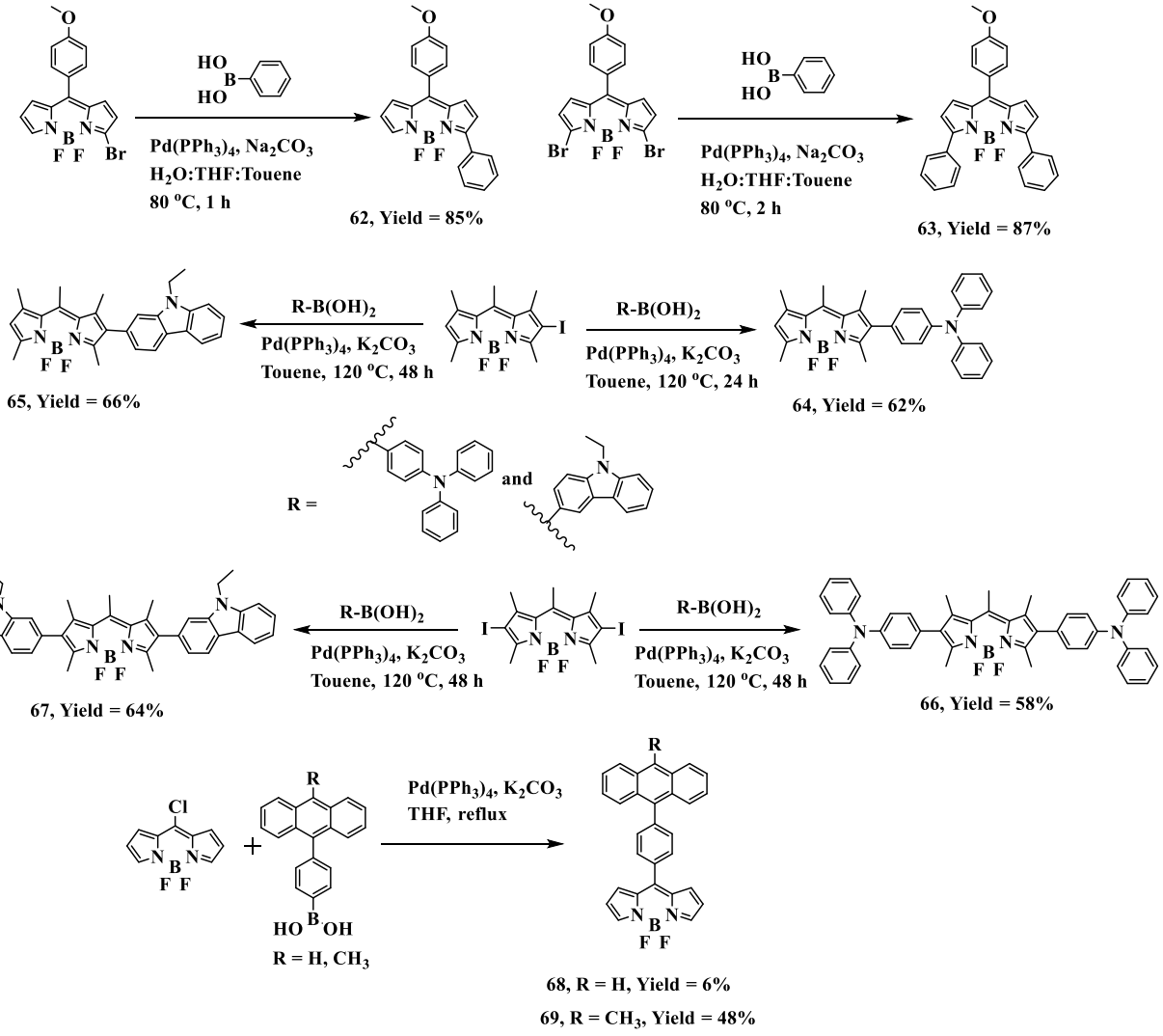

Scheme 15. Synthesis of the BODIPYs **62–69**.

Kim *et al.* have reported a set of 8-chloro BODIPY based chromophores **68** and **69** by Suzuki cross-coupling reaction which is useful for singlet oxygen generation ($^1O_2$). The 8-chloro BODIPY was

reacted with anthraphenylene boronic acid in the presence of palladium catalyst, potassium carbonate and THF solvent under reflux conditions resulting in orange color anthracene-based D–A BODIPYs **68** and **69** (Scheme 15). The BODIPYs **68** and **69** exhibit absorption band at 498 nm and emission bands at 517 nm and 519 nm respectively in MeOH solvent.[95]

1.3.5.3. Stille Cross-Coupling Reaction

In 2014, Ziessel *et al.* synthesized 3,5-substituted thiophene-benzothiadiazole-thiophene functionalized BODIPY **70** *via* Stille cross-coupling reaction. The *α*-di bromo BODIPY reacts with stannyl thiophene-benzothiadiazole-thiophene in the presence of Pd-catalyst and tri(*o*-tolyl)-phosphine using toluene at reflux condition which resulted in *α*-di thiophene-benzothiadiazole-thiophene substituted BODIPY **70** (purple color) in 83% yield (Scheme 16). The BODIPY **70** absorbs up to 800 nm in solution and up to 900 in thin film. The absorption spectra of the BODIPY **70** shows three peaks. The thiophene unit shows a peak at 320 nm overlapping with $S_0 \rightarrow S_2$ transition of the BODIPY unit and a CT peak was observed at 537 nm. The intense peak at 737 nm was assigned due to the $S_0 \rightarrow S_1$ (π–π*) transition of the BODIPY.[96] Yang *et al.* reported the D-A-D based BODIPYs **71** and **72** which were synthesized by Stille cross-coupling reaction for organic solar cells (OSCs). The *β*-di-bromo BODIPY reacts with tributyl(thiophen-2-yl)stannane and [2,2'-bithiophen].-5-yltributylstannane in the presence of Pd-catalyst using toluene solvent at 110 ^{o}C for 24 h which resulted in BODIPYs **71** and **72** respectively (Scheme 16). The decomposition temperature of the BODIPYs **71** and **72** exhibits at 221 ^{o}C and 305 ^{o}C respectively. The BODIPYs **71** and **72** show three absorption bands. The first absorption band at 280–350 nm region is due to π–π* transition of electron donors thiophene and bithiophene. The second band at 350–500 nm belongs to the π–π* of the BODIPY. The third absorption band at 500–800 nm region is attributed to the π–π* and ICT. The power conversion efficiency (η) of the organic

solar cells (OSC) based on BODIPYs/$PC_{61}BM$ (1:0.5, *w*/*w*) are 1.49% for BODIPY **71** and 2.15% for BODIPY **72**.[97]

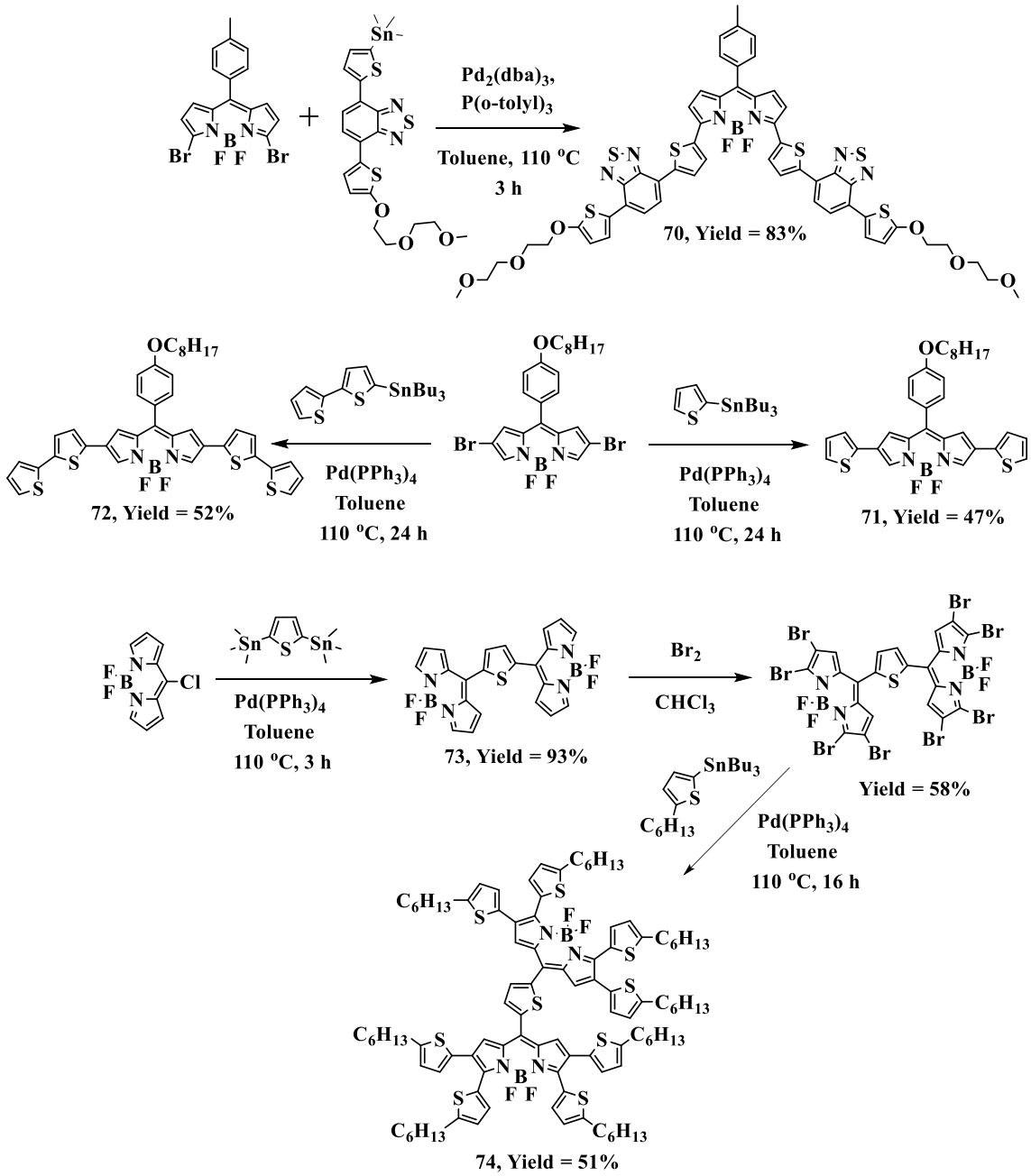

Scheme 16. Synthesis of thiophene functionalized BODIPYs **70–74**.

Leclerc *et al.* synthesized BODIPYs **73** and **74** through Stille cross-coupling reaction. The reaction of 8-chloro and octa-bromo substituted BODIPY with bis(trimethylstannyl)thiophene and tributyl(5-hexylthiophene2-yl)stannane using $Pd(PPh_3)_4$ and toluene at reflux condition for 3 h resulted in BODIPYs **73** and **74** in 93% and

51% yields respectively (Scheme 16). The BODIPYs **73** and **74** exhibit an absorption maximum at 520 nm, 486 nm, and 697 nm, 706 nm respectively. The absorption band at higher wavelength region are due to the $S_0 \rightarrow S_1$ transition and the second band are attributed to intramolecular charge transfer between donor thiophene and acceptor BODIPY moiety. The dimerization methodology of polycyclic aromatic units is a powerful strategy to synthesize BODIPY based material for organic solar cells application.[98]

1.3.5.4. Heck Cross-Coupling Reaction

In 2021, Knight *et al.* reported BODIPY derivative **75** which was synthesized by a Pd-catalyzed Heck coupling reaction. The α-di bromo BODIPY was reacted with styrene, $Pd(OAc)_2$, PPh_3, DMF and TEA to give 3,5-distyrene substituted BODIPY **75** in 51% yield (Scheme 17).[99] Hao *et al.* have reported regioselective and stepwise synthesis of BODIPYs **76–78** using Palladium(II) catalyzed Heck cross-coupling reaction. The bromo BODIPY reacts with 10–50 equivalent of methyl acrylate, $Pd(OAc)_2$, PPh_3, and Na_2CO_3 at different temperatures which resulted in alkenyl substituted BODIPYs **76–78** in 47%, 53% and 51% yield respectively (Scheme 17). The BODIPYs **76–78** exhibit absorption band at 612 nm, 622 nm and 634 nm and emission band at 628 nm, 655 nm and 669 nm respectively. The stokes shift of the BODIPYs **76–78** are 416 cm^{-1}, 810 $cm^{-1,}$ and 825 cm^{-1} respectively. The BODIPYs **76** and **77** (BODIPYs with bromo atoms at 2,6-position) shows efficient singlet oxygen ($^1O_2$) generation due to heavy atom effect.[100]

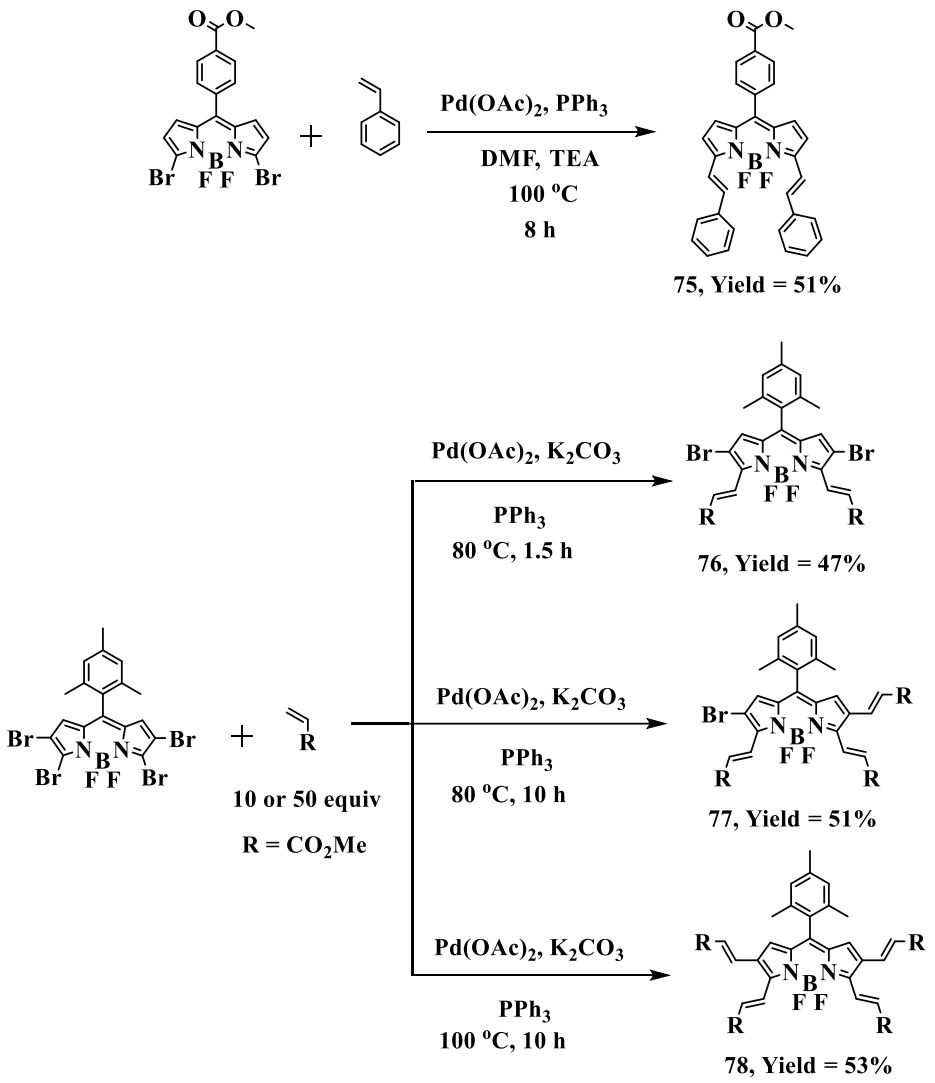

Scheme 17. Synthesis of phenyl substituted BODIPYs **75–78**.

1.3.6. C–H Amination of BODIPY

In 2018, You *et al.* reported a series of highly efficient BODIPYs **79–83** using Ag-mediated direct C-H amination for screening of ER (endoplasmic reticulum)-targeting reagents. The C-H amination of BODIPY was done with amines using 4.0 equivalents of AgOAc as an oxidant under a nitrogen atmosphere. The best result was obtained in DMSO (dimethyl sulfoxide) solvent at 80 °C for 12 h (Scheme 18). The BODIPYs with electron-withdrawing trifluoromethyl and cyano group and electron-donating methyl group on the *meso*-aryl group undergo a direct C-H amination reaction in high yields. The BODIPYs **79–83** show absorption band at 571 nm, 545 nm, 564 nm, 561 nm, 487 nm and

emission band at 587 nm, 576 nm, 636 592 nm, and 557 nm respectively. Most of these π-conjugated BODIPYs emit green and yellow fluorescence. The cell imaging experiments show that the BODIPYs **80** and **82** containing benzoimidazole have excellent ER-labelling capacities.[101]

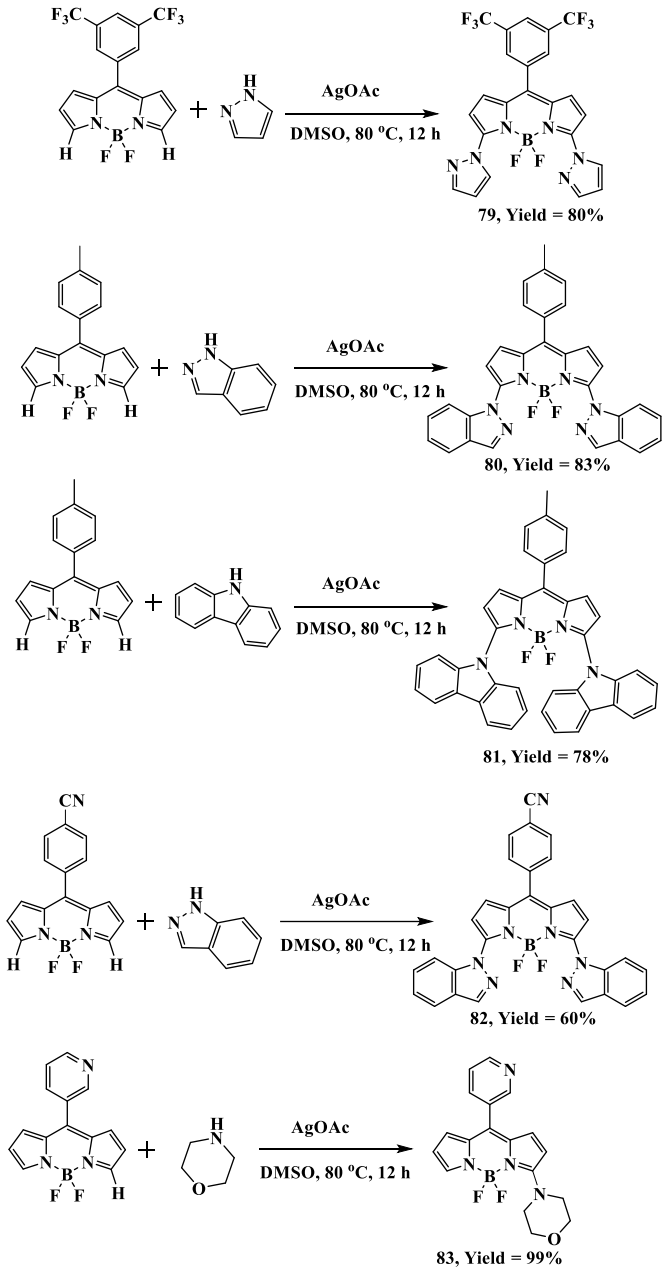

Scheme 18. Synthesis of α-mono and di-substituted BODIPYs **79–83** synthesized *via* C-H amination.

1.3.7. Grignard Reaction

Ziessel *et al.* synthesized a π-conjugated BODIPYs **84** and **85** based on substitution with alkynylaryl residue at the boron center of the BODIPY. The use of 2.0 equivalents of ethynyl-Grignard permitted the substitution of both fluorine atoms by two-ethynylpyrene groups using THF at reflux condition (Scheme 19).

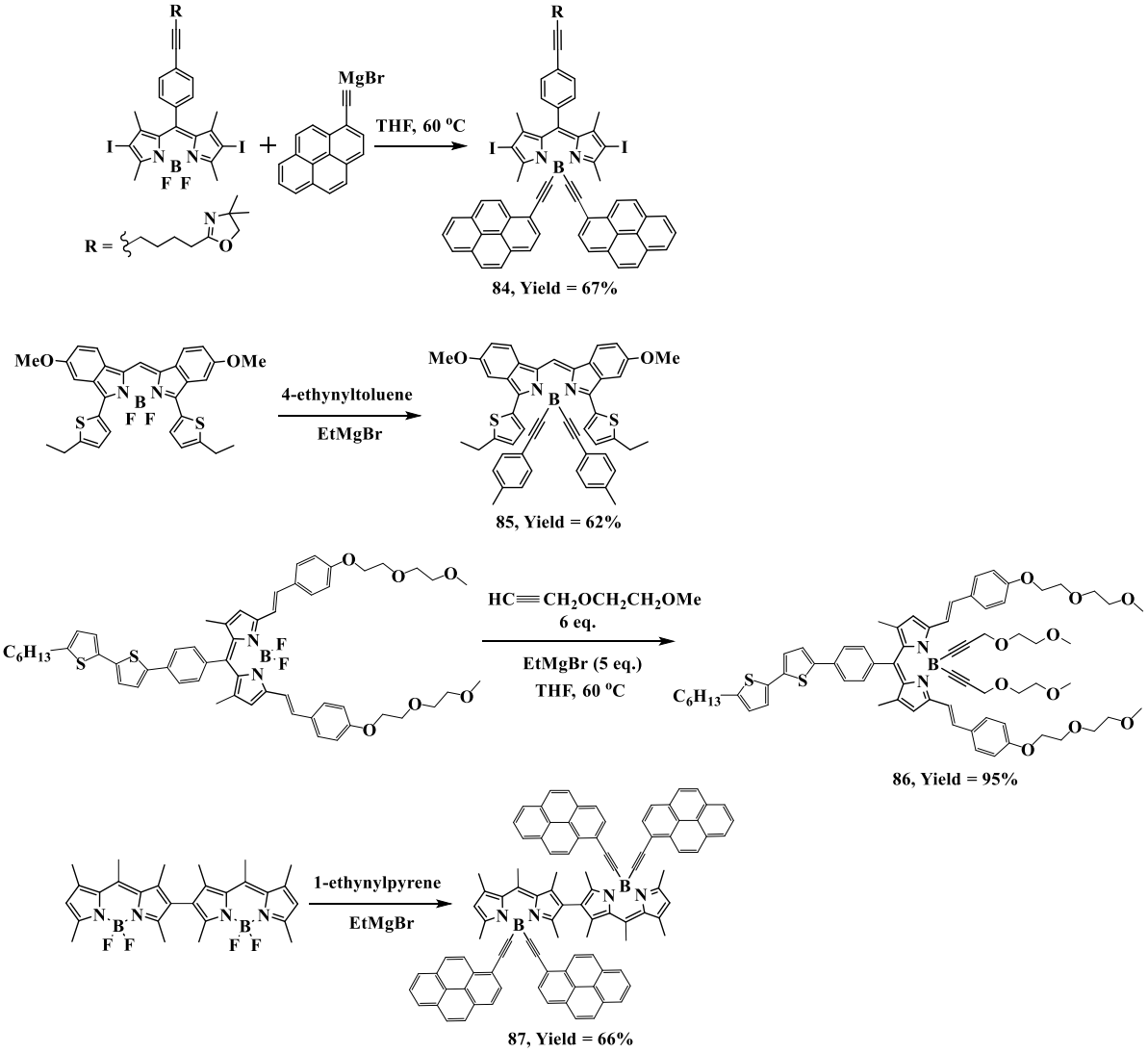

Scheme 19. Synthesis of BODIPYs **84–87** *via* Grignard reaction.

The BODIPY **84** shows absorption and emission band at 531 nm and 549 nm respectively in DCM. The BODIPY **85** shows absorption band at 709 nm and emission band 750 nm in DCM solvent with a stoke shift of 771 cm^{-1}. [102, 103] Rousseau *et al.* reported a 5-hexyl-2,2-

bithienyl substituted BODIPY **86** for bulk heterojunction solar cell application (Scheme 19). The BODIPY **86** was synthesized by using Grignard reagent to replace the fluorine atoms with ethynyl-residue resulting in 95% yield. The BODIPY **86** shows absorption band at 649 nm, emission at 661 nm and fluorescence quantum yield of 0.63.[104] Rihn *et al.* reported the BODIPY **87** by use of excess ethynyl-Grignard reagent in 66% yield (Scheme 19). The BODIPY **87** exhibit absorption band at 360 nm, 520 nm emission band at 562 nm and fluorescence quantum yield of 0.70. The substitution of the boron center by 1-ethynylpyrene does not affect the emission properties. The pyrene unit shows two absorption bands at 285 nm and 369 nm assigned to the π–π* transition.[105]

1.4. Similar Structures as BODIPY

1.4.1. BOIMPY (Bis(borondifluoride)-8-imidazodipyrromethene)

BOIMPY dyes are a new class of fluorophore with large π-conjugated skeletons and allow various functionalization to extend the absorption band toward the NIR region. In 2021, Werz *et al.* reported red-emitting BOIMPY (bis(borondifluoride)-8-imidazodipyrromethene) fluorophores **88** and **89** which exhibit high fluorescence quantum yield. The *meso*-position of the benzimidazole contains two BF_2 groups which results a rigid and planar conjugated system. The BOIMPY offers easy functionalization possibilities such as nucleophilic fluorine substitution, Knoevenagel condensation and cross-coupling reactions making them valuable fluorophores for optoelectronic applications. The BOIMPYs **88** and **89** were synthesized by the reaction of benzimidazole-2-carboxylic acid, oxalyl chloride, and pyrrole, followed by DBU and $BF_3.OEt_2$ in 39% and 31% yields respectively (Figure 1.5). The BOIMPYs **88** and **89** show absorption and emission band at 596 nm and 605 nm and the fluorescence quantum yields of 0.72 and 0.73 respectively.[106] Patalag *et al.* reported highly fluorescent and photostable fluorophores BOIMPYs **90–93** *via* Knoevenagel condensation reaction using substituted aldehydes (Figure

1.5). The BOIMPYs **90–93** shows an absorption band at 803 nm, 951 nm, 784 nm and 783 nm respectively. The computational studies show that the LUMO is partially delocalized outside the pyrrole unit whereas the HOMO is located over the BOIMPY core.[107] Werz and co-workers have reported a series of red- and NIR-absorbing push–pull BOIMPYs **94–96** (Figure 1.5) and studied their photophysical, electrochemical and computational properties. The BOIMPYs **94–96** show absorption band at 703 nm, 719 nm and 826 nm and the emission band at 736 nm, 811 nm and 835 nm with a fluorescence quantum yield of 0.13, 0.07 and 0.03 respectively. The absorption spectra reveal that the absorption band shifts towards a higher wavelength region upon increasing the donor strength which follows the order **96** > **95** > **94**. The introduction of electron-donating thienyl and furyl groups significantly altered the HOMO and LUMO energies, suggesting the BOIMPY motifs are useful candidates for molecular electronics or dye-sensitized solar cells (DSSCs) applications.[108]

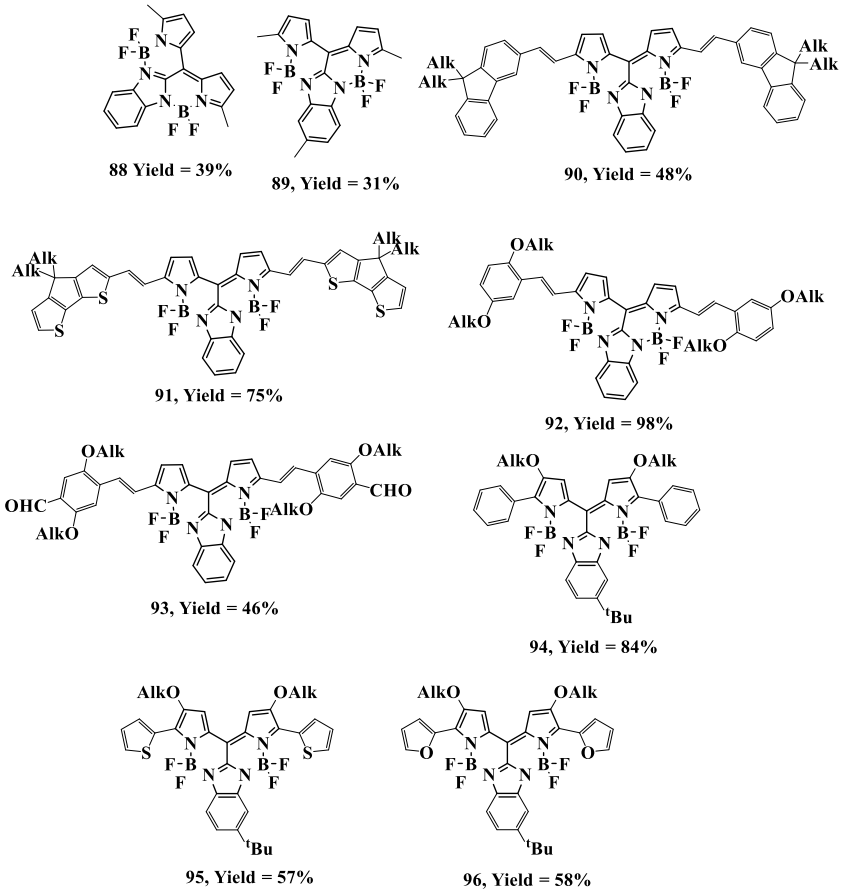

Figure 1.5. Molecular structures of the red-emitting BOIMPYs **88–96**.

1.4.2. BOPHY (Bis(difluoroboron)-1,2-bis ((1*H*-pyrrol-2-yl)methylene)hydrazine)

The tetracoordinate BF_2 complexes occupy a privileged position among all the fluorophores due to their easy synthetic procedure, facile structural modifications, good photochemical stability and photophysical properties. These properties have allowed the BOPHY dyes to be used in photoconductors *in vitro* and *in vivo* imaging agents, electrochromic devices and many more. Ziegler and co-workers have reported a new fluorophore (bis(difluoroboron)-1,2-bis ((1*H*-pyrrol-2-yl)methylene) hydrazine) (BOPHY). The BOPHY is a rigid planar fluorophore that possesses C_2h symmetry. The α, β- and *meso*-positions of the BOPHY can be functionalized to synthesize various donor–acceptor BOPHYs. The BOPHY was synthesized *via* a reaction of pyrrole-2-carboxaldehyde with hydrazine which results in pyrrole-imine dimeric chelate, followed by a complexation with $BF_3.OEt_2$.[109]

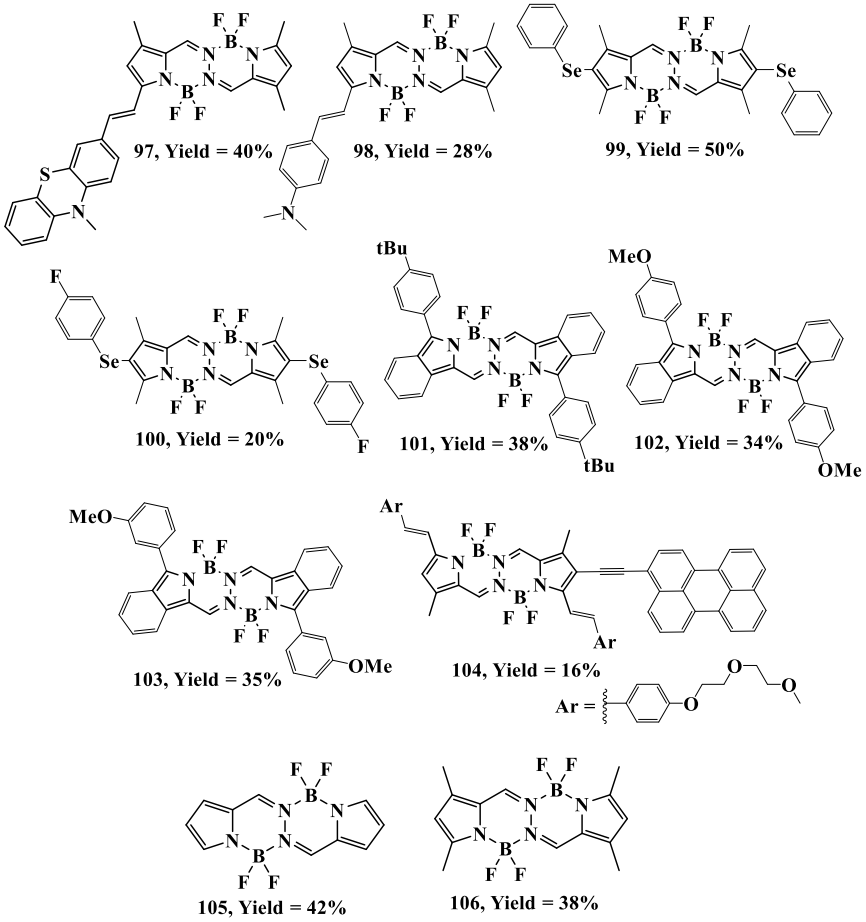

Figure 1.6. Structures of the BOPHY based derivatives **97–106**.

In 2018, Yu *et al.* reported a tetramethyl substituted fluorescent BOPHY **97** which was synthesized by knoevenagel condensation reaction with 10-methyl-10*H*-phenothiazine-3-carbaldehyde, and used for Cu^{2+} ion sensing (Figure 1.6). The Cu^{2+} ion was involved in the oxidation of the phenothiazine unit and inhibit the ICT process from donor to acceptor which results the strong fluorescence in solution.[110] Xiao and co-workers reported the design and synthesis of mono-substituted BOPHY **98** *via* knoevenagel condensation reaction with the (*p*-dimethylamino)styryl group (Figure 1.6). The BOPHY **98** was non-emissive due to the intramolecular charge transfer, and strong fluorescence was observed by the protonation of tertiary amine in BOPHY **98**. The BOPHY **98** was used as a pH probe in biological applications.[111] Hasegawa *et al.* reported the synthesis of BOPHYs **99** and **100** by introducing the arylselanyl group at the 2 and 7 positions (Figure 1.6). The direct C-Se bond formation facilitated the intersystem crossing (ISC) to the triplet state, which is useful for triplet sensitizer. The photophysical properties of the BOPHYs **99** and **100** were affected due to the presence of heavy atom selenium. The BOPHYs **99** and **100** exhibit an absorption maxima at 459 nm, 482 nm and emission maxima at 519 nm, 517 nm respectively.[112] Wang *et al.* reported fused BOPHYs **101–103** (Figure 1.6) and explored their photophysical and electrochemical properties. The BOPHYs **101–103** exhibit significant bathochromic shifts in absorption (up to 600 nm in solution), emission band (up to 648 nm in solution and 717 nm in the solid state) and high photochemical stability. The BOPHYs **101–103** exhibit absorption maxima at 423 nm, 571 nm and 563 nm whereas the emission band at 468 nm, 614 nm and 602 nm respectively in DCM solvent.[113] Ziessel and co-workers have reported the design and synthesis of BOPHY **104** (Figure 1.6) by Knoevenagel reaction, which shows an absorption maxima above 625 nm. The perylene unit was linked to BOPHY by Pd(0) catalyzed cross-coupling reaction. The BOPHY **104** is fluorescent and the intramolecular cascade energy transfer occurs from perylene to BOPHY, resulting in high stoke shifts (>5100 cm^{-1}).[114] Nemykin and co-workers reported fluorescent BOPHYs **105** and **106** by coupling of

pyrrole-2-carboxaldehyde with hydrazine and complexation reaction with boron complex in 42% and 38% yields respectively (Figure 1.6). The BOPHYs **105** and **106** exhibit absorption band at 424 nm, 442 nm and 444 nm, 467 nm with high fluorescence quantum yields of 0.95 and 0.92 respectively.[115]

1.4.3. Formazanate

Formazanates are a class of highly colored molecules containing electron-rich nitrogen atoms and have the formula Ar-NH-N=CR-N=N-Ar. Their bright color has led to their extensive use as dyes, particularly in cell biology, where they are frequently used to quantify cell viability. The formazanate ligands are highly conjugated with excellent optoelectronic and redox properties. These properties can be tuned *via* structural modification on formazanate unit. In 2021, Gilroy *et al.* reported the π-conjugated A–D–A based formazanate **107** (Figure 1.7) and explored its optoelectronic properties. The formazanate **107** exhibits excellent photophysical and electrochemical properties which can be tuned by using an appropriate group at *para*-position of N-aryl rings of the formazanate. The formazanate **107** shows an absorption band at 596 nm and molar extinction coefficient of 52400 M^{-1} cm^{-1}. The oxidation and reduction potentials of formazanate **107** was observed at 0.82 V, 1.07 V, and –1.96 V, –0.90 V respectively. The formazanate derivatives show their applications in fluorescence cell-imaging, electrochemiluminescent materials and organic solar cells (OSC).[116] Koenig *et al.* reported a non-fullerene acceptor formazanate **108** (Figure 1.7) end-capped with N-annulated perylene diimides. The electronic coupling between BF_2 formazanate and perylene diimides tuned the LUMO energy levels which resulted a bathochromic shift in absorption spectra. The BF_2 formazanate **108** in solution shows a broad absorption between 450–750 nm with maximum absorption at 543 nm.[117] Kumar *et al.* reported the thiophene-capped BF_2 formazanates **109** and **110** by using a Pd-catalyzed cross-coupling reaction (Figure 1.7). The formazanates **109** and **110** possess panchromatic absorption with low HOMO–LUMO gap and useful for light-harvesting organic materials.

The absorption band of formazanates **109** and **110** were obtained at 570 nm and 606 nm respectively. The ethylenedioxythiophenyl substituted formazanate **110** exhibits a red shift compared to thienophenyl substituted formazanate **109** because of donating nature of thiophene and extension of the π-conjugation.[118]

Barbon *et al.* have reported the boron difluoride (BF_2) formazanate dimers **111** and **112** (Figure 1.7) and investigated their photophysical and electrochemical properties. The dimer **112** exhibits bathochromic-shifted absorption and emission band as compared to the monomer due to an increase in conjugation; both the dimers **111** and **112** are non-emissive exhibiting high stokes shifts (>110 nm). The dimers **111** and **112** show absorption bands at 509 nm and 523 nm and the emission bands at 627 nm and 654 nm respectively in DCM solvent.[119] Gilroy and co-workers reported the flexidentate pyridine and toluene-substituted formazanates **113** and **114** respectively (Figure 1.7).

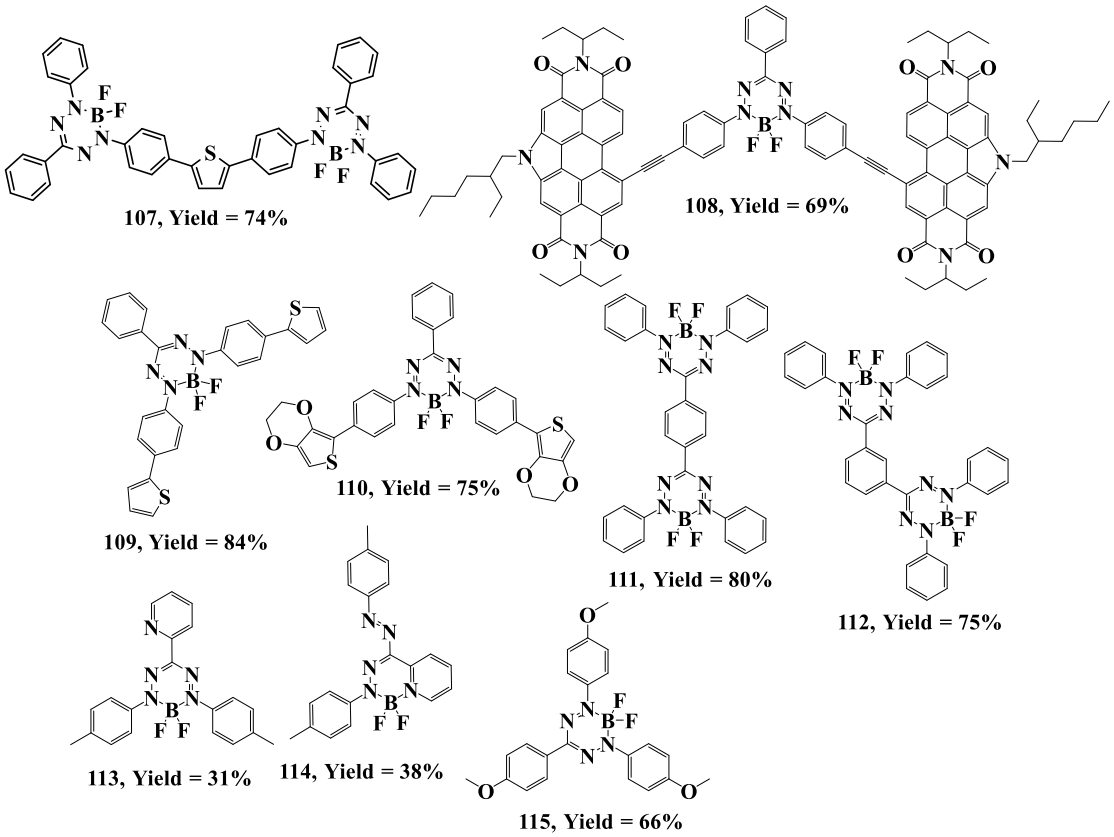

Figure 1.7. Structures of Formazanate derivatives **107–115**.

The coordination chemistry of both adducts was studied by reaction with nickel(II) bromide [$NiBr_2(CH_3CN)_2$], triflate [$Ni(OTf)_2$] salt. The photophysical properties of the formazanate adduct indicate a red-shifted absorption band with low reduction potentials when coordinated with nickel(II) ions. The electronic and physical properties of the formazanates **113** and **114** can be tuned through protonation.[120] Hesari *et al.* reported a boron difluoride formazanate **115** (Figure 1.7) containing a *p*-methoxyphenyl unit and explored their redox and electrogenerated chemiluminescence (ECL) properties. The formazanate **115** exhibits two quasi-reversible oxidation at 1.00 V and 1.30 V and two reversible reduction at –0.67 V and –1.80 V.[121]

1.5. Applications of BODIPY chromophores

The push–pull or donor–acceptor BODIPYs have a wide range of applications in optoelectronic and biological studies. Some of the important applications are summarized below.

1.5.1. Perovskite Solar Cell (PSCs)

In recent years the perovskite solar cells emerged as an important photovoltaic technology due to their excellent power conversion efficiency (PCE) in device architecture. The BODIPY based chromophores are well known for their strong chemical and photo-stability as well as easy synthetic modifications. In 2021, Cooke *et al.* reported the design and synthesis of the phenothiazine functionalized Y-shaped BODIPY derivative as HTM in perovskite solar cells.

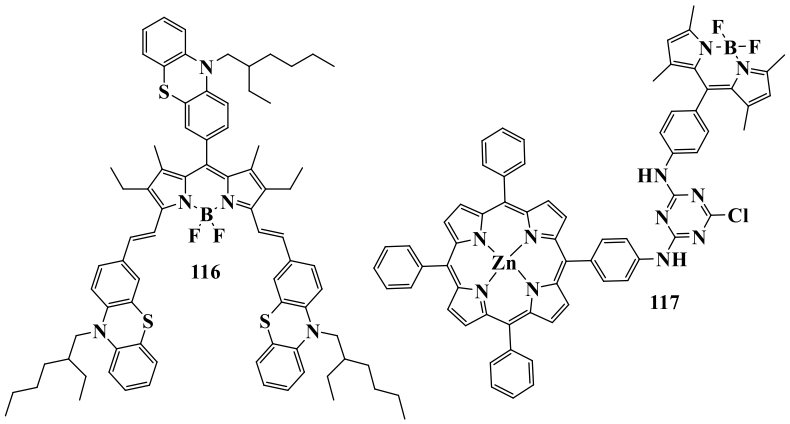

Figure 1.8. BODIPY based chromophores **116** and **117** for perovskite solar cells.

The PTZ substituted BODIPY **116** exhibited PCE of 14.6% (Figure 1.8).[122] In 2019, Vasilopoulou *et al.* reported a zinc porphyrin-triazine-bodipy (D-π-bridge-A) BODIPY **117** as a electron transfer mediator in organic and perovskite solar cell application (Figure 1.8).[123]

1.5.2. Organic Solar cells

Recently, Xu *et al.* have reported the star shaped π-conjugated truxene based BODIPY derivatives **118** and **119** for solar cell application. These BODIPYs shows strong absorption in visible to NIR range (Figure 1.9). The BODIPYs **118** and **119** exhibit a high electron mobility, superior short-circuit current density (J_{sc}) and open-circuit voltage. The BODIPYs **118** and **119** showed the power conversion efficiency (PCE) of 13.41 and 11.75%, respectively.[124]

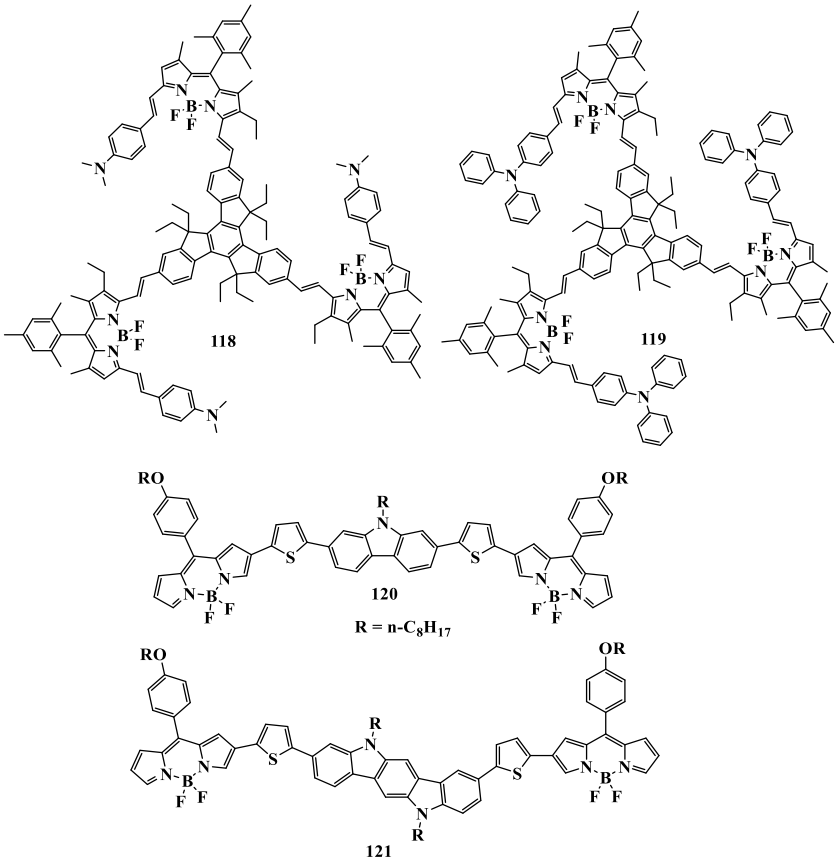

Figure 1.9. BODIPY based chromophores **118**–**121**.

Li *et al.* reported the design and synthesis of A-π-D-π-A-type BODIPYs **120** and **121** *via* Suzuki cross-coupling reaction in which carbazole and indolo-[3,2-*b*]carbazole as the electron-donating (D) groups attached with the acceptor BODIPY (A) and thiophane act as a π-bridge (Figure 1.9). The synthesized BODIPYs **120** and **121** exhibit low HOMO–LUMO gap and strong absorption in the range of 300–900 nm in film. The BODIPYs **120** and **121** exhibited PCE of 5.85 and 3.85 %, respectively.[125]

1.5.3. Sensing

Recently, Hibi *et al.* have reported the synthesis of hybrid BODIPY-based fluorescent sensor for fructose detection. The fructose is widely used in the food industry and it may be involved in diseases by generating harmful glycation end-products. The BODIPY-based fluorescent probe **122** was synthesized by combining phenylboronic acid group and a hydrophobic group in BODIPY. The BODIPY-probe

122 showed fluorescence response in different concentration with D-fructose (Figure 1.10).[126] Song *et al.* have synthesized BODIPY-based fluorescent sensor for detection of phosgene in both solution and gas phase. A highly selective BODIPY-based fluorescent sensor **123** exhibit rapid response of various acyl chlorides at low concentration in solution (Figure 1.10).[127]

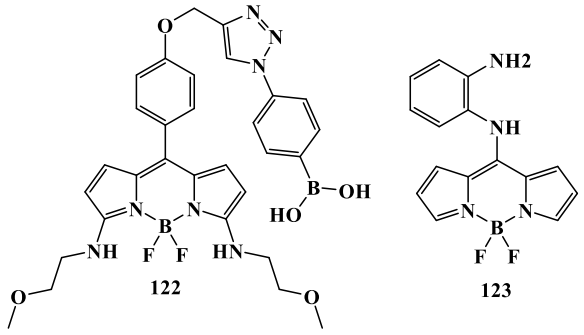

Figure 1.10. BODIPY based chromophores **122** and **123** for sensing application.

1.5.4. Bioimaging

In 2019, Cho *et al.* reported a triphenylamine substituted BODIPY derivatives and investigated the ICT characteristics in the S_1 state of BODIPY and TPA unit. The BODIPY containing TPA at the β-position exhibit strong red-color fluorescence at the 640 nm in moderate polar solvent.

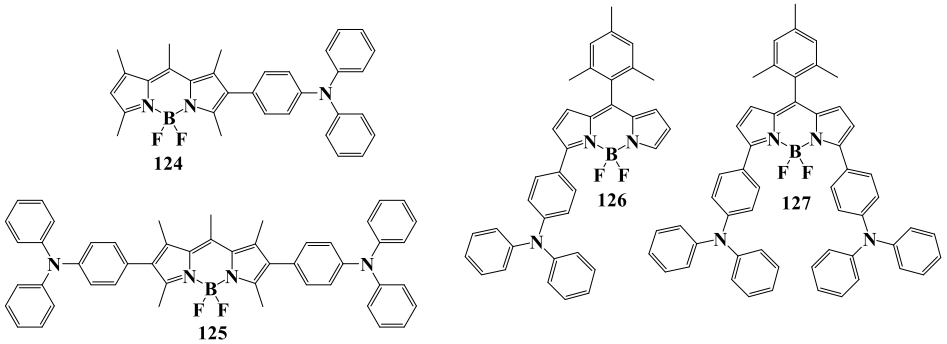

Figure 1.11. BODIPY based chromophores **124**–**127** for bioimaging application.

The red-color emission and AIIE property of the β-substituted BODIPYs with TPA are important characteristics for a biological application. The TPA substituted BODIPYs **124** and **125** were applied

to L-929 fibroblast cell for cellular imaging (Figure 1.11).[128] Recently, Guo *et al.* synthesized α-mono and di TPA substituted NIR fluorescent materials BODIPYs **126** and **127** with aggregation-induced emission (AIE) (Figure 1.11).

The nanoparticles of BODIPYs **126** and **127** were obtained by self-assembly and exhibit NIR emission with good photostability. The nanoparticles of the BODIPYs **126** and **127** shows remarkable bioimaging performance specially localized in LDs or lysosomes depending on the number of triphenylamine donor attached to the BODIPY.[129]

1.5.5. Photodynamic therapy

In 2021, Kim *et al.* have reported a phenylthiourea-conjugated BODIPY photosensitizer **128** for tyrosinase-positive melanoma targeted photodynamic therapy. Melanoma is the threatening form of metastatic skin cancer from melanocytes and causes death in majority. A non-invasive and clinically accepted method is photodynamic therapy (PDT).

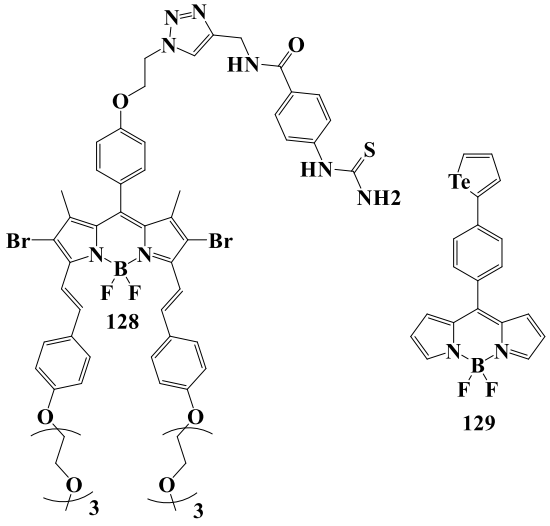

Figure 1.12. BODIPY based chromophores **128** and **129** for photodynamic therapy.

The BODIPY **128** shows excellent effects of increased oxidative stress by cellular uptake of the tyrosinase positive melanoma cell line (B16F10) (Figure 1.12).[130] Thompson *et al.* reported synthesis and

characterization of the BODIPY **129** which exhibits a five-membered heterocyclic tellurophene [Te] unit at *meso*-position (Figure 1.12). The tellurophene containing BODIPY **129** was synthesized by Suzuki-Miyaura coupling with tellurophene-2-B Pin. The presence of tellurophene moiety detected through mass cytometry, thus the tellurophene-containing BODIPY **129** act as a novel photodynamic-therapy-mass-cytometry theranostic agent.[131]

1.6. Current Work

The π-conjugated donor–acceptor molecular systems with a low HOMO–LUMO gap are an interesting class of materials due to wide application in the field of optoelectronics. A large variety of electron donors (phenothiazine, triphenylamine, carbazole, dimethylaniline) and strong acceptors (TCNE and TCNQ) have been incorporated to the BODIPY core to enhance and improve the optical characteristics and HOMO–LUMO gap. The photophysical and electrochemical properties of BODIPY based donor–acceptor chromophores were investigated.

The main objectives of the current work are as follows:

- ✓ To design and synthesize donor–acceptor based BODIPY derivatives for optoelectronic applications.
- ✓ To synthesize donor-acceptor functionalized chromophores *via* using the donor/acceptor moieties at the *β*-pyrrolic and *meso* position of the BODIPY core.
- ✓ To investigate the effect of different donor and acceptor units on the photophysical, electrochemical, thermal and HOMO–LUMO gap of the donor-acceptor BODIPYs.
- ✓ To tune the HOMO–LUMO gap, *via* varying the strength of donor/acceptor units or the π-linker at the *β*-pyrrolic and *meso* position of the BODIPY core.
- ✓ To understand the geometry, distribution of electron density and photonic properties of the donor–acceptor BODIPYs through density functional theory (DFT) and time-dependent functional

theory (TD-DFT) calculations as well as correlated with the experimental data.

1.7. Organization of thesis

Chapter 1 of the thesis describes the general introduction of the donor–acceptor system, followed by introduction of BODIPY dye, various synthetic methods and functionalization for designing various BODIPY chromophores as well as their application in different fields.

Chapter 2 of the thesis introduces about the instrumentation and general methods used in the present study.

Chapter 3 of the thesis describes the design and synthesis of the *β*-pyrrole functionalized push–pull or donor–acceptor BODIPYs. The photophysical, electrochemical and theoretical properties were investigated to analyze the effect of strong acceptor TCBD and cyclohexa-2,5-diene-1,4-diylidene-expanded TCBD units at the *β*-position of the BODIPY core.

Chapter 4 of the thesis describes the design and synthesis of the TCBD and cyclohexa-2,5-diene-1,4-diylidene-expanded TCBD substituted donor–acceptor BODIPYs and investigated their photophysical, electrochemical, thermal and computational studies.

Chapter 5 of the thesis describes the synthesis of meso-donor *N*,*N*-dimethylaniline functionalized BODIPYs. The photophysical, electrochemical, thermal, and theoretical studies were studied to understand the effect of acceptor TCBD and cyclohexa-2,5-diene-1,4-diylidene-expanded TCBD groups at the *meso*-position of the BODIPY.

Chapter 6 of the thesis describes the design and synthesis of phenothiazine and phenothiazine-5,5-dioxide functionalized BODIPY dyes and explored their photophysical, electrochemical and theoretical properties.

Chapter 7 of the thesis describes the synthesis of different donor (anisole, *N*,*N*-dimethyl anisole, *N*,*N*-dimethylaniline, *N*-phenyl

carbazole, *N*-phenyl phenothiazine and *N*-phenyl phenothiazine 5,5-dioxide) functionalized *β*-pyrrole BODIPYs and explored their photophysical, electrochemical, thermal and computational studies.

Chapter 8 of the thesis summarizes the salient features of the work and their future prospectus to develop the donor–acceptor (D–A) materials for optoelectronic applications.

References

1. Bijesh, S., & Misra, R. (2018). Triphenylamine Functionalized Unsymmetrical Quinoxalines. *Asian Journal of Organic Chemistry*, *7*(9), 1882–1892. https://doi.org/10.1002/ajoc.201800384

2. Camero, D. M., Grinalds, N. J., Kornman, C. T., Barba, S., Li, L., Weldeab, A. O., … Xue, J. (2022). Thin-Film Morphology and Optical Properties of Photoisomerizable Donor–Acceptor Oligothiophenes. *ACS Applied Materials & Interfaces*. https://doi.org/10.1021/acsami.2c05946

3. Cappello, D., Buguis, F. L., & Gilroy, J. B. (2022). Tuning the Properties of Donor–Acceptor and Acceptor–Donor–Acceptor Boron Difluoride Hydrazones via Extended π-Conjugation. *ACS Omega*. https://doi.org/10.1021/acsomega.2c04401

4. Funabiki, K., Yamada, K., Arisawa, Y., Watanabe, A., Agou, T., Kubota, Y., … Kutsumizu, S. (2022). Design, Regioselective Synthesis, and Photophysical Properties of Perfluoronaphthalene-Based Donor–Acceptor–Donor Fluorescent Dyes. *The Journal of Organic Chemistry*. https://doi.org/10.1021/acs.joc.2c01446

5. Garg, S., & Goel, N. (2022). Optoelectronic Applications of Conjugated Organic Polymers: Influence of Donor/Acceptor Groups through Density Functional Studies. *The Journal of Physical Chemistry C*, *126*(22), 9313–9323. https://doi.org/10.1021/acs.jpcc.2c02938

6. Geramita, K., Tao, Y., Segalman, R. A., & Tilley, T. D. (2010). Synthesis and Characterization of Fluorinated Heterofluorene-

Containing Donor−Acceptor Systems. *The Journal of Organic Chemistry*, *75*(6), 1871–1887. https://doi.org/10.1021/jo902488w

7. Guo, S., Liu, W., Wu, Y., Sun, J., Li, J., Jiang, H., … Yao, J. (2022). Distinctive Excited State Symmetry Breaking Dynamics in Typical Donor–Acceptor–Donor Fluorophore: Strong Photoluminescence and Ultrafast Charge Separation from a Partial Charge Transfer State. *The Journal of Physical Chemistry Letters*, *13*(32), 7547–7552. https://doi.org/10.1021/acs.jpclett.2c02342

8. Ishi-i, T., Ikeda, K., Ogawa, M., & Kusakaki, Y. (2015). Light-emitting properties of donor–acceptor and donor–acceptor–donor dyes in solution, solid, and aggregated states: structure–property relationship of emission behavior. *RSC Advances*, *5*(108), 89171–89187. https://doi.org/10.1039/C5RA18231J

9. Kowalski, K., Szczupak, Ł., Skiba, J., Abdel-Rahman, O. S., Winter, R. F., Czerwieniec, R., & Therrien, B. (2014). Synthesis, Structure, and Spectroelectrochemistry of Ferrocenyl–Meldrum's Acid Donor–Acceptor Systems. *Organometallics*, *33*(18), 4697–4705. https://doi.org/10.1021/om401191q

10. Li, G., Chen, Y., Qiao, Y., Lu, Y., & Zhou, G. (2018). Charge Transfer Switching in Donor–Acceptor Systems Based on BN-Fused Naphthalimides. *The Journal of Organic Chemistry*, *83*(10), 5577–5587. https://doi.org/10.1021/acs.joc.8b00597

11. Patil, Y., Jadhav, T., Dhokale, B., & Misra, R. (2016). Tuning of the HOMO–LUMO Gap of Symmetrical and Unsymmetrical Ferrocenyl-Substituted Diketopyrrolopyrroles. *European Journal of Organic Chemistry*, *2016*(4), 733–738. https://doi.org/10.1002/ejoc.201501123

12. Yadav, I. S., Alsaleh, A. Z., Martin, B., Misra, R., & D'Souza, F. (2022). Star-Shaped Triphenylamine–Tetracyanobutadiene–Phenothiazine Push–Pull Systems: Role of Terminal Phenothiazine in

Improving Charge Transfer. *The Journal of Physical Chemistry C*, *126*(31), 13300–13310. https://doi.org/10.1021/acs.jpcc.2c03495

13. Rout, Y., & Misra, R. (2021). Design and synthesis of 1,8-naphthalimide functionalized benzothiadiazoles. *New Journal of Chemistry*, *45*(22), 9838–9845. https://doi.org/10.1039/D1NJ00919B

14. Poddar, M., Sivakumar, G., & Misra, R. (2019). Donor–acceptor substituted 1,8-naphthalimides: design, synthesis, and structure–property relationship. *Journal of Materials Chemistry C*, *7*(47), 14798–14815. https://doi.org/10.1039/C9TC02634G

15. Poddar, M., & Misra, R. (2017). NIR-Absorbing Donor–Acceptor Based 1,1,4,4-Tetracyanobuta-1,3-Diene (TCBD)- and Cyclohexa-2,5-Diene-1,4-Ylidene-Expanded TCBD-Substituted Ferrocenyl Phenothiazines. *Chemistry – An Asian Journal*, *12*(22), 2908–2915. https://doi.org/10.1002/asia.201700879

16. Dhokale, B., Jadhav, T., Mobin, S. M., & Misra, R. (2015). Synergistic effect of donors on tetracyanobutadine (TCBD) substituted ferrocenyl pyrenes. *RSC Advances*, *5*(71), 57692–57699. https://doi.org/10.1039/C5RA11433K

17. Rout, Y., Gautam, P., & Misra, R. (2017). Unsymmetrical and Symmetrical Push–Pull Phenothiazines. *The Journal of Organic Chemistry*, *82*(13), 6840–6845. https://doi.org/10.1021/acs.joc.7b00991

18. Zhang, D., & Heeney, M. (2020). Organic Donor–Acceptor Systems. *Asian Journal of Organic Chemistry*, *9*(9), 1251–1251. https://doi.org/10.1002/ajoc.202000465

19. Gautam, P., Misra, R., & Sharma, G. D. (2016). Dicyanoquinodimethane-substituted benzothiadiazole for efficient small-molecule solar cells. *Physical Chemistry Chemical Physics*, *18*(10), 7235–7241. https://doi.org/10.1039/C6CP00243A

20. Piradi, V., Gao, Y., Yan, F., Imran, M., Zhao, J., Zhu, X., & So, S. K. (2022). Thiophene–Perylenediimide Bridged Dimeric Porphyrin

Donors Based on the Donor–Acceptor–Donor Structure for Organic Photovoltaics. *ACS Applied Energy Materials*, *5*(6), 7287–7296. https://doi.org/10.1021/acsaem.2c00819

21. Patil, Y., Misra, R., Sharma, A., & Sharma, G. D. (2016). D–A–D–π–D–A–D type diketopyrrolopyrrole based small molecule electron donors for bulk heterojunction organic solar cells. *Physical Chemistry Chemical Physics*, *18*(25), 16950–16957. https://doi.org/10.1039/C6CP02700H

22. Maragani, R., Sharma, R., & Misra, R. (2017). Donor-Acceptor Triphenylvinyl and Tetraphenyl Conjugates: Synthesis, Aggregation and Computational Studies. *ChemistrySelect*, *2*(31), 10033–10037. https://doi.org/10.1002/slct.201701373

23. Rout, Y., Jang, Y., Gobeze, H. B., Misra, R., & D'Souza, F. (2019). Conversion of Large-Bandgap Triphenylamine–Benzothiadiazole to Low-Bandgap, Wide-Band Capturing Donor–Acceptor Systems by Tetracyanobutadiene and/or Dicyanoquinodimethane Insertion for Ultrafast Charge Separation. *The Journal of Physical Chemistry C*, *123*(38), 23382–23389. https://doi.org/10.1021/acs.jpcc.9b06632

24. Li, S., He, M., Jin, X., Geng, W., Li, C., Li, X., … Hua, J. (2022). Extending the Stokes Shifts of Donor–Acceptor Fluorophores by Regulating the Donor Configuration for In Vivo Three-Photon Fluorescence Imaging. *Chemistry of Materials*, *34*(13), 5999–6008. https://doi.org/10.1021/acs.chemmater.2c01025

25. Zhao, Y., Zhang, Z., Lu, Z., Wang, H., & Tang, Y. (2019). Enhanced Energy Transfer in a Donor–Acceptor Photosensitizer Triggers Efficient Photodynamic Therapy. *ACS Applied Materials & Interfaces*, *11*(42), 38467–38474. https://doi.org/10.1021/acsami.9b12375

26. Zhang, D., & Heeney, M. (2020). Organic Donor–Acceptor Systems. *Asian Journal of Organic Chemistry*, *9*(9), 1251–1251. https://doi.org/10.1002/ajoc.202000465

27. Michinobu, T., Satoh, N., Cai, J., Li, Y., & Han, L. (2014). Novel design of organic donor–acceptor dyes without carboxylic acid anchoring groups for dye-sensitized solar cells. *Journal of Materials Chemistry C*, *2*(17), 3367–3372. https://doi.org/10.1039/C3TC32165G

28. Yadav, I. S., & Misra, R. (2022). Phenothiazine and phenothiazine-5,5-dioxide-based push–pull derivatives: synthesis, photophysical, electrochemical and computational studies. *New Journal of Chemistry*, *46*(33), 15999–16006. https://doi.org/10.1039/D2NJ03089F

29. Patil, Y., & Misra, R. (2019). Rational molecular design towards NIR absorption: efficient diketopyrrolopyrrole derivatives for organic solar cells and photothermal therapy. *Journal of Materials Chemistry C*, *7*(42), 13020–13031. https://doi.org/10.1039/C9TC03640G

30. Misra, R., Jadhav, T., Nevonen, D., Monzo, E. M., Mobin, S. M., & Nemykin, V. N. (2017). Synthesis, Structures, and Redox Properties of Tetracyano-Bridged Diferrocene Donor–Acceptor–Donor Systems. *Organometallics*, *36*(22), 4490–4498. https://doi.org/10.1021/acs.organomet.7b00728

31. Gautam, P., Misra, R., Siddiqui, S. A., & Sharma, G. D. (2015). Unsymmetrical Donor–Acceptor–Acceptor−π–Donor Type Benzothiadiazole-Based Small Molecule for a Solution Processed Bulk Heterojunction Organic Solar Cell. *ACS Applied Materials & Interfaces*, *7*(19), 10283–10292. https://doi.org/10.1021/acsami.5b02250

32. Tram, K., Yan, H., Jenkins, H. A., Vassiliev, S., & Bruce, D. (2009). The synthesis and crystal structure of unsubstituted 4,4-difluoro-4-bora-3a,4a-diaza-s-indacene (BODIPY). *Dyes and Pigments*, *82*(3), 392–395. https://doi.org/10.1016/j.dyepig.2009.03.001

33. Shinde, J., Thomas, M. B., Poddar, M., Misra, R., & D'Souza, F. (2021). Does Location of BF2-Chelated Dipyrromethene (BODIPY) Ring Functionalization Affect Spectral and Electron Transfer Properties? Studies on α-, β-, and Meso-Functionalized BODIPY-Derived Donor–Acceptor Dyads and Triads. *The Journal of Physical Chemistry C*, *125*(43), 23911–23921. https://doi.org/10.1021/acs.jpcc.1c06704

34. Maragani, R., Thomas, M. B., Misra, R., & D'Souza, F. (2018). C3-Symmetric Positional Isomers of BODIPY Substituted Triazines: Synthesis and Excited State Properties. *The Journal of Physical Chemistry A*, *122*(21), 4829–4837. https://doi.org/10.1021/acs.jpca.8b02967

35. Lakshmi, V., Rao, M. R., & Ravikanth, M. (2015). Halogenated boron-dipyrromethenes: synthesis, properties and applications. *Organic & Biomolecular Chemistry*, *13*(9), 2501–2517. https://doi.org/10.1039/C4OB02293A

36. Boens, N., Leen, V., & Dehaen, W. (2012). Fluorescent indicators based on BODIPY. *Chemical Society Reviews*, *41*(3), 1130–1172. https://doi.org/10.1039/C1CS15132K

37. Fron, E., Coutiño-Gonzalez, E., Pandey, L., Sliwa, M., Auweraer, M. V. der, Schryver, F. C. D., … Vosch, T. (2009). Synthesis and photophysical characterization of chalcogen substituted BODIPY dyes. *New Journal of Chemistry*, *33*(7), 1490–1496. https://doi.org/10.1039/B900786E

38. Miao, J., Wang, Y., Liu, J., & Wang, L. (2022). Organoboron molecules and polymers for organic solar cell applications. *Chemical Society Reviews*, *51*(1), 153–187. https://doi.org/10.1039/D1CS00974E

39. Gapare, R. L., & Thompson, A. (2022). Substitution at boron in BODIPYs. *Chemical Communications*, *58*(53), 7351–7359. https://doi.org/10.1039/D2CC02362H

40. Carlotti, B., Poddar, M., Elisei, F., Spalletti, A., & Misra, R. (2019). Energy-Transfer and Charge-Transfer Dynamics in Highly Fluorescent Naphthalimide–BODIPY Dyads: Effect of BODIPY Orientation. *The Journal of Physical Chemistry C*, *123*(40), 24362–24374. https://doi.org/10.1021/acs.jpcc.9b05851

41. Misra, R., Dhokale, B., Jadhav, T., & Mobin, S. M. (2014). Heteroatom-Connected Ferrocenyl BODIPYs: Synthesis, Structure, and Properties. *Organometallics*, *33*(7), 1867–1877. https://doi.org/10.1021/om5002292

42. Shen, B., & Qian, Y. (2016). A novel triphenylamine-BODIPY dendron: click synthesis, near-infrared emission and a multi-channel chemodosimeter for Hg2+ and Fe3+. *Journal of Materials Chemistry B*, *4*(47), 7549–7559. https://doi.org/10.1039/C6TB02469F

43. Zhou, Z., & Maki, T. (2021). Ratiometric Fluorescence Acid Probes Based on a Tetrad Structure Including a Single BODIPY Chromophore. *The Journal of Organic Chemistry*, *86*(24), 17560–17566. https://doi.org/10.1021/acs.joc.1c01328

44. Dhokale, B., Jadhav, T., Mobin, S. M., & Misra, R. (2014). Meso enamine substituted BODIPYs. *Chemical Communications*, *50*(65), 9119–9121. https://doi.org/10.1039/C4CC03857F

45. Obondi, C. O., Lim, G. N., Karr, P. A., Nesterov, V. N., & D'Souza, F. (2016). Photoinduced charge separation in wide-band capturing, multi-modular bis(donor styryl)BODIPY–fullerene systems. *Physical Chemistry Chemical Physics*, *18*(27), 18187–18200. https://doi.org/10.1039/C6CP03479A

46. Awuah, S. G., & You, Y. (2012). Boron dipyrromethene (BODIPY)-based photosensitizers for photodynamic therapy. *RSC Advances*, *2*(30), 11169–11183. https://doi.org/10.1039/C2RA21404K

47. Qin, Y., Liu, X., Jia, P.-P., Xu, L., & Yang, H.-B. (2020). BODIPY-based macrocycles. *Chemical Society Reviews*, *49*(16), 5678–5703. https://doi.org/10.1039/C9CS00797K

48. Aksoy, B. T., Dedeoglu, B., Zorlu, Y., Ayhan, M. M., & Çoşut, B. (2022). Exploring halogen···halogen interactions in supramolecular self-assemblies of BODIPY networks. *CrystEngComm*, *24*(31), 5630–5641. https://doi.org/10.1039/D2CE00776B

49. Li, P., Wu, F., Fang, Y., Dahiya, H., Keshtov, M. L., Xu, H., … Sharma, G. D. (2022). Truxene π-Expanded BODIPY Star-Shaped Molecules as Acceptors for Non-Fullerene Solar Cells with over 13% Efficiency. *ACS Applied Energy Materials*, *5*(2), 2279–2289. https://doi.org/10.1021/acsaem.1c03781

50. Gangada, S., Ramnagar, R. A., Sangolkar, A. A., Pawar, R., Nanubolu, J. B., Roy, P., … Chitta, R. (2020). Excitation-Wavelength-Dependent Light-Induced Electron Transfer and Twisted Intramolecular Charge Transfer in N,N-Bis(4′-tert-butylbiphenyl-4-yl)aniline Functionalized Borondipyrromethenes. *The Journal of Physical Chemistry A*, *124*(47), 9738–9750. https://doi.org/10.1021/acs.jpca.0c04789

51. Misra, R., Dhokale, B., Jadhav, T., & Mobin, S. M. (2014). The quenching of fluorescence as an indicator of donor-strength in meso arylethynyl BODIPYs. *Dalton Transactions*, *43*(12), 4854–4861. https://doi.org/10.1039/C3DT53056F

52. Umasekhar, B., Ganapathi, E., Chatterjee, T., & Ravikanth, M. (2015). Synthesis, structure, and spectral, electrochemical and fluoride sensing properties of meso-pyrrolyl boron dipyrromethene. *Dalton Transactions*, *44*(37), 16516–16527. https://doi.org/10.1039/C5DT02634B

53. Chen, Y., Zhao, J., Guo, H., & Xie, L. (2012). Geometry Relaxation-Induced Large Stokes Shift in Red-Emitting Borondipyrromethenes (BODIPY) and Applications in Fluorescent Thiol Probes. *The Journal of Organic Chemistry*, *77*(5), 2192–2206. https://doi.org/10.1021/jo202215x

54. Rao, M. R., Kumar, K. V. P., & Ravikanth, M. (2010). Synthesis of boron-dipyrromethene–ferrocene conjugates. *Journal of Organometallic Chemistry*, *695*(6), 863–869. https://doi.org/10.1016/j.jorganchem.2010.01.009

55. Gautam, P., Dhokale, B., Mobin, S. M., & Misra, R. (2012). Ferrocenyl BODIPYs: synthesis, structure and properties. *RSC Advances*, *2*(32), 12105–12107. https://doi.org/10.1039/C2RA21964F

56. Collado, D., Casado, J., González, S. R., Navarrete, J. T. L., Suau, R., Perez-Inestrosa, E., … Raposo, M. M. M. (2011). Enhanced Functionality for Donor–Acceptor Oligothiophenes by means of Inclusion of BODIPY: Synthesis, Electrochemistry, Photophysics, and Model Chemistry. *Chemistry – A European Journal*, *17*(2), 498–507. https://doi.org/10.1002/chem.201001942

57. El-Khouly, M. E., Fukuzumi, S., & D'Souza, F. (2014). Photosynthetic Antenna–Reaction Center Mimicry by Using Boron Dipyrromethene Sensitizers. *ChemPhysChem*, *15*(1), 30–47. https://doi.org/10.1002/cphc.201300715

58. Dhokale, B., Jadhav, T., Mobin, S. M., & Misra, R. (2015). Meso Alkynylated Tetraphenylethylene (TPE) and 2,3,3-Triphenylacrylonitrile (TPAN) Substituted BODIPYs. *The Journal of Organic Chemistry*, *80*(16), 8018–8025. https://doi.org/10.1021/acs.joc.5b01117

59. Mikulchyk, T., Karuthedath, S., Castro, C. S. P. D., Buglak, A. A., Sheehan, A., Wieder, A., … Filatov, M. A. (2022). Charge transfer mediated triplet excited state formation in donor–acceptor–donor BODIPY: Application for recording of holographic structures in photopolymerizable glass. *Journal of Materials Chemistry C*, *10*(32), 11588–11597. https://doi.org/10.1039/D2TC02263J

60. Bassan, E., Gualandi, A., Cozzi, P. G., & Ceroni, P. (2021). Design of BODIPY dyes as triplet photosensitizers: electronic properties tailored for solar energy conversion, photoredox catalysis and

photodynamic therapy. *Chemical Science*, *12*(19), 6607–6628. https://doi.org/10.1039/D1SC00732G

61. Merkes, J. M., Ostlender, T., Wang, F., Kiessling, F., Sun, H., & Banala, S. (2021). Tuning the optical properties of BODIPY dyes by N-rich heterocycle conjugation using a combined synthesis and computational approach. *New Journal of Chemistry*, *45*(42), 19641–19645. https://doi.org/10.1039/D1NJ01847G

62. An, F., Xin, J., Deng, C., Tan, X., Aras, O., Chen, N., … Ting, R. (2021). Facile synthesis of near-infrared bodipy by donor engineering for in vivo tumor targeted dual-modal imaging. *Journal of Materials Chemistry B*, *9*(45), 9308–9315. https://doi.org/10.1039/D1TB01883C

63. Liu, X., Chi, W., Qiao, Q., Kokate, S. V., Cabrera, E. P., Xu, Z., … Chang, Y.-T. (2020). Molecular Mechanism of Viscosity Sensitivity in BODIPY Rotors and Application to Motion-Based Fluorescent Sensors. *ACS Sensors*, *5*(3), 731–739. https://doi.org/10.1021/acssensors.9b01951

64. Sansalone, L., Tang, S., Garcia-Amorós, J., Zhang, Y., Nonell, S., Baker, J. D., … Raymo, F. M. (2018). A Photoactivatable Far-Red/Near-Infrared BODIPY To Monitor Cellular Dynamics in Vivo. *ACS Sensors*, *3*(7), 1347–1353. https://doi.org/10.1021/acssensors.8b00262

65. Chi, C.-C., Huang, Y.-J., & Chen, C.-T. (2012). Synthesis and Spectroscopic Characterization of Dual Absorption BODIPY Type Dyes and their Light Harvesting Application in Polymer-Based Bulk Hetrojunction Organic Photovoltaics. *Journal of the Chinese Chemical Society*, *59*(3), 305–316. https://doi.org/10.1002/jccs.201100612

66. Bulut, I., Huaulmé, Q., Mirloup, A., Chávez, P., Fall, S., Hébraud, A., … Leclerc, N. (2017). Rational Engineering of BODIPY-Bridged Trisindole Derivatives for Solar Cell Applications. *ChemSusChem*, *10*(9), 1878–1882. https://doi.org/10.1002/cssc.201700465

67. Treibs, A., & Kreuzer, F.-H. (1968). Difluorboryl-Komplexe von Di- und Tripyrrylmethenen. *Justus Liebigs Annalen der Chemie*, *718*(1), 208–223. https://doi.org/10.1002/jlac.19687180119

68. Esnal, I., Urías-Benavides, A., Gómez-Durán, C. F. A., Osorio-Martínez, C. A., García-Moreno, I., Costela, A., … Peña-Cabrera, E. (2013). Reaction of Amines with 8-MethylthioBODIPY: Dramatic Optical and Laser Response to Amine Substitution. *Chemistry – An Asian Journal*, *8*(11), 2691–2700. https://doi.org/10.1002/asia.201300760

69. Boyer, J. H., Haag, A. M., Sathyamoorthi, G., Soong, M.-L., Thangaraj, K., & Pavlopoulos, T. G. (1993). Pyrromethene–BF2 complexes as laser dyes: 2. *Heteroatom Chemistry*, *4*(1), 39–49. https://doi.org/10.1002/hc.520040107

70. Zhang, M., Hao, E., Xu, Y., Zhang, S., Zhu, H., Wang, Q., … Jiao, L. (2012). One-pot efficient synthesis of pyrrolylBODIPY dyes from pyrrole and acyl chloride. *RSC Advances*, *2*(30), 11215–11218. https://doi.org/10.1039/C2RA22203E

71. Jiao, L., Yu, C., Wang, J., Briggs, E. A., Besley, N. A., Robinson, D., … Boens, N. (2015). Unusual spectroscopic and photophysical properties of meso-tert-butylBODIPY in comparison to related alkylated BODIPY dyes. *RSC Advances*, *5*(109), 89375–89388. https://doi.org/10.1039/C5RA17419H

72. Kolemen, S., Cakmak, Y., Kostereli, Z., & Akkaya, E. U. (2014). Atropisomeric Dyes: Axial Chirality in Orthogonal BODIPY Oligomers. *Organic Letters*, *16*(3), 660–663. https://doi.org/10.1021/ol403193f

73. Kim, D., Yamamoto, K., & Ahn, K. H. (2012). A BODIPY-based reactive probe for ratiometric fluorescence sensing of mercury ions. *Tetrahedron*, *68*(26), 5279–5282. https://doi.org/10.1016/j.tet.2012.01.091

74. Chi, W., Qiao, Q., Lee, R., Liu, W., Teo, Y. S., Gu, D., … Liu, X. (2019). A Photoexcitation-Induced Twisted Intramolecular Charge Shuttle. *Angewandte Chemie International Edition*, *58*(21), 7073–7077. https://doi.org/10.1002/anie.201902766

75. Boens, N., Verbelen, B., Ortiz, M. J., Jiao, L., & Dehaen, W. (2019). Synthesis of BODIPY dyes through postfunctionalization of the boron dipyrromethene core. *Coordination Chemistry Reviews*, *399*, 213024. https://doi.org/10.1016/j.ccr.2019.213024

76. Boens, N., Leen, V., Dehaen, W., Wang, L., Robeyns, K., Qin, W., … Alvarez-Pez, J. M. (2012). Visible Absorption and Fluorescence Spectroscopy of Conformationally Constrained, Annulated BODIPY Dyes. *The Journal of Physical Chemistry A*, *116*(39), 9621–9631. https://doi.org/10.1021/jp305551w

77. Boens, N., Verbelen, B., & Dehaen, W. (2015). Postfunctionalization of the BODIPY Core: Synthesis and Spectroscopy. *European Journal of Organic Chemistry*, *2015*(30), 6577–6595. https://doi.org/10.1002/ejoc.201500682

78. Zhu, S., Bi, J., Vegesna, G., Zhang, J., Luo, F.-T., Valenzano, L., & Liu, H. (2013). Functionalization of BODIPY dyes at 2,6-positions through formyl groups. *RSC Advances*, *3*(14), 4793–4800. https://doi.org/10.1039/C3RA22610G

79. Ji, J.-M., Zhou, H., & Kim, H. K. (2018). Rational design criteria for D–π–A structured organic and porphyrin sensitizers for highly efficient dye-sensitized solar cells. *Journal of Materials Chemistry A*, *6*(30), 14518–14545. https://doi.org/10.1039/C8TA02281J

80. Bassan, E., Gualandi, A., Cozzi, P. G., & Ceroni, P. (2021). Design of BODIPY dyes as triplet photosensitizers: electronic properties tailored for solar energy conversion, photoredox catalysis and photodynamic therapy. *Chemical Science*, *12*(19), 6607–6628. https://doi.org/10.1039/D1SC00732G

81. Rohand, T., Baruah, M., Qin, W., Boens, N., & Dehaen, W. (2006). Functionalisation of fluorescent BODIPY dyes by nucleophilic substitution. *Chemical Communications*, (3), 266–268. https://doi.org/10.1039/B512756D

82. Boens, N., Verbelen, B., Ortiz, M. J., Jiao, L., & Dehaen, W. (2019). Synthesis of BODIPY dyes through postfunctionalization of the boron dipyrromethene core. *Coordination Chemistry Reviews*, *399*, 213024. https://doi.org/10.1016/j.ccr.2019.213024

83. Meng, G., Velayudham, S., Smith, A., Luck, R., & Liu, H. (2009). Color Tuning of Polyfluorene Emission with BODIPY Monomers. *Macromolecules*, *42*(6), 1995–2001. https://doi.org/10.1021/ma8023975

84. Lu, H., Wang, Q., Gai, L., Li, Z., Deng, Y., Xiao, X., … Shen, Z. (2012). Tuning the Solid-State Luminescence of BODIPY Derivatives with Bulky Arylsilyl Groups: Synthesis and Spectroscopic Properties. *Chemistry – A European Journal*, *18*(25), 7852–7861. https://doi.org/10.1002/chem.201200169

85. Zhang, Y., Shao, X., Wang, Y., Pan, F., Kang, R., Peng, F., … Zhao, W. (2015). Dual emission channels for sensitive discrimination of Cys/Hcy and GSH in plasma and cells. *Chemical Communications*, *51*(20), 4245–4248. https://doi.org/10.1039/C4CC08687B

86. Leen, V., Yuan, P., Wang, L., Boens, N., & Dehaen, W. (2012). Synthesis of Meso-Halogenated BODIPYs and Access to Meso-Substituted Analogues. *Organic Letters*, *14*(24), 6150–6153. https://doi.org/10.1021/ol3028225

87. Madhu, S., Rao, M. R., Shaikh, M. S., & Ravikanth, M. (2011). 3,5-Diformylboron Dipyrromethenes as Fluorescent pH Sensors. *Inorganic Chemistry*, *50*(10), 4392–4400. https://doi.org/10.1021/ic102499h

88. Madhu, S., Kumar, S., Chatterjee, T., & Ravikanth, M. (2014). Synthesis, X-ray structure, spectral and electrochemical properties of a

β- meso covalently linked BODIPY–Ru(ii) dipyrrin complex. *New Journal of Chemistry*, *38*(11), 5551–5558. https://doi.org/10.1039/C4NJ01114G

89. Zhang, X., Zhang, Y., Chen, L., & Xiao, Y. (2015). Star-shaped carbazole-based BODIPY derivatives with improved hole transportation and near-infrared absorption for small-molecule organic solar cells with high open-circuit voltages. *RSC Advances*, *5*(41), 32283–32289. https://doi.org/10.1039/C5RA02414E

90. Obondi, C. O., Lim, G. N., Karr, P. A., Nesterov, V. N., & D'Souza, F. (2016). Photoinduced charge separation in wide-band capturing, multi-modular bis(donor styryl)BODIPY–fullerene systems. *Physical Chemistry Chemical Physics*, *18*(27), 18187–18200. https://doi.org/10.1039/C6CP03479A

91. Shinde, J., Thomas, M. B., Poddar, M., Misra, R., & D'Souza, F. (2021). Does Location of BF2-Chelated Dipyrromethene (BODIPY) Ring Functionalization Affect Spectral and Electron Transfer Properties? Studies on α-, β-, and Meso-Functionalized BODIPY-Derived Donor–Acceptor Dyads and Triads. *The Journal of Physical Chemistry C*, *125*(43), 23911–23921. https://doi.org/10.1021/acs.jpcc.1c06704

92. Rao, M. R., Kumar, K. V. P., & Ravikanth, M. (2010). Synthesis of boron-dipyrromethene–ferrocene conjugates. *Journal of Organometallic Chemistry*, *695*(6), 863–869. https://doi.org/10.1016/j.jorganchem.2010.01.009

93. Lakshmi, V., & Ravikanth, M. (2013). Synthesis, spectral and electrochemical properties of phenylated boron-dipyrromethenes. *Dyes and Pigments*, *96*(3), 665–671. https://doi.org/10.1016/j.dyepig.2012.10.012

94. Wanwong, S., Khomein, P., & Thayumanavan, S. (2018). BODIPY dyads and triads: synthesis, optical, electrochemical and

transistor properties. *Chemistry Central Journal*, *12*(1), 60. https://doi.org/10.1186/s13065-018-0430-5

95. Kim, S., Zhou, Y., Tohnai, N., Nakatsuji, H., Matsusaki, M., Fujitsuka, M., … Majima, T. (2018). Aggregation-Induced Singlet Oxygen Generation: Functional Fluorophore and Anthrylphenylene Dyad Self-Assemblies. *Chemistry – A European Journal*, *24*(3), 636–645. https://doi.org/10.1002/chem.201703686

96. Mirloup, A., Leclerc, N., Rihn, S., Bura, T., Bechara, R., Hébraud, A., … Ziessel, R. (2014). A deep-purple-grey thiophene–benzothiadiazole–thiophene BODIPY dye for solution-processed solar cells. *New Journal of Chemistry*, *38*(8), 3644–3653. https://doi.org/10.1039/C4NJ00294F

97. Liao, J., Zhao, H., Xu, Y., Cai, Z., Peng, Z., Zhang, W., … Yang, X. (2016). Novel D–A–D type dyes based on BODIPY platform for solution processed organic solar cells. *Dyes and Pigments*, *128*, 131–140. https://doi.org/10.1016/j.dyepig.2016.01.020

98. Huaulmé, Q., Fall, S., Lévêque, P., Ulrich, G., & Leclerc, N. (2019). Pairing of α-Fused BODIPY: Towards Panchromatic n-Type Semiconducting Materials. *Chemistry – A European Journal*, *25*(26), 6613–6620. https://doi.org/10.1002/chem.201900536

99. Frank, F. J., Waddell, P. G., Hall, M. J., & Knight, J. G. (2021). Synthesis and Reactivity of 3,5-Diiodo-BODIPYs via a Concerted, Double Aromatic Finkelstein Reaction. *Organic Letters*, *23*(21), 8595–8599. https://doi.org/10.1021/acs.orglett.1c03317

100. Feng, Z., Jiao, L., Feng, Y., Yu, C., Chen, N., Wei, Y., … Hao, E. (2016). Regioselective and Stepwise Syntheses of Functionalized BODIPY Dyes through Palladium-Catalyzed Cross-Coupling Reactions and Direct C–H Arylations. *The Journal of Organic Chemistry*, *81*(15), 6281–6291. https://doi.org/10.1021/acs.joc.6b00858

101. Zhang, H., Chen, X., Lan, J., Liu, Y., Zhou, F., Wu, D., & You, J. (2018). Silver-mediated direct C–H amination of BODIPYs for

screening endoplasmic reticulum-targeting reagents. *Chemical Communications*, *54*(26), 3219–3222. https://doi.org/10.1039/C8CC00238J

102. Goeb, S., & Ziessel, R. (2007). Convenient Synthesis of Green Diisoindolodithienylpyrromethene−Dialkynyl Borane Dyes. *Organic Letters*, *9*(5), 737–740. https://doi.org/10.1021/ol0627404

103. Bonardi, L., Ulrich, G., & Ziessel, R. (2008). Tailoring the Properties of Boron−Dipyrromethene Dyes with Acetylenic Functions at the 2,6,8 and 4-B Substitution Positions. *Organic Letters*, *10*(11), 2183–2186. https://doi.org/10.1021/ol800560b

104. Rousseau, T., Cravino, A., Ripaud, E., Leriche, P., Rihn, S., Nicola, A. D., … Roncali, J. (2010). A tailored hybrid BODIPY–oligothiophene donor for molecular bulk heterojunction solar cells with improved performances. *Chemical Communications*, *46*(28), 5082–5084. https://doi.org/10.1039/C0CC01144D

105. Rihn, S., Erdem, M., De Nicola, A., Retailleau, P., & Ziessel, R. (2011). Phenyliodine(III) Bis(trifluoroacetate) (PIFA)-Promoted Synthesis of Bodipy Dimers Displaying Unusual Redox Properties. *Organic Letters*, *13*(8), 1916–1919. https://doi.org/10.1021/ol200189y

106. Freese, T., Patalag, L. J., Merz, J. L., Jones, P. G., & Werz, D. B. (2021). One-Pot Strategy for Symmetrical and Unsymmetrical BOIMPY Fluorophores. *The Journal of Organic Chemistry*, *86*(3), 3089–3095. https://doi.org/10.1021/acs.joc.0c02860

107. Patalag, L. J., Jones, P. G., & Werz, D. B. (2016). BOIMPYs: Rapid Access to a Family of Red-Emissive Fluorophores and NIR Dyes. *Angewandte Chemie International Edition*, *55*(42), 13340–13344. https://doi.org/10.1002/anie.201606883

108. Patalag, L. J., Loch, M., Jones, P. G., & Werz, D. B. (2019). Exploring the π-System of the (Aza-)BOIMPY Scaffold: Electron-Rich Pyrrole Moieties Working in Concert with Electron-Depleted Meso-

Positions. *The Journal of Organic Chemistry*, *84*(12), 7804–7814. https://doi.org/10.1021/acs.joc.9b00603

109. Lv, F., Liu, D., Zheng, W., Zhao, Y., & Song, F. (2021). BOPHY-Based Aggregation-Induced-Emission Nanoparticle Photosensitizers for Photodynamic Therapy. *ACS Applied Nano Materials*, *4*(6), 6012–6019. https://doi.org/10.1021/acsanm.1c00862

110. He, C., Zhou, H., Yang, N., Niu, N., Hussain, E., Li, Y., & Yu, C. (2018). A turn-on fluorescent BOPHY probe for Cu2+ ion detection. *New Journal of Chemistry*, *42*(4), 2520–2525. https://doi.org/10.1039/C7NJ03911E

111. Jiang, X.-D., Su, Y., Yue, S., Li, C., Yu, H., Zhang, H., … Xiao, L.-J. (2015). Synthesis of mono-(p-dimethylamino)styryl-containing BOPHY dye for a turn-on pH sensor. *RSC Advances*, *5*(22), 16735–16739. https://doi.org/10.1039/C4RA15914D

112. Hasegawa, R., Iwakiri, S., & Kubo, Y. (2021). Synthesis and triplet sensitization of bis(arylselanyl)BOPHYs; potential application in triplet–triplet annihilation upconversion. *New Journal of Chemistry*, *45*(13), 6091–6099. https://doi.org/10.1039/D1NJ00721A

113. Wang, J., Wu, Q., Yu, C., Wei, Y., Mu, X., Hao, E., & Jiao, L. (2016). Aromatic Ring Fused BOPHYs as Stable Red Fluorescent Dyes. *The Journal of Organic Chemistry*, *81*(22), 11316–11323. https://doi.org/10.1021/acs.joc.6b02291

114. Huaulmé, Q., Mirloup, A., Retailleau, P., & Ziessel, R. (2015). Synthesis of Highly Functionalized BOPHY Chromophores Displaying Large Stokes Shifts. *Organic Letters*, *17*(9), 2246–2249. https://doi.org/10.1021/acs.orglett.5b00858

115. Tamgho, I.-S., Hasheminasab, A., Engle, J. T., Nemykin, V. N., & Ziegler, C. J. (2014). A New Highly Fluorescent and Symmetric Pyrrole–BF2 Chromophore: BOPHY. *Journal of the American Chemical Society*, *136*(15), 5623–5626. https://doi.org/10.1021/ja502477a

116. Dhindsa, J. S., Buguis, F. L., Anghel, M., & Gilroy, J. B. (2021). Band Gap Engineering in Acceptor-Donor-Acceptor Boron Difluoride Formazanates. *The Journal of Organic Chemistry*, *86*(17), 12064–12074. https://doi.org/10.1021/acs.joc.1c01416

117. Koenig, J. D. B., Farahat, M. E., Dhindsa, J. S., Gilroy, J. B., & Welch, G. C. (2020). Near-IR absorption and photocurrent generation using a first-of-its-kind boron difluoride formazanate non-fullerene acceptor. *Materials Chemistry Frontiers*, *4*(6), 1643–1647. https://doi.org/10.1039/D0QM00109K

118. Kumar, C., Agrawal, A. R., Ghosh, N. G., Karmakar, H. S., Das, S., Kumar, N. R., … Zade, S. S. (2020). Boron difluoride formazanates with thiophene and 3,4-ethylenedioxythiophene capping and their electrochemical polymerization. *Dalton Transactions*, *49*(38), 13202–13206. https://doi.org/10.1039/D0DT02905J

119. Barbon, S. M., Price, J. T., Yogarajah, U., & Gilroy, J. B. (2015). Synthesis and characterization of conjugated/cross-conjugated benzene-bridged boron difluoride formazanate dimers. *RSC Advances*, *5*(69), 56316–56324. https://doi.org/10.1039/C5RA09505K

120. Barbon, S. M., Buddingh, J. V., Maar, R. R., & Gilroy, J. B. (2017). Boron Difluoride Adducts of a Flexidentate Pyridine-Substituted Formazanate Ligand: Property Modulation via Protonation and Coordination Chemistry. *Inorganic Chemistry*, *56*(19), 12003–12011. https://doi.org/10.1021/acs.inorgchem.7b01984

121. Hesari, M., Barbon, S. M., Mendes, R. B., Staroverov, V. N., Ding, Z., & Gilroy, J. B. (2018). Structural Tuning of Boron Difluoride Formazanate Electrochemiluminescence Mediated by Tri-n-propylamine. *The Journal of Physical Chemistry C*, *122*(2), 1258–1266. https://doi.org/10.1021/acs.jpcc.7b10246

122. Santos, J. M. D., Jagadamma, L. K., Cariello, M., Samuel, I. D. W., & Cooke, G. (2022). A BODIPY small molecule as hole

transporting material for efficient perovskite solar cells. *Sustainable Energy & Fuels*. https://doi.org/10.1039/D2SE00667G

123. Gkini, K., Verykios, A., Balis, N., Kaltzoglou, A., Papadakis, M., Adamis, K. S., … Vasilopoulou, M. (2020). Enhanced Organic and Perovskite Solar Cell Performance through Modification of the Electron-Selective Contact with a Bodipy–Porphyrin Dyad. *ACS Applied Materials & Interfaces*, *12*(1), 1120–1131. https://doi.org/10.1021/acsami.9b17580

124. Li, P., Wu, F., Fang, Y., Dahiya, H., Keshtov, M. L., Xu, H., … Sharma, G. D. (2022). Truxene π-Expanded BODIPY Star-Shaped Molecules as Acceptors for Non-Fullerene Solar Cells with over 13% Efficiency. *ACS Applied Energy Materials*, *5*(2), 2279–2289. https://doi.org/10.1021/acsaem.1c03781

125. Xie, B., Yin, L., Fan, J., Liu, C., & Li, Y. (2022). Novel A-π-D-π-A-type BODIPY dyads as small-molecule donors for solution-processed organic solar cells. *Journal of Materials Chemistry C*, *10*(8), 3248–3258. https://doi.org/10.1039/D1TC04981J

126. Kashiwazaki, G., Watanabe, R., Nishikawa, A., Kawamura, K., Kitayama, T., & Hibi, T. (2022). A selective hybrid fluorescent sensor for fructose detection based on a phenylboronic acid and BODIPY-based hydrophobicity probe. *RSC Advances*, *12*(24), 15083–15090. https://doi.org/10.1039/D2RA01569B

127. Xia, H.-C., Xu, X.-H., & Song, Q.-H. (2017). BODIPY-Based Fluorescent Sensor for the Recognization of Phosgene in Solutions and in Gas Phase. *Analytical Chemistry*, *89*(7), 4192–4197. https://doi.org/10.1021/acs.analchem.7b00203

128. Bui, H. T., Mai, D. K., Kim, B., Choi, K.-H., Park, B. J., Kim, H.-J., & Cho, S. (2019). Effect of Substituents on the Photophysical Properties and Bioimaging Application of BODIPY Derivatives with Triphenylamine Substituents. *The Journal of Physical Chemistry B*, *123*(26), 5601–5607. https://doi.org/10.1021/acs.jpcb.9b04782

129. Guo, X., Tang, B., Wu, Q., Bu, W., Zhang, F., Yu, C., … Hao, E. (2022). Engineering BODIPY-based near-infrared nanoparticles with large Stokes shifts and aggregation-induced emission characteristics for organelle specific bioimaging. *Journal of Materials Chemistry B, 10*(29), 5612–5623. https://doi.org/10.1039/D2TB00921H

130. Jung, E., Shim, I., An, J., Ji, M. S., Jangili, P., Chi, S.-G., & Kim, J. S. (2021). Phenylthiourea-Conjugated BODIPY as an Efficient Photosensitizer for Tyrosinase-Positive Melanoma-Targeted Photodynamic Therapy, 8.

131. Campbell, J. W., Tung, M. T., Diaz-Rodriguez, R. M., Robertson, K. N., Beharry, A. A., & Thompson, A. (2021). Introducing the Tellurophene-Appended BODIPY: PDT Agent with Mass Cytometry Tracking Capabilities. *ACS Medicinal Chemistry Letters*, *12*(12), 1925–1931. https://doi.org/10.1021/acsmedchemlett.1c00492

Chapter 2

Materials and Experimental Techniques

2.1. Introduction

This chapter discusses about the materials used, spectroscopic techniques, the computational calculations and the instrumentation employed in the characterization of synthesized molecules.

2.2. Chemicals for synthesis

Common solvents used for syntheses were purified according to known procedures.[1] Anisaldehyde, Benzaldehyde, Pyrrole, Thiophosgene, Phosphorus oxychloride, Boron trifluoride etherate, Phenothiazine, propyl iodide, sodium hydroxide, anhydrous sodium sulphate, glacial acetic acid, bromine, hydrogen peroxide, bis(pinacolato)diboron, potassium acetate, N-Bromo succinimide, hydrochloric acid, Triphenylamine, *N*,*N*-dimethylaniline and carbazole were obtained from S. D. Fine chem. Ltd. DDQ, was obtained from Spectrochem, bis(triphenylphosphine)palladium(II) ($PdCl_2(PPh_3)_2$), [1,1′-bis(diphenylphosphino)ferrocene]dichloro- palladium(II)dichloride, tetrakis(triphenylphosphine)palladium(0) ($Pd(PPh_3)_4$), tetrabutylammonium hexafluorophosphate ($TBAPF_6$), 4-ethynyl-*N*,*N*-dimethylaniline were procured from Aldrich chemicals USA. Silica gel (100–200 mesh and 230–400 mesh) were purchased from Rankem chemicals, India. TLC pre-coated silica gel plates (Kieselgel 60F254, Merck) were obtained from Merck, India.

Dry solvents chloroform ($CHCl_3$), dichloromethane (DCM), *N*,*N*-dimethylformamide (DMF), tetrahydrofuran (THF), 1,2-dichloroethane, acetone, toluene and methanol were obtained from S. D. Fine chem. Ltd and Spectrochem India. All moisture sensitive reactions were performed under nitrogen/argon atmosphere using standard schlenk method. The N-Bromo succinimide was recrystallized from hot water before use. The solvents and reagents were used as received unless otherwise indicated.

Photophysical and electrochemical studies were performed using spectroscopic grade solvents.

2.3. Spectroscopic Measurements

2.3.1. NMR Spectroscopy

^{1}H NMR (400 MHz and 500 MHz), and ^{13}C NMR (101 MHz and 126 MHz) spectra were recorded on the Bruker Avance (III) 400 MHz and Model AVNACE NEO500 Ascend Bruker 500 MHz, using $CDCl_3$ as solvent. Chemical shifts in ^{1}H, and ^{13}C NMR spectra were reported in parts per million (ppm). In ^{1}H NMR chemical shifts are reported relative to the residual solvent peak ($CDCl_3$, 7.26 ppm). Multiplicities are given as: s (singlet), d (doublet), t (triplet), q (quartet), m (multiplet). ^{13}C NMR chemical shifts are reported relative to the solvent residual peak ($CDCl_3$, 77.02 ppm).

2.3.2. Mass Spectrometry

High resolution mass spectra (HRMS) were recorded on Brucker-Daltonics, micrOTOF-Q II mass spectrometer using positive and negative mode electrospray ionizations.

2.3.3. UV-Vis Spectroscopy

UV-Vis absorption spectra were recorded using a Varian Cary100 Bio UV-Vis and PerkinElmer LAMBDA 35 UV/Vis spectrophotometer.

2.4. Electrochemical Studies

Cyclic voltammograms (CVs) were recorded on PalmSens 4 electrochemical analyzer using Glassy carbon as working electrode and Pt wire as the counter electrode, Ag/AgCl as the reference electrode. The scan rate was 100 mVs^{-1}. A solution of tetrabutylammonium hexafluorophosphate ($TBAPF_6$) in CH_2Cl_2 (0.1 M) was used as the supporting electrolyte.

2.5. Thermal Analysis

Thermogravimetric analysis was performed on the Mettler Toledo thermal analysis system at a heating rate of 10 ℃ min^{-1} under the nitrogen atmosphere.

2.6. Computational Calculations

The density functional theory (DFT) calculation was carried out at the B3LYP/6-31G level for C, H, N, O, B, F and S in the Gaussian 09 program.[2]

2.7. References

[1] (a) Vogel A. I., Tatchell A. R., Furnis B. S., Hannaford A. J., Smith, P. W. G. (1996), Vogel's Textbook of Practical Organic Chemistry (5th Edition) (5th ed.). (b) Wei Ssberger A. Proskraner E. S. Riddick J. A., Toppos Jr. E. F. (1970). Organic Solvents in Techniques of Organic Chemistry, Vol. IV, 3rd Edition, Inc. New York.

[2] (a) Frisch, M. J.; Trucks, G. W.; Schlegel, H. B.; Scuseria, G. E.; Robb, M. A.; Cheeseman, J. R.; Scalmani, G.; Barone, V.; Mennucci, B.; Petersson, G. A.; Nakatsuji, H.; Caricato, M.; Li, X.; Hratchian, H. P.; Izmaylov, A. F.; Bloino, J.; Zheng, G.; Sonnenberg, J. L.; Hada, M.; Ehara, M.; Toyota, K.; Fukuda, R.; Hasegawa, J.; Ishida, M.; Nakajima, T.; Honda, Y.; Kitao, O.; Nakai, H.; Vreven, T.; Montgomery, J. A. Jr.; Peralta, J. E.; Ogliaro, F.; Bearpark, M.; Heyd, J. J.; Brothers, E.; Kudin, K. N.; Staroverov, V. N.; Kobayashi, R.; Normand, J.; Raghavachari, K.; Rendell, A.; Burant, J. C.; Iyengar, S. S.; Tomasi, J.; Cossi, M.; Rega, N.; Millam, N. J.; Klene, M.; Knox, J. E.; Cross, J. B.; Bakken, V.; Adamo, C.; Jaramillo, J.; Gomperts, R.; Stratmann, R. E.; Yazyev, O.; Austin, A. J.; Cammi, R.; Pomelli, C.; Ochterski, J. W.; Martin, R. L.; Morokuma, K.; Zakrzewski, V. G.; Voth, G. A.; Salvador, P.; Dannenberg, J. J.; Dapprich, S.; Daniels, A. D.; Farkas, O.; Foresman, J. B.; Ortiz, J. V.; Cioslowski, J.; Fox, D. J. (2009). Gaussian 09, revision A.02; *Gaussian, Inc.*: Wallingford, CT. (b) Lee, C., Yang, W., & Parr, R. G. (1988). Development of the Colle-Salvetti correlation-energy

formula into a functional of the electron density. *Physical Review B*, 37(2), 785–789. (DOI: 10.1103/PhysRevB.37.785) (c) Becke, A. D. (1993). A new mixing of Hartree-Fock and local density-functional theories. *J. Chem. Phys*. 98, 1372–377. (DOI: 10.1063/1.464304).

Chapter 3

Phenothiazine and Carbazole Substituted Push–Pull Boron-Dipyrromethenes: Synthesis, Photophysical, Electrochemical and Computational Studies

3.1. Introduction

Over the last few decades, the design and synthesis of π-conjugated donor–acceptor materials have emerged as an interesting topic of research due to their potential applications in organic photovoltaics and bioimaging.[1–6] The donor–acceptor (D–A) interactions are one way to modify the frontier molecular orbital energies and HOMO–LUMO gap of the π-conjugated chromophores.[7] In these donor–acceptor chromophores, the heterocyclic conjugates (containing N, O, and S) were introduced to tune their photophysical and redox properties.[8] The electronic and photonic properties of the push–pull chromophores can be improved by various synthetic modifications at the *meso*, α and β-pyrrolic-position of the BODIPY.[3] During the past couple of decades, the 4,4-difluoro-4-bora-3a,4a-diaza-*s*-indacene dyes (BODIPY) have attracted a lot of interest because of their unique properties such as high absorption and fluorescence quantum yields, low toxicity, excellent photo and chemical stability.[9–14] Phenothiazine is a heterocyclic, non-planar, bowl-shaped structure that exhibits electron-rich nitrogen (N) and sulfur (S) heteroatoms.[15–18] The high electron density and good electron donor ability of phenothiazine have found a wide range of applications in electrochromic displays, semiconductors, organic field-effect transistors, dye-sensitized solar cells, and organic light-emitting diodes.[18–20] The 9*H*-carbazole is a nitrogen-containing heterocyclic donor molecule exhibits an absorption bands around 300–400 nm in the UV-visible spectra and an essential building block for synthesizing the π-conjugated chromophores.[21, 22] It is an electron donating group which show an excellent thermal and chemical stability as well as allows the easy structural modification.[23] Several carbazole-based

derivatives were reported, showing the application in organic light-emitting diodes (OLEDs), organic field-effect transistors, and organic photovoltaic devices.[24]

The electron-rich alkynes react with electron acceptor tetracyanoethylene (TCNE) and 7,7,8,8-tetracyanoquinodimethane (TCNQ) *via* [2+2] cycloaddition−retroelectrocyclization reaction which results in D–A type molecular systems.[25–29] It has been found that the cross-conjugated molecular system containing TCBD or cyclohexa-2,5-diene-1,4-ylidene-expanded TCBD groups are useful for tuning the HOMO–LUMO gap and exhibit intramolecular charge transfer (ICT) band in the UV-visible spectra.[26, 30] Michinobu *et al.* have explored a variety of TCBD and cyclohexa-2,5-diene-1,4-ylidene-expanded TCBD substituted donor–acceptor (D–A) chromophores for various optoelectronic applications.[31, 32] Diederich, Shoji, Butenschön, Trolez and Nakamura *et al.* have reported various TCBD and cyclohexa-2,5-diene-1,4-ylidene-expanded TCBD substituted push–pull chromophores and studied their photophysical and redox properties.[33–38] Our group has reported a variety of TCBD, and cyclohexa-2,5-diene-1,4-ylidene-expanded TCBD substituted push–pull chromophores and explored their photophysical and electrochemical characteristics for various optoelectronic applications.[39–42]

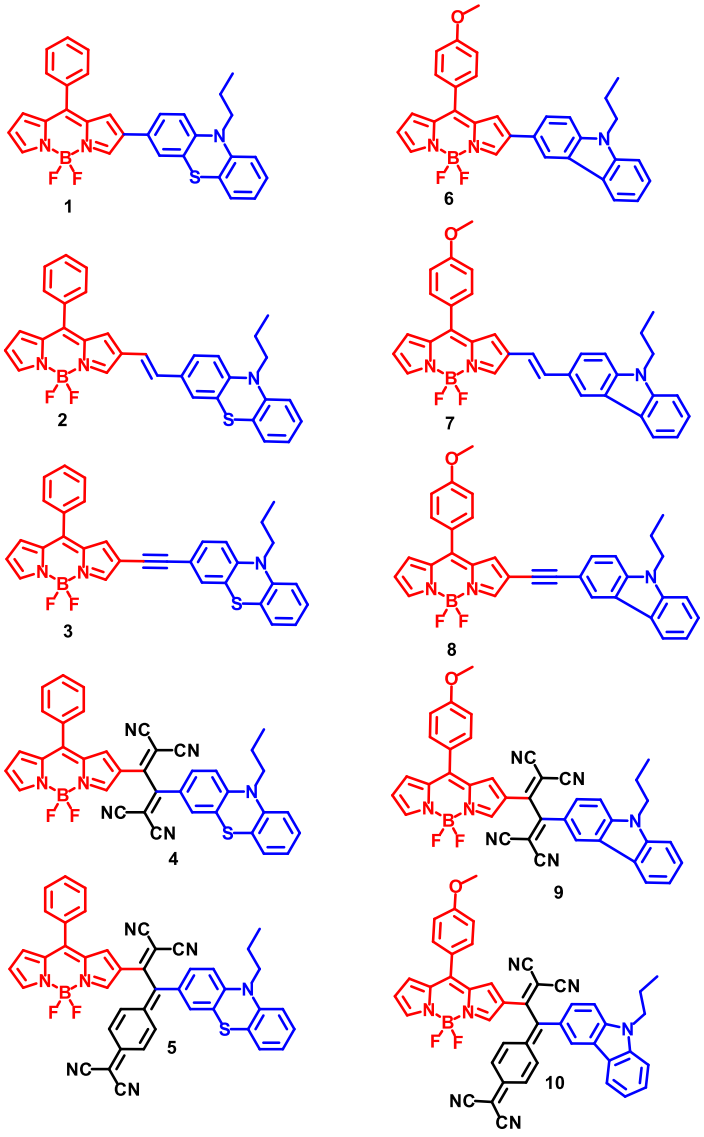

Chart 3.1. Molecular structures of the push–pull BODIPYs **1–10**.

In this study, we wish to report the design and synthesis of donor–acceptor BODIPYs **1–10** *via* *β*-pyrrole functionalization in good yields (Chart 3.1). The phenothiazine and carbazole groups used as donor and BODIPY, TCBD and cyclohexa-2,5-diene-1,4-ylidene-expanded TCBD as an acceptor unit. Therefore, we have investigated the photophysical, electrochemical and theoretical properties of the push–pull BODIPYs **1–10**, in order to analyze the effect of donor and acceptor on the donor–acceptor BODIPYs.

3.2. Results and Discussion

The donor–acceptor BODIPYs **1–10** were designed and synthesized by the Pd-catalyzed Suzuki, Heck, Sonogashira cross-coupling and [2+2] cycloaddition-retroelectrocyclic ring-opening reactions in good yields. The BODIPYs **1** and **6** were synthesized by the Suzuki cross-coupling reaction using boronate ester of phenothiazine **12** and boronate ester of carbazole **16**, respectively. The *β*-mono-iodo BODIPY **11** was synthesized by the reported procedure.[43] The *β*-mono-iodo BODIPYs **11** and **15** were reacted with boronate ester of phenothiazine **12** and boronate ester of carbazole **16** in the catalytic amount of $Pd(PPh_3)_4$ at 80 ℃ for 12 h using Toluene: EtOH: H_2O (9:3:1) solvent to give BODIPYs **1** and **6** in 72% and 75% yields, respectively (Scheme 3.1 and 3.2). The BODIPYs **2** and **7** were synthesized *via* a Pd-catalyzed Heck coupling reaction. The *β*-mono-iodo BODIPYs **11** and **15** reacted with compound **13** and **17** using $Pd(OAc)_2$ and tetrabutylammonium bromide (Bu_4NBr) in the presence of dimethylformamide (DMF) solvent, resulting the BODIPYs **2** and **7** in 35% and 40% yields, respectively (Scheme 3.1 and 3.2). The *β*-mono-iodo BODIPYs **11** and **15** reacts with compounds **14** (3-ethynyl-10-propyl-10*H*-phenothiazine) and compound **18** (3-ethynyl-9-propyl-9*H*-carbazole) in presence of catalytic amount of $Pd(PPh_3)_4$ using THF:DIPEA solvent at 60 ℃ for 12 hours resulted in BODIPY **3** and **8** in 70% and 60% yields, respectively (Scheme 3.1 and 3.2).

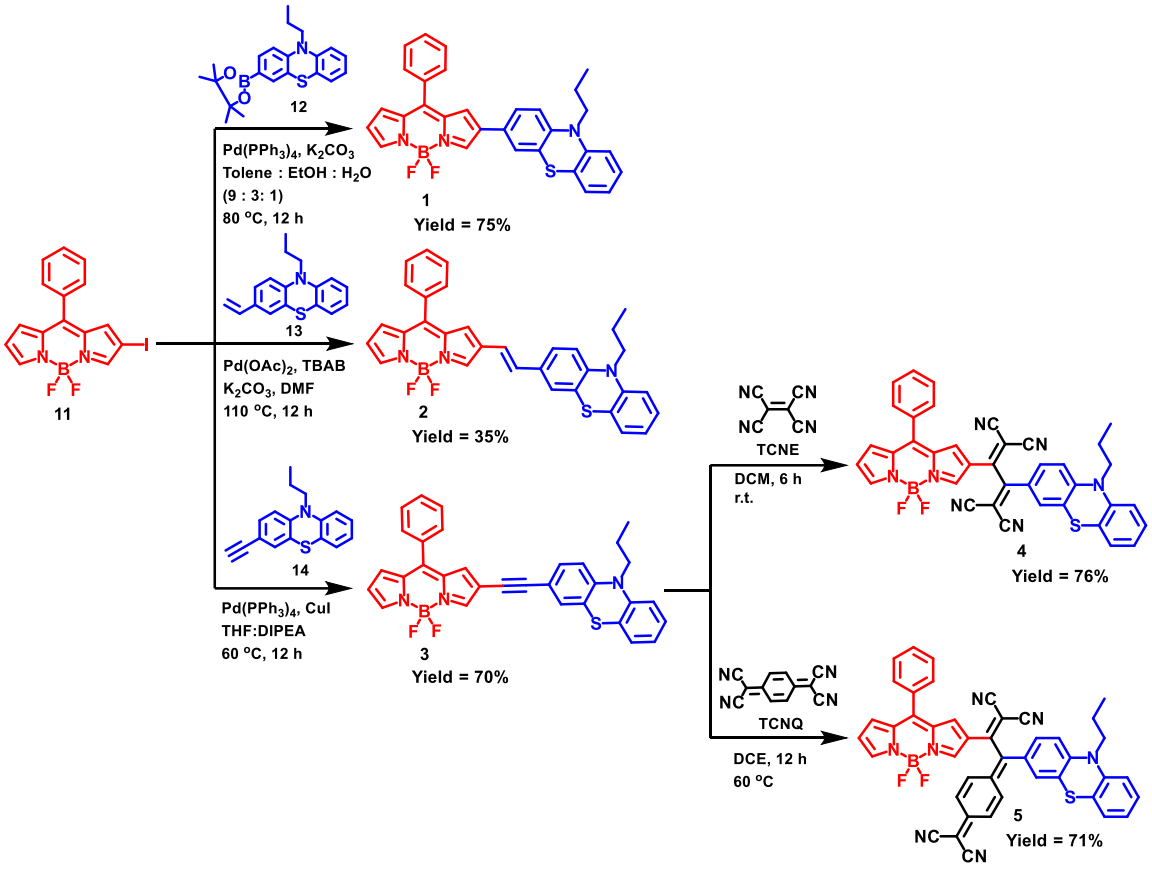

Scheme 3.1. Synthetic methodology of the BODIPYs **1**–**5**.

The reaction of BODIPYs 3 and 8 with strong electron acceptor tetracyanoethylene (TCNE) in dichloromethane (DCM) solvent at room temperature for 6 h gave TCBD substituted BODIPYs **4** and **9** in 76% and 80% yields, respectively. Similarly, the BODIPYs **3** and **8** reacts with strong electron acceptor 7,7,8,8-tetracyanoquinodimethane (TCNQ) in dichloroethane (DCE) solvent at 60 °C for 12 h, resulting in cyclohexa-2,5-diene-1,4-ylidene-expanded TCBD substituted BODIPYs **5** and **10** in 76% and 73% yields, respectively (Scheme 3.1 and 3.2).

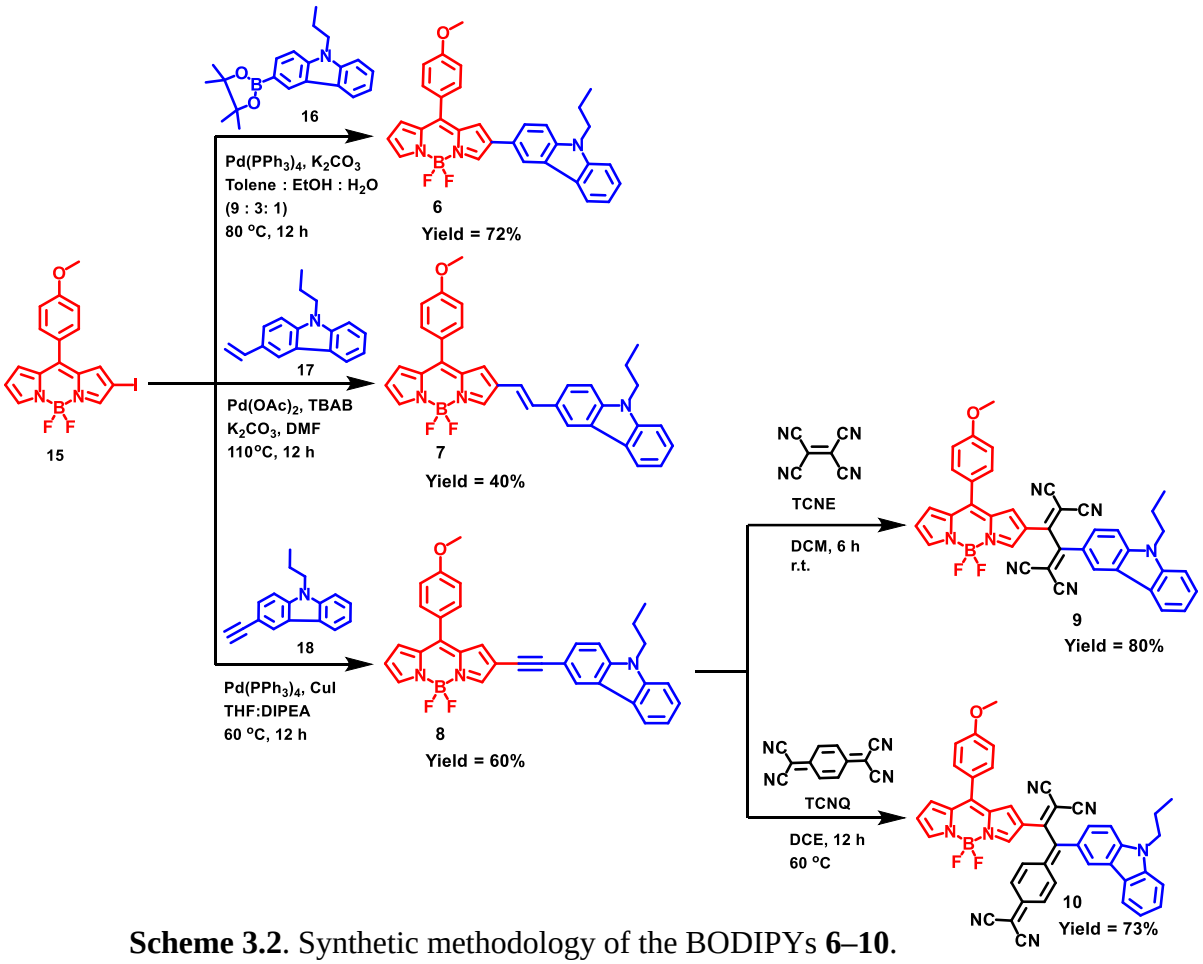

Scheme 3.2. Synthetic methodology of the BODIPYs **6–10**.

The π-conjugated push–pull BODIPYs **1–10** were purified by column chromatography (silica gel size = 100–200 mesh) using Hexane: DCM as a solvent. ^{1}H NMR, ^{13}C NMR, and HRMS techniques were used to characterize the molecular structures of all push–pull BODIPYs. The push–pull BODIPYs **1–10** are readily soluble in common organic solvents such as acetone, chloroform, dichloromethane, and acetonitrile.

Reaction Mechanism for TCNE :

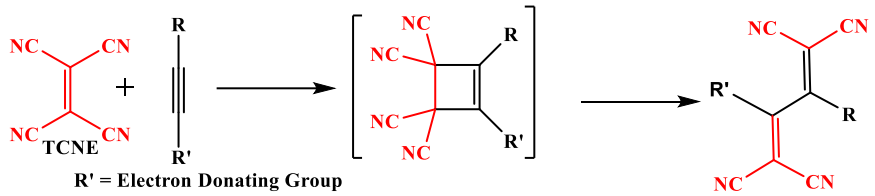

Reaction Mechanism for TCNQ :

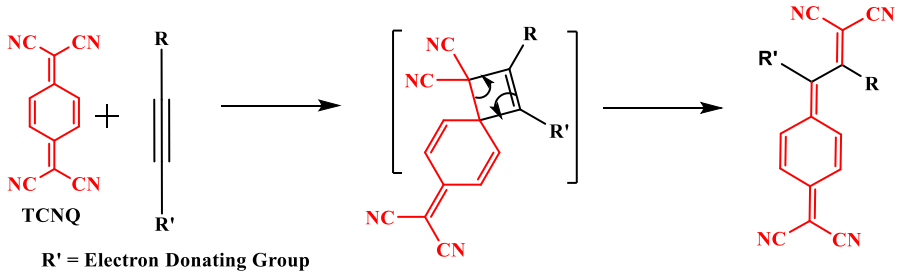

3.3. Photophysical properties

The normalized electronic absorption spectra of the push–pull BODIPYs **1–10** were recorded in dry dichloromethane at room temperature (Figures 3.1a and 3.2b), and the data are compiled in Table 3.1.

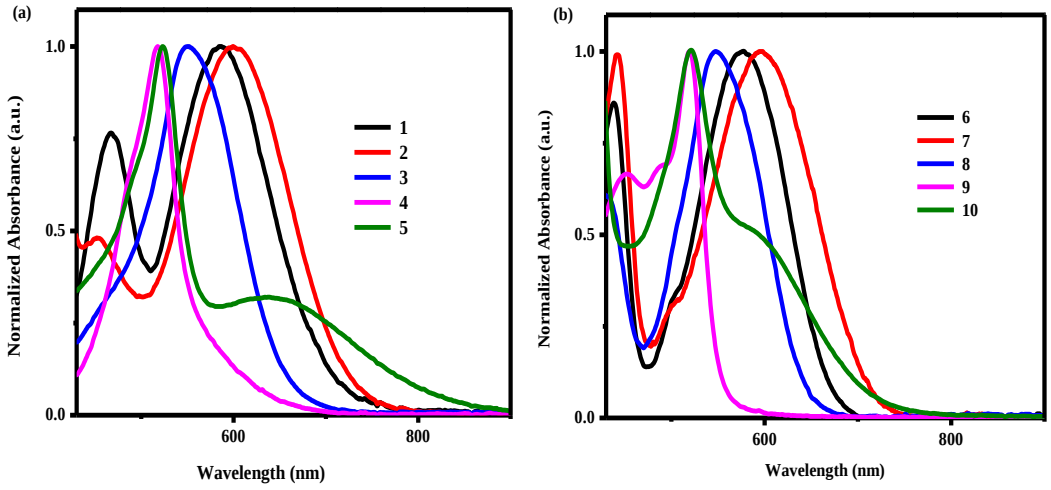

Figure 3.1. Normalized electronic absorption spectra of the push–pull BODIPYs (a) BODIPY-PTZ **1–5** and (b) BODIPY-CBZ **6–10** were recorded in DCM solvent (10^{-5} M).

BODIPY generally exhibits an intense sharp absorption band in the green part of the visible spectrum.[2] The electron donor

phenothiazine and carbazole unit exhibit an intense absorption band at 316 nm and 300–400 nm, respectively.[15, 22] The BODIPYs **1–10** exhibit strong donor–acceptor interaction and displays two absorption bands in the UV-visible spectra; the first band from 400–500 nm and the second from 500–600 nm. The BODIPYs **1** and **6** exhibit absorption band at 467 nm, 587 nm, and 438 nm, 576 nm, respectively due to π–π* transition. The BODIPY **1** exhibits a slight bathochromic shift compared to the BODIPY **6** due to the strong electron donor ability of the phenothiazine unit. The vinylene bridged BODIPYs **2** and **7** exhibit two absorption bands at 457 nm, 599 nm, and 411 nm, 595 nm, respectively, due to π–π* transition. The ethynyl bridged BODIPY **3** exhibits an absorption band at 550 nm, and BODIPY **8** exhibits two absorption bands at 432 nm and 548 nm in the UV-visible spectra. The phenothiazine substituted BODIPYs show a bathochromic shift compared to carbazole substituted BODIPYs due to the strong electron-donating nature of the phenothiazine unit. The TCBD-substituted BODIPYs **4** and **9** show an intense intramolecular charge transfer (ICT) band at 519 nm and 518 nm, respectively, due to strong electronic communication between the donor and acceptor group. The cyclohexa-2,5-diene-1,4-ylidene-expanded TCBD functionalized BODIPYs **5,** and **10** exhibit two absorption bands at 523 nm, 643 nm, and 523 nm, 597 nm, respectively. The higher energy transition bands correspond to the π–π* transition, and the lower energy transition bands belong to the ICT transition from donor to acceptor moiety. The electronic absorption spectra of cyclohexa-2,5-diene-1,4-ylidene-expanded TCBD substituted BODIPYs show a bathochromic shift compared to the TCBD substituted BODIPYs due to strong donor–acceptor (D–A) interactions.

Table 3.1. Photophysical and electrochemical data of the push–pull BODIPYs **1–10**.

Photophysical data[a]				**Electrochemical data[b]**	
Compound	**λ_{abs} (nm)**	**ε (M^{-1} cm^{-1})**	**Optical band gap (eV)**	**E_{ox} (V)**	**E_{red} (V)**
1	467 587	7220 9410	1.69	0.61 1.27	-0.65
2	457 599	5610 11790	1.71	0.60 1.13	-0.68
3	550	16930	1.78	0.68 1.33	-0.62
4	373 519	7060 18410	2.02	0.95 1.38	-0.23 -0.39 -0.81
5	523 643	34330 10960	1.29	0.86 1.47	-0.05 -0.25 -0.85
6	438 576	10620 12350	1.78	0.99 1.30	-0.76
7	411 595	3610 3640	1.73	0.84 1.17	-0.74
8	432 548	6470 10720	1.81	1.03 1.28	-0.64
9	450 518	32540 48980	2.20	1.03 1.26	-0.33 -0.52 -0.87
10	523 597	40220 19820	1.46	0.13 1.09	-0.31 -0.87

[a] Absorbance recorded in dry DCM at 1×10^{-5} M conc. λ_{abs}: absorption wavelength. ε: extinction coefficient. [b] Electrochemical analysis was estimated by differential pulse voltammetry in 0.1 M solution of Bu_4NPF_6 in DCM at 100 mV s^{-1} scan rate *versus* Ag/AgCl at 25 °C. E_{oxi} and E_{red} values are based on DPV analysis.

The experimentally calculated optical bandgap of TCBD and cyclohexa-2,5-diene-1,4-ylidene-expanded TCBD substituted push–pull BODIPYs **4**, **9**, **5,** and **10** follow the order **9**>**4**>**10**>**5**. The optical bandgap trend clearly indicates that the incorporation of cyclohexa-2,5-diene-1,4-ylidene-expanded TCBD unit results in a bathochromic shift in the UV-visible spectra compared to the TCBD due to strong electronic communication between donor and acceptor unit.

3.4. Electrochemical properties

Cyclic voltammetry (CV) and differential pulse voltammetry (DPV) were performed to investigate the redox behaviour of the push–pull BODIPYs **1–10**. The electrochemical data of BODIPYs **1–10** are compiled in Table 3.1. All the measurements were recorded in dry dichloromethane (DCM) solvent at room temperature using tetrabutylammonium hexafluorophosphate (Bu_4NPF_6) as a supporting electrolyte. The representative CV and DPV plots of the push–pull BODIPYs **1**–**10** are shown in Figure 3.2.

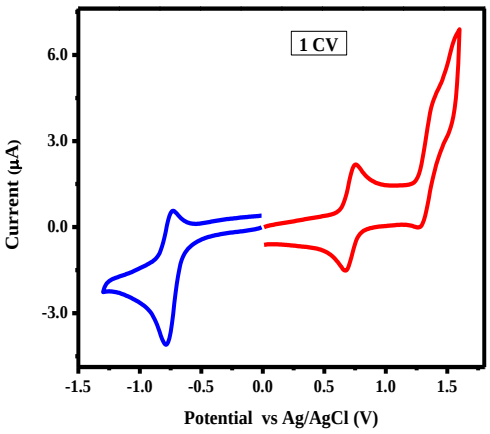
1 CV
Current (µA)
Potential vs Ag/AgCl (V)

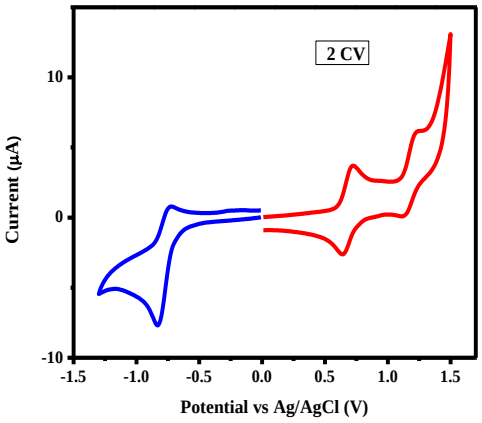
2 CV
Current (µA)
Potential vs Ag/AgCl (V)

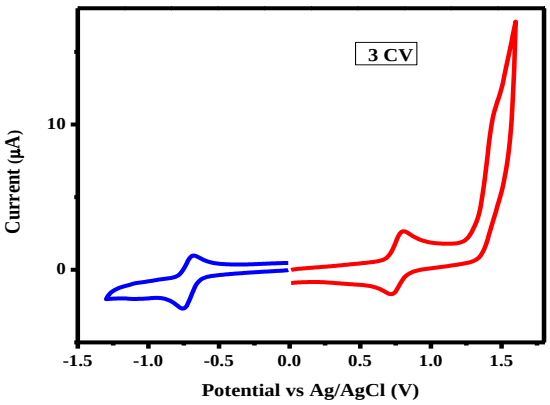
3 CV
Current (µA)
Potential vs Ag/AgCl (V)

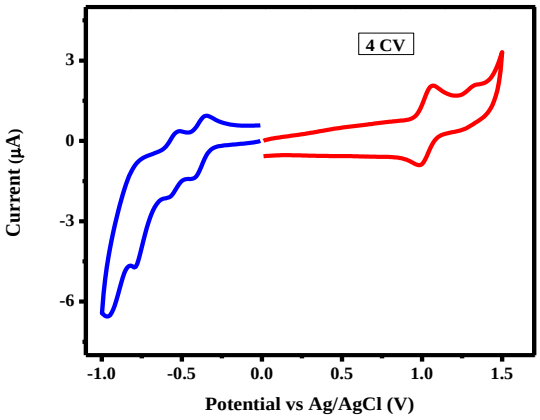
4 CV
Current (µA)
Potential vs Ag/AgCl (V)

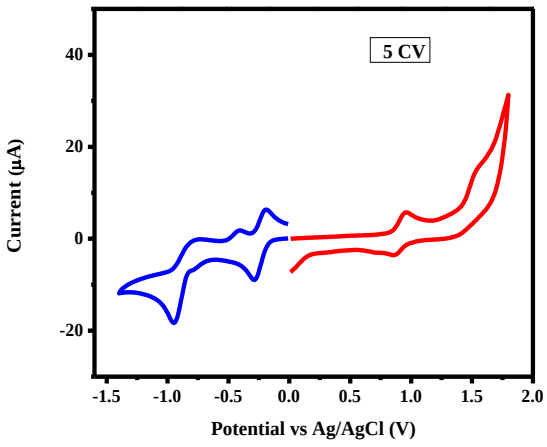
5 CV
Current (µA)
Potential vs Ag/AgCl (V)

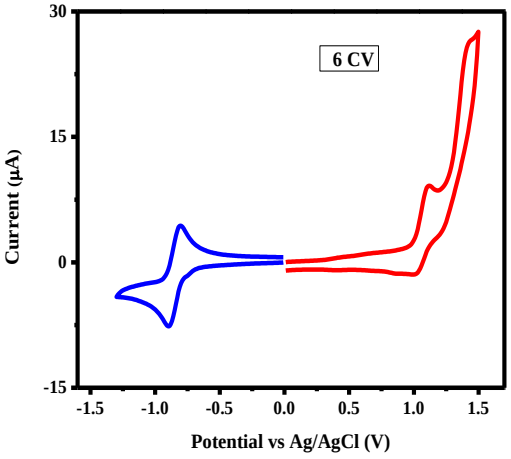
6 CV
Current (µA)
Potential vs Ag/AgCl (V)

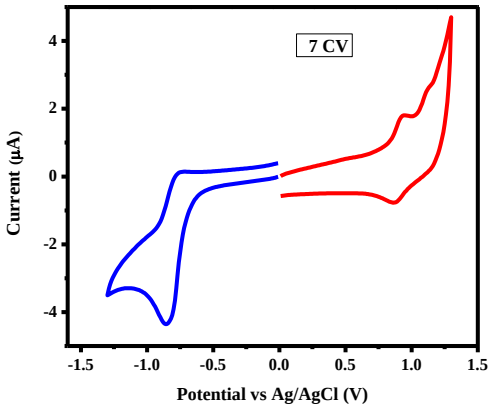
7 CV
Current (µA)
Potential vs Ag/AgCl (V)

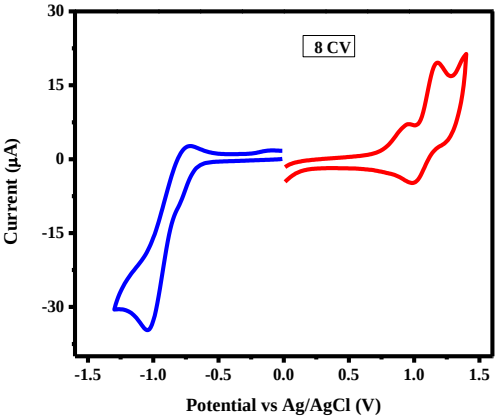
8 CV
Current (µA)
Potential vs Ag/AgCl (V)

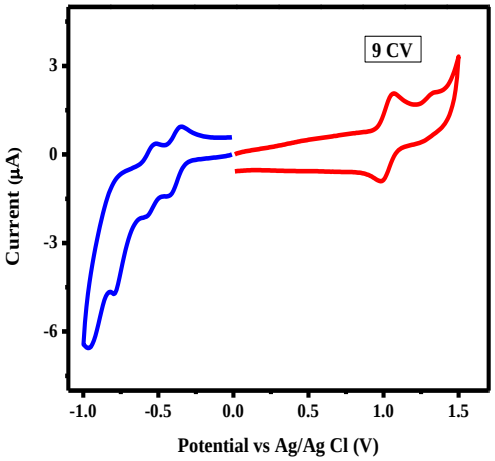
9 CV
Current (µA)
Potential vs Ag/Ag Cl (V)

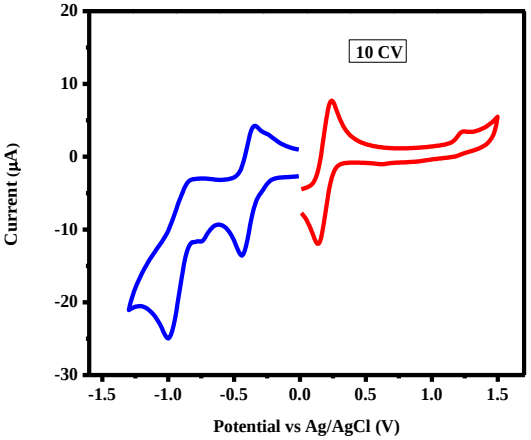
10 CV
Current (µA)
Potential vs Ag/AgCl (V)

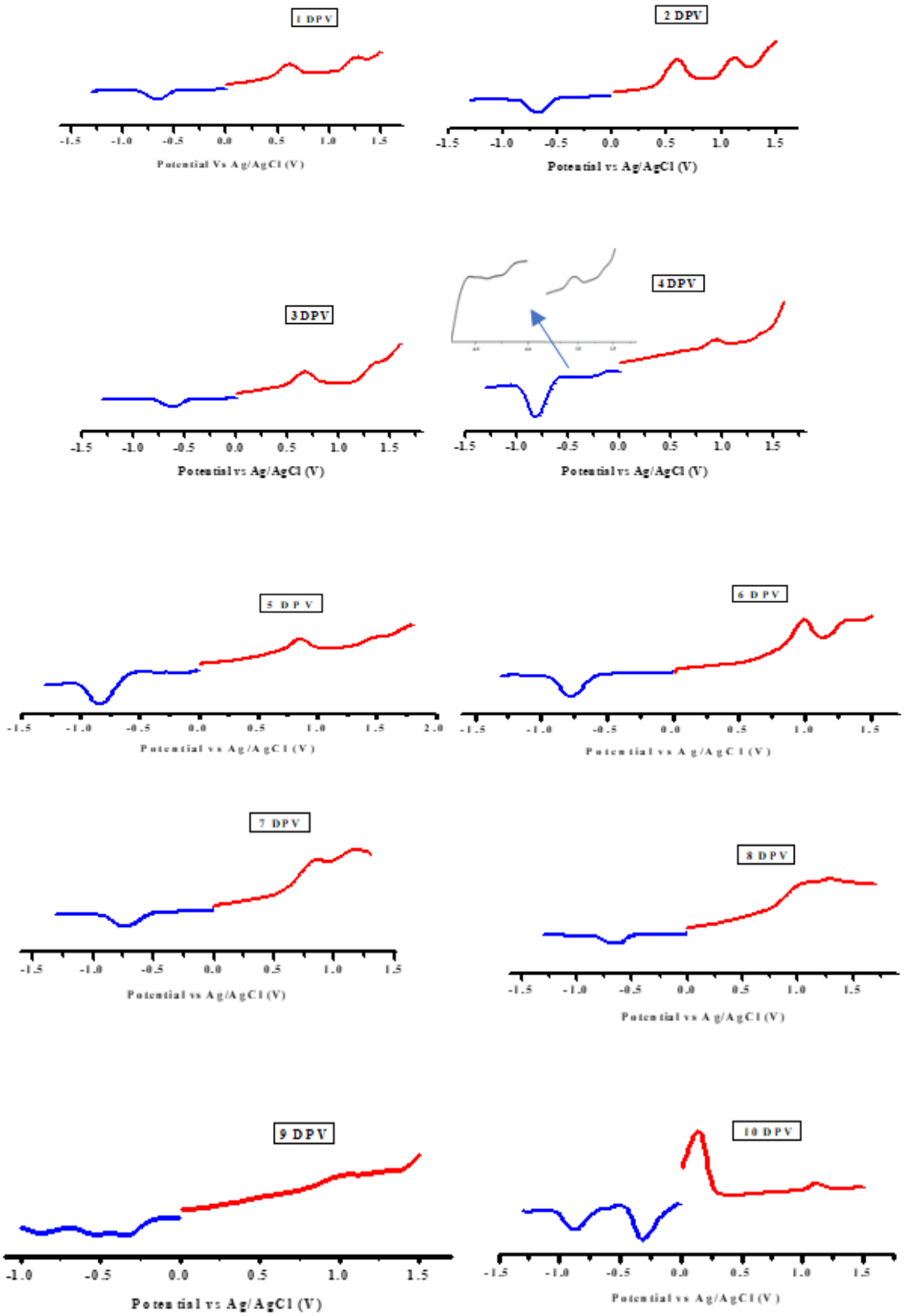

Figure 3.2. CV and DPV plots of the push–pull BODIPYs **1**–**10** in 0.1 M solution of Bu_4NPF_6 using DCM at 100 mV s^{-1} scan rate *versus* Ag/AgCl at 25 °C.

The push–pull BODIPYs **1–10** exhibit multiple oxidations and reduction waves at different potentials, which play a key role in determining the donor ability in the electron transfer process. The phenothiazine exhibits one reversible oxidation wave at low potential [44], and the BODIPY unit exhibits one oxidation and one reduction wave, each signifying the formation of a mono π-radical cation and a mono π-radical anion.[45] The oxidation and reduction potential values of the push–pull BODIPYs **1–10** were identified by DPV analysis. The push–pull BODIPYs **1–5** exhibit oxidation potentials at +0.61, +1.27 V; +0.61, +1.13 V; +0.68, +1.33 V; +0.95, +1.38 V; +0.86, 1.47 V and reduction potentials at –0.65 V; –0.68 V; –0.62 V; –0.23, –0.39, –0.81 V; –0.05, –0.25, –0.85 V, respectively (Table 3.1). Similarly, the BODIPYs **6–10** exhibits two oxidation potentials at +0.99, +1.30 V; +0.84, +1.17 V; +1.03, +1.28 V; +1.03, +1.26 V; +0.13, +1.09 V and reduction potentials at –0.76 V; –0.74 V; –0.64 V; –0.33, –0.52, –0.87 V; –0.31, –0.87 V, respectively (Table 3.1). The push–pull BODIPYs **1–10** exhibits two oxidation waves the first oxidation wave at lower potential due to donor phenothiazine/carbazole unit and the second oxidation wave at higher potential attributed to BODIPY unit. The BODIPYs **1–3** and **6–8** exhibit only one reduction wave due to the presence of the acceptor BODIPY unit.

The TCBD and cyclohexa-2,5-diene-1,4-ylidene-expanded TCBD substituted BODIPYs **4**, **5** and **9**, **10** exhibit two reversible reduction waves at low potential, and each step belongs to one-electron transfer and an additional one reduction wave from –0.81 to –0.87 V range which are attributed to acceptor BODIPY unit. Compared to conventional electron acceptors quinone and fullerene, the TCBD and cyclohexa-2,5-diene-1,4-ylidene-expanded TCBD functionalized BODIPYs exhibit easy reduction at a low potential.[46] The electrochemical data reveals that incorporation of a cyano-based electron acceptor can perturb the redox properties of BODIPYs and the cyclohexa-2,5-diene-1,4-ylidene-expanded TCBD unit and stabilize the LUMO energy level more as compared to TCBD unit. Comparing the first oxidation potential of phenothiazine functionalized BODIPYs **1–5**

with carbazole substituted BODIPYs **6–10** reflects that the phenothiazines are more facile to oxidize than carbazole due to the strong electron-donating nature of the phenothiazine unit.

3.5. Theoretical calculations

To understand the geometry and the electronic structures of the push–pull BODIPYs **1–10**, density functional theory (DFT) and time-dependent density functional theory (TD-DFT) calculations were performed using Gaussian 09W program at the B3LYP/6-31G (d, p) level. The frontier molecular orbitals and energy gap values of all the investigated push–pull BODIPYs **1–10** are shown in Figures 3 and 4. In the case of BODIPYs **1–3** and **6–8,** the HOMOs are delocalized over the whole molecule, whereas the LUMOs are centered on the BODIPY core. The BODIPYs **4**, **5**, **9,** and **10** exhibit non-planar molecular structure due to the incorporation of TCBD and cyclohexa-2,5-diene-1,4-diylidene-expanded TCBD moiety.

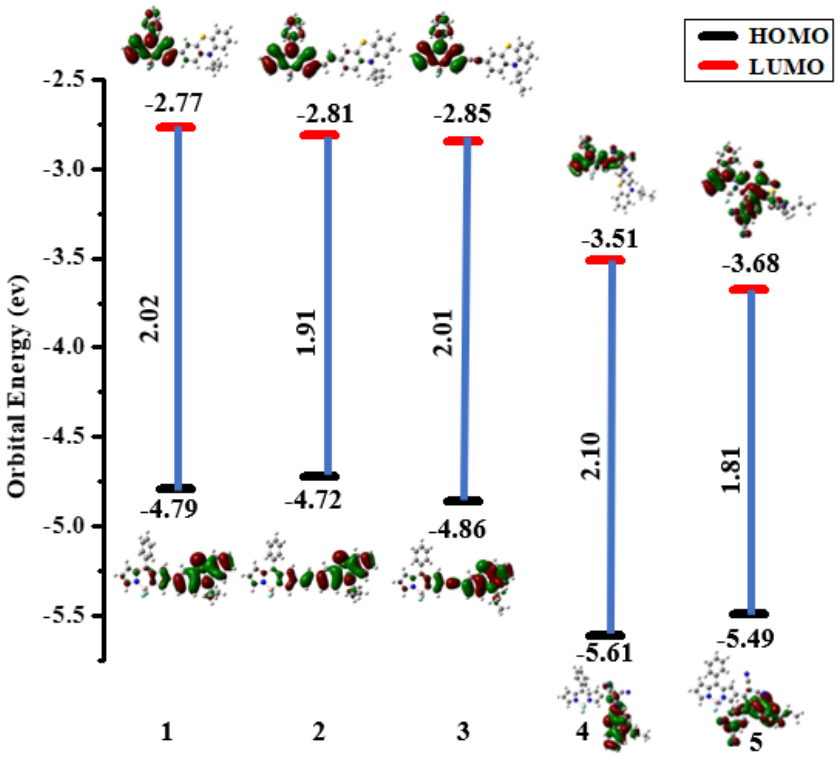

Figure 3.3. Energy profile diagram and frontier molecular orbitals of the push–pull BODIPYs **1–5** estimated by DFT calculations (B3LYP/6-31G (d,p) level).

The theoretically calculated HOMO and LUMO energy levels of multi-modular push–pull BODIPYs **1–10** shows that the donor (phenothiazine and carbazole), acceptors, and π-linker groups can tune the HOMO and LUMO energy levels. The HOMO energy levels of BODIPYs **1–10** are –4.79 eV, –4.72 eV, –4.86 eV, –5.61 eV, –5.49 eV, –5.10 eV, –4.91 eV, –5.02 eV, –5.91 eV and –5.60 eV and associated LUMO energy levels are –2.77 eV, –2.81 eV, –2.85 eV, –3.51 eV, –3.68 eV, –2.62 eV, –2.66 eV, –2.70 eV, –3.37 eV and –3.56 eV, respectively (Figure 3.3 and 3.4).

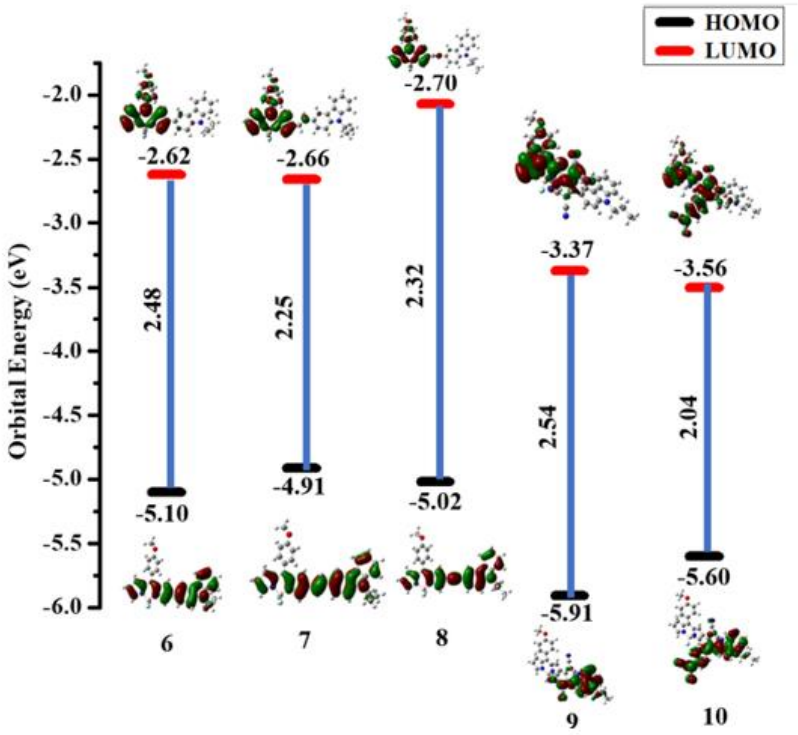

Figure 3.4. Energy profile diagram and frontier molecular orbitals of the push–pull BODIPYs **6–10** estimated by DFT calculations (B3LYP /6-31G (d, p) level).

The HOMO–LUMO gap values of the BODIPYs **1–10** are 2.02, 1.91, 1.70, 2.10, 1.81, 2.48, 2.25, 2.32, 2.53 and 2.04 eV, respectively (Figure 3.3 and 3.4). The theoretically calculated HOMO–LUMO gap of the BODIPYs **1–10** follows the trend **9>6>8>7>4>10>1>2>5>3**. The theoretically calculated HOMO–LUMO energy gap values of BODIPYs **1–10** exhibit good agreement with experimentally calculated optical bandgap (E_{gap}) values. In the case of BODIPYs **4**, **5, 9,** and **10**, the

HOMOs are delocalized over donor phenothiazine and carbazole units, while LUMOs are mainly centered on the acceptor TCBD and cyclohexa-2,5-diene-1,4-ylidene-expanded TCBD unit, which shows good electronic communication between donor and acceptor unit. The cyclohexa-2,5-diene-1,4-ylidene-expanded TCBD functionalized BODIPYs exhibit low LUMO energy levels as compared to TCBD substituted BODIPYs due to strong donor–acceptor interactions.

Table 3.2. Theoretically calculated electronic transitions for the push–pull BODIPYs **1–10**.

BODIPYs	**Wavelength (nm)**	**Composition**	**f[a]**	**Assignment**
1	381	HOMO-1→LUMO (0.55)	0.24	π–π*
	476	HOMO→LUMO (0.58)	0.63	π–π*
2	380	HOMO-1→LUMO (0.45)	0.15	π–π*
	501	HOMO→LUMO (0.55)	0.82	π–π*
3	471	HOMO→LUMO (0.51)	0.87	π–π*
4	425	HOMO-1→LUMO (0.56)	0.61	π–π*
	443	HOMO→LUMO+1 (0.42)	0.72	ICT
5	571	HOMO-1→LUMO (0.60)	0.11	π–π*
	668	HOMO→LUMO+1 (0.64)	0.20	ICT
6	361	HOMO-2→LUMO (0.47)	0.29	π–π*
	464	HOMO→LUMO (0.62)	0.66	π–π*
7	366	HOMO-2→LUMO (0.44)	0.28	π–π*
	494	HOMO→LUMO (0.62)	0.78	π–π*
8	364	HOMO-3→LUMO (0.53)	0.31	π–π*
	466	HOMO→LUMO (0.59)	0.83	π–π*
9	399	HOMO→LUMO+1 (0.44)	0.43	π–π*
	431	HOMO-1→LUMO (0.44)	0.96	ICT
10	443	HOMO-2→LUMO (0.48)	0.75	π–π*
	538	HOMO→LUMO (0.67)	1.19	ICT

f[a] oscillator strength

The time-dependent DFT calculation was performed to evaluate the electronic transitions of push–pull BODIPYs **1–4** and **6–10** at CAM-B3LYP/6-31G (d, p) level in DCM solvent, and for BODIPY **5** the B3LYP/6-31G (d, p) level in gas phase used for calculation. The TD-DFT data of push–pull BODIPYs **1–10** are compiled in Table 3.2. The polarized continuum model (PCM) was used to analyse the solvent effect in TD-DFT calculation. The push–pull BODIPYs **1–3** and **6–8** exhibit two major electronic absorption bands in the UV-vis region in which both the absorption bands correspond to the π–π* transition. The absorption band of BODIPY **1** and **6** obtained at 476 nm and 464 nm respectively, originating from HOMO → LUMO due to the π–π* transition (Figure 3.5). The cyclohexa-2,5-diene-1,4-ylidene-expanded TCBD substituted push–pull BODIPYs **5** and **10** exhibits absorption bands at 571 nm, 668 nm, and 443 nm, 538 nm, respectively, in which the absorption spectra in the lower wavelength region corresponds to π–π* transition and the spectra in the longer wavelength region corresponds to the ICT transition. The absorption band at lower wavelength region originating from HOMO–1 → LUMO at 571 nm for BODIPY **5** and HOMO–2 → LUMO at 443 nm for BODIPY **10**, attributed to π–π* transition. The push–pull BODIPY **5** shows a strong absorption band at longer wavelength region which corresponds from HOMO → LUMO+1 at 668 nm attributed to the intramolecular charge transfer (ICT) transition. The BODIPY **10** exhibits an absorption band at 538 nm, occurs from HOMO → LUMO which belongs to the ICT transition from donor to acceptor unit (Figure 3.6). Overall, the TD-DFT calculations suggest that the intramolecular charge transfer (ICT) band of the BODIPYs **5** and **10** exhibits a bathochromic shift with low HOMO–LUMO gap as compared to the TCBD substituted BODIPYs **4**

and **8** due to strong accepting nature of the cyclohexa-2,5-diene-1,4-ylidene-expanded TCBD unit.

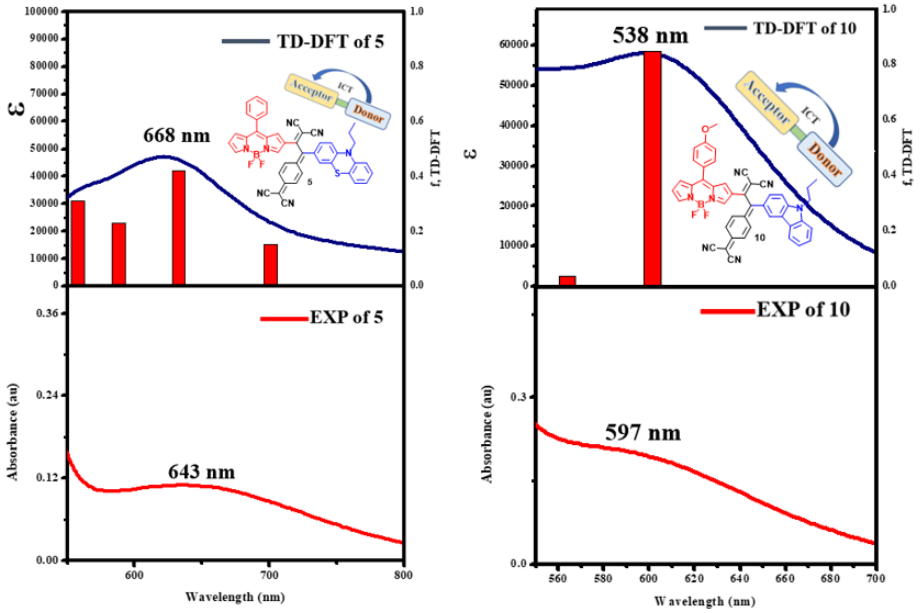

Figure 3.5. UV-vis absorption spectra of the push–pull BODIPYs **1** and **6**. Experimental (bottom) and TD-DFT predicted (top) in DCM solvent.

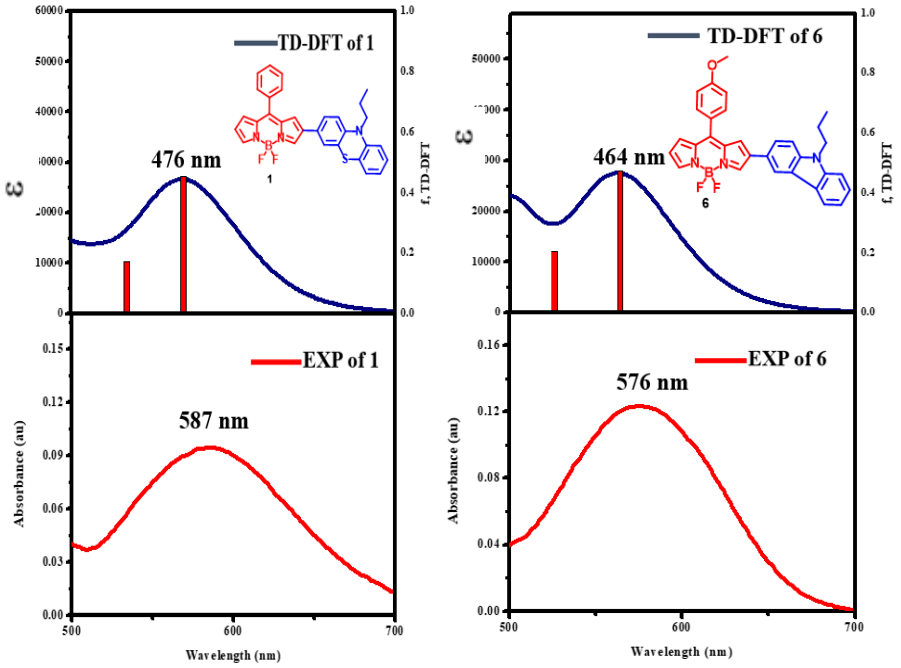

Figure 3.6. UV-vis absorption spectra of the push–pull BODIPYs **5** and **10**. Experimental (bottom) and TD-DFT predicted (top).

The theoretically calculated electronic transitions were observed more than the experimental values due to many factors like solvent effect, temperature, and dipole moment. The UV-vis transitions with composition, assignment, and oscillator strength are shown in Table 3.2.

3.6. Experimental Section

General Methods

All the moisture and oxygen-sensitive reactions were performed in an inert atmosphere using the standard inert atmosphere method. ^{1}H NMR was measured in Bruker Avance (III) 400 MHz, and ^{13}C NMR spectra were measured in 100 MHz using $CDCl_3$ as the internal solvent. The ^{1}H NMR chemical shifts are recorded in parts per million (ppm) relative to the solvent residual peak ($CDCl_3$, 7.26 ppm). The ^{13}C NMR shifts are reported relative to the solvent residual peak ($CDCl_3$, 77.00 ppm). The multiplicities are given as s (singlet), d (doublet), t (triplet), q (quartet), m (multiplet), and the coupling constants values (*J*) are reported in Hz. The UV-visible absorption spectra of all compounds were recorded in PerkinElmer's LAMBDA 35 UV-visible Spectrophotometer in DCM solvent at room temperature. High-Resolution Mass Spectrometry (HRMS) was recorded on a Bruker-Daltonics micrOTOF-Q II mass spectrometer. Cyclic voltammogram and differential voltammogram (DPVs) were recorded on an electrochemical analyzer using glassy carbon as the working electrode, Pt wire as the counter electrode, and the Ag/AgCl as the reference electrode.

Synthesis and characterization of BODIPY 1: Compound **11** (0.1 g, 0.25 mmol), compound **12** (0.102 g, 0.27 mmol), $Pd(PPh_3)_4$ (0.015 g, 0.01 mmol), and potassium carbonate (0.115 g, 0.83 mmol) was dissolved in Toluene/ethanol/ water (9/3/1 v/v/v) and heated to reflux for 12 h under a nitrogen atmosphere. The reaction mixture was cooled to room temperature and poured into water. The organic layer was extracted with dichloromethane and the combined organic layers were washed with saturated brine solution and water and dried over anhydrous sodium sulphate. After filtration and solvent evaporation, the

residue was purified by silica-gel column chromatography using hexane/dichloromethane (60/40 v/v) as the eluent. A light purple solid of BODIPY **1** was obtained in 75% yield (0.096 g). **^{1}H NMR ($CDCl_3$, 400 MHz, ppm):** δ 8.22 (s, 1H), 7.93 (s, 1H), 7.64-7.55 (m, 5H), 7.31-7.27 (m, 2H), 7.16-7.11 (m, 2H), 6.99 (s, 1H), 6.92-6.89 (m, 2H), 6.86-6.82 (m, 2H), 6.55 (s, 1H), 3.82 (t, *J* = 4 Hz, 2H), 1.87-1.79 (m, 2H), 1.01 (t, *J* = 8 Hz, 3H). **^{13}C NMR ($CDCl_3$, 100 MHz, ppm):** 146.5, 144.8, 144.6, 143.7, 142.0, 135.6, 135.0, 133.8, 131.1, 130.7. 130.4, 128.5, 127.4, 127.2, 126.8, 125.4, 124.5, 124.2, 124.1, 124.1, 122.4, 118.3, 115.5, 115.4, 49.1, 20.0, 11.2; **HRMS (ESI, positive)** m/z calculated for $C_{30}H_{24}BF_2N_3S$ 507.1752 $[M]^+$,measured 507.1769 $[M]^+$.

Synthesis and characterization of BODIPY 2: Compound **11** (0.1 g, 0.25 mmol), compound **13** (0.074 g, 0.27 mmol), palladium acetate (0.003 g, 0.01 mmol), potassium carbonate (0.042 g, 0.30 mmol), and tetra-*n*-butylammonium bromide (0.098 g, 0.30 mmol) were mixed with 20 ml DMF. The reaction mixture was heated under Ar atm at 110 °C for 12 h. The resultant mixture was diluted with DCM and washed with 1 N HCl solution. The organic layer was collected, dried over anhydrous Na_2SO_4 and evaporated under vacuum. The solid was adsorbed on silica gel and purified by column chromatography, using hexane/dichloromethane (60/40 v/v) as the eluent. A dark green solid of BODIPY **2** was obtained in 35% yield (0.047 g). **^{1}H NMR ($CDCl_3$, 400 MHz, ppm):** δ 8.14 (s, 1H), 7.92 (s, 1H), 7.59-7.54 (m, 5H), 7.21-7.12 (m, 4H), 6.91-6.80 (m, 7H), 6.55 (s, 1H), 3.82 (t, *J* = 4 Hz, 2H), 1.86-1.81 (m, 2H), 1.02 (t, *J* = 4 Hz, 3H). **^{13}C NMR ($CDCl_3$, 100 MHz, ppm):** 146.2, 144.8, 143.5, 143.5, 135.6, 135.0, 133.9, 132.6, 131.4, 130.9, 130.7, 130.4, 128.5, 128.3, 127.5, 127.4, 127.2, 125.7, 125.4, 124.7, 124.2, 123.5, 122.4, 118.2, 117.7, 115.9, 115.4, 115.3, 49.2, 20.1, 11.3; **HRMS (ESI, positive)** m/z calculated for $C_{32}H_{26}BF_2N_3S$ 533.1909 $[M]^+$, measured 533.1927 $[M]^+$.

Synthesis and characterization of BODIPY 3: Under argon atmosphere a solution of compound **11** (0.1 g, 0.25 mmol) and the corresponding compound **14** (0.074 g, 0.27 mmol) in dry THF (20 ml),

added *N*,*N*-Diisopropylethylamine (DIPEA) (20 ml), $Pd(PPh_3)_4$ (0.016 g, 0.014 mmol), CuI (0.002 g, 0.014 mmol), stirred for 12 h at 60 ^oC, after completion of the reaction, the reaction mixture was concentrated under reduced pressure, the crude compound was purified by column chromatography on silica, using Hexane/DCM (70:30, v/v), and afforded pure BODIPY **3** (Purple colour) around 70% yield. **^{1}H NMR ($CDCl_3$, 400 MHz, ppm):** δ 8.01 (d, *J* = 16 Hz, 2H), 7.16-7.52 (m, 5H), 7.23-7.20 (m, 2H), 7.16-7.10 (m, 2H), 6.99 (s, 2H), 6.91 (t, *J* = 4 Hz, 1H), 6.84 (d, *J* = 8 Hz, 1H), 6.76 (d, *J* = 8 Hz, 1H), 6.59 (s, 1H), 3.80 (t, *J* = 8 Hz, 2H), 1.86-1.77 (m, 2H), 1.00 (t, *J* = 8 Hz, 3H). **^{13}C NMR ($CDCl_3$, 100 MHz, ppm):** 147.2, 145.6, 145.4, 144.5, 135.5, 134.2, 133.4, 132.4, 131.5, 130.9, 130.5, 130.4, 129.9, 128.5, 127.4, 127.3, 124.7, 124.0, 122.7, 119.1, 116.5, 115.5, 115.0, 91.5, 81.8, 49.2, 20.0, 11.2; **HRMS (ESI, positive)** m/z calculated for $C_{32}H_{24}BF_2N_3S$ 532.1830 $[M + H]^+$, measured 532.1838 $[M + H]^+$.

Synthesis and characterization of BODIPY 4: In a 50 mL round bottomed flask, tetracyanoethylene (TCNE, 24 mg, 0.1 mmol) was added to solution of compound **3** (100 mg, 0.1 mmol) in DCM (20 mL). The reaction mixture was stirred in room temperature for 6 h. After completion of reaction, the reaction mix. was dried under vacuum and purified by column chromatography with hexane/DCM (30:70, v/v) as eluent to give BODIPY **4** as dark red solid (Yield: 76%). **^{1}H NMR (400 MHz, $CDCl_3$):** *δ* 8.27 (s, 1H), 7.92 (s, 1H), 7.73-7.61 (m, 7H), 7.35 (s, 1H), 7.28 (s, 1H), 7.17 (t, *J* = 8 Hz, 1H), 7.06 (d, *J* = 8 Hz, 1H), 6.99 (t, *J* = 8 Hz, 1H), 6.90-6.82 (m, 3H), 3.86 (t, *J* = 8 Hz, 2H), 1.90-1.81 (m, 2H), 1.04 (t, *J* = 8 Hz, 3H). **^{13}C NMR ($CDCl_3$, 100 MHz, ppm):** *δ* 162.3, 159.0, 152.0, 151.4, 148.7, 141.8, 141.5, 138.0, 136.5, 135.6, 132.3, 132.2, 130.6, 130.3, 129.1, 127.9, 127.6, 127.5, 126.6, 125.5, 124.5, 123.8, 122.5, 116.2, 115.1, 112.8, 112.7, 112.1, 111.6, 80.0, 79.9, 49.9, 20.0, 11.1; **HRMS (ESI, positive)** m/z calculated for $C_{38}H_{24}BF_2N_7S$ 660.1954 $[M + H]^+$, measured 660.1966 $[M + H]^+$.

Synthesis and characterization of BODIPY 5: In 50 mL round bottomed flask, tetracyanoquinodimethane (TCNQ, 38 mg, 0.1 mmol)

was added to solution of compound **3** (100 mg, 0.1 mmol) in DCE (20 ml) under argon atmosphere. The reaction mixture was heated at 60 °C for overnight. After completion of reaction, the reaction mixture was dried under vacuum and purified by column chromatography with hexane/DCM (20:80, v/v) (eluent: CH_2Cl_2) BODIPY **5** as dark black (Yield: 71%). **^{1}H NMR (400 MHz, $CDCl_3$):** δ 8.22 (s, 1H), 7.87 (s, 1H), 7.68 (t, *J* = 8 Hz, 1H), 7.62-7.55 (m, 5H), 7.50-7.47 (m, 1H), 7.31-7.29 (m, 1H), 7.24-7.07 (m, 5H), 7.01-6.92 (m, 3H), 6.89-6.86 (m, 2H), 6.78 (d, *J* = 4 Hz, 1H), 3.85 (t, *J* = 8 Hz, 2H), 1.90-1.81 (m, 2H), 1.04 (t, *J* = 8 Hz, 3H); **^{13}C NMR (100 MHz, $CDCl_3$, ppm):** δ 162.5, 154.0, 151.4, 148.8, 148.6, 147.9, 142.8, 142.5, 136.2, 134.4, 133.8, 132.3, 132.2, 131.6, 130.5, 129.0, 128.8, 127.7, 127.5, 126.3, 125.9, 125.8, 123.8, 122.9, 122.8, 116.0, 115.4, 113.7, 113.5, 112.5, 80.5, 75.9, 49.7, 20.0, 11.1; **HRMS (ESI, positive)** m/z $[M]^+$ calculated for $C_{44}H_{28}BF_2N_7S$ 737.2268, measured 737.2309 $[M]^+$.

Synthesis and characterization of BODIPY 6: Compound **15** (0.1 g, 0.23 mmol), Compound **16** (0.086 g, 0.25 mmol), $Pd(PPh_3)_4$ (0.013 g, 0.01 mmol), and potassium carbonate (0.107 g, 0.77 mmol) was dissolved in Toluene/ethanol/ water (9/3/1 v/v/v) and heated to reflux for 12 h under a nitrogen atmosphere. The reaction mixture was cooled to room temperature and poured into water. The organic layer was extracted with dichloromethane and the combined organic layers were washed with saturated brine solution and water and dried over anhydrous sodium sulphate. After filtration and solvent evaporation, the residue was purified by silica-gel column chromatography using hexane/dichloromethane (60/40 v/v) as the eluent. A light purple solid of BODIPY **6** was obtained in 72% yield (0.085 g). **^{1}H NMR ($CDCl_3$, 400 MHz, ppm):** δ 8.42 (s, 1H), 8.27 (s, 1H), 8.12 (d, *J* = 8 Hz, 1H), 7.92 (s, 1H), 7.65 (d, *J* = 8 Hz, 3H), 7.49 (t, *J* = 8 Hz, 1H), 7.43-7.41 (m, 2H), 7.25-7.22 (m, 2H), 7.12 (d, *J* = 8 Hz, 2H), 6.97 (s, 1H), 6.56 (s, 1H), 4.29 (t, *J* = 8 Hz, 2H), 3.96 (s, 3H), 1.97-1.90 (m, 2H), 0.99 (t, *J* = 8 Hz, 3H). **^{13}C NMR ($CDCl_3$, 100 MHz, ppm):** 162.0, 146.5, 144.8, 144.7, 143.7, 142.4, 142.0, 135.7, 135.0, 133.8, 132.4, 131.19, 130.7,

130.4, 128.5, 127.4, 127.3, 126.8, 125.9, 125.5, 124.5, 124.2, 124.1, 123.5, 122.5, 120.4, 119.0, 118.3, 117.2, 115.5, 115.4, 114.1, 109.1, 108.9, 55.5, 49.2, 20.1, 11.3; **HRMS (ESI, positive)** m/z calculated for $C_{31}H_{26}BF_2N_3O$ 528.2035 $[M + Na]^+$, measured 528.2071 $[M + Na]^+$.

Synthesis and characterization of BODIPY 7: *β*-mono-iodo BODIPY **15** (0.1 g, 0.23 mmol), compound **17** (0.060 g, 0.25 mmol), palladium acetate (0.003 g, 0.01 mmol), potassium carbonate (0.039 g, 0.28 mmol), and tetra-*n*-butylammonium bromide (0.091 g, 0.28 mmol) were mixed with 20 ml DMF. The reaction mixture was heated under Ar atm at 110 °C for 12 h. The resultant mixture was diluted with DCM and washed with 1 N HCl solution. The organic layer was collected, dried over anhydrous Na_2SO_4 and evaporated under vacuum. The solid was adsorbed on silica gel and purified by column chromatography, using hexane/dichloromethane (60/40 v/v) as the eluent. A dark green solid of BODIPY **7** was obtained in 40% yield (0.050 g). **^{1}H NMR ($CDCl_3$, 400 MHz, ppm):** δ 8.20 (s, 1H), 8.16 (s, 1H), 8.11 (d, *J* = 8 Hz, 2H), 7.90 (s, 1H), 7.62-7.59 (m, 2H), 7.48 (t, *J* = 8 Hz, 1H), 7.42-7.38 (m, 2H), 7.25-7.24 (m, 1H), 7.18 (s,1H), 7.15 (s, 1H), 7.10 (d, *J* = 8 Hz, 2H), 7.01 (s, 1H), 6.97-6.96 (m, 1H), 6.55 (s, 2H), 4.28 (t, *J* = 8 Hz, 2H), 3.95 (s, 3H), 1.97-1.90 (m, 2H), 0.99 (t, *J* = 8 Hz, 3H). **^{13}C NMR ($CDCl_3$, 100 MHz, ppm):** 162.0, 143.1, 142.5, 140.9, 140.4, 134.9, 132.4, 130.5, 128.2, 126.5, 125.8, 125.1, 124.2, 123.2, 122.8, 120.4, 119.1, 118.5, 117.1, 116.8, 114.1, 109.0, 55.5, 44.7, 22.3, 11.7; **HRMS (ESI, positive)** m/z calculated for $C_{33}H_{28}BF_2N_3O$ 531.2294 $[M]^+$, measured 531.2308 $[M]^+$.

Synthesis and characterization of BODIPY 8: Under argon atmosphere a solution of compound **15** (0.1 g, 0.23 mmol) and the corresponding compound **18** (0.060 g, 0.25 mmol) in dry THF (20 ml), added *N*,*N*-Diisopropylethylamine (DIPEA) (20 ml), $Pd(PPh_3)_2Cl_2$ (0.008 g, 0.011 mmol), CuI (0.002 g, 0.011 mmol), stirred for 12 h at 60 °C, after completion of the reaction, the reaction mixture was concentrated under reduced pressure, the crude compound was purified by column chromatography on silica, using Hexane/DCM (70:30, v/v),

and afforded pure BODIPY **8** (Purple colour) around 60% yield (0.074 g). **^{1}H NMR ($CDCl_3$, 400 MHz, ppm** δ 8.24 (s, 1H), 8.08-8.07 (m, 2H), 7.97 (s, 1H), 7.48 (t, *J* = 8 Hz, 1H), 7.41 (d, *J* = 8 Hz, 1H), 7.36 (d, *J* = 8 Hz, 2H), 7.08 (t, *J* = 8 Hz, 3H),7.03 (d, *J* = 4 Hz, 1H), 6.58 (s, 1H), 4.27 (t, *J* = 8 Hz, 2H), 3.93 (s, 3H), 1.95-1.89 (m, 2H), 0.98 (t, *J* = 4 Hz, 3H). **^{13}C NMR ($CDCl_3$, 100 MHz, ppm):** 162.2, 147.1, 145.1, 144.2, 140.8, 140.1, 135.3,134.1, 132.4, 131.9, 131.4, 129.0, 126.1, 123.8, 122.8, 122.3, 120.4, 119.3, 118.7, 114.1, 112.8, 108.9, 108.7, 93.4, 80.2, 55.5, 44.7, 22.2, 11.7; **HRMS (ESI, positive)** m/z calculated for $C_{33}H_{26}BF_2N_3O$ 552.2035 $[M + Na]^+$, measured 552.2067 $[M + Na]^+$.

Synthesis and characterization of BODIPY 9: In a 50 mL round bottomed flask, tetracyanoethylene (TCNE, 12 mg, 0.09 mmol) was added to solution of compound **8** (50 mg, 0.09 mmol) in DCM (20 mL). The reaction mixture was stirred in room temperature for 6 h. After completion of reaction, the reaction mix. was dried under vacuum and purified by column chromatography with hexane/DCM (50:50, v/v) as eluent to give BODIPY **9** as dark red solid 80% yield (0.049 g). **^{1}H NMR ($CDCl_3$, 400 MHz, ppm)** δ 8.57 (s, 1H), 8.19 (s, 1H), 8.14 (d, *J* = 8 Hz, 1H), 7.98-7.94 (m, 2H), 7.78 (s, 1H), 7.61-7.55 (m, 3H), 7.51-7.47 (m, 2H), 7.35 (t, *J* = 8 Hz, 1H), 7.29 (d, *J* = 4 Hz, 1H), 7.12 (d, *J* = 8 Hz, 2H), 6.81 (d, *J* = 4 Hz, 1H), 4.33 (t, *J* = 4 Hz, 2H), 3.94 (s, 3H), 2.00-1.92 (m, 2H), 1.01 (t, *J* = 4 Hz, 3H). **^{13}C NMR ($CDCl_3$, 100 MHz, ppm):** 165.4, 163.5, 160.0, 150.5, 148.7, 144.1, 141.4, 141.3, 137.5, 136.1, 135.6, 132.9, 127.3, 126.5, 124.9, 124.2, 123.0, 122.5, 122.4, 121.3, 121.2, 121.1, 114.8, 113.4, 113.1, 112.4, 111.8, 110.2, 109.8, 80.0, 79.8, 55.7, 45.1, 22.3, 11.7; **HRMS (ESI, positive)** m/z calculated for $C_{39}H_{26}BF_2N_7O$ 680.2159 $[M + Na]^+$,measured 680.2160 $[M + Na]^+$.

Synthesis and characterization of BODIPY 10: In 50 mL round bottomed flask, tetracyanoquinodimethane (TCNQ, 19 mg, 0.09 mmol) was added to solution of compound **8** (50 mg, 0.09 mmol) in DCE (20 mL) under argon atmosphere. The reaction mixture was heated at 60 °C for overnight. After completion of reaction, the reaction mixture was dried under vacuum and purified by column chromatography with

hexane/DCM (20:80, v/v) as eluent to give BODIPY **10** as dark black solid 73% yield (0.050 g). **^{1}H NMR ($CDCl_3$, 400 MHz, ppm):** δ 8.13 (s, 1H), 8.11-8.10 (m, 1H), 7.93 (s, 1H), 7.71 (s, 1H) 7.61 (d, *J* = 4 Hz, 1H), 7.59 (d, *J* = 4 Hz, 1H), 7.56 (s, 3H), 7.53 (s, 1H), 7.51 (s, 1H), 7.48 (s, 2H), 7.46 (s, 1H), 7.35 (s, 1H), 7.34-7.33 (m, 1H), 7.24-7.22 (m, 1H), 7.08 (d, *J* = 4 Hz, 1H), 7.06-7.05 (m, 1H), 6.76 (d, *J* = 4 Hz, 1H), 4.32 (t, *J* = 4 Hz, 2H), 3.91 (s, 3H), 1.99-1.92 (m, 2H), 1.01 (t, *J* = 4 Hz, 3H). **^{13}C NMR ($CDCl_3$, 100 MHz, ppm):** 163.4, 154.2, 151.2, 150.0, 142.5, 142.3, 141.2, 135.9, 135.7, 134.3, 132.8, 132.3, 131.1, 129.2, 127.3, 127.1, 126.3, 125.9, 125.6, 125.0, 124.3, 124.1, 122.3, 121.0, 120.6, 114.7, 113.9, 110.0, 109.6, 80.4, 74.9, 55.6, 45.0, 22.3, 11.7; **HRMS (ESI, positive)** m/z calculated for $C_{45}H_{30}BF_2N_7O$ 756.2473 $[M + Na]^+$, measured 756.2471 $[M + Na]^+$.

3.7. Conclusion

The design and synthesis of push–pull BODIPYs **1**–**10** *via* Pd-catalyzed Suzuki, Heck, Sonogashira cross-coupling, and [2+2] cycloaddition−retroelectrocyclization reactions in good yields were explored. The UV-visible absorption spectra of cyclohexa-2,5-diene-1,4-ylidene-expanded TCBD functionalized BODIPYs exhibit intramolecular charge transfer (ICT) band in the longer wavelength region as compared to TCBD substituted BODIPYs due to strong donor–acceptor interactions. The electrochemical studies of push–pull BODIPYs **4**, **5**, **9** and **10** demonstrate that the cyclohexa-2,5-diene-1,4-ylidene-expanded TCBD unit acts as a strong electron acceptor and exhibit multiple reduction wave at low potential as compared to TCBD unit. The theoretically predicted HOMOs of BODIPYs **1–10** are delocalized on the donor phenothiazine and carbazole unit, whereas the LUMOs are localized over acceptor BODIPY, TCBD, and cyclohexa-2,5-diene-1,4-ylidene-expanded TCBD unit. These findings suggest that the introduction of strong acceptor cyclohexa-2,5-diene-1,4-ylidene-expanded TCBD decreases the HOMO–LUMO gap more as compared to the TCBD unit which resulted in a bathochromic shift in UV-vis spectra. This research work opens new avenue to explore the design and

synthesis of push–pull chromophores with low HOMO–LUMO gap for various optoelectronic applications.

3.8. References

1. Cherumukkil, S., Ghosh, S., Praveen, V. K., & Ajayaghosh, A. (2017). An unprecedented amplification of near-infrared emission in a Bodipy derived π-system by stress or gelation. *Chemical Science*, *8*(8), 5644–5649. https://doi.org/10.1039/C7SC01696D

2. Poddar, M., Sharma, V., Mobin, S. M., & Misra, R. (2018). 1,8-Naphthalimide-Substituted BODIPY Dyads: Synthesis, Structure, Properties, and Live-Cell Imaging. *Chemistry – An Asian Journal*, *13*(19), 2881–2890. https://doi.org/10.1002/asia.201800816

3. Dhokale, B., Gautam, P., Mobin, S. M., & Misra, R. (2013). Donor–acceptor, ferrocenyl substituted BODIPYs with marvelous supramolecular interactions. *Dalton Transactions*, *42*(5), 1512–1518. https://doi.org/10.1039/C2DT31632C

4. Gautam, P., Yu, C. P., Zhang, G., Hillier, V. E., & Chan, J. M. W. (2017). Pulling with the Pentafluorosulfanyl Acceptor in Push–Pull Dyes. *The Journal of Organic Chemistry*, *82*(20), 11008–11020. https://doi.org/10.1021/acs.joc.7b01972

5. Homnick, P. J., Tinkham, J. S., Devaughn, R., & Lahti, P. M. (2014). Engineering Frontier Energy Levels in Donor–Acceptor Fluoren-9-ylidene Malononitriles versus Fluorenones. *The Journal of Physical Chemistry A*, *118*(2), 475–486. https://doi.org/10.1021/jp407854r

6. Sartor, S. M., Lattke, Y. M., McCarthy, B. G., Miyake, G. M., & Damrauer, N. H. (2019). Effects of Naphthyl Connectivity on the Photophysics of Compact Organic Charge-Transfer Photoredox Catalysts. *The Journal of Physical Chemistry A*, *123*(22), 4727–4736. https://doi.org/10.1021/acs.jpca.9b03286

7. Dhindsa, J. S., Buguis, F. L., Anghel, M., & Gilroy, J. B. (2021). Band Gap Engineering in Acceptor-Donor-Acceptor Boron Difluoride Formazanates. *The Journal of Organic Chemistry*, *86*(17), 12064–12074. https://doi.org/10.1021/acs.joc.1c01416

8. Rout, Y., Montanari, C., Pasciucco, E., Misra, R., & Carlotti, B. (2021). Tuning the Fluorescence and the Intramolecular Charge Transfer of Phenothiazine Dipolar and Quadrupolar Derivatives by Oxygen Functionalization. *Journal of the American Chemical Society*, *143*(26), 9933–9943. https://doi.org/10.1021/jacs.1c04173

9. Popere, B. C., Della Pelle, A. M., & Thayumanavan, S. (2011). BODIPY-Based Donor–Acceptor π-Conjugated Alternating Copolymers. *Macromolecules*, *44*(12), 4767–4776. https://doi.org/10.1021/ma200839q

10. Gómez, A. M., Uriel, C., Oliden-Sánchez, A., Bañuelos, J., Garcia-Moreno, I., & López, J. C. (2021). A Concise Route to Water-Soluble 2,6-Disubstituted BODIPY-Carbohydrate Fluorophores by Direct Ferrier-Type C-Glycosylation. *The Journal of Organic Chemistry*, *86*(13), 9181–9188. https://doi.org/10.1021/acs.joc.1c00413

11. Wang, J.-L., Zhang, L., Zhao, M.-J., Zhang, T., Liu, Y., & Jiang, F.-L. (2021). Mitochondria-Targeted BODIPY Nanoparticles for Enhanced Photothermal and Photoacoustic Imaging In Vivo. *ACS Applied Bio Materials*, *4*(2), 1760–1770. https://doi.org/10.1021/acsabm.0c01509

12. Lu, H., Mack, J., Yang, Y., & Shen, Z. (2014). Structural modification strategies for the rational design of red/NIR region BODIPYs. *Chemical Society Reviews*, *43*(13), 4778–4823. https://doi.org/10.1039/C4CS00030G

13. Umasekhar, B., Ganapathi, E., Chatterjee, T., & Ravikanth, M. (2015). Synthesis, structure, and spectral, electrochemical and fluoride sensing properties of meso-pyrrolyl boron dipyrromethene. *Dalton*

Transactions, *44*(37), 16516–16527. https://doi.org/10.1039/C5DT02634B

14. Bui, H. T., Mai, D. K., Kim, B., Choi, K.-H., Park, B. J., Kim, H.-J., & Cho, S. (2019). Effect of Substituents on the Photophysical Properties and Bioimaging Application of BODIPY Derivatives with Triphenylamine Substituents. *The Journal of Physical Chemistry B*, *123*(26), 5601–5607. https://doi.org/10.1021/acs.jpcb.9b04782

15. Huang, Z.-S., Meier, H., & Cao, D. (2016). Phenothiazine-based dyes for efficient dye-sensitized solar cells. *Journal of Materials Chemistry C*, *4*(13), 2404–2426. https://doi.org/10.1039/C5TC04418A

16. Rout, Y., Misra, R., Singhal, R., Biswas, S., & Sharma, G. D. (2018). Phenothiazine-based small-molecule organic solar cells with power conversion efficiency over 7% and open circuit voltage of about 1.0 V using solvent vapor annealing. *Physical Chemistry Chemical Physics*, *20*(9), 6321–6329. https://doi.org/10.1039/C7CP08308D

17. Ramachandran, E., & Dhamodharan, R. (2015). Rational design of phenothiazine (PTz) and ethylenedioxythiophene (EDOT) based donor–acceptor compounds with a molecular aggregation breaker for solid state emission in red and NIR regions. *Journal of Materials Chemistry C*, *3*(33), 8642–8648. https://doi.org/10.1039/C5TC01423A

18. Poddar, M., Cesaretti, A., Ferraguzzi, E., Carlotti, B., & Misra, R. (2020). Singlet and Triplet Excited-State Dynamics of 3,7-Bis(arylethynyl)phenothiazines: Intramolecular Charge Transfer and Reverse Intersystem Crossing. *The Journal of Physical Chemistry C*, *124*(33), 17864–17878. https://doi.org/10.1021/acs.jpcc.0c01786

19. Kowalski, J. A., Casselman, M. D., Kaur, A. P., Milshtein, J. D., Elliott, C. F., Modekrutti, S., … Odom, S. A. (2017). A stable two-electron-donating phenothiazine for application in nonaqueous redox flow batteries. *Journal of Materials Chemistry A*, *5*(46), 24371–24379. https://doi.org/10.1039/C7TA05883G

20. Sun, D., Rosokha, S. V., & Kochi, J. K. (2004). Donor−Acceptor (Electronic) Coupling in the Precursor Complex to Organic Electron Transfer: Intermolecular and Intramolecular Self-Exchange between Phenothiazine Redox Centers. *Journal of the American Chemical Society*, *126*(5), 1388–1401. https://doi.org/10.1021/ja038746v

21. Chen, S., Wang, L., Zhang, J., Hao, Z., Huang, H., & Deng, G.-J. (2017). Modular Synthesis of Carbazole-Based Conjugated Molecules through a One-Pot Annulation/Dehydrogenation Sequence. *The Journal of Organic Chemistry*, *82*(20), 11182–11191. https://doi.org/10.1021/acs.joc.7b02305

22. Reddy, G., Duvva, N., Seetharaman, S., D'Souza, F., & Giribabu, L. (2018). Photoinduced energy transfer in carbazole–BODIPY dyads. *Physical Chemistry Chemical Physics*, *20*(43), 27418–27428. https://doi.org/10.1039/C8CP05509B

23. Kato, S., Noguchi, H., Jin, S., & Nakamura, Y. (2016). Synthesis and Electronic, Optical, and Electrochemical Properties of a Series of Tetracyanobutadiene-Substituted Carbazoles. *Asian Journal of Organic Chemistry*, *5*(2), 246–256. https://doi.org/10.1002/ajoc.201500431

24. Blouin, N., & Leclerc, M. (2008). Poly(2,7-carbazole)s: Structure−Property Relationships. *Accounts of Chemical Research*, *41*(9), 1110–1119. https://doi.org/10.1021/ar800057k

25. Shoji, T., Ito, S., Toyota, K., Yasunami, M., & Morita, N. (2008). Synthesis, Properties, and Redox Behavior of Mono-, Bis-, and Tris[1,1,4,4,-tetracyano-2-(1-azulenyl)-3-butadienyl] Chromophores Binding with Benzene and Thiophene Cores. *Chemistry – A European Journal*, *14*(27), 8398–8408. https://doi.org/10.1002/chem.200701981

26. Rout, Y., Gautam, P., & Misra, R. (2017). Unsymmetrical and Symmetrical Push–Pull Phenothiazines. *The Journal of Organic Chemistry*, *82*(13), 6840–6845. https://doi.org/10.1021/acs.joc.7b00991

27. Yadav, I. S., Alsaleh, A. Z., Misra, R., & D'Souza, F. (2021). Charge stabilization *via* electron exchange: excited charge separation in

symmetric, central triphenylamine derived, dimethylaminophenyl–tetracyanobutadiene donor–acceptor conjugates. *Chemical Science*, *12*(3), 1109–1120. https://doi.org/10.1039/D0SC04648E

28. Banziger, S. D., Clendening, R. A., Oxley, B. M., & Ren, T. (2020). Spectroelectrochemical and Computational Analysis of a Series of Cycloaddition–Retroelectrocyclization-Derived Donor–Acceptor Chromophores. *The Journal of Physical Chemistry B*, *124*(52), 11901–11909. https://doi.org/10.1021/acs.jpcb.0c09450

29. Nielsen, M. B. (2023). Clicking together Alkynes and Tetracyanoethylene. *ChemPhysChem*, *24*(15), e202300236. https://doi.org/10.1002/cphc.202300236

30. Rout, Y., Chauhan, V., & Misra, R. (2020). Synthesis and Characterization of Isoindigo-Based Push–Pull Chromophores. *The Journal of Organic Chemistry*, *85*(7), 4611–4618. https://doi.org/10.1021/acs.joc.9b03267

31. Poddar, M., & Misra, R. (2017). NIR-Absorbing Donor–Acceptor Based 1,1,4,4-Tetracyanobuta-1,3-Diene (TCBD)- and Cyclohexa-2,5-Diene-1,4-Ylidene-Expanded TCBD-Substituted Ferrocenyl Phenothiazines. *Chemistry – An Asian Journal*, *12*(22), 2908–2915. https://doi.org/10.1002/asia.201700879

32. Michinobu, T. (2008). Click-Type Reaction of Aromatic Polyamines for Improvement of Thermal and Optoelectronic Properties. *Journal of the American Chemical Society*, *130*(43), 14074–14075. https://doi.org/10.1021/ja8061612

33. Sharma, R., Thomas, M. B., Misra, R., & D'Souza, F. (2019). Strong Ground- and Excited-State Charge Transfer in C_3 -Symmetric Truxene-Derived Phenothiazine-Tetracyanobutadine and Expanded Conjugates. *Angewandte Chemie*, *131*(13), 4394–4399. https://doi.org/10.1002/ange.201814388

34. Sharma, R., Maragani, R., & Misra, R. (2018). C 3-Symmetric star shaped donor–acceptor truxenes: synthesis and photophysical,

electrochemical and computational studies. *New Journal of Chemistry*, *42*(2), 882–890. https://doi.org/10.1039/C7NJ03934D

35. Kato, S., Kijima, T., Shiota, Y., Abe, T., Kuwako, S., Miyauchi, H., … Nakamura, Y. (2020). Chemical transformations of push–pull fluorenones: push–pull dibenzodicyanofulvenes as well as fluorenone– and dibenzodicyanofulvene–tetracyanobutadiene conjugates. *Organic & Biomolecular Chemistry*, *18*(22), 4198–4209. https://doi.org/10.1039/C9OB02706H

36. Kraußе, N., Kielmann, M., Ma, J., & Butenschön, H. (2015). Reactions of Alkynyl- and 1,1′-Dialkynylferrocenes with Tetracyanoethylene – Unanticipated Addition at the Less Electron-Rich of Two Triple Bonds. *European Journal of Organic Chemistry*, *2015*(12), 2622–2631. https://doi.org/10.1002/ejoc.201500105

37. Kato, S., & Diederich, F. (2010). Non-planar push–pull chromophores. *Chemical Communications*, *46*(12), 1994–2006. https://doi.org/10.1039/B926601A

38. Bui, A. T., Philippe, C., Beau, M., Richy, N., Cordier, M., Roisnel, T., … Trolez, Y. (2020). Synthesis, characterization and unusual near-infrared luminescence of 1,1,4,4-tetracyanobutadiene derivatives. *Chemical Communications*, *56*(24), 3571–3574. https://doi.org/10.1039/C9CC09560H

39. Poddar, M., Jang, Y., Misra, R., & D'Souza, F. (2020). Excited-State Electron Transfer in 1,1,4,4-Tetracyanobuta-1,3-diene (TCBD)- and Cyclohexa-2,5-diene-1,4-diylidene-Expanded TCBD-Substituted BODIPY-Phenothiazine Donor–Acceptor Conjugates. *Chemistry – A European Journal*, *26*(30), 6869–6878. https://doi.org/10.1002/chem.202000346

40. Yadav, I. S., Jang, Y., Rout, Y., Thomas, M. B., Misra, R., & D'Souza, F. (2022). Near-IR Intramolecular Charge Transfer in Strongly Interacting Diphenothiazene-TCBD and Diphenothiazene-

DCNQ Push-Pull Triads. *Chemistry – A European Journal*, *28*(25), e202200348. https://doi.org/10.1002/chem.202200348

41. Pinjari, D., Alsaleh, A. Z., Patil, Y., Misra, R., & D'Souza, F. (2020). Interfacing High-Energy Charge-Transfer States to a Near-IR Sensitizer for Efficient Electron Transfer upon Near-IR Irradiation. *Angewandte Chemie*, *132*(52), 23905–23913. https://doi.org/10.1002/ange.202013036

42. Khan, F., Jang, Y., Patil, Y., Misra, R., & D'Souza, F. (2021). Photoinduced Charge Separation Prompted Intervalence Charge Transfer in a Bis(thienyl)diketopyrrolopyrrole Bridged Donor-TCBD Push-Pull System. *Angewandte Chemie*, *133*(37), 20681–20690. https://doi.org/10.1002/ange.202108293

43. Gautam, P., Dhokale, B., Mobin, S. M., & Misra, R. (2012). Ferrocenyl BODIPYs: synthesis, structure and properties. *RSC Advances*, *2*(32), 12105–12107. https://doi.org/10.1039/C2RA21964F

44. Christensen, J. A., Phelan, B. T., Chaudhuri, S., Acharya, A., Batista, V. S., & Wasielewski, M. R. (2018). Phenothiazine Radical Cation Excited States as Super-oxidants for Energy-Demanding Reactions. *Journal of the American Chemical Society*, *140*(15), 5290–5299. https://doi.org/10.1021/jacs.8b01778

45. Gautam, P., Dhokale, B., M. Mobin, S., & Misra, R. (2012). Ferrocenyl BODIPYs: synthesis, structure and properties. *RSC Advances*, *2*(32), 12105–12107. https://doi.org/10.1039/C2RA21964F

46. Gautam, P., Misra, R., Thomas, M. B., & D'Souza, F. (2017). Ultrafast Charge-Separation in Triphenylamine-BODIPY-Derived Triads Carrying Centrally Positioned, Highly Electron-Deficient, Dicyanoquinodimethane or Tetracyanobutadiene Electron-Acceptors. *Chemistry – A European Journal*, *23*(38), 9192–9200. https://doi.org/10.1002/chem.201701604

Chapter 4

β-Functionalized Donor-Acceptor BODIPYs: Design, Synthesis and Properties

4.1. Introduction

The donor-acceptor (D-A) based π-conjugated systems have been widely studied for their valuable applications in molecular electronics, organic photovoltaics and nonlinear optics.[1–5] To achieve high efficiency in optoelectronic applications, it is essential to fine-tune the photonic and electronic properties of the donor-acceptor systems by modulating the strength of the donor/acceptor or π-linker groups.[5, 6] Recently, the BF_2-chelated dipyrromethenes have received considerable interest in the scientific community as a building component for artificial photosynthetic systems, light-harvesting arrays, fluorescent switches, tunable laser dyes, and molecular probes, among others.[7–9] The BODIPY core is electron-deficient (acceptor); therefore, incorporating electron-donating (donor) groups induces a donor-acceptor interaction in the molecule.[3] The BODIPY-based fluorophores are of considerable interest because of their remarkable optical properties, including high photostability, significant absorption coefficients, robust fluorescence quantum yields, and adjustable redox potential. These properties have a wide range of applications in optoelectronics and biological chemistry.[10–15]

Triphenylamine (TPA) has a non-planar molecular structure due to the sp^3 hybridization of nitrogen atom.[16–18] The triphenylamine is the most extensively studied donor unit in the designing of donor-acceptor chromophores due to its more vital electron-donor ability, electrochemical stability, and relatively low HOMO–LUMO gap. These properties of the triphenylamine unit make it a good candidate in photovoltaics materials, hole-transport layer in organic field-effect transistors (OFRT), organic solar cells (OSCs), and organic light-emitting diodes (OLEDs).[1, 16, 19–21] The [2+2] cycloaddition of

electron-deficient olefin bonds is one of the most straightforward and valuable reaction of acetylene-containing compounds.[22–25] Material scientists have explored the cycloaddition-retroelectrocyclization (CA–RE) reaction to synthesize non-planar π-conjugated donor-acceptor chromophores for various optoelectronic applications.[26–29] It is common for TCNE and TCNQ units to undergo two reversible one-electron reductions, which makes CA-RE derivatives suitable for use as p-type dopants in organic electronics.[26] Diederich *et al*. synthesized TCBD-linked small molecules for organic semiconductors.[24, 30–32] Michinobu *et al.* reported several TCBD derivatives, emphasizing the reactivity of the alkyne bond *via* substitution of donor unit.[33, 34] Butenschön, Soji, and Trolez *et al.* have reported various TCBD and cyclohexa-2,5-diene-1,4-ylidene-expanded TCBD functionalized push-pull chromophores and investigated their photophysical and redox properties.[35–38]

Our group reported various TCBD and cyclohexa-2,5-diene-1,4-ylidene-expanded TCBD substituted π-conjugated push-pull dyes and explored their photophysical and electrochemical properties for applications of optoelectronic devices.[39–42] In this research context, we have synthesized a new π-conjugated push-pull chromophore *via* Sonogashira cross-coupling and formal [2+2] cycloaddition retroelectrocyclization (CA–RE) reactions between electron-rich alkynes and electron-deficient olefins. These chromophores have a tunable near-infrared absorbance, amphoteric redox activity, and reduction potentials comparable to those of the organic acceptors tetracyanoethylene (TCNE) and 7,7,8,8-tetracyanoquinodimethane (TCNQ).

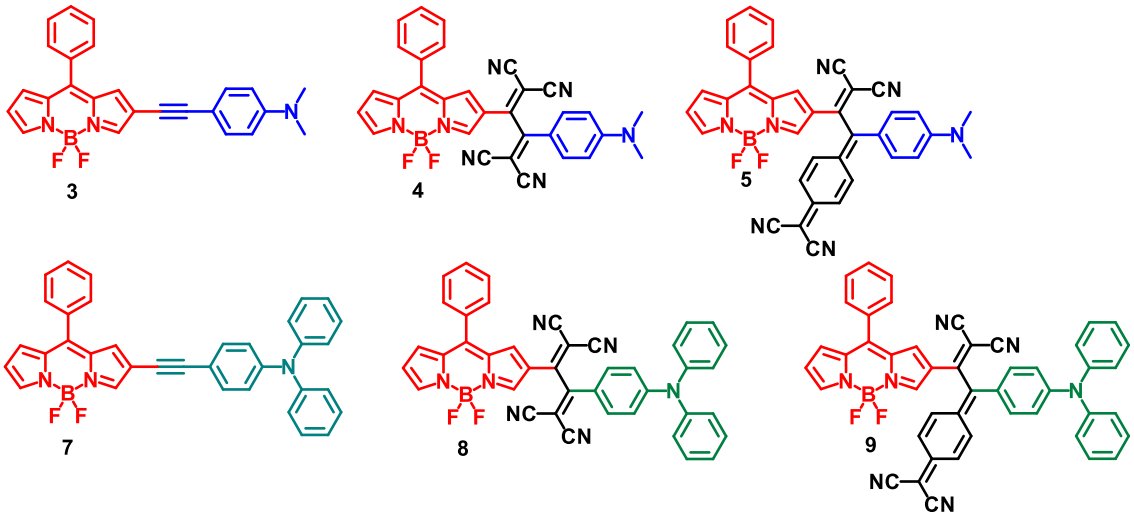

Chart 4.1. Molecular structures of the push–pull BODIPYs **3–5** and **7–9**.

Herein, the donor-acceptor BODIPYs **3–5** and **7–9** were synthesized. The variation of electron donor and acceptor units on the photophysical, electrochemical, and theoretical properties of the BODIPY were investigated (Chart 4.1). The incorporation of the cyclohexa-2,5-diene-1,4-diylidene-expanded TCBD unit shows a bathochromic shift in electronic absorption spectra due to strong donor-acceptor interactions compared to the TCBD unit. The redox properties of donor-acceptor BODIPYs **4, 5, 8,** and **9** exhibit multiple reduction waves at low potential due to the presence of TCBD and cyclohexa-2,5-diene-1,4-diylidene-expanded TCBD unit. The computational calculations of BODIPYs **4**, **5**, **8,** and **9** show that the incorporation of cyclohexa-2,5-diene-1,4-diylidene-expanded TCBD unit decreases the HOMO–LUMO gap more compared to the TCBD unit.

4.2. Results and Discussion

The multi-modular π-conjugated donor-acceptor based chromophore BODIPYs **3–5** and **7–9** were synthesized by palladium-catalyzed Sonogashira cross-coupling and [2+2] cycloaddition retroelectrocyclization reactions in good yields. The *N*,*N*-dimethylaniline (NND), and triphenylamine (TPA) units were used as electron donors, and BODIPY, tetracyanoethylene (TCNE), and 7,7,8,8-

tetracyanoquinodimethane (TCNQ) units act as a strong electron acceptor. The BODIPY **1** reacts with compounds **2** and **6** using a catalytic amount of $Pd(PPh_3)_4$ in THF: DIPEA solvent at 60 °C for 12 hours, resulted in BODIPYs **3** and **7** in 74% and 70% yields, respectively. The ethynyl bridged BODIPYs **3** and **7** further react with strong electron acceptor tetracyanoethylene (TCNE) in dichloromethane (DCM) solvent at room temperature for 6 h offered TCBD substituted BODIPYs **4** and **8** in 83% and 80% yields, respectively. Similarly, the reaction of BODIPY **3** and **7** reacts with strong acceptor tetracyanoquinodimethane (TCNQ) using dichloroethane (DCE) solvent at reflux condition for 6 h resulted in cyclohexa-2,5-diene-1,4-diylidene-expanded TCBD functionalized BODIPYs **5** and **9** in 77% and 75% yields, respectively (Scheme 4.1).

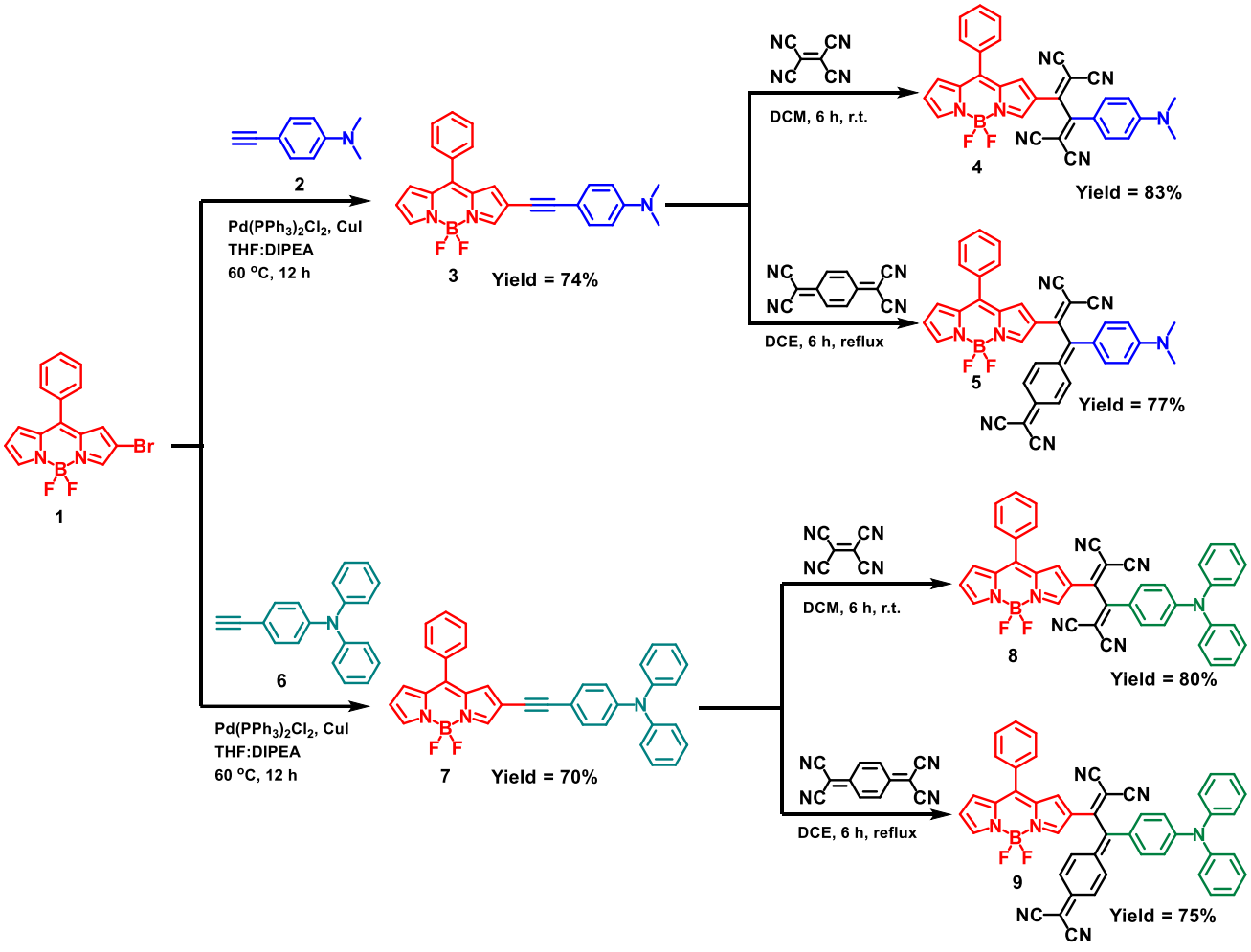

Scheme 4.1. Synthetic route of the BODIPYs **3**–**5** and **7**–**9**.

The donor-acceptor BODIPYs **3–5** and **7–9** are easily soluble in common organic solvents such as chloroform, dichloromethane, acetonitrile, tetrahydrofuran. The purification was done by column chromatography (silica gel size = 100–200 mesh) using Hexane and DCM solvents. The ^{1}H NMR, ^{13}C NMR and high-resolution mass spectrometry (HRMS) techniques were used to characterize the molecular structures of all BODIPYs.

4.3. Photophysical properties

The normalized electronic absorption spectra of donor-acceptor conjugates BODIPY **3–5** and **7–9** were recorded in dry dichloromethane (DCM) solvent at room temperature (Figures 4.1a and 4.1b), and the corresponding data are tabulated in Table 4.1.

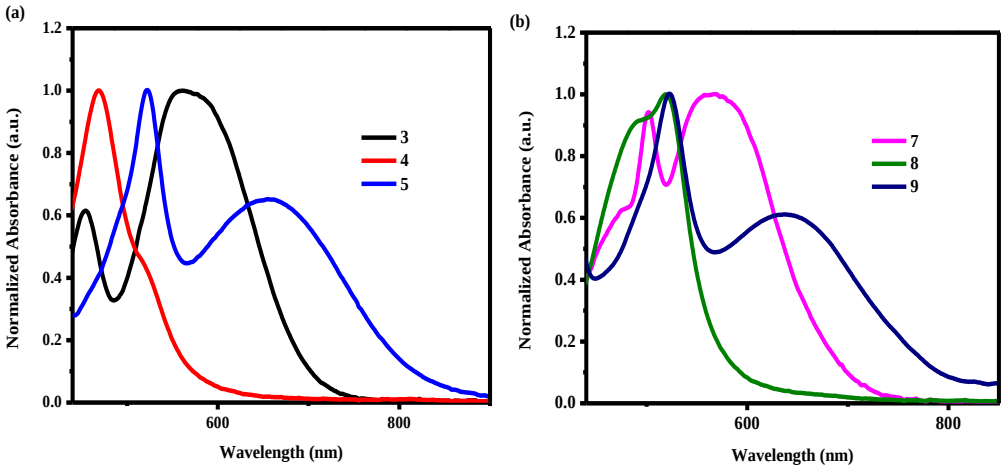

Figure 4.1. Normalized absorption spectra of donor-acceptor BODIPYs **3–5** (Figure 4.1a) and **7–9** (Figure 4.1b) in DCM (10^{-5} M).

The donor-acceptor BODIPYs **3** & **7** exhibits two intense absorption band at 454 nm, 561 nm, and 503 nm, 565 nm, respectively, and both electronic absorption bands correspond to π-π* transition. The TCBD-functionalized BODIPYs **4** and **8** exhibit two absorption bands at 468 nm, 521 nm, and 492 nm, 520 nm, respectively, and at the lower wavelength region, the absorption band attributed to π-π* transition, and at the longer wavelength region, the electronic absorption band belongs to intramolecular charge transfer (ICT) transition from donor to acceptor moiety. Similarly, the cyclohexa-2,5-diene-1,4-ylidene-expanded TCBD functionalized BODIPYs **5** and **9** exhibit absorption bands at 521

nm, 662 nm, and 524 nm, 643 nm, respectively. At the higher wavelength region, the electronic absorption band belongs to the intramolecular charge transfer (ICT) transition. The cyclohexa-2,5-diene-1,4-ylidene-expanded TCBD substituted BODIPYs exhibit an intramolecular charge transfer (ICT) band at the higher wavelength region compared to TCBD substituted BODIPYs due to strong donor-acceptor interactions.

Table 4.1. Photophysical and electrochemical data of push-pull BODIPYs **3–5** and **7–9**.

Photophysical data[a]				**Electrochemical data[b]**	
Compound	**λ_{abs} (nm)**	**ε (M^{-1} cm^{-1})**	**Optical band gap (eV)**	**E_{ox} (V)**	**E_{red} (V)**
3	454 561	10600 17200	1.77	0.72 1.15	-0.68
4	468 521	34500 15370	2.16	0.80 1.25	-0.54 -0.78 -1.15
5	521 662	25100 16300	1.51	0.07 0.72	-0.30 -0.85 -1.48
7	503 565	10800 11500	1.73	0.86 1.24	-0.69
8	492 520	34600 37800	2.12	0.93 1.86	-0.31 -0.45 -1.08
9	524 643	16900 10300	1.54	0.11 0.91	-0.35 -0.90 -1.49

[a] Absorbance recorded in dry DCM at 1×10^{-5} M conc. λ_{abs}: absorption wavelength. ε: extinction coefficient. [b] Electrochemical analysis was estimated by differential pulse voltammetry in 0.1 M solution of Bu_4NPF_6 in DCM at 100 mV s^{-1} scan rate *versus* Ag/AgCl at 25 °C. E_{oxi} and E_{red} values are based on DPV analysis.

The optical bandgap values calculated from UV-vis absorption spectra of TCBD and cyclohexa-2,5-diene-1,4-ylidene-expanded-TCBD functionalized push-pull BODIPYs **4**, **8**, **5,** and **9** follow the order **4**>**8**>**9**>**5**. The trend suggests that the incorporation of the cyclohexa-2,5-diene-1,4-ylidene-expanded TCBD resulted in a bathochromic shift with a low optical bandgap compared to TCBD functionalized BODIPYs due to strong donor-acceptor interactions.

4.4. Electrochemical properties

The electrochemical properties of push-pull BODIPYs **3–5** and **7–9** were explored by cyclic voltammetry (CV) and differential pulse voltammetry (DPV) in dry dichloromethane (DCM) solvent at room temperature using tetrabutylammonium hexafluorophosphate (Bu_4NPF_6) as a supporting electrolyte. The glassy carbon is used as a working electrode, Pt wire as a counter electrode, and Ag/AgCl as the reference electrode. The electrochemical data are tabulated in Table 4.1, and representative CV and DPV plots of BODIPYs **3–5** and **7–9** are shown in Figure 4.2.

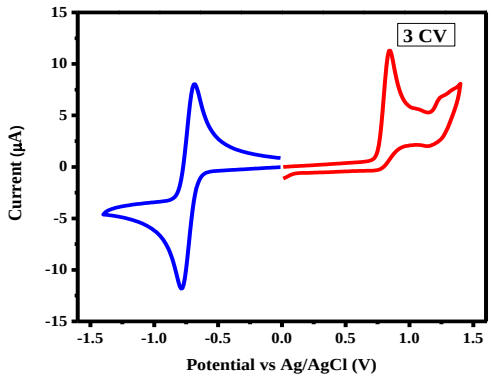
3 CV
Current (µA)
Potential vs Ag/AgCl (V)

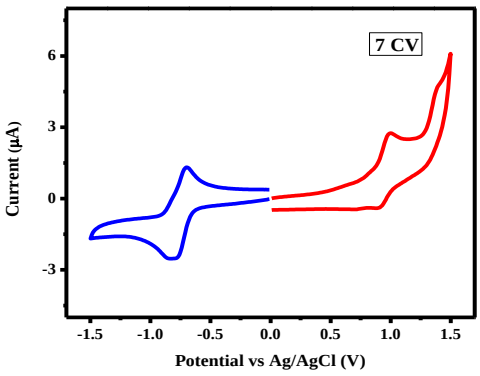
7 CV
Current (µA)
Potential vs Ag/AgCl (V)

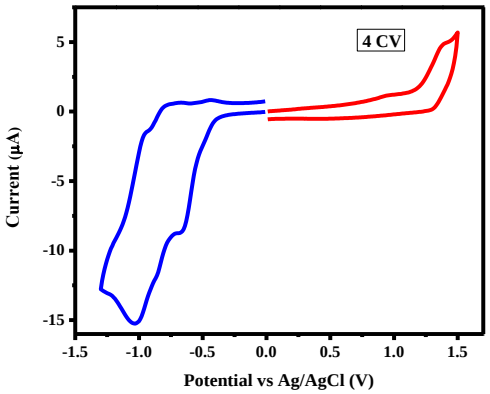
4 CV
Current (µA)
Potential vs Ag/AgCl (V)

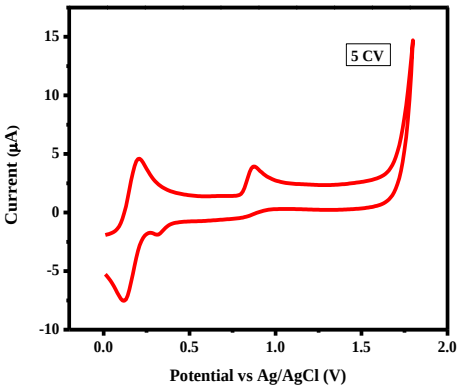
5 CV
Current (µA)
Potential vs Ag/AgCl (V)

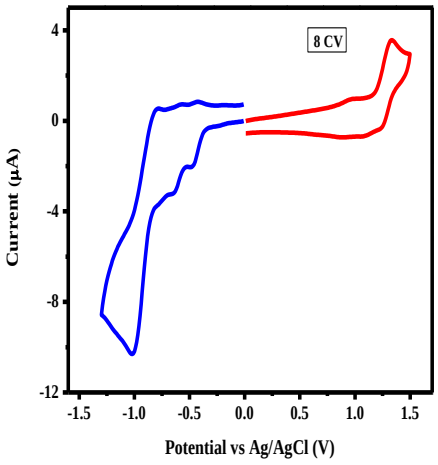
8 CV
Current (µA)
Potential vs Ag/AgCl (V)

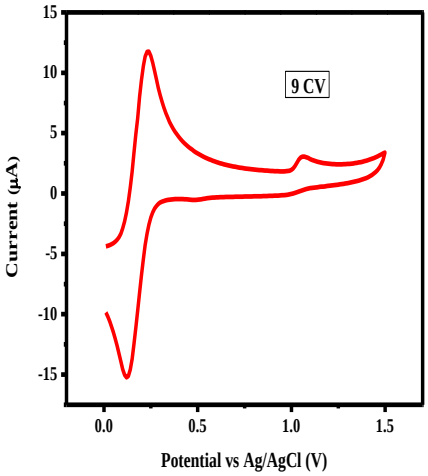
9 CV
Current (µA)
Potential vs Ag/AgCl (V)

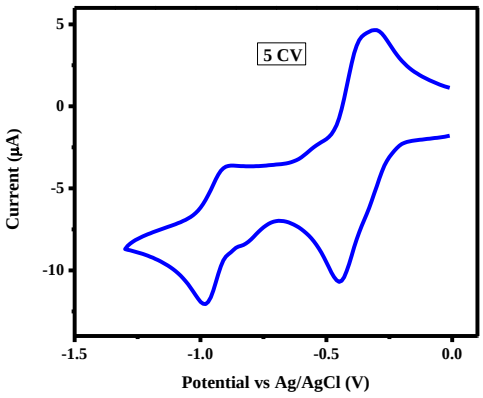
5 CV
Current (µA)
Potential vs Ag/AgCl (V)

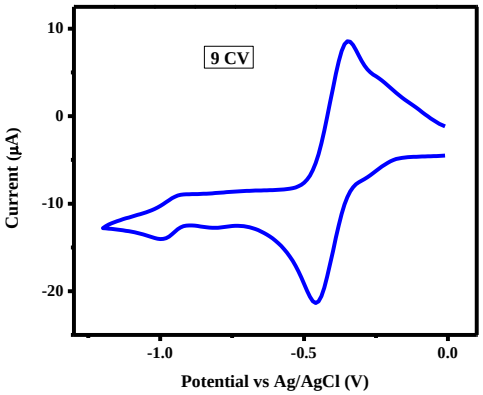
9 CV
Current (µA)
Potential vs Ag/AgCl (V)

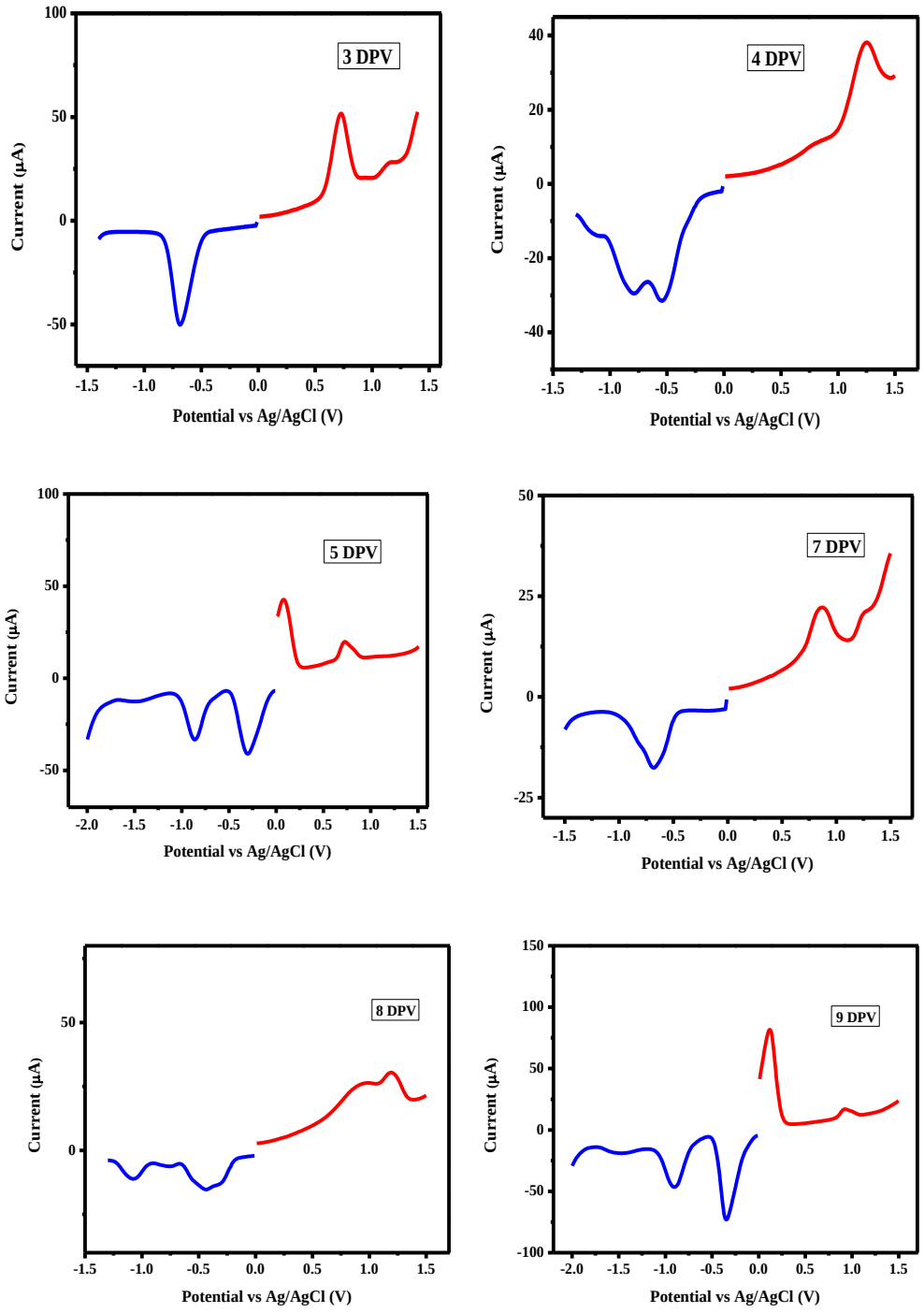

Figure 4.2. CV and DPV plots of the BODIPYs **3–5** and **7–9** in 0.1 M solution of Bu_4NPF_6 in dry dichloromethane solvent at 100 mV s^{-1} scan rate versus Ag/AgCl at 25 °C.

The BODIPY exhibits a single oxidation and reduction wave at low potential due to the formation of a mono π-radical cation and a mono π-radical anion. The BODIPYs **3** and **7** exhibit two oxidation waves at +0.72 V, +1.15 V, and +0.86 V, +1.24 V, respectively (Table 4.1). The

first oxidation at lower potential due to the presence of the donor unit, and the second oxidation at higher potential belongs to the BODIPY unit. The BODIPYs **3** and **7** exhibit one reduction wave at -0.68 V and -0.69 V, respectively, due to the presence of the acceptor BODIPY unit. The TCBD functionalized BODIPYs **4** and **8** exhibit two oxidation waves at +0.80 V, +1.25 V and +0.93 V, +1.86 V and three reduction waves at -0.54 V, -0.78 V, -1.15 V and -0.31 V, -0.45 V, -1.08 V, respectively (Table 4.1). The first oxidation wave belongs to the donor groups, and the second oxidation wave corresponds to the BODIPY unit. In the reduction region, the first two reduction waves correspond to TCBD, and each step corresponds to one-electron transfer due to the generation of mono and di-anion. The third reduction wave corresponds to the acceptor BODIPY unit. The cyclohexa-2,5-diene-1,4-ylidene-expanded TCBD substituted BODIPYs **5** and **9** exhibit multiple reduction waves due to acceptor BODIPY and cyclohexa-2,5-diene-1,4-ylidene-expanded TCBD unit. The BODIPYs **5** and **9** show oxidation at +0.07 V and +0.72 V and +0.11 V and +0.91 V, respectively. In the reduction region, the push-pull BODIPYs **5** and **9** show multiple reduction waves at -0.54 V, -0.85 V, -1.48 V, and -0.35 V, -0.90 V, and -1.49 V, respectively (Table 4.1). The first two reduction wave corresponds to cyclohexa-2,5-diene-1,4-ylidene-expanded TCBD unit at lower potential related to the generation of mono and di-anion, and each step exhibits single electron transfer. The third reduction wave corresponds to the BODIPY unit. The cyclic voltammetry results show that the incorporation of strong acceptor cyclohexa-2,5-diene-1,4-ylidene-expanded TCBD decreases the LUMO energy level more than TCBD unit.

4.5. Thermal Properties

The thermal stability is an important characterization of the material for various optoelectronic applications. The thermal properties of the push–pull BODIPYs **3–5** and **7–9** were measured by thermogravimetric analysis (TGA) at a heating rate of 10 °C min^{-1} and

monitoring the weight loss against temperature under the nitrogen atmosphere.

The donor–acceptor BODIPYs **3–5** and **7–9** exhibit excellent thermal stability and the corresponding thermograms are shown in Figure 4.3. The decomposition temperatures for the BODIPYs **3–5** and **7–9** at 5% weight loss were found to be at 328 ℃, 144 ℃, 232 ℃ and 253 ℃, 201 ℃ and 221 ℃, respectively. The *N*,*N*-dimethylaniline substituted donor–acceptor BODIPY **3** exhibits the highest thermal stability as compared to BODIPYs **4, 5, 7, 8,** and **9**. The thermal stability of the donor–acceptor BODIPYs **3–5** and **7–9** follows the order **3**> **7**> **5**> **9**> **8**> **4**.

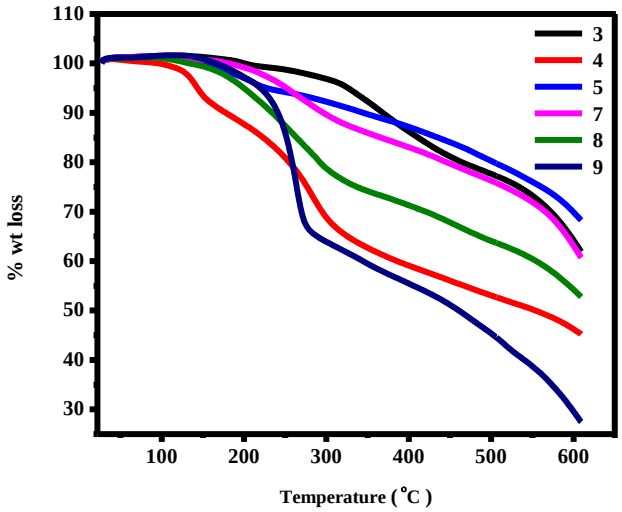

Figure 4.3. Thermogravimetric analysis (TGA) of the donor–acceptor BODIPYs **3–5** and **7–9** measured at a heating rate of 10 ℃ min^{-1} under a nitrogen atmosphere.

4.6. Theoretical calculations

To understand the geometry and electronic properties of the push-pull chromophore BODIPYs **3–5** and **7–9,** we have performed density functionalized theory (DFT) at the B3LYP/6-31G (d, p) level in the Gaussian 09W program.

The computationally estimated HOMO and LUMO energy levels of the multi-modular BODIPYs **3–5** and **7–9** revels that the terminal donor groups (*N*,*N*-dimethylaniline, and triphenylamine) can

tune the HOMO and LUMO energy levels. The highest occupied molecular orbitals (HOMOs) of the BODIPYs **3** and **7** are spread over the whole molecule, whereas the lowest unoccupied molecular orbitals (LUMOs) are localized on the BODIPY unit.

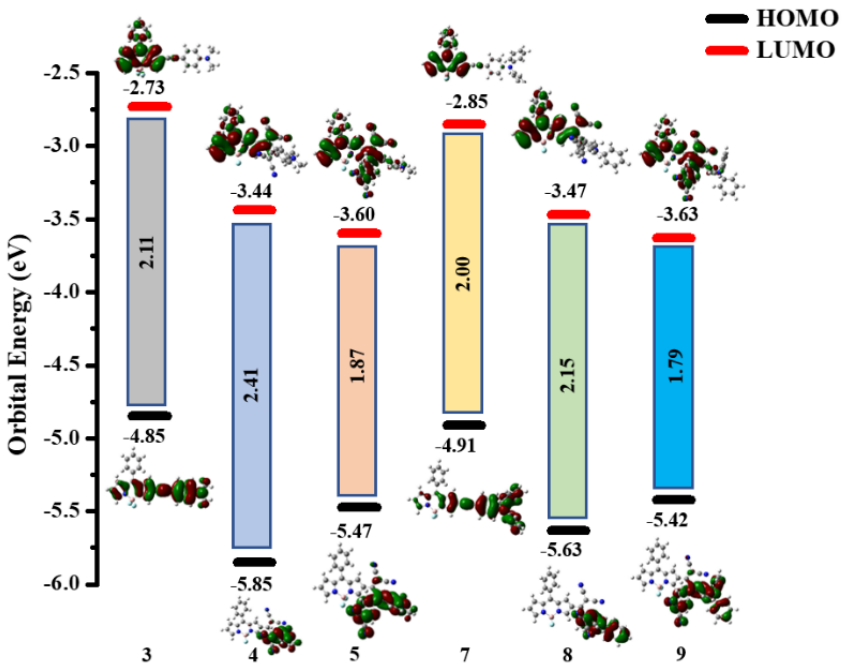

Figure 4.4. Energy level diagram and frontier molecular orbitals of the push-pull BODIPYs **3–5** and **7–9** estimated by DFT calculation at the B3LYP/6-31G (d, p) level.

The optimized structure of TCBD and cyclohexa-2,5-diene-1,4-ylidene-expanded TCBD substituted push-pull BODIPYs **4**, **5**, **8,** and **9** exhibit non-planer geometry. The HOMOs are mainly spread over donor NND and TPA units, whereas LUMOs are cantered on acceptor TCBD and cyclohexa-2,5-diene-1,4-ylidene-expanded TCBD unit in BODIPYs **4**, **5**, **8** and **9**. The theoretically estimated HOMO levels of push-pull BODIPYs **3–5** and **7–9** are –4.85, –5.85, –5.47, –4.91, –5.63 and –5.42 eV, respectively whereas the LUMO levels are –2.73, –3.44, –3.60, –2.85, –3.47 and –3.63 eV, respectively. The theoretical band gap of the push-pull BODIPYs **3–5** and **7–9** were estimated to be 2.11, 2.41, 1.87, 2.00, 2.15, and 1.79 eV, respectively (Figure 4.4). The cyclohexa-2,5-diene-1,4-ylidene-expanded TCBD substituted BODIPYs exhibit a low HOMO–LUMO energy gap and shows bathochromic shift in the

UV-visible spectrum as compared to TCBD functionalized BODIPYs (Figure 4.4).

The time-dependent DFT calculation was performed to evaluate the electronic transitions of the push–pull BODIPYs **3, 5, 7, 8, 9** and **4** at CAM-B3LYP/6-31G (d, p) level in DCM solvent and B3LYP/6-31G (d, p) level in gas phase, respectively. The polarized continuum model (PCM) was used to analyse the solvent effect in TD-DFT calculation. The electronic transitions with composition, oscillator strengths, and assignments of the donor–acceptor BODIPYs **3–5** and **7–9** are compiled in Table 4.2. The donor-acceptor BODIPYs **3** and **7** exhibit absorption bands at 369 nm, 488 nm and 366 nm, 473 nm, respectively.

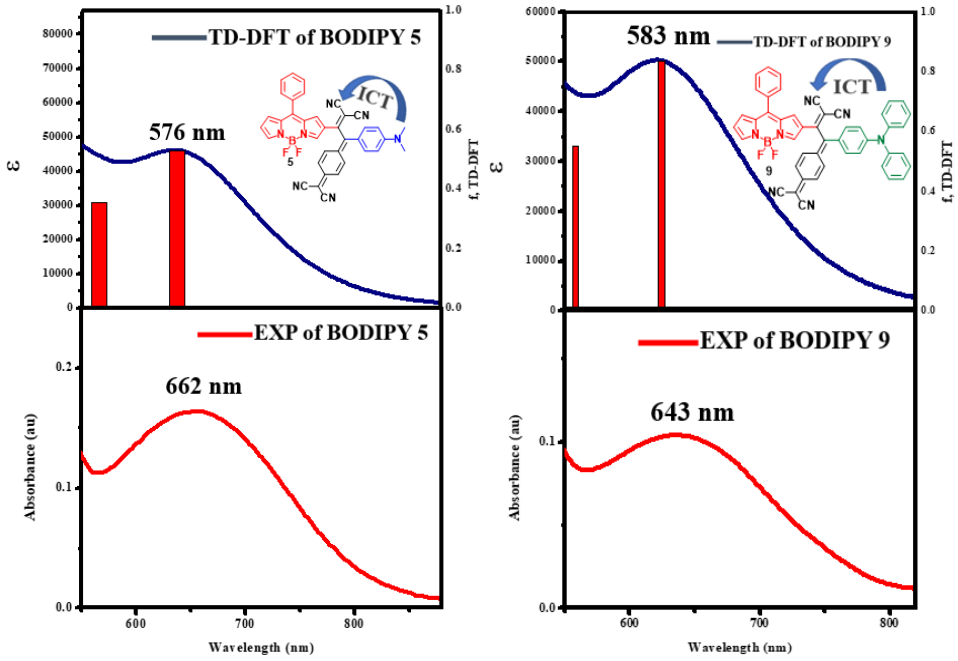

Figure 4.5. UV-vis absorption spectra of donor–acceptor BODIPYs **5** and **9**. Experimental (bottom) and TD-DFT predicted (top) at CAM-B3LYP/6-31G (d, p) level in DCM solvent.

The absorption band at lower wavelength region originating from HOMO –1 → LUMO and at longer wavelength region originating from HOMO → LUMO for BODIPYs **3** and **7** which corresponding to the π–π* transition. The TCBD substituted BODIPYs **4** and **8** exhibit ICT band at 459 nm and 445 nm, respectively which attributed to HOMO → LUMO+1 transition (Table 4.2). The cyclohexa-2,5-diene-1,4-ylidene-

expanded TCBD functionalized BODIPYs **5** and **9** exhibit ICT band at 576 nm and 583 nm respectively originating from HOMO → LUMO transition (Figure 4.5). The theoretical calculation reveals that the cyclohexa-2,5-diene-1,4-ylidene-expanded TCBD substituted BODIPYs exhibits low HOMO–LUMO gap compared to the TCBD functionalized BODIPYs due to strong donor–acceptor interactions.

Table 4.2. Calculated electronic transitions for donor-acceptor BODIPYs **3–5** and **7–9.**

Compound	**Wavelength (nm)**	**Composition**	**f[a]**	**Assignment**
3	369 488	HOMO-1→LUMO (0.57) HOMO→LUMO (0.61)	0.26 0.75	π–π* π–π*
4	378 459	HOMO→LUMO+2 (0.56) HOMO→LUMO+1 (0.61)	0.53 0.10	π–π* ICT
5	447 576	HOMO-1→LUMO (0.49) HOMO→LUMO (0.66)	0.69 1.04	π–π* ICT
7	366 473	HOMO-1→LUMO (0.42) HOMO→LUMO (0.53)	0.15 0.90	π–π* π–π*
8	421 445	HOMO-1→LUMO (0.54) HOMO→LUMO+1 (0.40)	0.61 0.98	π–π* ICT
9	446 583	HOMO-2→LUMO (0.52) HOMO→LUMO (0.66)	0.77 1.17	π–π* ICT

f[a] oscillator strength

The theoretically calculated electronic absorption wavelengths were found to be longer than experimental data, which could be due to several factors such as solvent effect, temperature, and dipole moment.

4.7. Experimental Section

All the moisture and oxygen-sensitive reactions were performed in an inert atmosphere using the standard inert atmosphere method .^{1}H NMR were measured in Bruker Avance (III) 400 MHz, and ^{13}C NMR spectra were measured in 100 MHz using $CDCl_3$ as the internal solvent. The ^{1}H NMR chemical shifts are recorded in parts per million (ppm) relative to the solvent residual peak ($CDCl_3$, 7.26). The ^{13}C NMR shifts are reported relative to the solvent residual peak ($CDCl_3$, 77.00 ppm). The multiplicities are given as s (singlet), d (doublet), t (triplet), q (quartet), m (multiplet), and the coupling constants values (*J*) are reported in Hz. The UV-visible absorption spectra of all compounds were recorded in PerkinElmer's LAMBDA 35 UV-visible Spectrophotometer in DCM solvent at room temperature. High-Resolution Mass Spectrometry (HRMS) was recorded on a Bruker-Daltonics micrOTOF-Q II mass spectrometer. Cyclic voltammogram and differential voltammogram (DPVs) were recorded on an electrochemical analyzer using glassy carbon as the working electrode, Pt wire as the counter electrode, and the Ag/AgCl as the reference electrode. Thermogravimetric analysis was performed on the Mettler Toledo thermal analysis system.

Synthesis and characterization of BODIPY 3: Under argon atmosphere a solution of compound **1** (0.1 g, 0.28 mmol) and corresponding compound **2** (4-ethynyl-*N*,*N*-dimethylaniline) (0.050 g, 0.34 mmol) in dry THF (20 ml), added *N*,*N*-Diisopropylethylamine (DIPEA) (20 ml), $Pd(PPh_3)_4$ (0.016 g, 0.014 mmol), CuI (0.002 g, 0.014 mmol), stirred for 12 h at 60 °C, after completion of the reaction, the reaction mixture was concentrated under reduced pressure, the crude compound was purified by column chromatography on silica, using Hexane/ DCM (70:30, v/v), and afforded pure BODIPY **3** (Purple colour) around 74 % yield. **^{1}H NMR ($CDCl_3$, 400 MHz, ppm):** δ 8.04

(s, 1H), 7.96 (s, 1H), 7.59-7.53 (m, 5H), 7.34 (d, *J* = 8 Hz, 2H), 6.98-6.96 (m, 2H), 6.64 (d, *J* = 8 Hz, 2H), 6.57 (s, 1H) 2.98 (s, 6H); **^{13}C NMR (CDCl$_3$, 100 MHz, ppm):** 150.1, 146.1, 144.7, 133.6, 132.6, 131.9, 131.3, 130.9, 130.5, 128.5, 118.8, 111.8, 109.5, 93.5, 79.5, 40.1; **HRMS (ESI, positive)** m/z calculated for $C_{25}H_{20}BF_2N_3$ 412.1796 $[M + H]^+$, measured 412.1802 $[M + H]^+$.

Synthesis and characterization of BODIPY 4: In a 50 mL round bottomed flask, tetracyanoethylene (TCNE, 31 mg, 0.2 mmol) was added to solution of compound **3** (100 mg, 0.2 mmol) in DCM (20 mL). The reaction mixture was stirred in room temperature for 6 h. After completion of reaction, the reaction mix. was dried under vacuum and purified by column chromatography with hexane/DCM (30:70, v/v) as eluent to give compound **4** as dark red solid (Yield: 83 %). **^{1}H NMR (400 MHz, CDCl$_3$):** δ 8.24 (s, 1H), 7.89 (s, 1H), 7.78 (d, *J* = 8 Hz, 2H), 7.71-7.68 (m, 2H), 7.61 (d, *J* = 4 Hz, 4H), 7.26 (s, 1H), 6.80 (d, *J* = 4 Hz, 1H), 6.69 (d, *J* = 12 Hz, 2H), 3.17 (s, 6H); **^{13}C NMR (CDCl$_3$, 100 MHz, ppm):** δ 162.0, 160.4, 154.5, 151.5, 148.8, 142.1, 137.8, 136.3, 135.5, 132.4, 130.6, 129.1, 126.9, 122.8, 117.4, 114.2, 113.0, 112.2, 111.7, 80.0, 73.8, 40.1; **HRMS (ESI, positive)** m/z calculated for $C_{31}H_{20}BF_2N_7$ 562.1739 $[M + Na]^+$, measured 562.1782 $[M + Na]^+$.

Synthesis and characterization of BODIPY 5: In 50 mL round bottomed flask, tetracyanoquinodimethane (TCNQ, 49 mg, 0.2 mmol) was added to solution of compound **3** (100 mg, 0.2 mmol) in DCE (20 mL) under argon atmosphere. The reaction mixture was heated at 60 °C for overnight. After completion of reaction, the reaction mixture was dried under vacuum and purified by column chromatography with hexane/DCM (20:80, v/v) (eluent: CH_2Cl_2) compound **5** as dark purple (Yield: 77%). **^{1}H NMR (400 MHz, CDCl$_3$):** δ 8.20 (s, 1H), 7.80 (s, 1H), 7.68 (s, 2H), 7.62-7.52 (m, 7H), 7.32 (d, *J* = 12 Hz, 2H), 7.23 (d, *J* = 4 Hz, 1H), 7.15 (d, *J* = 12 Hz, 1H), 6.91 (d, *J* = 8 Hz, 1H) 6.78-6.72 (m, 2H), 3.15 (s, 6H); **^{13}C NMR (100 MHz, CDCl$_3$):** δ 163.7, 154.3, 153.0, 151.1, 150.7, 143.0, 136.0, 135.4, 134.2, 132.4, 130.5, 130.2, 129.0, 127.1, 125.2, 124.6, 122.9, 122.6, 114.8, 113.7, 112.6, 112.5, 80.8, 71.2,

40.1 ppm; **HRMS (ESI, positive)** m/z calculated for $C_{37}H_{24}BF_2N_7$ 638.2053 $[M + Na]^+$, measured 638.2066 $[M + Na]^+$.

Synthesis and characterization of BODIPY 7: Under argon atmosphere a solution of compound **1** (0.1 g, 0.28 mmol) and corresponding compound **6** (4-ethynyl-triphenylamine) (0.077 g, 0.28 mmol) in dry THF (20 ml), added *N*,*N*-Diisopropylethylamine (DIPEA) (20 ml), $Pd(PPh_3)_4$ (0.010 g, 0.014 mmol), CuI (0.002 g, 0.014 mmol), stirred for 12 h at 60 °C, after completion of the reaction, the reaction mixture was concentrated under reduced pressure, the crude compound was purified by column chromatography on silica, using Hexane/ DCM (70:30, v/v), and afforded pure BODIPY **7** (Purple colour) around 70 % yield. **^{1}H NMR ($CDCl_3$, 400 MHz, ppm):** δ 8.05 (s, 1H), 8.00 (s, 1H), 7.96 (s, 1H), 7.63-7.59 (m, 2H), 7.57-7.52 (m, 2H), 7.32-7.28 (m, 5H), 7.16-7.11 (m, 3H), 7.09-7.06 (m, 3H), 7.01-6.89 (m, 4H), 6.60-6.56 (m, 2H); **^{13}C NMR ($CDCl_3$, 100 MHz, ppm):** 148.0, 147.0, 145.7, 145.2, 144.1, 135.5, 134.2, 133.5, 132.3, 131.5, 130.9, 130.7, 130.4, 129.3, 128.5, 128.4, 125.4, 125.0, 123.6, 122.0, 119.1, 115.5, 92.4, 81.1; **HRMS (ESI, positive)** m/z calculated for $C_{35}H_{24}BF_2N_3$ 558.1930 $[M + Na]^+$, measured 558.1963 $[M + Na]^+$.

Synthesis and characterization of BODIPY 8: In a 50 mL round bottomed flask, tetracyanoethylene (TCNE, 11 mg, 0.08 mmol) was added to solution of compound **7** (50 mg, 0.08 mmol) in DCM (20 mL). The reaction mixture was stirred in room temperature for 6 h. After completion of reaction, the reaction mix. was dried under vacuum and purified by column chromatography with hexane/DCM (30:70, v/v) as eluent to give compound **8** as dark red solid (Yield: 80 %). **^{1}H NMR (400 MHz, $CDCl_3$):** *δ* 8.26 (s, 1H),7.89 (s, 1H), 7.70-7.60 (m, 8H), 7.40-7.38 (m, 5H), 7.26-7.22 (m, 6H), 6.92 (d, *J* = 8Hz, 2H), 6.82 (s, 1H); **^{13}C NMR ($CDCl_3$, 100 MHz, ppm):** *δ* 162.4, 159.8, 153.9, 151.8, 148.8, 144.4, 141.9, 137.9, 136.4, 135.5, 132.3, 131.7, 130.0, 129.1, 126.9, 126.7, 123.0, 120.7, 118.1, 113.4, 112.8, 112.7, 111.7, 79.9; **HRMS (ESI, positive)** m/z calculated for $C_{41}H_{24}BF_2N_7$ 686.2053 $[M + Na]^+$, measured 686.2055 $[M + Na]^+$.

Synthesis and characterization of BODIPY 9: In 50 mL round bottomed flask, tetracyanoquinodimethane (TCNQ, 18 mg, 0.08 mmol) was added to solution of compound **7** (100 mg, 0.08 mmol) in DCE (20 mL) under argon atmosphere. The reaction mixture was heated at 60 ℃ for overnight. After completion of reaction, the reaction mixture was dried under vacuum and purified by column chromatography with hexane/DCM (20:80, v/v) compound **9** as dark purple (Yield: 75%). **^{1}H NMR (400 MHz, $CDCl_3$):** δ 8.22 (s, 1H), 7.82 (s, 1H), 7.68-7.67 (m, 1H), 7.62-7.54 (m, 5H), 7.39 (t, *J* = 8Hz, 4H), 7.30-7.27 (m, 2H), 7.23-7.15 (m, 10H), 6.98 (d, *J* = 8Hz, 2H), 6.94-6.92 (m, 1H), 6.80 (d, *J* = 4Hz, 1H); **^{13}C NMR (100 MHz, $CDCl_3$):** δ 163.1, 154.1, 151.7, 151.3, 142.8, 136.1, 135.3, 134.9, 134.0, 133.0, 132.3, 130.5, 129.8, 129.0, 127.0, 126.5, 125.8, 125.4, 119.5, 114.1, 113.6, 112.5, 80.6, 74.1; **HRMS (ESI, positive)** m/z calculated for $C_{47}H_{28}BF_2N_7$ 762.2367 $[M + Na]^+$, measured 762.2388 $[M + Na]^+$.

4.8. Conclusion

A set of push–pull BODIPYs **3**–**5** and **7**–**9** were synthesized *via* Pd-catalyzed Sonogashira cross-coupling followed by [2+2] cycloaddition retroelectrocyclization reaction in good yields were explored. The photophysical results show that the ICT band of cyclohexa-2,5-diene-1,4-ylidene-expanded TCBD functionalized BODIPYs **5** and **9** exhibits a bathochromic shift compared to TCBD functionalized BODIPYs **4** and **8** because of strong–donor interaction. The redox properties of TCBD and cyclohexa-2,5-diene-1,4-ylidene-expanded TCBD substituted BODIPYs **4**, **5**, **8** and **9** display multiple reduction waves at low potential due to the formation of mono and di-radical anion on TCBD unit. The computational calculations revel that the incorporation of cyclohexa-2,5-diene-1,4-ylidene-expanded TCBD unit decreases the HOMO–LUMO gap more compared to TCBD substituted BODIPYs due to strong donor–acceptor interactions. The research reports a new avenue to design π-conjugated push-pull chromophores with low HOMO–LUMO gap for various optoelectronic applications.

4.9. Reference

1. Yadav, I. S., Alsaleh, A. Z., Misra, R., & D'Souza, F. (2021). Charge stabilization via electron exchange: excited charge separation in symmetric, central triphenylamine derived, dimethylaminophenyl–tetracyanobutadiene donor–acceptor conjugates. *Chemical Science*, *12*(3), 1109–1120. https://doi.org/10.1039/D0SC04648E

2. Philippe, C., Bui, A. T., Batsongo-Boulingui, S., Pokladek, Z., Matczyszyn, K., Mongin, O., … Trolez, Y. (2021). 1,1,4,4-Tetracyanobutadiene-Functionalized Anthracenes: Regioselectivity of Cycloadditions in the Synthesis of Small Near-IR Dyes. *Organic Letters*, *23*(6), 2007–2012. https://doi.org/10.1021/acs.orglett.1c00136

3. Xuan, S., Zhao, N., Ke, X., Zhou, Z., Fronczek, F. R., Kadish, K. M., … Vicente, M. G. H. (2017). Synthesis and Spectroscopic Investigation of a Series of Push–Pull Boron Dipyrromethenes (BODIPYs). *The Journal of Organic Chemistry*, *82*(5), 2545–2557. https://doi.org/10.1021/acs.joc.6b02941

4. Mondal, R., Braun, J. D., Sidhu, B. K., Nevonen, D. E., Nemykin, V. N., & Herbert, D. E. (2021). Catalytic Synthesis of Donor-Acceptor-Donor (D-A-D) and Donor-Acceptor-Acceptor (D-A-A) Pyrimidine-Ferrocenes via Acceptorless Dehydrogenative Coupling: Synthesis, Structures, and Electronic Communication. *Organometallics*, *40*(11), 1765–1775. https://doi.org/10.1021/acs.organomet.1c00232

5. Izumi, S., Higginbotham, H. F., Nyga, A., Stachelek, P., Tohnai, N., Silva, P. de, … Minakata, S. (2020). Thermally Activated Delayed Fluorescent Donor–Acceptor–Donor–Acceptor π-Conjugated Macrocycle for Organic Light-Emitting Diodes. *Journal of the American Chemical Society*, *142*(3), 1482–1491. https://doi.org/10.1021/jacs.9b11578

6. Gautam, P., Misra, R., Thomas, M. B., & D'Souza, F. (2017). Ultrafast Charge-Separation in Triphenylamine-BODIPY-Derived Triads Carrying Centrally Positioned, Highly Electron-Deficient,

Dicyanoquinodimethane or Tetracyanobutadiene Electron-Acceptors. *Chemistry – A European Journal*, *23*(38), 9192–9200. https://doi.org/10.1002/chem.201701604

7. Can, A., Choi, G.-S., Ozdemir, R., Park, S., Park, J. S., Lee, Y., … Usta, H. (2022). Meso-π-Extended/Deficient BODIPYs and Low-Band-Gap Donor–Acceptor Copolymers for Organic Optoelectronics. *ACS Applied Polymer Materials*, *4*(3), 1991–2005. https://doi.org/10.1021/acsapm.1c01856

8. LaMaster, D. J., Kaufman, N. E. M., Bruner, A. S., & Vicente, M. G. H. (2018). Structure Based Modulation of Electron Dynamics in meso-(4-Pyridyl)-BODIPYs: A Computational and Synthetic Approach. *The Journal of Physical Chemistry A*, *122*(31), 6372–6380. https://doi.org/10.1021/acs.jpca.8b05153

9. Uriel, C., Gómez, A. M., García Martínez de la Hidalga, E., Bañuelos, J., Garcia-Moreno, I., & López, J. C. (2021). Access to 2,6-Dipropargylated BODIPYs as "Clickable" Congeners of Pyrromethene-567 Dye: Photostability and Synthetic Versatility. *Organic Letters*, *23*(17), 6801–6806. https://doi.org/10.1021/acs.orglett.1c02380

10. Popere, B. C., Della Pelle, A. M., & Thayumanavan, S. (2011). BODIPY-Based Donor–Acceptor π-Conjugated Alternating Copolymers. *Macromolecules*, *44*(12), 4767–4776. https://doi.org/10.1021/ma200839q

11. Shinde, J., Thomas, M. B., Poddar, M., Misra, R., & D'Souza, F. (2021). Does Location of BF_2-Chelated Dipyrromethene (BODIPY) Ring Functionalization Affect Spectral and Electron Transfer Properties? Studies on α-, β-, and Meso-Functionalized BODIPY-Derived Donor–Acceptor Dyads and Triads. *The Journal of Physical Chemistry C*, *125*(43), 23911–23921. https://doi.org/10.1021/acs.jpcc.1c06704

12. Schellhammer, K. S., Li, T.-Y., Zeika, O., Körner, C., Leo, K., Ortmann, F., & Cuniberti, G. (2017). Tuning Near-Infrared Absorbing

Donor Materials: A Study of Electronic, Optical, and Charge-Transport Properties of aza-BODIPYs. *Chemistry of Materials*, *29*(13), 5525–5536. https://doi.org/10.1021/acs.chemmater.7b00653

13. Dhokale, B., Jadhav, T., Mobin, S. M., & Misra, R. (2015). Meso Alkynylated Tetraphenylethylene (TPE) and 2,3,3-Triphenylacrylonitrile (TPAN) Substituted BODIPYs. *The Journal of Organic Chemistry*, *80*(16), 8018–8025. https://doi.org/10.1021/acs.joc.5b01117

14. Schäfer, C., Mony, J., Olsson, T., & Börjesson, K. (2022). Effect of the Aza-N-Bridge and Push–Pull Moieties: A Comparative Study between BODIPYs and Aza-BODIPYs. *The Journal of Organic Chemistry*, *87*(5), 2569–2579. https://doi.org/10.1021/acs.joc.1c02525

15. Carlotti, B., Poddar, M., Elisei, F., Spalletti, A., & Misra, R. (2019). Energy-Transfer and Charge-Transfer Dynamics in Highly Fluorescent Naphthalimide–BODIPY Dyads: Effect of BODIPY Orientation. *The Journal of Physical Chemistry C*, *123*(40), 24362–24374. https://doi.org/10.1021/acs.jpcc.9b05851

16. Tu, J., Fan, Y., Wang, J., Li, X., Liu, F., Han, M., … Li, Z. (2019). Halogen-substituted triphenylamine derivatives with intense mechanoluminescence properties. *Journal of Materials Chemistry C*, *7*(39), 12256–12262. https://doi.org/10.1039/C9TC03515J

17. Wang, J., Liu, K., Ma, L., & Zhan, X. (2016). Triarylamine: Versatile Platform for Organic, Dye-Sensitized, and Perovskite Solar Cells. *Chemical Reviews*, *116*(23), 14675–14725. https://doi.org/10.1021/acs.chemrev.6b00432

18. Karak, A., Manna, S. K., & Mahapatra, A. K. (2022). Triphenylamine-based small-molecule fluorescent probes. *Analytical Methods*, *14*(10), 972–1005. https://doi.org/10.1039/D2AY00134A

19. Wang, H., Wang, Y., Ye, X., Hayama, H., Sugino, H., Nakano, H., & Nakano, T. (2017). π-Stacked poly(vinyl ketone)s with accumulated push–pull triphenylamine moieties in the side chain.

Polymer Chemistry, *8*(4), 708–714. https://doi.org/10.1039/C6PY01737A

20. Wu, J.-H., & Liou, G.-S. (2015). Substituent and Charge Transfer Effects on Memory Behavior of the Ambipolar Poly(triphenylamine)s. *ACS Applied Materials & Interfaces*, *7*(29), 15988–15994. https://doi.org/10.1021/acsami.5b04123

21. Zhang, J., Xu, B., Johansson, M. B., Vlachopoulos, N., Boschloo, G., Sun, L., … Hagfeldt, A. (2016). Strategy to Boost the Efficiency of Mixed-Ion Perovskite Solar Cells: Changing Geometry of the Hole Transporting Material. *ACS Nano*, *10*(7), 6816–6825. https://doi.org/10.1021/acsnano.6b02442

22. Finke, A. D., Dumele, O., Zalibera, M., Confortin, D., Cias, P., Jayamurugan, G., … Diederich, F. (2012). 6,6-Dicyanopentafulvenes: Electronic Structure and Regioselectivity in [2 + 2] Cycloaddition–Retroelectrocyclization Reactions. *Journal of the American Chemical Society*, *134*(43), 18139–18146. https://doi.org/10.1021/ja309141r

23. Michinobu, T., & Diederich, F. (2018). The [2+2] Cycloaddition-Retroelectrocyclization (CA-RE) Click Reaction: Facile Access to Molecular and Polymeric Push-Pull Chromophores. *Angewandte Chemie International Edition*, *57*(14), 3552–3577. https://doi.org/10.1002/anie.201711605

24. Breiten, B., Jordan, M., Taura, D., Zalibera, M., Griesser, M., Confortin, D., … Diederich, F. (2013). Donor-Substituted Octacyano[4]dendralenes: Investigation of π-Electron Delocalization in Their Radical Ions. *The Journal of Organic Chemistry*, *78*(5), 1760–1767. https://doi.org/10.1021/jo301194y

25. Zhang, Z., Gou, G., Wan, J., Li, H., Wang, M., & Li, L. (2022). Synthesis, Structure, and Significant Energy Gap Modulation of Symmetrical Silafluorene-Cored Tetracyanobutadiene and Tetracyanoquinodimethane Derivatives. *The Journal of Organic Chemistry*, *87*(5), 2470–2479. https://doi.org/10.1021/acs.joc.1c02382

26. Banziger, S. D., Clendening, R. A., Oxley, B. M., & Ren, T. (2020). Spectroelectrochemical and Computational Analysis of a Series of Cycloaddition–Retroelectrocyclization-Derived Donor–Acceptor Chromophores. *The Journal of Physical Chemistry B*, *124*(52), 11901–11909. https://doi.org/10.1021/acs.jpcb.0c09450

27. Erden, K., & Dengiz, C. (2022). 3-Alkynylindoles as Building Blocks for the Synthesis of Electronically Tunable Indole-Based Push–Pull Chromophores. *The Journal of Organic Chemistry*, *87*(6), 4385–4399. https://doi.org/10.1021/acs.joc.2c00067

28. Srinivasa Rao, P., Brixi, S., Shaikh, D. B., Al Kobaisi, M., Lessard, B. H., Bhosale, S. V., & Bhosale, S. V. (2021). The Effect of TCNE and TCNQ Acceptor Units on Triphenylamine-Naphthalenediimide Push-Pull Chromophore Properties. *European Journal of Organic Chemistry*, *2021*(18), 2615–2624. https://doi.org/10.1002/ejoc.202100198

29. Khan, F., Jang, Y., Patil, Y., Misra, R., & D'Souza, F. (2021). Photoinduced Charge Separation Prompted Intervalence Charge Transfer in a Bis(thienyl)diketopyrrolopyrrole Bridged Donor-TCBD Push-Pull System. *Angewandte Chemie*, *133*(37), 20681–20690. https://doi.org/10.1002/ange.202108293

30. Reutenauer, P., Kivala, M., Jarowski, P. D., Boudon, C., Gisselbrecht, J.-P., Gross, M., & Diederich, F. (2007). New strong organic acceptors by cycloaddition of TCNE and TCNQ to donor-substituted cyanoalkynes. *Chemical Communications*, (46), 4898–4900. https://doi.org/10.1039/B714731G

31. Kivala, M., Boudon, C., Gisselbrecht, J.-P., Seiler, P., Gross, M., & Diederich, F. (2007). A novel reaction of 7,7,8,8-tetracyanoquinodimethane (TCNQ): charge-transfer chromophores by [2 + 2] cycloaddition with alkynes. *Chemical Communications*, (45), 4731–4733. https://doi.org/10.1039/B713683H

32. Dengiz, C., Breiten, B., Gisselbrecht, J.-P., Boudon, C., Trapp, N., Schweizer, W. B., & Diederich, F. (2015). Synthesis and Optoelectronic Properties of Janus-Dendrimer-Type Multivalent Donor–Acceptor Systems. *The Journal of Organic Chemistry*, *80*(2), 882–896. https://doi.org/10.1021/jo502367h

33. Michinobu, T., Satoh, N., Cai, J., Li, Y., & Han, L. (2014). Novel design of organic donor–acceptor dyes without carboxylic acid anchoring groups for dye-sensitized solar cells. *Journal of Materials Chemistry C*, *2*(17), 3367–3372. https://doi.org/10.1039/C3TC32165G

34. Morimoto, M., Murata, K., & Michinobu, T. (2011). Photochemical control of a highly efficient addition reaction between electron-rich alkynes and tetracyanoethylene. *Chemical Communications*, *47*(35), 9819–9821. https://doi.org/10.1039/C1CC13476K

35. Kraußе, N., Kielmann, M., Ma, J., & Butenschön, H. (2015). Reactions of Alkynyl- and 1,1′-Dialkynylferrocenes with Tetracyanoethylene – Unanticipated Addition at the Less Electron-Rich of Two Triple Bonds. *European Journal of Organic Chemistry*, *2015*(12), 2622–2631. https://doi.org/10.1002/ejoc.201500105

36. Shoji, T., Higashi, J., Ito, S., Okujima, T., Yasunami, M., & Morita, N. (2012). Synthesis of donor–acceptor chromophores by the [2 + 2] cycloaddition of arylethynyl-2H-cyclohepta[b]furan-2-ones with 7,7,8,8-tetracyanoquinodimethane. *Organic & Biomolecular Chemistry*, *10*(12), 2431–2438. https://doi.org/10.1039/C2OB06931H

37. Shoji, T., Ito, S., Toyota, K., Iwamoto, T., Yasunami, M., & Morita, N. (2009). Reactions between 1-Ethynylazulenes and 7,7,8,8-Tetracyanoquinodimethane (TCNQ): Preparation, Properties, and Redox Behavior of Novel Azulene-Substituted Redox-Active Chromophores. *European Journal of Organic Chemistry*, *2009*(25), 4316–4324. https://doi.org/10.1002/ejoc.200900539

38. Thy Bui, A., Philippe, C., Beau, M., Richy, N., Cordier, M., Roisnel, T., … Trolez, Y. (2020). Synthesis, characterization and unusual near-infrared luminescence of 1,1,4,4-tetracyanobutadiene derivatives. *Chemical Communications*, *56*(24), 3571–3574. https://doi.org/10.1039/C9CC09560H

39. Rout, Y., Chauhan, V., & Misra, R. (2020). Synthesis and Characterization of Isoindigo-Based Push–Pull Chromophores. *The Journal of Organic Chemistry*, *85*(7), 4611–4618. https://doi.org/10.1021/acs.joc.9b03267

40. Poddar, M., & Misra, R. (2017). NIR-Absorbing Donor–Acceptor Based 1,1,4,4-Tetracyanobuta-1,3-Diene (TCBD)- and Cyclohexa-2,5-Diene-1,4-Ylidene-Expanded TCBD-Substituted Ferrocenyl Phenothiazines. *Chemistry – An Asian Journal*, *12*(22), 2908–2915. https://doi.org/10.1002/asia.201700879

41. Gautam, P., Misra, R., & Sharma, G. D. (2016). Dicyanoquinodimethane-substituted benzothiadiazole for efficient small-molecule solar cells. *Physical Chemistry Chemical Physics*, *18*(10), 7235–7241. https://doi.org/10.1039/C6CP00243A

42. Rout, Y., & Misra, R. (2021). Design and synthesis of 1,8-naphthalimide functionalized benzothiadiazoles. *New Journal of Chemistry*, *45*(22), 9838–9845. https://doi.org/10.1039/D1NJ00919B

Chapter 5

Meso-Donor *N,N*-dimethylaniline Functionalized BODIPYs: Synthesis, Photophysical, Electrochemical, Thermal and Theoretical Studies

5.1. Introduction

The π-conjugated donor-acceptor molecular systems have gained considerable interest in the scientific community due to their tunable optoelectronic properties and wide range of applications such as in organic field-effect transistors, bio-imaging, sensors, organic light-emitting diodes.[1–7] The optoelectronic properties and HOMO–LUMO gap of the π-conjugated chromophores can be altered by modifying the donor (D) or acceptor (A) unit or the π-linker.[8, 9] The 4,4-difluoro-4-bora-3a,4a-diaza-*s*-indacene dyes, frequently known as BODIPY has attracted a lot of attention in the last few decades because of their excellent chemical and photophysical properties including strong absorption, high fluorescence quantum yields and molar absorption coefficients, low toxicity, long fluorescence lifetime as well as good photochemical stability.[10–18] The optoelectronic characteristics of the BODIPYs can be tuned by expanding the conjugation and incorporation of appropriate D/A group at the *meso* and pyrrolic locations (α- and β-positions).[19–22] As a result, the BODIPY-based π-conjugated dyes have been extensively used as an efficient candidate for fluorescent imaging agents, molecular switches, chemosensors, laser dyes, light-emitting devices, photosensitizers, and organic optoelectronic materials.[23–28] The BODIPY unit act as strong acceptor and exhibits reversible oxidation and reduction waves at low potential.[29, 30] The optoelectronic properties of the donor-acceptor chromophores can be tuned through modifying the strong donor or acceptor group. Recently, the cross-conjugation has been used

as a good way to modify the HOMO–LUMO gap using acceptor units.[31]

The [2+2] cycloaddition-retroelectrocyclization is a catalyst-free and excellent-yielding reaction.[32] The electron-rich alkynes react with the acceptor TCNE, and TCNQ resulting in the nonplanar donor-acceptor molecules with low HOMO–LUMO gap.[33–35] The push-pull molecular systems based on TCBD and cyclohexa-2,5-diene-1,4-diylidene-expanded TCBD groups exhibit strong ICT band at higher wavelength due to strong donor-acceptor interactions.[32, 36, 37] The cross-conjugated chromophores containing TCBD and cyclohexa-2,5-diene-1,4-diylidene-expanded TCBD moieties have emerged as potential candidates in optoelectronics.[38, 39] Diederich, Michinobu, Shoji, Trolez, and Butenschön *et al.* have explored the synthesis, photophysical and redox properties of TCBD and cyclohexa-2,5-diene-1,4-diylidene-expanded TCBD functionalized donor-acceptor chromophores as redox-active chromophores for various optoelectronic applications.[40–45] Recently, Our group has reported the TCBD and cyclohexa-2,5-diene-1,4-diylidene-expanded TCBD functionalized donor-acceptor systems and explored their photophysical and redox properties for photovoltaic and optoelectronic applications.[46]

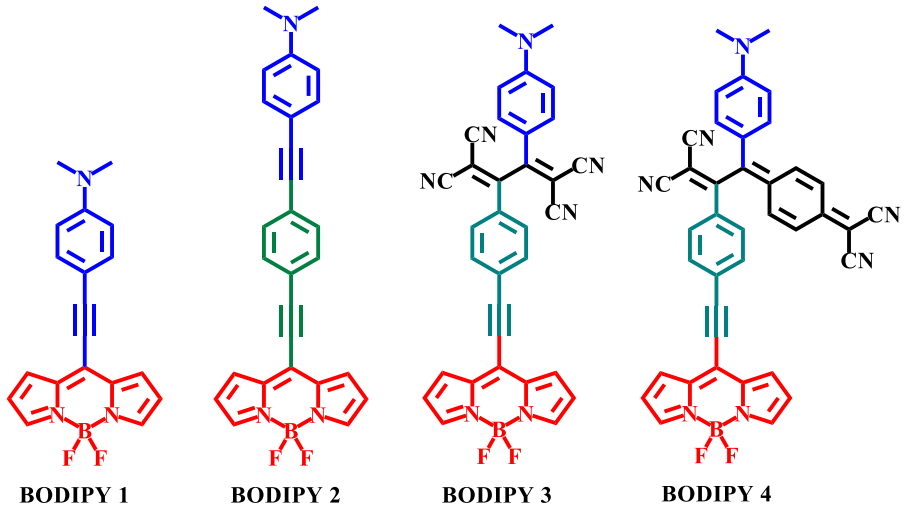

Chart 5.1. Molecular structures of the push-pull **BODIPYs 1–4**.

Herein, we report the donor-acceptor **BODIPYs 1–4** which were synthesized by the palladium-catalyzed Sonogashira cross-coupling and

[2+2] cycloaddition-retroelectrocyclization reactions (Chart 5.1). The TCBD and cyclohexa-2,5-diene-1,4-diylidene-expanded TCBD substituted **BODIPYs 3** and **4** exhibit intramolecular charge transfer band (ICT) at a longer wavelength region due to strong donor-acceptor interaction. The redox properties of the donor-acceptor **BODIPYs 3** and **4** show multiple redox waves at low potential due to presence of redox active TCBD, TCNQ and BODIPY unit. Additionally, the theoretical studies were carried out to analyze the molecular geometry and electronic properties of the donor-acceptor **BODIPYs 1–4**.

5.2. Results and Discussion

The donor-acceptor **BODIPYs 1** and **2** were designed and synthesized by the palladium-catalyzed Sonogashira cross-coupling reaction in good yields. The **BODIPYs 3** and **4** were synthesized by the [2+2] cycloaddition-retroelectrocyclization (CA-RE) reaction of **BODIPY 2** with strong acceptor TCNE and TCNQ units. The precursor 8-chloro BODIPY were synthesized by the reported procedure in good yield.[19] The **BODIPY 1** was synthesized by the reaction of 8-chloro BODIPY **1** with compound **2** (4-ethynyl-*N*,*N*-dimethylaniline) using catalytic amount of $Pd(PPh_3)_2Cl_2$ in tetrahydrofuran (THF) and triethylamine (TEA) solvent at 0 °C for 2 hours, resulted in 80% yield. Similarly, the **BODIPY 2** was synthesized *via* reaction of 8-chloro BODIPY **1** with compound **3** (4-((4-ethynylphenyl)ethynyl)-*N*, *N*-dimethylaniline) using a catalytic amount of Pd $(PPh_3)_2Cl_2$ in tetrahydrofuran (THF) and triethylamine (TEA) solvent at 0 °C for 2 hours, resulted in 70% yield (Scheme 5.1).

The donor-acceptor **BODIPY 3** was synthesized by the reaction of **BODIPY 2** with electron acceptor TCNE at room temperature for 6 h using dichloromethane (DCM) solvent, resulted in 75% yield**.** Similarly, the **BODIPY 4** was synthesized by the reaction of **BODIPY 2** with strong acceptor TCNQ using DCE solvent at reflux condition for 8 h, resulted in 71% yield (Scheme 5.1).

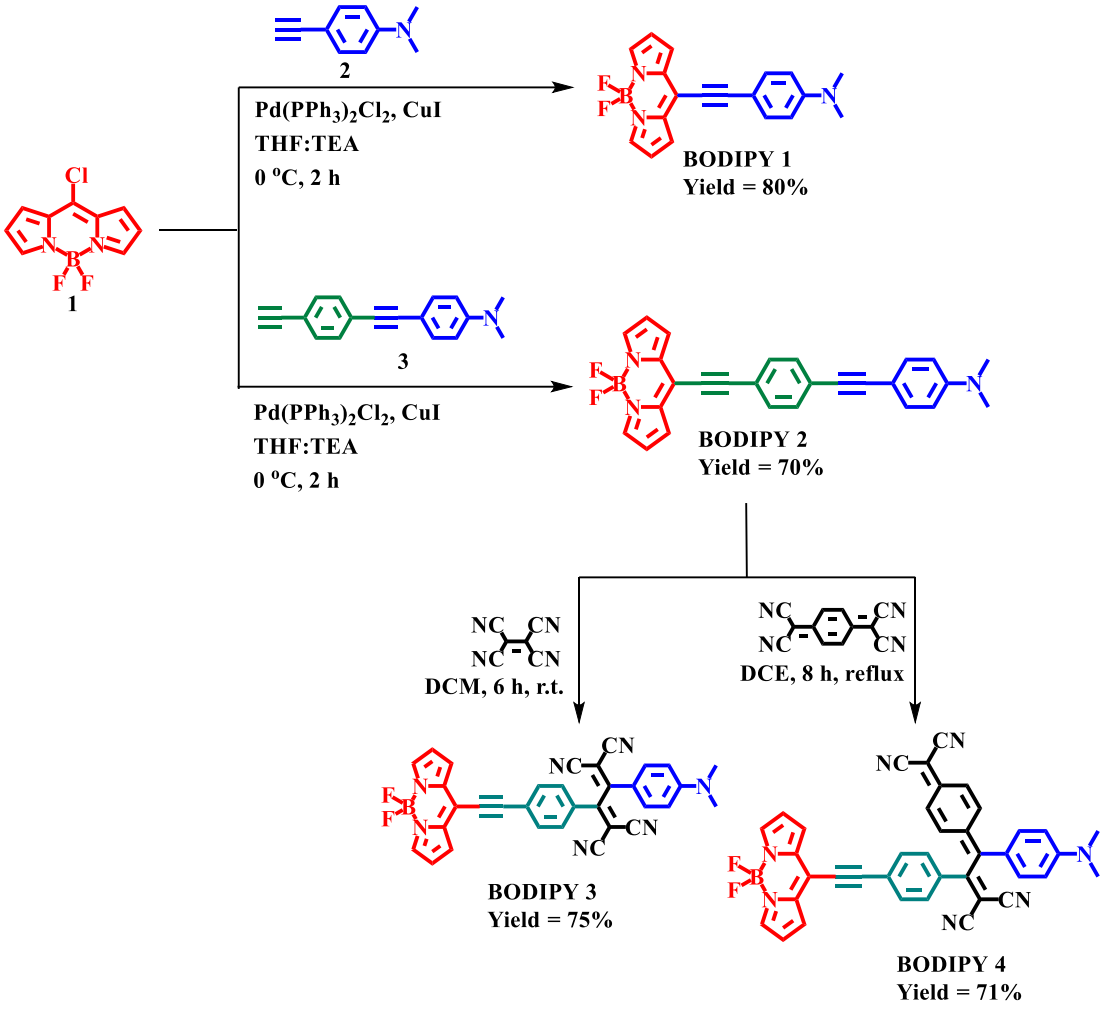

Scheme 5.1. Synthetic methodology of push-pull **BODIPYs 1–4**.

The **BODIPYs 1–4** were purified by silica-gel column chromatography (silica gel size = 100–200 mesh) using Hexane: DCM solvent and exhibit good solubility in common organic solvent acetone, chloroform, dichloromethane, acetonitrile. The ^{1}H NMR, ^{13}C NMR, and HRMS techniques were used to characterize the molecular structures of donor-acceptor BODIPYs.

5.3. Photophysical properties

The electronic absorption spectra of the studied donor-acceptor **BODIPYs 1–4** were recorded in dry dichloromethane (DCM) solvent at room temperature as shown in Figure 5.1 and the data are summarized in Table 5.1.

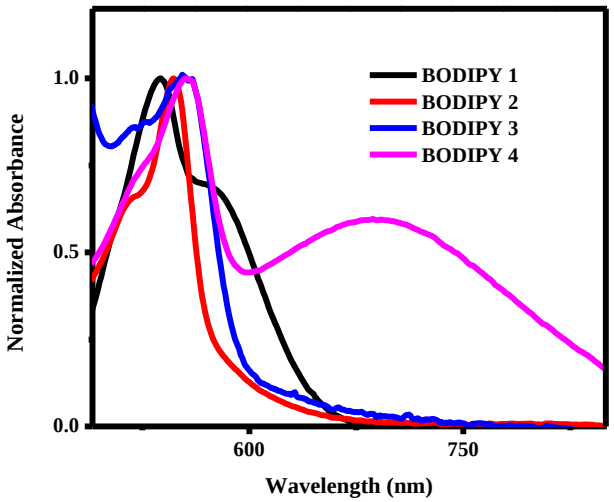

Figure 5.1. Normalized absorption spectra of the donor-acceptor **BODIPYs 1–4** in DCM solvent (10^{-5} M).

In general, the BODIPY exhibits an absorption band around 500–530 nm. The NND-BODIPYs exhibit intense absorption band at 450–550 nm region due to the $S_0 \rightarrow S_1$ (π–π*) transition. Additionally, a weak electronic absorption band was observed at lower wavelength region which could be attributed to $S_0 \rightarrow S_2$ (π–π*) transition of the BODIPY with contribution from NND unit. The **BODIPY 3** exhibited a broad $S_0 \rightarrow S_1$ transition from 550–750 nm range. Similarly, in the **BODIPY 4** showed broadening of the $S_0 \rightarrow S_1$ peak at 600–800 nm range. The **BODIPY 3** and **4** exhibits a new broad intramolecular charge transfer (ICT) band due to strong D-A interactions.[47] The **BODIPYs 1** and **2** shows the absorption band at 537 nm, 576 nm, and 516 nm, 548 nm, respectively, and both electronic absorption bands correspond to π–π* transitions. The **BODIPYs 3** and **4** exhibit absorption at 465 nm, 553 nm, and 557 nm, 695 nm, respectively. The absorption bands at the shorter wavelength region corresponds to π–π* transitions, and at the higher wavelength region were associated to ICT transition. The donor-acceptor **BODIPYs 3** and **4** display a bathochromic shift compared to **BODIPYs 1** and **2** due to significant donor-acceptor interaction.

Table 5.1. Photophysical and electrochemical data of donor-acceptor **BODIPYs 1–4**.

Photophysical data[a]				**Electrochemical data[b]**	
Compound	λ_{abs} **(nm)**	ε **(M^{-1} cm^{-1})**	**Optical band gap (eV)**	E_{ox} **(V)**	E_{red} **(V)**
BODIPY 1	537 576	12750 8824	1.83	1.08 1.53	-0.75
BODIPY 2	516 548	10710 16410	1.66	0.89 1.66	-0.61
BODIPY 3	465 553	8141 6340	2.01	1.15 1.29	-0.53 -0.88 -1.16
BODIPY 4	557 695	12790 7540	1.18	0.72 0.90	-0.26 -0.40 -0.68

[a] Absorbance recorded in dry DCM at 1×10^{-5} M conc. λ_{abs}: absorption wavelength. ε: extinction coefficient. **[b]** Electrochemical analysis was estimated by differential pulse voltammetry in 0.1 M solution of Bu_4NPF_6 in DCM at 100 mV s^{-1} scan rate *versus* Ag/AgCl at 25 °C. E_{oxi} and E_{red} values are based on DPV analysis.

The optical bandgap calculated from the onset wavelength of the UV-visible spectrum of the donor-acceptor **BODIPYs 1–4** follows the order **3** >**1** > **2**> **4**, which indicates that the introduction of strong acceptor results in low optical band gap with a red-shifted ICT band in electronic absorption spectra. The cyclohexa-2,5-diene-1,4-ylidene-expanded TCBD substituted **BODIPY 4** exhibit a red shifted ICT band at longer wavelength region compared to TCBD substituted **BODIPY 3** due to strong electronic communication between donor and acceptor unit.

5.4. Electrochemical properties

The electrochemical properties of the donor-acceptor **BODIPYs 1–4** were explored by using cyclic voltammetry (CV) and differential pulse voltammetry (DPV) techniques. All the measurements were recorded in dry dichloromethane solvent at room temperature using tetrabutylammonium hexafluorophosphate (Bu_4NPF_6) as a supporting electrolyte. The representative CV and DPV plots of the **BODIPYs 1–4** are shown in Figure 5.2, and the data are summarized in Table 5.1.

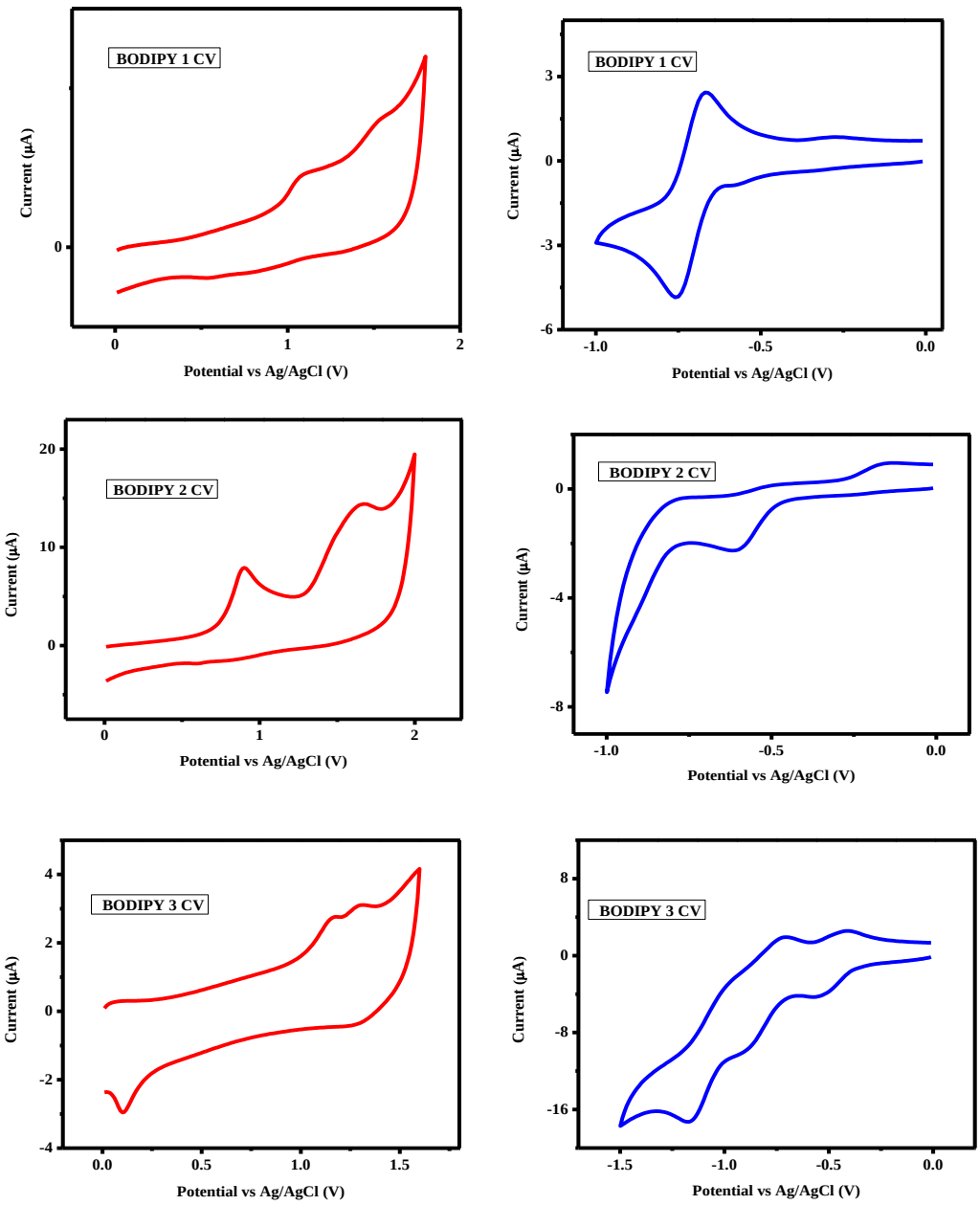

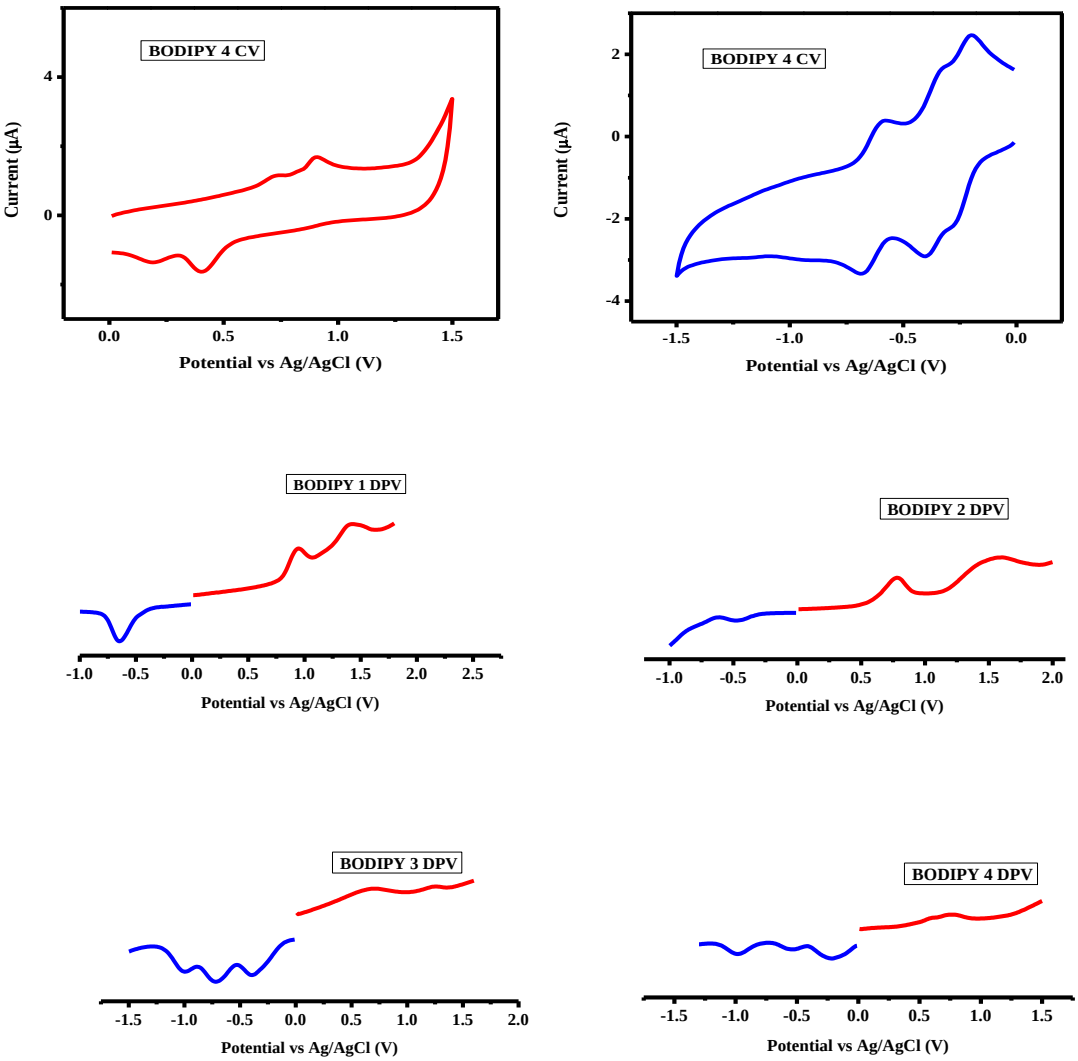

Figure 5.2. CV and DPV of the donor-acceptor **BODIPYs 1–4** using 0.1 M solution of Bu_4NPF_6 in dichloromethane at 100 mV s^{-1} scan rate *versus* Ag/AgCl at 25 °C.

The redox active moieties exhibit an individual oxidation and reduction potential which are crucial in determining their ability in the electron transfer system. The donor NND unit exhibits a reversible single oxidation wave at low potential. The BODIPY generally show single oxidation and single reduction wave due to formation of a mono π-radical cation and a mono π-radical anion.[48] The **BODIPYs 1–4** exhibits two oxidation potential at +1.08, +1.53 V; +0.89, +1.66 V; +1.15, +1.29 V; +0.72, +0.90 V and reduction potential at –0.75 V; –0.61 V; –0.53, –0.88, –1.16 V; –0.26, –0.40, –0.68 V, respectively (Table 5.1). The **BODIPYs 1–4** exhibit two oxidation and one reduction

waves: the first oxidation wave belongs to the donor unit, and the second oxidation corresponds to the BODIPY unit and one reduction wave at –0.26 to –1.16 V range due to BODIPY unit. The donor–acceptor **BODIPYs 3** and **4** exhibits three reduction waves at low potential. The initial first two reduction waves are attributed to the formation of mono and di-anion formation of the TCBD unit and each step corresponds to a one electron transfer and additional third reduction wave measured due to formation of the BODIPY mono-radical anion.[32, 49] In comparison of the **BODIPYs 3** and **4** indicates that the **BODIPY 4** is easier to reduce than the **BODIPY 3**, which can be attributed to the cyclohexa-2,5-diene-1,4-diyliden-expanded TCBD unit.[38] The HOMO energy levels of the **BODIPYs 1**–**4** estimated from CV plots are −5.52, −5.29, −5.59, and −5.16 and the associated LUMO energy levels are −3.69, −3.83, −3.91, and −4.18 eV, respectively. These electrochemical findings suggest that the cyclohexa-2,5-diene-1,4-ylidene-expanded TCBD unit decreases the LUMO energy level more than TCBD unit.

5.5. Thermal Properties

The thermal stability is an important characterization of the material for various optoelectronic applications. The thermal properties of the **BODIPYs 1–4** were measured by thermogravimetric analysis (TGA) at a heating rate of 10 ℃ min^{-1} and monitoring the weight loss against temperature under the nitrogen atmosphere.

The **BODIPYs 1–4** exhibit excellent thermal stability and the corresponding thermograms are shown in Figure 5.3. The decomposition temperatures for the **BODIPYs 1–4** at 5% weight loss were found to be at 315 ℃, 364 ℃, 261 ℃, 275 ℃, respectively. The phenyl incorporated *N*,*N*-dimethylaniline functionalized donor–acceptor **BODIPY 2** exhibits the highest thermal stability as compared to **BODIPYs 1, 3** and **4**. The cyclohexa-2,5-diene-1,4-ylidene-expanded TCBD functionalized **BODIPY 4** exhibits high thermal stability than TCBD functionalized **BODIPY 3**. The thermal stability of the donor–acceptor **BODIPYs 1–4** follows the order **2**> **1**> **4**> **3**.

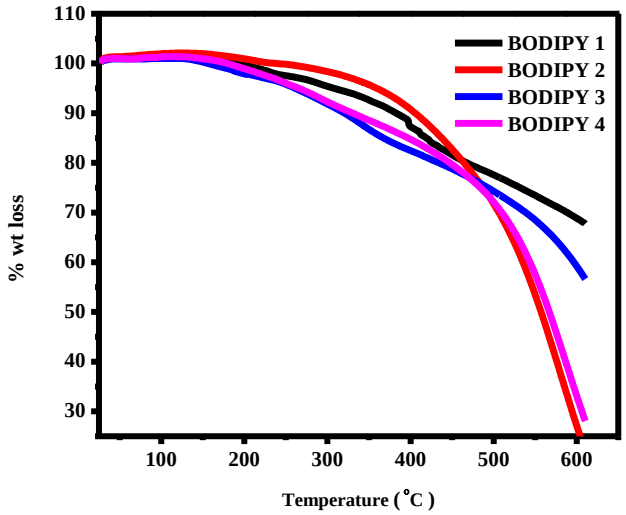

Figure 5.3. Thermogravimetric analysis (TGA) of the donor-acceptor **BODIPYs 1–4** measured at a heating rate of 10 °C min^{-1} under a nitrogen atmosphere.

5.6. Theoretical calculations

The density functional theory (DFT) calculations were performed to understand the geometry and electronic properties of **BODIPYs 1–4** at the B3LYP/6-31G (d, p) level for C, H, N, B, and F using Gaussian 09W program. The optimized structures of the **BODIPYs 3** and **4** exhibit twisted geometry due to incorporation of strong acceptor TCBD and cyclohexa-2,5-diene-1,4-ylidene-expanded TCBD. The donor-acceptor **BODIPYs 1–4** shows that the HOMOs are localized over both donor NND and BODIPY unit, whereas the LUMOs are localized on strong acceptor TCBD, cyclohexa-2,5-diene-1,4-ylidene-expanded TCBD and BODIPY unit. In case of **BODIPY 4** the HOMOs are localized on the donor NND unit and LUMOs are mostly cantered on strong acceptor cyclohexa-2,5-diene-1,4-ylidene-expanded TCBD unit which indicates a strong charge transfer from donor to

acceptor unit. The energy level diagram and frontier molecular orbitals of **BODIPYs 1–4** are shown in Figure 5.4.

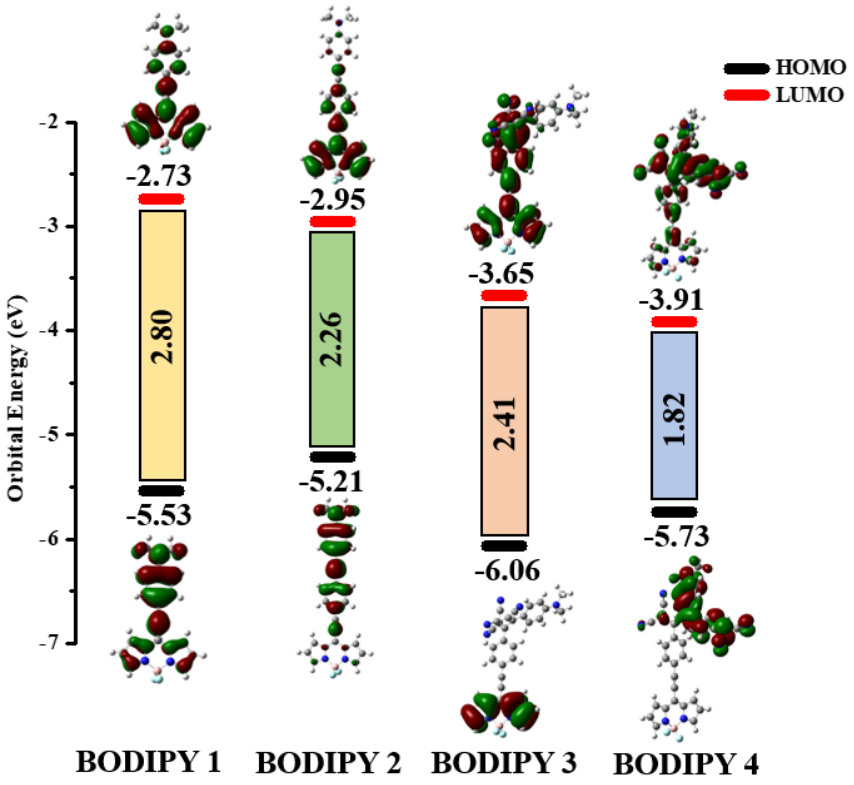

Figure 5.4. Energy level diagram and frontier HOMO and LUMO orbitals of donor-acceptor **BODIPYs 1–4** estimated by DFT calculations (B3LYP/631G (d, p) level).

The donor-acceptor **BODIPY 4** exhibits the lowest HOMO–LUMO gap and signifies that the TCNQ units act as strong acceptor compared to TCNE unit. The theoretically predicted HOMO energy levels of the donor-acceptor **BODIPYs 1–4** are –5.53 eV, –5.21 eV, –6.06 eV, and –5.73 eV, and associated LUMO levels are –2.73 eV, –2.95 eV, –3.65 eV and –3.91 eV, respectively (Figure 5.4). The introduction of TCBD and cyclohexa-2,5-diene-1,4-ylidene-expanded TCBD unit stabilize the LUMO energy levels, which results in a red shifted ICT band in electronic absorption spectra. The trend in the LUMO energy level of **BODIPYs 3** and **4** follows the order **3** > **4**, which suggest that the decreasing the LUMO energy levels with an increasing the strength of acceptor unit. The computationally calculated HOMO–LUMO gap values of the donor-acceptor **BODIPYs 1–4** are 2.80, 2.26,

2.41, and 1.82 eV, respectively. The electronic transitions with oscillator strengths, composition and assignment data are tabulated in Table 5.2. The optical bandgap (E_{gap}) values calculated from UV-visible spectra agreed well with the theoretically predicted HOMO–LUMO gap.

The time-dependent DFT calculation was performed to evaluate the electronic transitions of the donor-acceptor **BODIPYs 1–3** at B3LYP/6-31G (d, p) and CAM-B3LYP/6-31G (d, p) level for the **BODIPY 4**, in DCM solvent. The polarized continuum model (PCM) was used to analyse the solvent effect in TD-DFT calculation. The TD-DFT data of the donor-acceptor **BODIPYs 1–4** are compiled in Table 5.2. The **BODIPYs 1** and **2** exhibits absorption band at 441 nm, 542 nm and 456 nm, 693 nm, respectively.

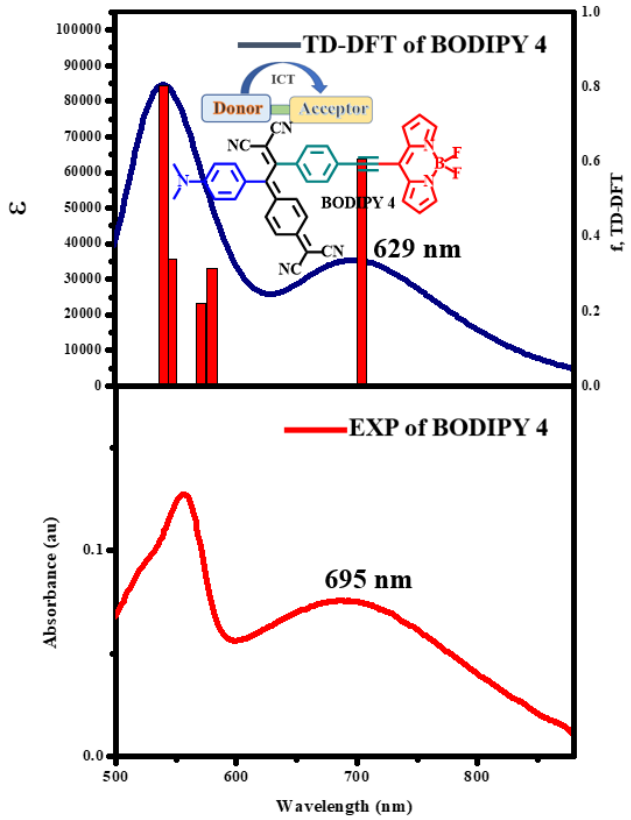

Figure 5.5. UV-vis absorption spectra of donor-acceptor **BODIPY 4**. Experimental (bottom) and TD-DFT predicted (top) in DCM solvent.

The absorption band at higher wavelength region originating from HOMO → LUMO, and at lower wavelength region occurs from HOMO–1 → LUMO, attributed to π–π* transition for **BODIPYs 1** and

2. The TCBD and cyclohexa-2,5-diene-1,4-ylidene-expanded TCBD substituted **BODIPYs 3** and **4** exhibits two absorption bands: at shorter wavelength region attributed to the π–π* transition and ICT at longer wavelength region. The **BODIPYs 3** and **4** exhibit absorption band at 447 nm, 505 nm and 452 nm, 629 nm, respectively. The absorption band at lower wavelength region for **BODIPYs 3** and **4**, originates from HOMO–2 → LUMO and HOMO–1 to LUMO+1 attributed to π–π* transition. The **BODIPYs 3** and **4** exhibit the ICT band at longer wavelength region originating from HOMO → LUMO+1 and HOMO → LUMO transition (Figure 5.5). The theoretically calculated electronic absorption wavelengths were found to be longer than experimental data, which could be due to a number of factors such as solvent effect, temperature, and dipole moment.

Table 5.2. Calculated electronic transitions of the donor-acceptor **BODIPYs 1–4**.

Compounds	**Wavelength (nm)**	**Composition**	**f[a]**	**Assignment**
BODIPY 1	441 542	HOMO-1→LUMO (0.69) HOMO→LUMO (0.70)	0.38 0.92	π–π* π–π*
BODIPY 2	456 693	HOMO-1→LUMO (0.69) HOMO→LUMO (0.70)	0.35 0.85	π–π* π–π*
BODIPY 3	447 505	HOMO-2→LUMO (0.69) HOMO→LUMO+1 (0.68)	1.20 0.12	π–π* ICT
BODIPY 4	452 629	HOMO-1→LUMO+1 (0.58) HOMO→LUMO (0.68)	0.44 0.85	π–π* ICT

f[a] oscillator strength

5.7. Experimental Section

General Methods

All the moisture and oxygen-sensitive reactions were performed in an inert atmosphere using the standard inert atmosphere method .^{1}H NMR was measured in Bruker Avance (III) 500 MHz, and ^{13}C NMR spectra were measured in 126 MHz using $CDCl_3$ as the internal solvent. The ^{1}H NMR chemical shifts are recorded in parts per million (ppm) relative to the solvent residual peak ($CDCl_3$, 7.26 ppm). The ^{13}C NMR shifts are reported relative to the solvent residual peak ($CDCl_3$, 77.00 ppm). The multiplicities are given as s (singlet), d (doublet), t (triplet), q (quartet), m (multiplet), and the coupling constants values (*J*) are reported in Hz. The UV-visible absorption spectra of all compounds were recorded in PerkinElmer's LAMBDA 35 UV-visible Spectrophotometer in DCM solvent at room temperature. High-Resolution Mass Spectrometry (HRMS) was recorded on a Bruker-Daltonics micrOTOF-Q II mass spectrometer. The cyclic voltammogram and differential voltammogram (DPVs) were recorded on electrochemical analyzer using glassy carbon as the working electrode, Pt wire as the counter electrode and the Ag/AgCl as the reference electrode. Thermogravimetric analysis was performed on the Mettler Toledo thermal analysis system.

Synthesis and characterization of BODIPY 1: Under argon atmosphere, a solution of compound **1** (8-chloro BODIPY) (0.1 g, 0.44 mmol) and the corresponding compound **2** (0.064 g, 0.44 mmol) in dry THF (20 ml), added triethylamine (TEA) (20 ml), $Pd(PPh_3)_4$ (0.016 g, 0.022 mmol), CuI (0.004 g, 0.022 mmol), stirred for 2 h at 0 ℃, after completion of the reaction, the reaction mixture was concentrated under reduced pressure, the crude compound was purified by column chromatography on silica, using Hexane/ DCM (70:30, v/v), and afforded pure **BODIPY 1** (Purple color) around 80 % yield. **^{1}H NMR (500 MHz, $CDCl_3$) δ** 7.76 (s, 2H), 7.54 (d, *J* = 8.9 Hz, 2H), 7.37 (d, *J* = 3.9 Hz, 2H), 6.69 (d, *J* = 8.9 Hz, 2H), 6.52 (d, *J* = 2.9 Hz, 2H), 3.09 (s, 6H); **^{13}C NMR (126 MHz, $CDCl_3$) δ** 152.21, 141.61, 136.03, 135.21, 129.16, 127.85, 117.59, 112.68, 111.88, 106.92, 86.68, 40.20; **HRMS**

(ESI, positive) m/z calculated for $C_{19}H_{16}BF_2N_3$ 358.1301 $[M + Na]^+$, measured 358.1306 $[M + Na]^+$.

Synthesis and characterization of BODIPY 2: Under argon atmosphere, a solution of compound **1** (8-chloro BODIPY) (0.1 g, 0.44 mmol) and the corresponding compound **3** (8-chloro BODIPY) (0.108 g, 0.44 mmol) in dry THF (20 ml), added triethylamine (TEA) (20 ml), $Pd(PPh_3)_4$ (0.016 g, 0.022 mmol), CuI (0.004 g, 0.022 mmol), stirred for 2 h at 0 ℃, after completion of the reaction, the reaction mixture was concentrated under reduced pressure, the crude compound was purified by column chromatography on silica, using Hexane/ DCM (60:40, v/v), and afforded pure **BODIPY 2** (Brown colour) around 70 % yield. **^{1}H NMR (500 MHz, $CDCl_3$) δ** 7.83 (s, 2H), 7.62 (d, *J* = 8.3 Hz, 2H), 7.55 (d, *J* = 8.3 Hz, 2H), 7.42 (dd, *J* = 12.9, 6.4 Hz, 4H), 6.67 (d, *J* = 8.8 Hz, 2H), 6.56 (d, *J* = 3.6 Hz, 2H), 3.02 (s, 6H); **^{13}C NMR (126 MHz, $CDCl_3$) δ** 150.64, 143.71, 133.17, 132.81, 131.59, 129.16, 127.53, 119.39, 118.51, 111.91, 109.19, 106.13, 95.58, 87.44, 85.80, 40.30; **HRMS (ESI, positive) m/z** calculated for $C_{27}H_{20}BF_2N_3$ 436.1796 $[M + H]^+$, measured 436.1836 $[M + H]^+$.

Synthesis and characterization of BODIPY 3: In a 50 mL round-bottomed flask, tetracyanoethylene (TCNE, 32 mg, 0.25 mmol) was added to the solution of BODIPY **2** (100 mg, 0.22 mmol) in DCM (20 mL). The reaction mixture was stirred at room temperature for 6 h. After completion of the reaction, the reaction mix. was dried under vacuum and purified by column chromatography with Hexane/DCM (30:70, v/v) as eluent to give BODIPY **3** as a dark red solid (Yield: 75 %). **^{1}H NMR (500 MHz, $CDCl_3$) δ** 7.86 (s, 2H), 7.82 – 7.77 (m, 6H), 7.36 (d, *J* = 4.1 Hz, 2H), 6.77 (d, *J* = 9.4 Hz, 2H), 6.58 (d, *J* = 3.9 Hz, 2H), 3.20 (s, 6H); **^{13}C NMR (126 MHz, $CDCl_3$) δ** 167.94, 162.50, 154.73, 144.91, 133.57, 132.67, 129.90, 129.57, 126.73, 119.11, 118.00, 112.59, 111.85, 101.76, 88.86, 87.48, 40.40; **HRMS (ESI, positive)** m/z calculated for $C_{33}H_{20}BF_2N_7$ 564.1920 $[M + H]^+$, measured 564.1940 $[M + H]^+$.

Synthesis and characterization of BODIPY 4: In 50 mL round-bottomed flask, tetracyanoquinodimethane (TCNQ, 51 mg, 0.25 mmol) was added to a solution of BODIPY **2** (100 mg, 0.22 mmol) in DCE (20

mL) under argon atmosphere. The reaction mixture was heated at 60 ℃ for 8 h. After completion of the reaction, the reaction mixture was dried under vacuum and purified by column chromatography with hexane/DCM (20:80, v/v) (eluent: CH_2Cl_2) BODIPY **4** as dark black (Yield: 71%). **^{1}H NMR (500 MHz, $CDCl_3$) δ** 7.86 (s, 2H), 7.72 (s, 4H), 7.48 (dd, *J* = 9.6, 1.8 Hz, 1H), 7.33 (d, *J* = 4.0 Hz, 2H), 7.30 (dd, *J* = 9.6, 1.8 Hz, 1H), 7.27 (s, 1H), 7.25 (s, 1H), 7.20 (dd, *J* = 9.5, 1.8 Hz, 1H), 6.97 (dd, *J* = 9.6, 1.8 Hz, 1H), 6.73 (d, *J* = 9.1 Hz, 2H), 6.56 (d, *J* = 3.7 Hz, 2H), 3.14 (s, 6H); **^{13}C NMR (126 MHz, $CDCl_3$) δ** 171.21, 153.98, 153.07, 150.77, 144.83, 136.68, 135.82, 134.57, 134.11, 133.52, 132.44, 130.00, 129.47, 125.85, 125.46, 123.53, 119.03, 114.70, 112.72, 102.05, 89.03, 87.18, 72.83, 40.32. **HRMS (ESI, positive) m/z** [M + Na] $^+$ calculated for $C_{39}H_{24}BF_2N_7$ 662.2053, measured 662.2063 [M+ Na] $^+$.

5.8. Conclusion

A set of donor–acceptor (D–A) based **BODIPYs 1**–**4** were designed and synthesized *via* palladium-catalyzed Sonogashira cross-coupling and subsequent [2+2] cycloaddition-retroelectrocyclization reactions were explored. The photophysical properties reveal that the **BODIPY 4** exhibits a strong ICT band at a longer wavelength region due to strong donor–acceptor interaction. The redox properties of push–pull **BODIPYs 1–4** exhibits multiple reduction waves due to presence of multiple-redox active entities. The **BODIPYs 3** and **4** exhibit multiple reduction waves at low potential as compared to **BODIPYs 1** and **2** due presence of strong acceptor groups. The theoretical results reveal that the incorporation of phenyl spacer, TCBD, and cyclohexa-2,5-diene-1,4-ylidene-expanded TCBD unit perturbs the HOMO–LUMO gap. The push–pull **BODIPYs 1–4** shows that the HOMOs are delocalized on both donor and acceptor BODIPY unit, whereas the LUMOs are localized on acceptor TCBD and cyclohexa-2,5-diene-1,4-ylidene-expanded TCBD unit. The **BODIPY 4** exhibits low HOMO–LUMO gap compared to **BODIPY 3** due to strong accepting nature of cyclohexa-

2,5-diene-1,4-ylidene-expanded TCBD unit. This report provides an important route for synthesizing a push–pull chromophores with low HOMO–LUMO gap for optoelectronic applications.

5.9. References

1. Li, G., Chen, Y., Qiao, Y., Lu, Y., & Zhou, G. (2018). Charge Transfer Switching in Donor–Acceptor Systems Based on BN-Fused Naphthalimides. *The Journal of Organic Chemistry*, *83*(10), 5577–5587. https://doi.org/10.1021/acs.joc.8b00597

2. Larsen, C. B., van der Salm, H., Shillito, G. E., Lucas, N. T., & Gordon, K. C. (2016). Tuning the Rainbow: Systematic Modulation of Donor–Acceptor Systems through Donor Substituents and Solvent. *Inorganic Chemistry*, *55*(17), 8446–8458. https://doi.org/10.1021/acs.inorgchem.6b01039

3. McLay, J. R. W., Sutton, J. J., Shillito, G. E., Larsen, C. B., Huff, G. S., Lucas, N. T., & Gordon, K. C. (2021). Transitioning from Intraligand π,π* to Charge-Transfer Excited States Using Thiophene-Based Donor–Acceptor Systems. *Inorganic Chemistry*, *60*(1), 130–139. https://doi.org/10.1021/acs.inorgchem.0c02555

4. Pop, F., Riobé, F., Seifert, S., Cauchy, T., Ding, J., Dupont, N., … Avarvari, N. (2013). Tetrathiafulvalene-1,3,5-triazines as (Multi)Donor–Acceptor Systems with Tunable Charge Transfer: Structural, Photophysical, and Theoretical Investigations. *Inorganic Chemistry*, *52*(9), 5023–5034. https://doi.org/10.1021/ic3027336

5. Mandal, A. (2022). Tuning p-type to n-type semiconductor nature by charge transfer cocrystallization: effect of transfer integral vs. reorganization energy. *CrystEngComm*, *24*(11), 2072–2080. https://doi.org/10.1039/D2CE00006G

6. Gautam, P., Misra, R., Thomas, M. B., & D'Souza, F. (2017). Ultrafast Charge-Separation in Triphenylamine-BODIPY-Derived Triads Carrying Centrally Positioned, Highly Electron-Deficient, Dicyanoquinodimethane or Tetracyanobutadiene Electron-Acceptors.

Chemistry – A European Journal, *23*(38), 9192–9200. https://doi.org/10.1002/chem.201701604

7. Poddar, M., Sharma, V., Mobin, S. M., & Misra, R. (2018). 1,8-Naphthalimide-Substituted BODIPY Dyads: Synthesis, Structure, Properties, and Live-Cell Imaging. *Chemistry – An Asian Journal*, *13*(19), 2881–2890. https://doi.org/10.1002/asia.201800816

8. Dhindsa, J. S., Buguis, F. L., Anghel, M., & Gilroy, J. B. (2021). Band Gap Engineering in Acceptor-Donor-Acceptor Boron Difluoride Formazanates. *The Journal of Organic Chemistry*, *86*(17), 12064–12074. https://doi.org/10.1021/acs.joc.1c01416

9. Donor-Acceptor Based 1,8-Naphthalimide Substituted Phenothiazines: Tuning of HOMO-LUMO Gap. (n.d.). https://doi.org/10.1002/ajoc.202100628

10. Popere, B. C., Della Pelle, A. M., & Thayumanavan, S. (2011). BODIPY-Based Donor–Acceptor π-Conjugated Alternating Copolymers. *Macromolecules*, *44*(12), 4767–4776. https://doi.org/10.1021/ma200839q

11. Carlotti, B., Poddar, M., Elisei, F., Spalletti, A., & Misra, R. (2019). Energy-Transfer and Charge-Transfer Dynamics in Highly Fluorescent Naphthalimide–BODIPY Dyads: Effect of BODIPY Orientation. *The Journal of Physical Chemistry C*, *123*(40), 24362–24374. https://doi.org/10.1021/acs.jpcc.9b05851

12. Niu, S., Ulrich, G., Retailleau, P., & Ziessel, R. (2011). Regioselective Synthesis of 5-Monostyryl and 2-Tetracyanobutadiene BODIPY Dyes. *Organic Letters*, *13*(19), 4996–4999. https://doi.org/10.1021/ol201600s

13. Kong, L., Wong, H.-L., Tam, A. Y.-Y., Lam, W. H., Wu, L., & Yam, V. W.-W. (2014). Synthesis, Characterization, and Photophysical Properties of Bodipy-Spirooxazine and -Spiropyran Conjugates: Modulation of Fluorescence Resonance Energy Transfer Behavior via

Acidochromic and Photochromic Switching. *ACS Applied Materials & Interfaces*, *6*(3), 1550–1562. https://doi.org/10.1021/am404242a

14. Gomez-Duran, C. F. A., Hu, R., Feng, G., Li, T., Bu, F., Arseneault, M., … Tang, B. Z. (2015). Effect of AIE Substituents on the Fluorescence of Tetraphenylethene-Containing BODIPY Derivatives. *ACS Applied Materials & Interfaces*, *7*(28), 15168–15176. https://doi.org/10.1021/acsami.5b05033

15. Zatsikha, Y. V., Didukh, N. O., Swedin, R. K., Yakubovskyi, V. P., Blesener, T. S., Healy, A. T., … Kovtun, Y. P. (2019). Preparation of Viscosity-Sensitive Isoxazoline/Isoxazolyl-Based Molecular Rotors and Directly Linked BODIPY–Fulleroisoxazoline from the Stable meso-(Nitrile Oxide)-Substituted BODIPY. *Organic Letters*, *21*(14), 5713–5718. https://doi.org/10.1021/acs.orglett.9b02082

16. Gao, H., Gao, Y., Wang, C., Hu, D., Xie, Z., Liu, L., … Ma, Y. (2018). Anomalous Effect of Intramolecular Charge Transfer on the Light Emitting Properties of BODIPY. *ACS Applied Materials & Interfaces*, *10*(17), 14956–14965. https://doi.org/10.1021/acsami.7b13444

17. Nguyen, V.-N., Ha, J., Koh, C. W., Ryu, B., Kim, G., Park, J. H., … Yoon, J. (2021). Access to the Triplet Excited States of Heavy-Atom-Free Boron-Dipyrromethene Photosensitizers via Radical Pair Intersystem Crossing for Image-Guided Tumor-Targeted Photodynamic Therapy. *Chemistry of Materials*, *33*(19), 7889–7896. https://doi.org/10.1021/acs.chemmater.1c02776

18. Misra, R., Jadhav, T., Dhokale, B., Gautam, P., Sharma, R., Maragani, R., & Mobin, S. M. (2014). Carbazole-BODIPY conjugates: design, synthesis, structure and properties. *Dalton Transactions*, *43*(34), 13076–13086. https://doi.org/10.1039/C4DT00983E

19. Shinde, J., Thomas, M. B., Poddar, M., Misra, R., & D'Souza, F. (2021). Does Location of BF2-Chelated Dipyrromethene (BODIPY) Ring Functionalization Affect Spectral and Electron Transfer

Properties? Studies on α-, β-, and Meso-Functionalized BODIPY-Derived Donor–Acceptor Dyads and Triads. *The Journal of Physical Chemistry C*, *125*(43), 23911–23921. https://doi.org/10.1021/acs.jpcc.1c06704

20. Gapare, R. L., & Thompson, A. (2022). Substitution at boron in BODIPYs. *Chemical Communications*, *58*(53), 7351–7359. https://doi.org/10.1039/D2CC02362H

21. Kumar, B., Bhatta, A., Saraf, P., Rangan, K., Sarkar, M., Mitra, S., & Kumar, D. (2022). Iodine(III)-promoted regioselective and efficient synthesis of β-triazolyl BODIPYs for the selective recognition of nickel ions and bovine serum albumin. *Dalton Transactions*, *51*(21), 8169–8176. https://doi.org/10.1039/D2DT00946C

22. Lu, P., Chung, K.-Y., Stafford, A., Kiker, M., Kafle, K., & Page, Z. A. (2021). Boron dipyrromethene (BODIPY) in polymer chemistry. *Polymer Chemistry*, *12*(3), 327–348. https://doi.org/10.1039/D0PY01513J

23. Chong, H., Lin, H.-A., Shen, M.-Y., Liu, C.-Y., Zhao, H., & Yu, H. (2015). Step-Economical Syntheses of Functional BODIPY-EDOT π-Conjugated Materials through Direct C–H Arylation. *Organic Letters*, *17*(13), 3198–3201. https://doi.org/10.1021/acs.orglett.5b00875

24. Kaneza, N., Zhang, J., Liu, H., Archana, P. S., Shan, Z., Vasiliu, M., … Pan, S. (2016). Electrochemical and Spectroscopic Properties of Boron Dipyrromethene–Thiophene–Triphenylamine-Based Dyes for Dye-Sensitized Solar Cells. *The Journal of Physical Chemistry C*, *120*(17), 9068–9080. https://doi.org/10.1021/acs.jpcc.6b01611

25. Duan, C., Zhou, Y., Shan, G.-G., Chen, Y., Zhao, W., Yuan, D., … Niu, G. (2019). Bright solid-state red-emissive BODIPYs: facile synthesis and their high-contrast mechanochromic properties. *Journal of Materials Chemistry C*, *7*(12), 3471–3478. https://doi.org/10.1039/C8TC06421K

26. Obondi, C. O., Lim, G. N., Karr, P. A., Nesterov, V. N., & D'Souza, F. (2016). Photoinduced charge separation in wide-band capturing, multi-modular bis(donor styryl)BODIPY–fullerene systems. *Physical Chemistry Chemical Physics*, *18*(27), 18187–18200. https://doi.org/10.1039/C6CP03479A

27. Filatov, M. A., Karuthedath, S., Polestshuk, P. M., Callaghan, S., Flanagan, K. J., Telitchko, M., … Senge, M. O. (2018). Control of triplet state generation in heavy atom-free BODIPY–anthracene dyads by media polarity and structural factors. *Physical Chemistry Chemical Physics*, *20*(12), 8016–8031. https://doi.org/10.1039/C7CP08472B

28. Wei, Z., Sharma, S., Philip, A. M., Sengupta, S., & Grozema, F. C. (2021). Excited state dynamics of BODIPY-based acceptor–donor–acceptor systems: a combined experimental and computational study. *Physical Chemistry Chemical Physics*, *23*(14), 8900–8907. https://doi.org/10.1039/D1CP00453K

29. Thompson, B. L., Kieffer, I. A., & Heiden, Z. M. (2022). Utilization of BODIPY-based redox events to manipulate the Lewis acidity of fluorescent boranes. *Chemical Communications*, *58*(16), 2646–2649. https://doi.org/10.1039/D1CC06400B

30. Misra, R., Dhokale, B., Jadhav, T., & Mobin, S. M. (2014). The quenching of fluorescence as an indicator of donor-strength in meso arylethynyl BODIPYs. *Dalton Transactions*, *43*(12), 4854–4861. https://doi.org/10.1039/C3DT53056F

31. Poddar, M., & Misra, R. (2017). NIR-Absorbing Donor–Acceptor Based 1,1,4,4-Tetracyanobuta-1,3-Diene (TCBD)- and Cyclohexa-2,5-Diene-1,4-Ylidene-Expanded TCBD-Substituted Ferrocenyl Phenothiazines. *Chemistry – An Asian Journal*, *12*(22), 2908–2915. https://doi.org/10.1002/asia.201700879

32. Patil, Y., Popli, C., & Misra, R. (2018). Near-infrared absorbing tetracyanobutadiene-bridged diketopyrrolopyrroles. *New Journal of Chemistry*, *42*(5), 3892–3899. https://doi.org/10.1039/C7NJ05162J

33. Misra, R., Jadhav, T., Nevonen, D., Monzo, E. M., Mobin, S. M., & Nemykin, V. N. (2017). Synthesis, Structures, and Redox Properties of Tetracyano-Bridged Diferrocene Donor–Acceptor–Donor Systems. *Organometallics*, *36*(22), 4490–4498. https://doi.org/10.1021/acs.organomet.7b00728

34. Zhang, Z., Gou, G., Wan, J., Li, H., Wang, M., & Li, L. (2022). Synthesis, Structure, and Significant Energy Gap Modulation of Symmetrical Silafluorene-Cored Tetracyanobutadiene and Tetracyanoquinodimethane Derivatives. *The Journal of Organic Chemistry*, *87*(5), 2470–2479. https://doi.org/10.1021/acs.joc.1c02382

35. Khan, F., Jang, Y., Patil, Y., Misra, R., & D'Souza, F. (2021). Photoinduced Charge Separation Prompted Intervalence Charge Transfer in a Bis(thienyl)diketopyrrolopyrrole Bridged Donor-TCBD Push-Pull System. *Angewandte Chemie*, *133*(37), 20681–20690. https://doi.org/10.1002/ange.202108293

36. Shoji, T., Maruyama, M., Shimomura, E., Maruyama, A., Ito, S., Okujima, T., … Morita, N. (2013). Synthesis, Properties, and Redox Behavior of Tetracyanobutadiene and Dicyanoquinodimethane Chromophores Bearing Two Azulenyl Substituents. *The Journal of Organic Chemistry*, *78*(24), 12513–12524. https://doi.org/10.1021/jo402104n

37. Banziger, S. D., Clendening, R. A., Oxley, B. M., & Ren, T. (2020). Spectroelectrochemical and Computational Analysis of a Series of Cycloaddition–Retroelectrocyclization-Derived Donor–Acceptor Chromophores. *The Journal of Physical Chemistry B, 124*(52), 11901–11909. https://doi.org/10.1021/acs.jpcb.0c09450

38. Rout, Y., Gautam, P., & Misra, R. (2017). Unsymmetrical and Symmetrical Push–Pull Phenothiazines. *The Journal of Organic Chemistry*, *82*(13), 6840–6845. https://doi.org/10.1021/acs.joc.7b00991

39. Yadav, I. S., Alsaleh, A. Z., Misra, R., & D'Souza, F. (2021). Charge stabilization via electron exchange: excited charge separation in

symmetric, central triphenylamine derived, dimethylaminophenyl–tetracyanobutadiene donor–acceptor conjugates. *Chemical Science*, *12*(3), 1109–1120. https://doi.org/10.1039/D0SC04648E

40. Finke, A. D., Dumele, O., Zalibera, M., Confortin, D., Cias, P., Jayamurugan, G., … Diederich, F. (2012). 6,6-Dicyanopentafulvenes: Electronic Structure and Regioselectivity in [2 + 2] Cycloaddition–Retroelectrocyclization Reactions. *Journal of the American Chemical Society*, *134*(43), 18139–18146. https://doi.org/10.1021/ja309141r

41. Dengiz, C., Breiten, B., Gisselbrecht, J.-P., Boudon, C., Trapp, N., Schweizer, W. B., & Diederich, F. (2015). Synthesis and Optoelectronic Properties of Janus-Dendrimer-Type Multivalent Donor–Acceptor Systems. *The Journal of Organic Chemistry*, *80*(2), 882–896. https://doi.org/10.1021/jo502367h

42. Li, Y., Tsuboi, K., & Michinobu, T. (2010). Double Click Synthesis and Second-Order Nonlinearities of Polystyrenes Bearing Donor−Acceptor Chromophores. *Macromolecules*, *43*(12), 5277–5286. https://doi.org/10.1021/ma100869m

43. Shoji, T., Miura, K., Araki, T., Maruyama, A., Ohta, A., Sekiguchi, R., … Okujima, T. (2018). Synthesis of 2-Methyl-1-azulenyl Tetracyanobutadienes and Dicyanoquinodimethanes: Substituent Effect of 2-Methyl Moiety on the Azulene Ring toward the Optical and Electrochemical Properties. *The Journal of Organic Chemistry*, *83*(12), 6690–6705. https://doi.org/10.1021/acs.joc.8b01067

44. Philippe, C., Bui, A. T., Batsongo-Boulingui, S., Pokladek, Z., Matczyszyn, K., Mongin, O., … Trolez, Y. (2021). 1,1,4,4-Tetracyanobutadiene-Functionalized Anthracenes: Regioselectivity of Cycloadditions in the Synthesis of Small Near-IR Dyes. *Organic Letters*, *23*(6), 2007–2012. https://doi.org/10.1021/acs.orglett.1c00136

45. Kraußе, N., Kielmann, M., Ma, J., & Butenschön, H. (2015). Reactions of Alkynyl- and 1,1′-Dialkynylferrocenes with Tetracyanoethylene – Unanticipated Addition at the Less Electron-Rich

of Two Triple Bonds. *European Journal of Organic Chemistry*, *2015*(12), 2622–2631. https://doi.org/10.1002/ejoc.201500105

46. Yadav, I. S., Jang, Y., Rout, Y., Thomas, M. B., Misra, R., & D'Souza, F. (2022). Near-IR Intramolecular Charge Transfer in Strongly Interacting Diphenothiazene-TCBD and Diphenothiazene-DCNQ Push-Pull Triads. *Chemistry – A European Journal*, *28*(25), e202200348. https://doi.org/10.1002/chem.202200348

47. Poddar, M., Jang, Y., Misra, R., & D'Souza, F. (2020). Excited-State Electron Transfer in 1,1,4,4-Tetracyanobuta-1,3-diene (TCBD)- and Cyclohexa-2,5-diene-1,4-diylidene-Expanded TCBD-Substituted BODIPY-Phenothiazine Donor–Acceptor Conjugates. *Chemistry – A European Journal*, *26*(30), 6869–6878. https://doi.org/10.1002/chem.202000346

48. Gautam, P., Dhokale, B., Mobin, S. M., & Misra, R. (2012). Ferrocenyl BODIPYs: synthesis, structure and properties. *RSC Advances*, *2*(32), 12105–12107. https://doi.org/10.1039/C2RA21964F

49. Dhokale, B., Jadhav, T., Mobin, S. M., & Misra, R. (2016). Tetracyanobutadiene functionalized ferrocenyl BODIPY dyes. *Dalton Transactions*, *45*(4), 1476–1483. https://doi.org/10.1039/C5DT04037J

Chapter 6

Phenothiazine and Phenothiazine-5,5-dioxide Based BODIPYs: Synthesis, Photophysical, Electrochemical and Theoretical Studies

6.1. Introduction

The π-conjugated donor–acceptor (D–A) materials has emerged as a hot area of research over the past few decades due to their potential applications in electroluminescent devices, dye-sensitized solar cells and chemosensors.[1–5] The donor–acceptor type of molecular system involves an intramolecular charge transfer (ICT) transition from an electron-rich donor to an electron-deficient acceptor unit, which can affect the properties like absorption, emission wavelength, energy levels of the highest occupied molecular orbitals (HOMOs) and the lowest unoccupied molecular orbitals (LUMOs).[6] The π-conjugated molecules, whose optical and electrochemical properties can be improved through molecular engineering, are an important class of materials and useful in semiconducting devices like field-effect transistors, light-emitting diodes (LEDs), and organic solar cells (OSCs). The synthesis of conjugated molecules *via* incorporating heteroatoms such as N, O, and S are a method that result in modified electronic structures with improved HOMO–LUMO gap.[7] The 4,4-Difluoro-4-borata-3a-azonia-4a-aza-*s*-indacene (BODIPY) dyes are one of the most active groups of fluorophores because of the easy synthetic modifications and unique properties such as strong absorption in the visible to near-infrared (NIR) range, high molar extinction coefficient, narrow emission band, a high fluorescence quantum yield, strong photo and chemical stability.[8–15] The electrochemical characteristics of the BODIPY-based dyes are reversible during oxidation and reduction, indicating that the BODIPY core can stabilize an extra electron and a hole in the π-conjugated molecular system.[16] Light capture and conversion efficiency of the BODIPY chromophores may be fine-tuned

by incorporating the appropriate donor or acceptor units, and π-linker group.[17] The BODIPY dyes are a type of versatile fluorophores that can be used in various applications such as bioimaging, organic solar cells, photodynamic therapy (PDT), organic fluorescence emitting devices (OFEDs), and chemo-sensors.[18–22]

The 10*H*-phenothiazine is an active building block for synthesizing push–pull molecular systems due to its strong electron donor-ability.[23] The phenothiazine (PTZ) is a tricyclic and non-planar molecule, which shows an absorption band at 316 nm in DCM solvent.[24, 25] Phenothiazine shows one-electron oxidation at low potential due to the presence of electron-rich sulfur (S) and nitrogen (N) atoms and useful in field effect transistors (OFETs), non-linear optics (NLO), dye-sensitized solar cells (DSSCs), perovskite solar cells (PSCs) and organic light-emitting diodes (OLEDs).[26–33] The phenothiazine unit exhibit high electron density that is primarily focused on the sulfur atom.[34] Converting an electron-donating sulfur atom to an electron-withdrawing sulfone group decreases the donor ability and resist the phenothiazine towards oxidation.[35, 36] However, the research on altering the oxidation state of the sulfur atom in the thiazine ring of phenothiazine is limited and uncommon. The phenothiazine 5,5-dioxide derivatives have been proved as an efficient building block for organic RTP materials and valuable for optoelectronic fields such as display, organic light emitting diodes (OLEDs), and bioimaging.[37] Recently, Ren *et al.* reported a series of phenothiazine 5,5-dioxide derivatives and studied room temperature phosphorescence (RTP) properties.[38] Xiang *et al.* reported phenothiazine 5,5-dioxide-based donor–acceptor chromophores for thermally activated delayed fluorescence (TADF) and aggregation-induced delayed fluorescence (AIDF) materials.[39]

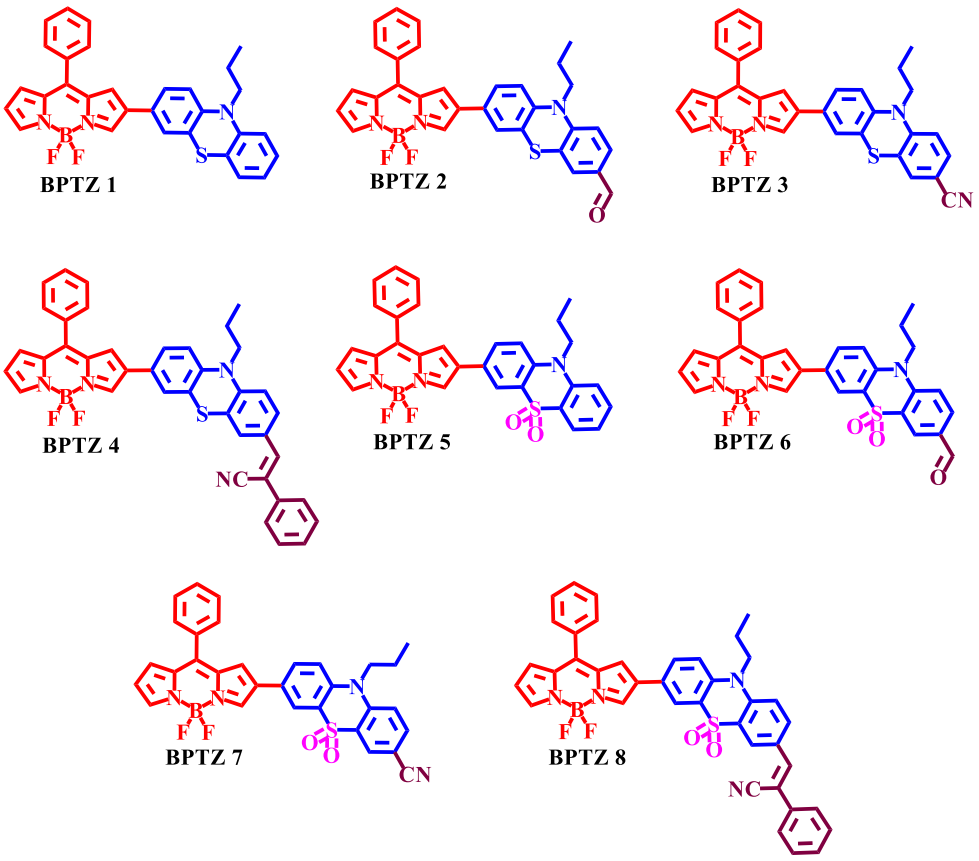

Chart 6.1. Molecular structures of the investigated push–pull BODIPYs **BPTZ 1–8**.

Herein, we report the design and synthesis of π-conjugated push–pull chromophores **BPTZ 1–8** in which the phenothiazine and phenothiazine 5,5-dioxide used as donor unit, whereas BODIPY were used as acceptor unit (Chart 6.1). We explored the effect of electron donor phenothiazine and phenothiazine 5,5-dioxide units on the photophysical and redox properties of the BODIPYs. The photophysical properties of the push–pull BODIPYs **BPTZ 1–4** shows a bathochromic shift in the UV-visible spectra compared to **BPTZ 5–8** due to the strong donor ability of the phenothiazine unit. The electrochemical studies reveal that the push–pull BODIPYs **BPTZ 1–8** exhibit two oxidation and one reduction waves at low potential due to redox-active phenothiazine, phenothiazine 5,5-dioxide and BODIPY entities. The computational studies of the BODIPYs **BPTZ 1–8** show that the HOMOs are delocalized over phenothiazine, phenothiazine 5,5-dioxide and BODIPY unit, whereas LUMOs are cantered on acceptor BODIPY

core. The push–pull conjugates **BPTZ 1–4** exhibit a low HOMO–LUMO gap relative to the **BPTZ 5–8** due to strong push-pull interaction.

6.2. Result and Discussion

The push–pull conjugates **BPTZ 1–8** were synthesized *via* Palladium-catalyzed Suzuki cross-coupling reaction and incorporation of oxygen atoms on the phenothiazine unit. The *β*-bromo BODIPY **1** reacts with boronate ester of phenothiazine **2** in the presence of $Pd(PPh_3)_4$ as catalyst at 90 ℃ for 12 h using Toluene: EtOH: H_2O (6:3:1), resulted **BPTZ 1** in 75% yield. The **BPTZ 1** further reaction of 3 equivalents of 3-chloroperbenzoic acid (*m*-CPBA) in dichloromethane (DCM) solution at room temperature for 1 h, resulted **BPTZ 5** in 78% yield. The **BPTZ 2–4** were synthesized by the Suzuki cross-coupling reaction of *β*-bromo BODIPY **1** with boronate ester of phenothiazines **3–5**, resulted in 72%, 80%, and 75% yields, respectively. The **BPTZ 2–4** were further reacted with 3 equivalent of *m*-CPBA in dry DCM solvent at room temperature for 1 h, resulted **BPTZ 6–8** in 80%, 79%, and 76% yields, respectively (Scheme 6.1). The push–pull chromophores **BPTZ 1–8** were purified by column chromatography (silica gel size = 100–200 mesh) using hexane and dichloromethane solvent. The synthesized conjugates **BPTZ 1–8** are readily soluble in solvents such as acetone, chloroform, dichloromethane, acetonitrile, and tetrahydrofuran. The ^{1}H NMR, ^{13}C NMR and HRMS techniques were used to characterize the molecular structures of push–pull conjugates **BPTZ 1–8**.

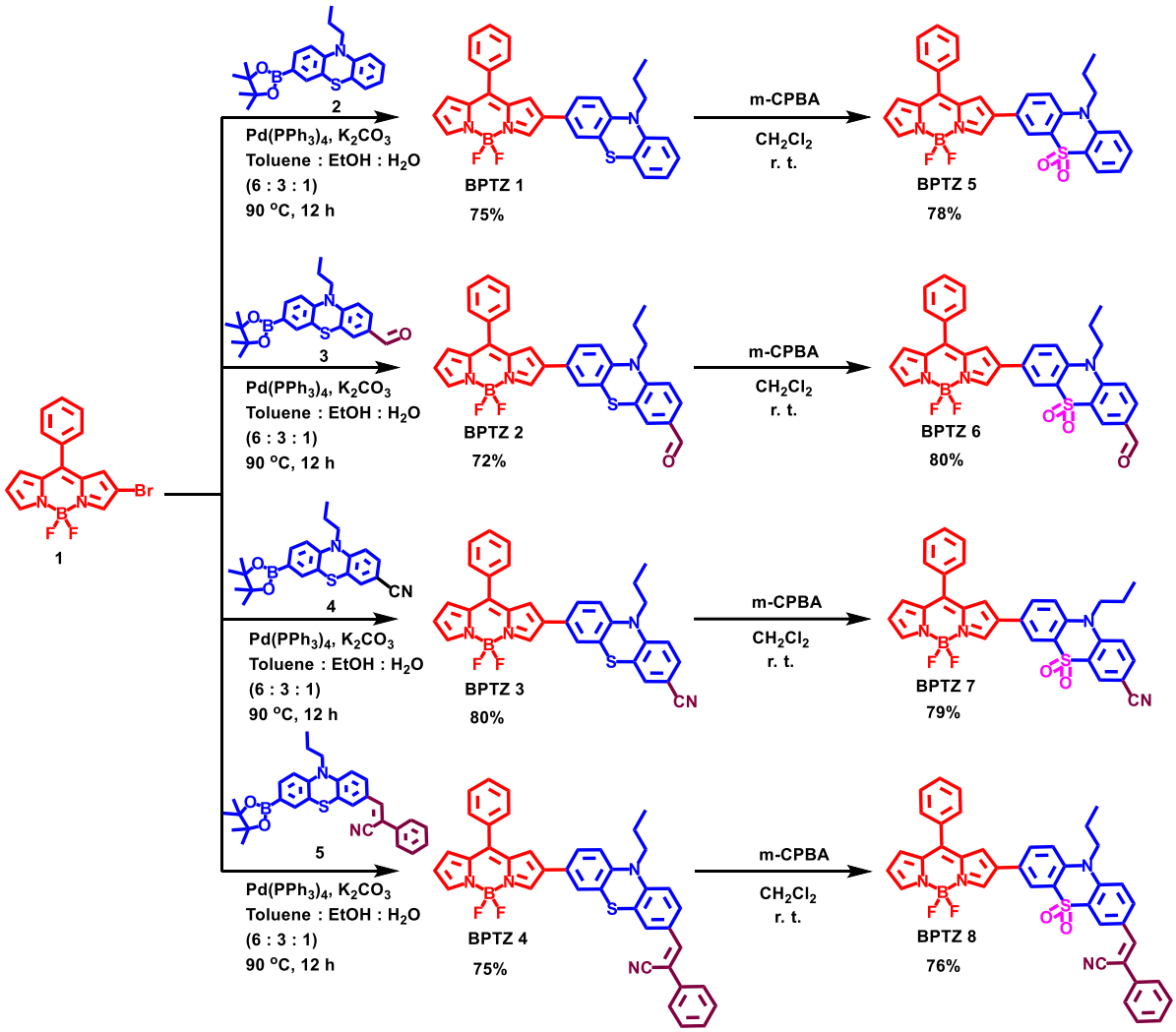

Scheme 6.1. Synthetic route of push–pull conjugates **BPTZ 1–8**.

6.3. Photophysical properties

The electronic absorption spectra of the push–pull conjugates **BPTZ 1–8** were recorded in dry dichloromethane (DCM) solvent at room temperature (Figure 6.1), and the data are tabulated in Table 6.1. Generally, the BODIPY exhibits an intense electronic absorption band around 500 nm range in the UV-visible spectra.[40] The π-conjugated push–pull conjugates **BPTZ 1–8** exhibit two absorption bands in UV-visible spectra: the first absorption band at 419–468 nm and the second at 553–590 nm, range. The absorption band at the lower wavelength region is attributed to phenothiazine and phenothiazine-5,5-dioxide unit and at the higher wavelength region corresponds to the BODIPY.

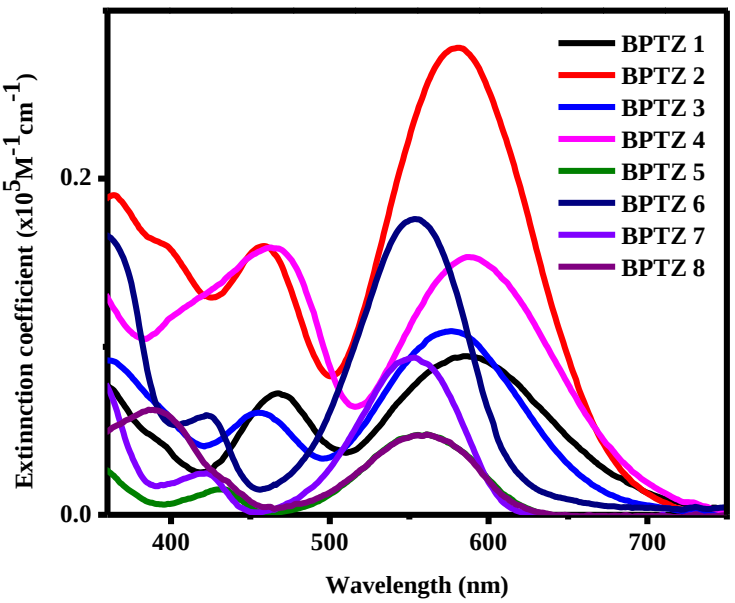

Figure 6.1. Absorption spectra of the push–pull conjugates **BPTZ 1–8** in dichloromethane (10^{-5} M).

The phenothiazine functionalized BODIPYs **BPTZ 1** and **2** exhibit two absorption bands at 468 nm, 589 nm, and 456 nm, 579 nm, respectively. The **BPTZ 3** and **4** exhibit absorption bands at 454 nm, 576 nm, and 464 nm, 589 nm, respectively. The phenothiazine-5,5-dioxide functionalized push–pull chromophores **BPTZ 5–8** exhibit two electronic absorption bands in UV-visible spectra. The phenothiazine-5,5-dioxide substituted BODIPYs **BPTZ 5** and **6** exhibit absorption bands at 432 nm, 562 nm, and 423 nm, 554 nm, respectively. The **BPTZ 7** and **8** exhibit absorption band at 419 nm, 553 nm, and 390 nm, 559 nm, respectively. The phenothiazine and phenothiazine-5,5-dioxide substituted push–pull chromophores **BPTZ 1–8** exhibit two absorption band in UV-visible region and both corresponds to the π–π* transition (Figure 6.1).

Table 6.1. Photophysical and electrochemical data of push–pull chromophores **BPTZ 1–8**.

Photophysical data[a]				**Electrochemical data[b]**	
Compound	**λ_{abs} (nm)**	**ε (M^{-1} cm^{-1})**	**Optical band gap (eV)**	**E_{oxi} (V)**	**E_{red} (V)**
BPTZ 1	468 589	7220 9410	1.69	0.61 1.27	-0.65
BPTZ 2	456 579	15970 27780	1.68	0.81 1.35	-0.71
BPTZ 3	454 576	6080 10930	1.67	0.84 1.35	-0.71
BPTZ 4	464 590	15850 15320	1.58	0.71 1.29	-0.74
BPTZ 5	432 562	1490 4750	1.70	1.56 1.83	-0.69
BPTZ 6	423 554	5890 17580	1.89	1.32 1.83	-0.68
BPTZ 7	419 553	2440 9340	1.86	1.27 1.86	-0.67
BPTZ 8	390 559	6210 4730	1.71	1.25 1.80	-0.67

[a] Absorbance recorded in dry DCM at 1×10^{-5} M conc. λ_{abs}: absorption wavelength. ε: extinction coefficient. **[b]** Electrochemical analysis was estimated by differential pulse voltammetry in 0.1 M solution of Bu_4NPF_6 in DCM at 100 mV s^{-1} scan rate *versus* Ag/AgCl at 25 °C. E_{oxi} and E_{red} values are based on DPV analysis.

The bathochromically shifted absorption spectra observed for the phenothiazine functionalized **BPTZ 1–4** compared to phenothiazine-5,5-dioxide substituted BODIPYs **BPTZ 5–8**, which indicate that the phenothiazine is a strong electron donor relative to phenothiazine-5,5-dioxide unit.

The optical bandgap estimated from the onset wavelength of the absorption spectrum, increase upon increasing the oxygen atoms attached to the phenothiazine sulfur. The optical bandgap of the push–pull conjugates **BPTZ 1–8** follow the order **BPTZ 6> BPTZ 7> BPTZ 8> BPTZ 5> BPTZ 1> BPTZ 2> BPTZ 3> BPTZ 4**. The trend indicates that the incorporation of the oxygen atoms on the phenothiazine unit increases the optical band, which resulted in the hypsochromic (blue) shift due to weak donor ability of phenothiazine-5,5-dioxide unit.

6.4. Electrochemical properties

Cyclic voltammetry (CV) and differential pulse voltammetry (DPV) were used to explore the redox behaviour and potentials of the push–pull conjugates **BPTZ 1–8**. All the measurements were recorded in dry dichloromethane (DCM) solvent at room temperature using tetrabutylammonium hexafluorophosphate (Bu_4NPF_6) as a supporting electrolyte. The CVs and DPVs of the push–pull **BPTZ 1–4** are depicted in Figure 6.2. The electrochemical data of the BODIPYs **BPTZ 1–8** are tabulated in Table 6.1.

The push–pull conjugates **BPTZ 1–8** exhibit multiple redox-waves due to redox-active phenothiazine, phenothiazine-5,5-dioxide and BODIPY unit. The oxidation and reduction potentials are crucial in determining the donor ability of chromophores in the electron transfer activities. In general, phenothiazine exhibits single reversible oxidation wave at low potential, whereas BODIPY unit shows one oxidation and a one reduction wave due to the formation of a mono π-radical cation and a mono π-radical anion.[40–42]

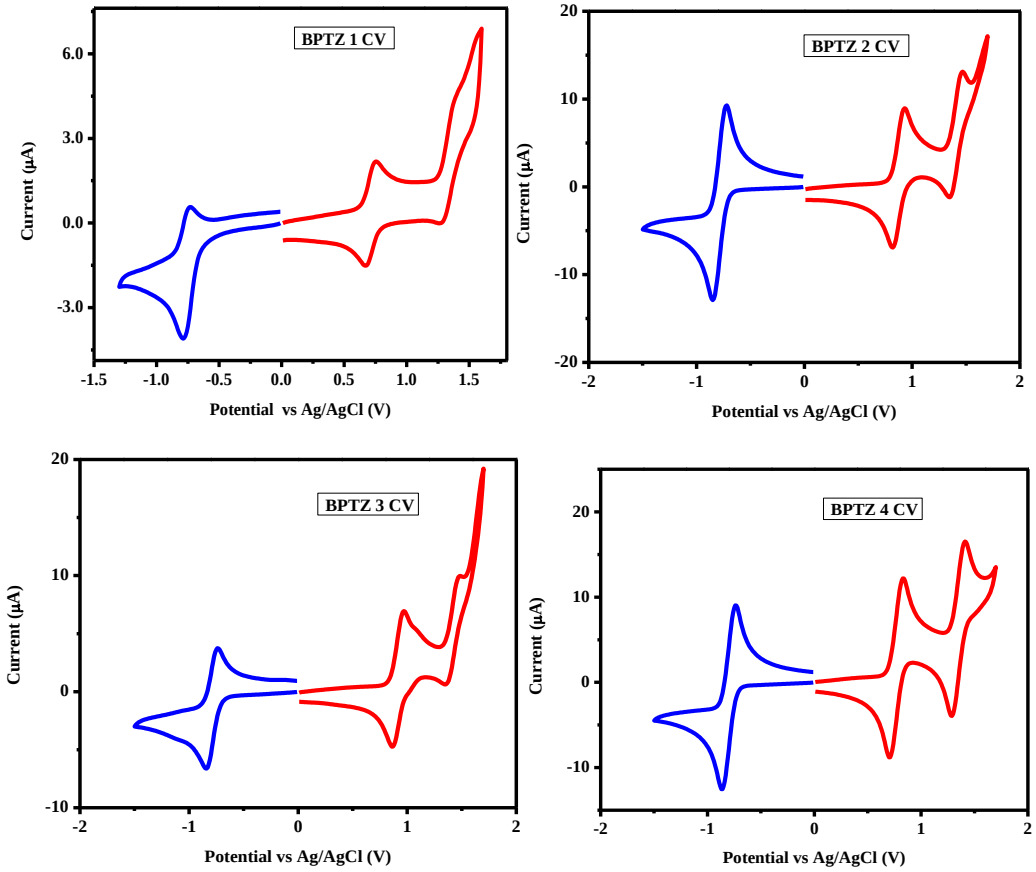
BPTZ 1 CV
Current (µA)
Potential vs Ag/AgCl (V)
BPTZ 2 CV
Current (µA)
Potential vs Ag/AgCl (V)
BPTZ 3 CV
Current (µA)
Potential vs Ag/AgCl (V)
BPTZ 4 CV
Current (µA)
Potential vs Ag/AgCl (V)

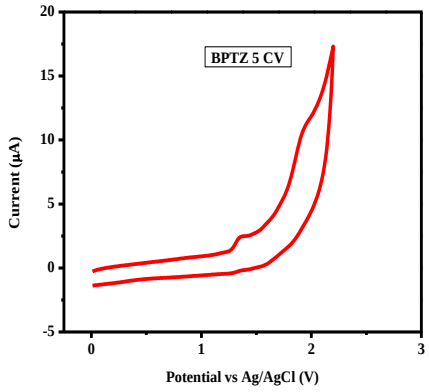
BPTZ 5 CV
Current (µA)
Potential vs Ag/AgCl (V)

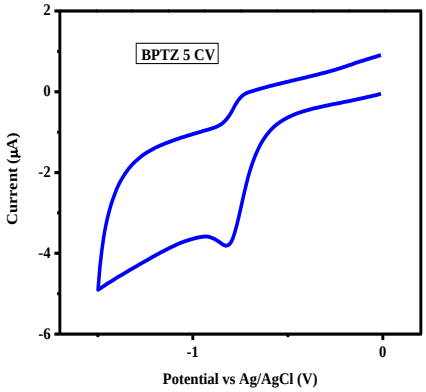
BPTZ 5 CV
Current (µA)
Potential vs Ag/AgCl (V)

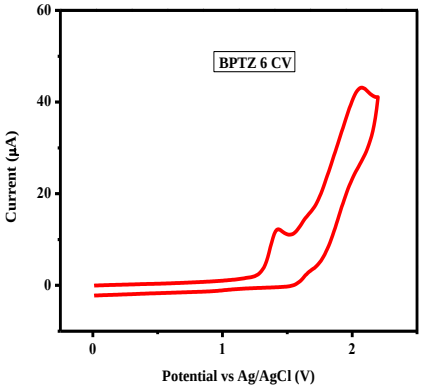
BPTZ 6 CV
Current (µA)
Potential vs Ag/AgCl (V)

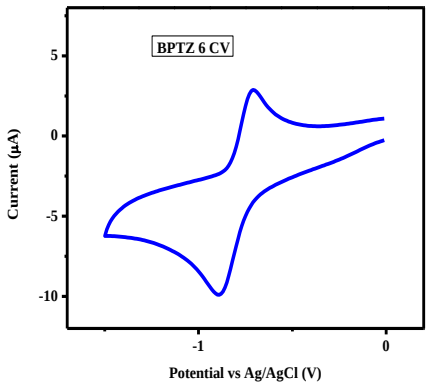
BPTZ 6 CV
Current (µA)
Potential vs Ag/AgCl (V)

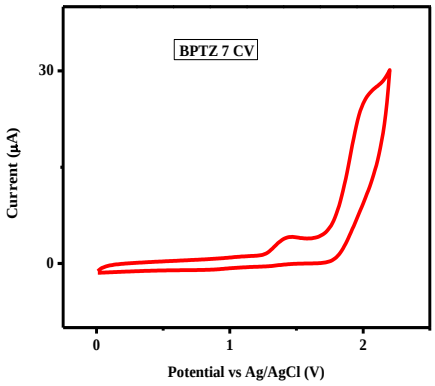
BPTZ 7 CV
Current (µA)
Potential vs Ag/AgCl (V)

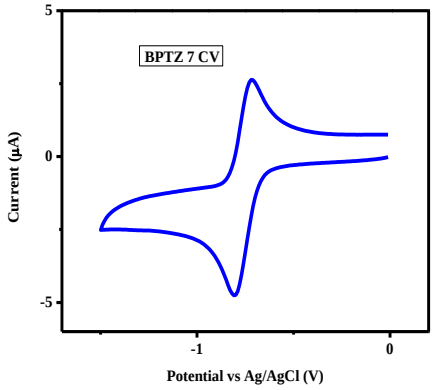
BPTZ 7 CV
Current (µA)
Potential vs Ag/AgCl (V)

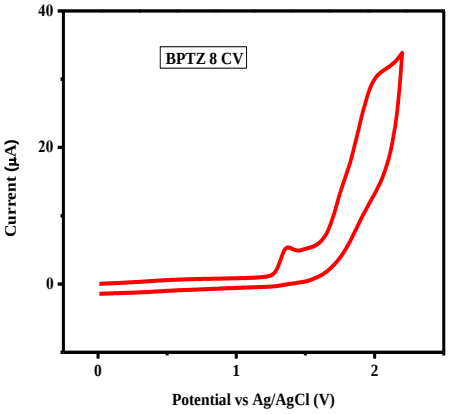
BPTZ 8 CV
Current (µA)
Potential vs Ag/AgCl (V)

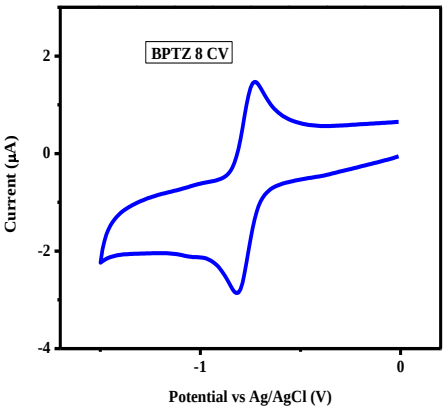
BPTZ 8 CV
Current (µA)
Potential vs Ag/AgCl (V)

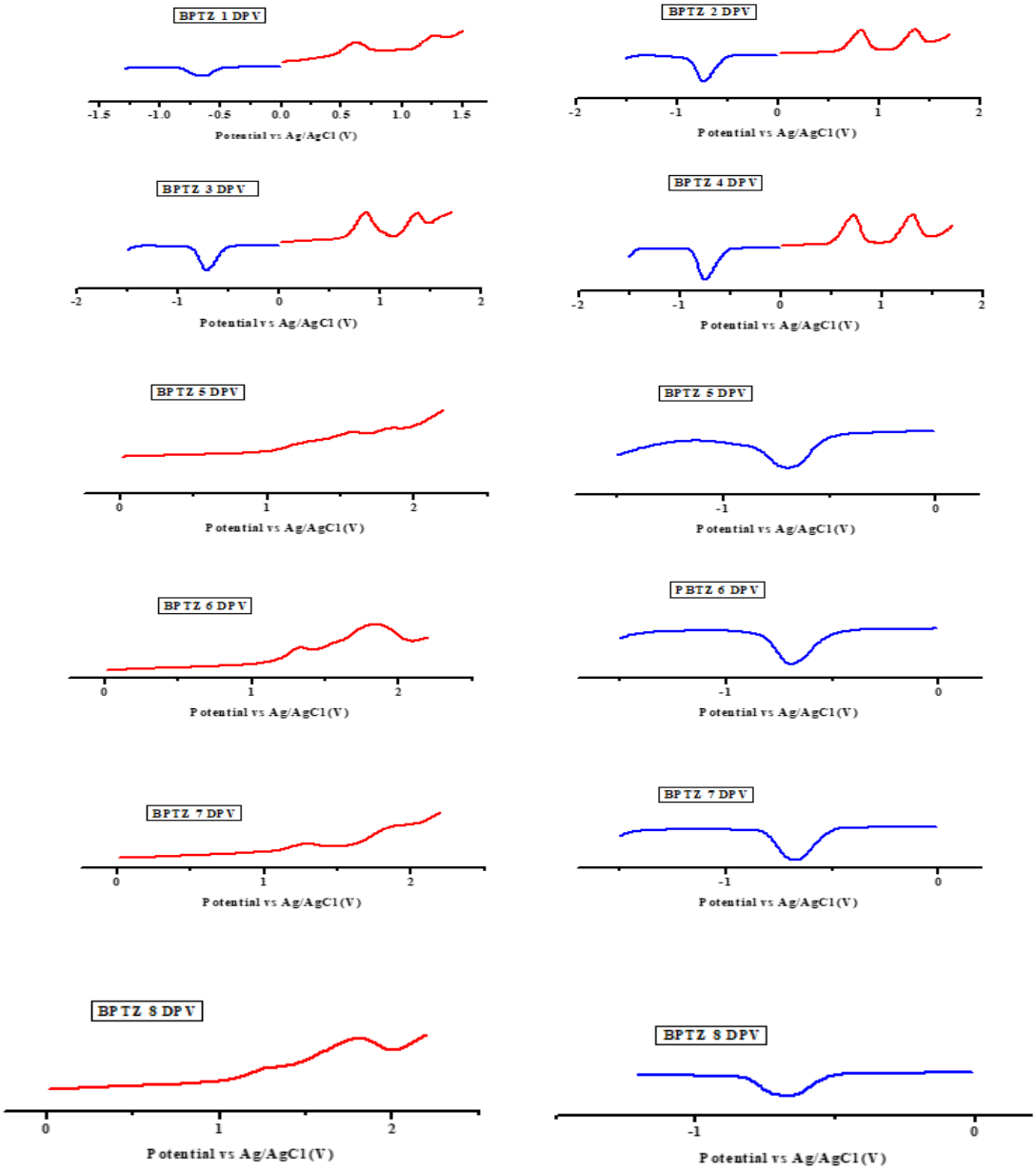

Figure 6.2. CVs and DPVs of the push–pull conjugates **BPTZ 1–8** in 0.1 M solution of Bu_4NPF_6 using dichloromethane solvent at 100 mV s^{-1} scan rate *versus* Ag/AgCl at 25 °C.

The push–pull conjugates **BPTZ 1–8** exhibits two oxidation waves at +0.61, +1.27 V; +0.81, +1.35 V; +0.84, +1.35 V; +0.71, +1.29 V; +1.56, 1.83 V; +1.32 V, +1.83 V; +1.27 V, +1.86 V; +1.25 V and +1.80 V and one reduction wave at –0.65 V; –0.71 V; –0.71 V; –0.74, –0.69 V, –0.68 V; –0.67 and –0.67 V, respectively (Table 6.1). The first oxidation wave at low potential corresponds to the phenothiazine and

phenothiazine-5,5-dioxide unit, and the second oxidation wave corresponds to the BODIPY. The push–pull conjugates **BPTZ 1–8** exhibits a single reduction wave at –0.65 to –0.74 V range due to formation of mono-radical anion of the BODIPY unit. The electrochemical results suggest that on the anodic side the oxidation wave of the phenothiazine-5,5-dioxide functionalized conjugates **BPTZ 5–8** were shifted towards more positive potentials relative to the phenothiazine functionalized BODIPYs **BPTZ 1–4** due to weak donor ability of phenothiazine-5,5-dioxide unit. The HOMO and LUMO energy levels of push-pull conjugates **BPTZ 1–8** were estimated by using the first onset potential of the oxidation and reduction waves. The HOMOs for the phenothiazine and phenothiazine-5,5-dioxide functionalized BODIPYs **BPTZ 1–8** estimated at –5.05, –5.25, –5.27, –5.10, –5.73, –5.72, –5.71, and –5.74 eV and the LUMOs are at –3.80, –3.75, –3.76, –3.77, –3.82, –3.74, –3.78, and –3.75 eV, respectively. These findings suggest that increasing of sulfur oxidation state has more effects on the HOMO compared to the LUMO energy levels.

6.5. Theoretical calculations

The geometry and electronic properties of the push–pull chromophores **BPTZ 1–8** were investigated by density functional theory (DFT) calculations at the B3LYP/6-31G (d,p) level in the Gaussian 09W program. The optimized frontier molecular orbitals of push–pull conjugates **BPTZ 1–8** are represented in Figure 6.3. The push–pull chromophores **BPTZ 1–8** exhibits a non-planar geometry due to the butterfly structure of phenothiazine and phenothiazine-5,5-dioxide unit. The highest occupied molecular orbitals (HOMOs) of the push–pull conjugates **BPTZ 1–8** are delocalized over phenothiazine, phenothiazine-5,5-dioxide and BODIPY unit, whereas the lowest unoccupied molecular orbitals (LUMOs) are cantered on the acceptor BODIPY core. The theoretically estimated HOMO energy levels of the push–pull conjugates **BPTZ 1–8** are –4.79 eV, –5.30 eV, –5.39 eV, –5.17 eV, –5.51 eV, –5.73 eV, –5.78 eV and –5.60 eV and associated

LUMO energy levels are –2.77 eV, –2.91 eV, –2.93 eV, –2.89 eV, –2.88 eV, –3.00 eV, –3.03 eV and –2.97 eV, respectively (Figure 6.3). The theoretical HOMO–LUMO gaps of push–pull conjugates **BPTZ 1–8** are 2.02 V, 2.39 V, 2.46 V, 2.28 V, 2.63 V, 2.73 V, 2.75 V, and 2.63 V, respectively (Figure 6.3). The phenothiazine substituted BODIPYs **BPTZ 1–4** exhibits a low HOMO–LUMO gap relative to phenothiazine-5,5-dioxide functionalized BODIPYs **BPTZ 5–8** due to the strong donor–acceptor interaction. The optical bandgap (E_{gap}) calculated from UV-vis absorption spectra reasonably agrees with the HOMO–LUMO gap calculated from DFT calculations.

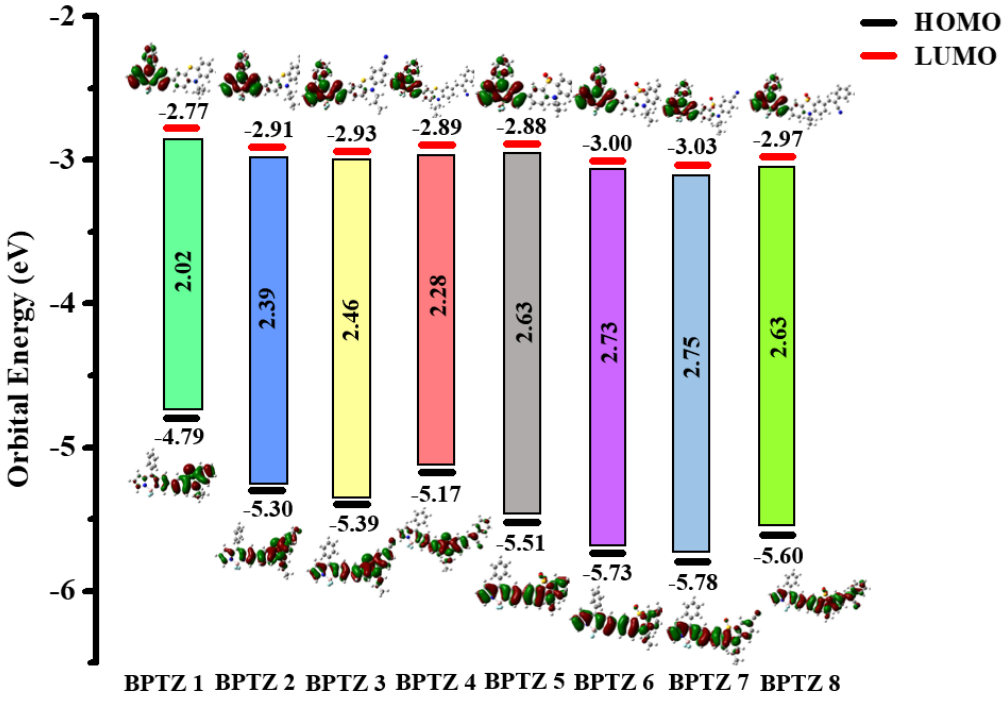

Figure 6.3. Energy profile diagram and optimized frontier HOMO and LUMO orbitals of the push–pull BODIPYs **BPTZ 1–8** estimated by DFT calculations (B3LYP/6-31G (d, p) level).

The TD-DFT calculations were performed on the optimized push–pull conjugates **BPTZ 1–8** at CAM-B3LYP/6-31G (d, p) using DCM solvent to evaluate the electronic properties. The polarized continuum model (PCM) was used to analyse the solvent effect in TD-DFT calculation. The electronic transitions with composition, assignment, and oscillator strength of push–pull chromophores **BPTZ**

1–8 are summarized in the Table 6.2. The theoretical results reveal that the BODIPYs **BPTZ 1**–**8** exhibit two major electronic transitions in UV/visible region, and both correspond to the π–π* transition. The TD-DFT calculations of the push–pull conjugates **BPTZ 1**–**8** exhibits an absorption band in the longer wavelength region at 476 nm, 456 nm, 454 nm, 459 nm, 449 nm, 446 nm, 445 nm and 446 nm, originating from the HOMO→LUMO, attributed to the π–π* transition. The push–pull BODIPYs **BPTZ 1**–**4** exhibits bathochromic shift compared to phenothiazine-5,5-dioxide substituted push–pull BODIPYs **BPTZ 5**–**8** due to the strong donor ability of phenothiazine unit. The UV-vis absorption spectra of the push–pull BODIPYs **BPTZ 1** and **BPTZ 2** experimental (bottom) and TD-DFT predicted (top) in DCM solvent are shown in the Figure 6.4.

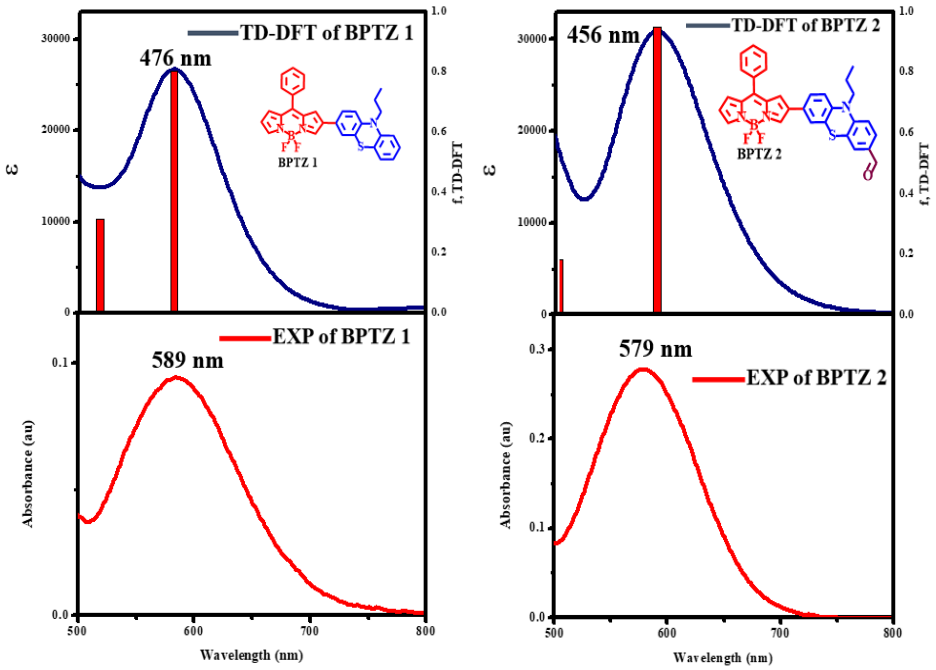

Figure 6.4. UV-vis absorption spectra of the push–pull BODIPYs **BPTZ 1** and **BPTZ 2**. Experimental (bottom) and TD-DFT predicted (top) in DCM solvent.

The theoretically calculated electronic absorption wavelengths were found to be longer than experimental data, which could be due to several factors such as solvent effect, temperature, and dipole moment.

Table 6.2. Calculated electronic transitions of push–pull BODIPYs **BPTZ 1–8**.

Compound	Wavelength (nm)	Composition	f[a]	Assignment
BPTZ1	381	HOMO-1→LUMO (0.55)	0.24	π–π*
	476	HOMO→LUMO (0.58)	0.63	π–π*
BPTZ 2	357	HOMO-1→LUMO (0.49)	0.14	π–π*
	456	HOMO→LUMO (0.55)	0.75	π–π*
BPTZ 3	354	HOMO-1→LUMO (0.49)	0.15	π–π*
	454	HOMO→LUMO (0.56)	0.75	π–π*
BPTZ 4	371	HOMO→LUMO+1(0.59)	0.58	π–π*
	459	HOMO→LUMO (0.51)	0.83	π–π*
BPTZ 5	345	HOMO-1→LUMO (0.55)	0.17	π–π*
	449	HOMO→LUMO (0.62)	0.77	π–π*
BPTZ 6	340	HOMO-1→LUMO (0.56)	0.14	π–π*
	446	HOMO→LUMO (0.64)	0.83	π–π*
BPTZ 7	339	HOMO-1→LUMO (0.56)	0.15	π–π*
	445	HOMO→LUMO (0.65)	0.82	π–π*
BPTZ 8	350	HOMO→LUMO+1(0.53)	1.04	π–π*
	446	HOMO→LUMO (0.56)	0.93	π–π*

f[a] oscillator strength

6.6. Experimental Section

General Methods

All the moisture and oxygen-sensitive reactions were performed in an inert atmosphere using the standard inert atmosphere method .^{1}H NMR was measured in Bruker Avance (III) 400 MHz/ 500 MHz and ^{13}C NMR spectra were measured in 126 MHz using $CDCl_3$ as the internal solvent. The ^{1}H NMR chemical shifts are recorded in parts per million (ppm) relative to the solvent residual peak ($CDCl_3$, 7.26 ppm). The ^{13}C NMR shifts are reported relative to the solvent residual peak ($CDCl_3$, 77.00 ppm). The multiplicities are given as s (singlet), d (doublet), t (triplet), q (quartet), m (multiplet), and the coupling constants values (*J*) are

reported in Hz. The UV-visible absorption spectra of all compounds were recorded in PerkinElmer's LAMBDA 35 UV-visible Spectrophotometer in DCM solvent at room temperature. High-Resolution Mass Spectrometry (HRMS) was recorded on a Bruker-Daltonics micrOTOF-Q II mass spectrometer. Cyclic voltammograms (CVs) were recorded on a PalmSens 4 electrochemical analyzer using Glassy carbon as a working electrode, Pt wire as the counter electrode, and Ag/AgCl as the reference electrode. The scan rate was 100 mV s^{-1} for cyclic voltammetry. A solution of tetrabutylammonium hexafluorophosphate (Bu_4NPF_6) in CH_2Cl_2 (0.1 M) was used as the supporting electrolyte.

Synthesis and characterization of BPTZ 1: Compound 1 (0.1 g, 0.25 mmol), **compound 2** (0.102 g, 0.27 mmol), $Pd(PPh_3)_4$ (0.015 g, 0.01 mmol), and potassium carbonate (0.115 g, 0.83 mmol) was dissolved in Toluene/ethanol/water (6/3/1 v/v/v) and heated to reflux for 12 h under a nitrogen atmosphere. The reaction mixture was cooled to room temperature and poured into water. The organic layer was extracted with dichloromethane, and the combined organic layers were washed with saturated brine solution and water and dried over anhydrous sodium sulphate. After filtration and solvent evaporation, the residue was purified by silica-gel column chromatography using hexane/dichloromethane (60/40 v/v) as the eluent. A light purple solid of **BPTZ 1** was obtained in 75% yield (0.096 g). **^{1}H NMR (400 MHz, $CDCl_3$) δ** 8.22 (s, 1H), 7.93 (s, 1H), 7.64-7.55 (m, 5H), 7.31-7.27 (m, 2H), 7.16-7.11 (m, 2H), 6.99 (s, 1H), 6.92-6.89 (m, 2H), 6.86-6.82 (m, 2H), 6.55 (s, 1H), 3.82 (t, *J* = 4 Hz, 2H), 1.87-1.79 (m, 2H), 1.01 (t, *J* = 8 Hz, 3H). **^{13}C NMR (126 MHz, $CDCl_3$) δ** 146.66, 144.97, 143.89, 143.83, 142.17, 135.85, 135.21, 133.98, 131.32, 130.91, 130.63, 128.68, 127.59, 126.97, 125.64, 124.69, 124.41, 124.31, 124.28, 122.65, 118.47, 115.61, 49.35, 20.24, 11.44; **HRMS (ESI-TOF)** m/z calculated for $C_{30}H_{24}BF_2N_3S$ = 507.1752 $[M]^+$, measured 507.1769 $[M]^+$.

Synthesis and characterization of BPTZ 2: Compound 1 (0.1 g, 0.28 mmol), **compound 3** (0.125 g, 0.31 mmol), $Pd(PPh_3)_4$ (0.016 g, 0.01

mmol), and potassium carbonate (0.131 g, 0.9 mmol) was dissolved in Toluene/ethanol/water (6/3/1 v/v/v) and heated to reflux for 12 h under a nitrogen atmosphere. The reaction mixture was cooled to room temperature and poured into water. The organic layer was extracted with dichloromethane, and the combined organic layers were washed with saturated brine solution and water and dried over anhydrous sodium sulphate. After filtration and solvent evaporation, the residue was purified by silica-gel column chromatography using hexane/dichloromethane (70/30 v/v) as the eluent. A dark purple solid of **BPTZ 2** was obtained in 72% yield (0.111 g). **^{1}H NMR (500 MHz, $CDCl_3$) δ** 9.78 (s, 1H), 8.20 (s, 1H), 7.95 (s, 1H), 7.67 – 7.53 (m, 7H), 7.30 (dd, *J* = 8.4, 1.9 Hz, 1H), 7.23 (d, *J* = 1.9 Hz, 1H), 7.03 – 6.79 (m, 4H), 6.59 – 6.53 (m, 1H), 3.92 – 3.77 (m, 2H), 1.89 – 1.76 (m, 2H), 1.03 (t, *J* = 7.3 Hz, 3H). **^{13}C NMR (126 MHz, $CDCl_3$) δ** 190.09, 150.34, 146.93, 144.41, 142.74, 141.68, 135.75, 135.34, 133.89, 132.94, 131.74, 131.25, 131.01, 130.62, 130.36, 128.73, 128.41, 124.83, 124.51, 118.77, 116.28, 114.95, 49.91, 20.13, 11.30; **HRMS (ESI-TOF)** m/z calculated for $C_{31}H_{24}BF_2N_3OS$ = 535.1701 $[M]^+$, measured 535.1768 $[M]^+$.

Synthesis and characterization of BPTZ 3: Compound 1 (0.1 g, 0.28 mmol), **compound 4** (0.124 g, 0.31 mmol), $Pd(PPh_3)_4$ (0.016 g, 0.01 mmol), and potassium carbonate (0.131 g, 0.9 mmol) was dissolved in Toluene/ethanol/water (6/3/1 v/v/v) and heated to reflux for 12 h under a nitrogen atmosphere. The reaction mixture was cooled to room temperature and poured into water. The organic layer was extracted with dichloromethane, and the combined organic layers were washed with saturated brine solution and water and dried over anhydrous sodium sulphate. After filtration and solvent evaporation, the residue was purified by silica-gel column chromatography using hexane/dichloromethane (70/30 v/v) as the eluent. A dark purple solid of **BPTZ 3** was obtained in 80% yield (0.123 g). **^{1}H NMR (500 MHz, $CDCl_3$) δ** 8.19 (s, 1H), 7.96 (s, 1H), 7.63 – 7.55 (m, 4H), 7.39 (d, *J* = 7.2 Hz, 1H), 7.30 (d, *J* = 7.4 Hz, 2H), 7.22 (d, *J* = 8.7 Hz, 1H), 7.05 – 6.73 (m, 5H), 6.56 (s, 1H), 3.83 – 3.79 (m, 2H), 1.81 (dd, *J* = 14.2, 7.1 Hz, 2H), 1.01 (t, *J* = 7.2 Hz, 3H). **^{13}C NMR (126 MHz, $CDCl_3$) δ**

149.06, 148.92, 146.97, 144.51, 142.81, 141.56, 135.71, 135.28, 133.85, 131.88, 131.82, 131.02, 130.54, 128.73, 128.46, 125.83, 125.41, 125.16, 124.81, 124.40, 124.22, 118.89, 118.80, 116.32, 115.23, 105.37, 49.68, 20.04, 11.28; **HRMS (ESI-TOF)** m/z calculated for $C_{31}H_{23}BF_2N_4S$ = 532.1705 $[M]^+$, measured 532.1703 $[M]^+$.

Synthesis and characterization of BPTZ 4: Compound 1 (0.1 g, 0.28 mmol), **compound 5** (0.157 g, 0.31 mmol), $Pd(PPh_3)_4$ (0.016 g, 0.01 mmol), and potassium carbonate (0.131 g, 0.9 mmol) was dissolved in Toluene/ethanol/water (6/3/1 v/v/v) and heated to reflux for 12 h under a nitrogen atmosphere. The reaction mixture was cooled to room temperature and poured into water. The organic layer was extracted with dichloromethane, and the combined organic layers were washed with saturated brine solution and water and dried over anhydrous sodium sulphate. After filtration and solvent evaporation, the residue was purified by silica-gel column chromatography using hexane/dichloromethane (70/30 v/v) as the eluent. A dark purple solid of **BPTZ 4** was obtained in 75% yield (0.137 g). **^{1}H NMR (500 MHz, $CDCl_3$) δ** 7.95 (s, 1H), 7.81 (dd, *J* = 8.6, 1.7 Hz, 1H), 7.67 – 7.52 (m, 9H), 7.43 (t, *J* = 7.6 Hz, 2H), 7.38 – 7.34 (m, 2H), 7.30 (dd, *J* = 8.4, 1.8 Hz, 1H), 7.24 (d, *J* = 1.8 Hz, 1H), 7.00 (s, 1H), 6.93 (d, *J* = 3.9 Hz, 1H), 6.85 (m, 2H), 6.55 (d, *J* = 2.5 Hz, 1H), 3.84 (t, *J* = 7.2 Hz, 2H), 1.90 – 1.81 (m, 2H), 1.04 (t, *J* = 7.3 Hz, 3H). **^{13}C NMR (126 MHz, $CDCl_3$) δ** 146.74, 144.21, 143.38, 141.90, 140.82, 134.86, 130.98, 130.63, 129.16, 128.97, 128.73, 128.27, 127.80, 125.92, 124.60, 124.37, 115.90, 115.32, 108.97, 49.67, 20.16, 11.36; **HRMS (ESI-TOF)** m/z calculated for $C_{39}H_{29}BF_2N_4S$ + Na = 657.2073 $[M + Na]^+$, measured 657.2112 $[M + Na]^+$.

Synthesis and characterization of BPTZ 5: In a 50 mL round-bottomed flask, m-Chloroperbenzoic acid (0.102 g, 0.59 mmol) was added to **BPTZ 1** (0.1 g, 0.19 mmol) in DCM (20 ml) at room temperature for 1h. Upon the completion of the reaction, the mixture was purified by silica gel column chromatography with CH_2Cl_2 to get the desired **BPTZ 5** as a pink solid. Yield 0.82 g (78%). **^{1}H NMR (500 MHz, $CDCl_3$) δ** 8.09 (s, 5H), 8.00 (d, *J* = 7.8 Hz, 5H), 7.60 – 7.58 (m,

4H), 7.43 (s, 3H), 4.25 – 4.07 (m, 2H), 1.97 (dt, *J* = 13.9, 7.5 Hz, 2H), 1.10 (t, *J* = 7.4 Hz, 3H). **^{13}C NMR (126 MHz, $CDCl_3$) δ** 170.77, 134.88, 134.05, 131.09, 130.64, 130.43, 130.01, 128.89, 128.48, 123.93, 122.08, 120.20, 116.79, 116.13, 50.21, 20.33, 11.15; **HRMS (ESI-TOF)** m/z calculated for $C_{30}H_{24}BF_2N_3O_2S$ + Na = 562.1548 $[M + Na]^+$, measured 562.1563 $[M + Na]^+$.

Synthesis and characterization of BPTZ 6: In a 50 mL round-bottomed flask, m-Chloroperbenzoic acid (0.96 g, 0.56 mmol) was added to **BPTZ 2** (0.1 g, 0.18 mmol) in DCM (20 ml) at room temperature for 1h. Upon the completion of the reaction, the mixture was purified by silica gel column chromatography with CH_2Cl_2 to get the desired **BPTZ 6** as a pink solid. Yield 0.84 g (80%). **^{1}H NMR (500 MHz, $CDCl_3$) δ** 10.01 (s, 1H), 8.60 (d, *J* = 1.9 Hz, 1H), 8.30 – 8.23 (m, 2H), 8.14 (dd, *J* = 8.9, 1.9 Hz, 1H), 8.02 (s, 1H), 7.82 (dd, *J* = 8.9, 2.1 Hz, 1H), 7.70 – 7.56 (m, 5H), 7.43 (m, 2H), 7.16 (s, 1H), 7.02 (d, *J* = 4.1 Hz, 1H), 6.61 (d, *J* = 2.9 Hz, 1H), 4.24 – 4.15 (m, 2H), 1.99 (dq, *J* = 15.0, 7.4 Hz, 2H), 1.11 (t, *J* = 7.4 Hz, 3H). **^{13}C NMR (126 MHz, $CDCl_3$) δ** 189.22, 147.72, 145.67, 144.55, 140.42, 138.82, 135.66, 133.79, 133.61, 133.73, 132.35, 131.28, 130.61, 130.29, 130.08, 129.95, 128.91, 128.59, 128.17, 125.43, 123.91, 120.12, 119.44, 117.45, 116.82, 50.68, 20.44, 11.07; **HRMS (ESI-TOF)** m/z calculated for $C_{31}H_{24}BF_2N_3O_3S$ + K = 606.1237 $[M + K]^+$, measured 606.1222 $[M + K]^+$.

Synthesis and characterization of BPTZ 7: In a 50 mL round-bottomed flask, m-Chloroperbenzoic acid (0.97 g, 0.56 mmol) was added to **BPTZ 3** (0.1 g, 0.18 mmol) in DCM (20 ml) at room temperature for 1h. Upon the completion of the reaction, the mixture was purified by silica gel column chromatography with CH_2Cl_2 to get the desired **BPTZ 7** as a pink solid. Yield 0.83 g (79%). **^{1}H NMR (500 MHz, $CDCl_3$) δ** 8.41 (d, *J* = 2.0 Hz, 1H), 8.26 (s, 1H), 8.21 (d, *J* = 2.2 Hz, 1H), 8.03 (s, 1H), 7.83 (dt, *J* = 8.9, 2.1 Hz, 2H), 7.62 (d, *J* = 6.7 Hz, 5H), 7.40 (dd, *J* = 9.0, 2.8 Hz, 2H), 7.16 (s, 1H), 7.02 (d, *J* = 4.2 Hz, 1H), 6.62 (d, *J* = 2.7 Hz, 1H), 4.21 – 4.14 (m, 2H), 1.97 (dd, *J* =15.4,7.6 Hz, 2H), 1.10 (t, *J* = 7.4 Hz, 3H). **^{13}C NMR (126 MHz, $CDCl_3$) δ** 145.69, 143.14, 135.77, 133.71, 131.16, 130.46, 130.28, 129.84, 128.88,

128.78, 120.05, 117.30, 116.86, 105.03, 50.44, 20.25, 10.93; **HRMS (ESI-TOF)** m/z calculated for $C_{31}H_{23}BF_2N_4O_2S$ + K = 603.1240 $[M + K]^+$, measured 603.1222 $[M + K]^+$.

Synthesis and characterization of BPTZ 8: In a 50 mL round-bottomed flask, m-Chloroperbenzoic acid (0.81 g, 0.47 mmol) was added to **BPTZ 4** (0.1 g, 0.15 mmol) in DCM (20 ml) at room temperature for 1h. Upon the completion of the reaction, the mixture was purified by silica gel column chromatography with CH_2Cl_2 to get the desired **BPTZ 8** as a pink solid. Yield 0.79 g (76%). **^{1}H NMR (500 MHz, $CDCl_3$) δ** 8.55 (dd, *J* = 9.0, 1.9 Hz, 1H), 8.36 – 8.15 (m, 3H), 7.99 (s, 1H), 7.79 (dd, *J* = 8.9, 2.0 Hz, 1H), 7.71 – 7.55 (m, 7H), 7.41 (m, 6H), 7.14 (s, 1H), 6.99 (d, *J* = 4.0 Hz, 1H), 6.59 (d, *J* = 3.0 Hz, 1H), 4.29 – 4.00 (m, 2H), 1.98 (dq, *J* = 14.8, 7.3 Hz, 2H), 1.11 (t, *J* = 7.3 Hz, 3H). **^{13}C NMR (126 MHz, $CDCl_3$) δ** 145.48, 141.39, 140.64, 139.40, 139.07, 134.18, 133.69, 132.57, 131.83, 131.24, 130.63, 130.23, 129.59, 129.33, 128.91, 127.90, 127.70, 127.06, 126.09, 125.37, 125.03, 124.06, 120.23, 118.11, 117.09, 116.84, 111.52, 50.43, 20.41, 11.11; **HRMS (ESI-TOF)** m/z calculated for $C_{39}H_{29}BF_2N_6O_2S$ + Na = 689.1971 $[M + Na]^+$, measured 689.1975 $[M + Na]^+$.

6.7. Conclusion

A set of push–pull chromophores **BPTZ 1–8**, which were synthesized *via* palladium-catalyzed Suzuki cross-coupling reaction and modulate the oxidation state of the sulfur atom on the phenothiazine unit by two oxygen functionalization were explored. The photophysical study reveals that the phenothiazine substituted BODIPYs **BPTZ 1**–**4** exhibits a bathochromic (red) shift compared to phenothiazine-5,5-dioxide substituted BODIPYs **BPTZ 5**–**8** due to the good donor ability of phenothiazine unit, which resulted in strong donor-acceptor interaction. The electrochemical properties of the phenothiazine-5,5-dioxide substituted BODIPYs **BPTZ 5–8** show reduced electron donating ability relative to the phenothiazine substituted BODIPYs **BPTZ 1–4**. DFT and TD-DFT calculations provided a broad

understanding of the electronic structures and absorption spectra of the push–pull chromophores **BPTZ 1–8**, and show that upon modulating the oxidation state of the sulfur atom on phenothiazine unit increases the HOMO–LUMO gap, resulted a blue shift in the absorption spectra. These findings suggest that oxygen functionalization is an effective strategy to synthesize new push–pull dyes with low HOMO–LUMO gap for various optoelectronic applications.

6.8. References

1. Revoju, S., Matuhina, A., Canil, L., Salonen, H., Hiltunen, A., Abate, A., & Vivo, P. (2020). Structure-induced optoelectronic properties of phenothiazine-based materials. *Journal of Materials Chemistry C*, *8*(44), 15486–15506. https://doi.org/10.1039/D0TC03421E

2. Rout, Y., Montanari, C., Pasciucco, E., Misra, R., & Carlotti, B. (2021). Tuning the Fluorescence and the Intramolecular Charge Transfer of Phenothiazine Dipolar and Quadrupolar Derivatives by Oxygen Functionalization. *Journal of the American Chemical Society*, *143*(26), 9933–9943. https://doi.org/10.1021/jacs.1c04173

3. Izumi, S., Higginbotham, H. F., Nyga, A., Stachelek, P., Tohnai, N., Silva, P. de, … Minakata, S. (2020). Thermally Activated Delayed Fluorescent Donor–Acceptor–Donor–Acceptor π-Conjugated Macrocycle for Organic Light-Emitting Diodes. *Journal of the American Chemical Society*, *142*(3), 1482–1491. https://doi.org/10.1021/jacs.9b11578

4. Wang, Z., Feng, Y., Wang, N., Cheng, Y., Quan, Y., & Ju, H. (2018). Donor–Acceptor Conjugated Polymer Dots for Tunable Electrochemiluminescence Activated by Aggregation-Induced Emission-Active Moieties. *The Journal of Physical Chemistry Letters*, *9*(18), 5296–5302. https://doi.org/10.1021/acs.jpclett.8b02087

5. Barnsley, J. E., Shillito, G. E., Mapley, J. I., Larsen, C. B., Lucas, N. T., & Gordon, K. C. (2018). Walking the Emission Tightrope:

Spectral and Computational Analysis of Some Dual-Emitting Benzothiadiazole Donor–Acceptor Dyes. *The Journal of Physical Chemistry A*, *122*(40), 7991–8006. https://doi.org/10.1021/acs.jpca.8b05361

6. Wang, Z., Wang, C., Gan, Q., Cao, Y., Yuan, H., & Hua, D. (2019). Donor–Acceptor-Type Conjugated Polymer-Based Multicolored Drug Carriers with Tunable Aggregation-Induced Emission Behavior for Self-Illuminating Cancer Therapy. *ACS Applied Materials & Interfaces*, *11*(45), 41853–41861. https://doi.org/10.1021/acsami.9b11237

7. Dhindsa, J. S., Buguis, F. L., Anghel, M., & Gilroy, J. B. (2021). Band Gap Engineering in Acceptor-Donor-Acceptor Boron Difluoride Formazanates. *The Journal of Organic Chemistry*, *86*(17), 12064–12074. https://doi.org/10.1021/acs.joc.1c01416

8. Miao, J., Wang, Y., Liu, J., & Wang, L. (2022). Organoboron molecules and polymers for organic solar cell applications. *Chemical Society Reviews*, *51*(1), 153–187. https://doi.org/10.1039/D1CS00974E

9. Barattucci, A., Gangemi, C. M. A., Santoro, A., Campagna, S., Puntoriero, F., & Bonaccorsi, P. (2022). Bodipy-carbohydrate systems: synthesis and bio-applications. *Organic & Biomolecular Chemistry*, *20*(14), 2742–2763. https://doi.org/10.1039/D1OB02459K

10. Kumar, B., Bhatta, A., Saraf, P., Rangan, K., Sarkar, M., Mitra, S., & Kumar, D. (2022). Iodine(III)-promoted regioselective and efficient synthesis of β-triazolyl BODIPYs for the selective recognition of nickel ions and bovine serum albumin. *Dalton Transactions*, *51*(21), 8169–8176. https://doi.org/10.1039/D2DT00946C

11. Zhang, Z., Yuan, D., Liu, X., Kim, M.-J., Nashchadin, A., Sharapov, V., & Yu, L. (2020). BODIPY-Containing Polymers with Ultralow Band Gaps and Ambipolar Charge Mobilities. *Macromolecules*, *53*(6), 2014–2020. https://doi.org/10.1021/acs.macromol.9b02653

12. Carlotti, B., Poddar, M., Elisei, F., Spalletti, A., & Misra, R. (2019). Energy-Transfer and Charge-Transfer Dynamics in Highly Fluorescent Naphthalimide–BODIPY Dyads: Effect of BODIPY Orientation. *The Journal of Physical Chemistry C*, *123*(40), 24362–24374. https://doi.org/10.1021/acs.jpcc.9b05851

13. Liu, H., Liu, L., Fu, Y., Liu, E., & Xue, B. (2019). Theoretical Design of D−π–A–A Sensitizers with Narrow Band Gap and Broad Spectral Response Based on Boron Dipyrromethene for Dye-Sensitized Solar Cells. *Journal of Chemical Information and Modeling*, *59*(5), 2248–2256. https://doi.org/10.1021/acs.jcim.9b00187

14. Ozdemir, M., Choi, D., Kwon, G., Zorlu, Y., Cosut, B., Kim, H., … Usta, H. (2016). Solution-Processable BODIPY-Based Small Molecules for Semiconducting Microfibers in Organic Thin-Film Transistors. *ACS Applied Materials & Interfaces*, *8*(22), 14077–14087. https://doi.org/10.1021/acsami.6b02788

15. Misra, R., Jadhav, T., Dhokale, B., Gautam, P., Sharma, R., Maragani, R., & Mobin, S. M. (2014). Carbazole-BODIPY conjugates: design, synthesis, structure and properties. *Dalton Transactions*, *43*(34), 13076–13086. https://doi.org/10.1039/C4DT00983E

16. Popere, B. C., Della Pelle, A. M., & Thayumanavan, S. (2011). BODIPY-Based Donor–Acceptor π-Conjugated Alternating Copolymers. *Macromolecules*, *44*(12), 4767–4776. https://doi.org/10.1021/ma200839q

17. Shinde, J., Thomas, M. B., Poddar, M., Misra, R., & D'Souza, F. (2021). Does Location of BF2-Chelated Dipyrromethene (BODIPY) Ring Functionalization Affect Spectral and Electron Transfer Properties? Studies on α-, β-, and Meso-Functionalized BODIPY-Derived Donor–Acceptor Dyads and Triads. *The Journal of Physical Chemistry C*, *125*(43), 23911–23921. https://doi.org/10.1021/acs.jpcc.1c06704

18. Thompson, B. L., Kieffer, I. A., & Heiden, Z. M. (2022). Utilization of BODIPY-based redox events to manipulate the Lewis acidity of fluorescent boranes. *Chemical Communications*, *58*(16), 2646–2649. https://doi.org/10.1039/D1CC06400B

19. Ayhan, M. M., Özcan, E., Alkan, F., Çetin, M., Ün, İ., Bardelang, D., & Çoşut, B. (2022). External complexation of BODIPYs by CB[7] improves in-cell fluorescence imaging. *Materials Advances*, *3*(1), 547–553. https://doi.org/10.1039/D1MA00931A

20. Zatsikha, Y. V., Blesener, T. S., King, A. J., Healy, A. T., Goff, P. C., Didukh, N. O., … Nemykin, V. N. (2021). Fully Conjugated Pyrene–BODIPY and Pyrene–BODIPY–Ferrocene Dyads and Triads: Synthesis, Characterization, and Selective Noncovalent Interactions with Nanocarbon Materials. *The Journal of Physical Chemistry B*, *125*(1), 360–371. https://doi.org/10.1021/acs.jpcb.0c10074

21. Deckers, J., Cardeynaels, T., Doria, S., Tumanov, N., Lapini, A., Ethirajan, A., … Maes, W. (2022). Balancing fluorescence and singlet oxygen formation in push–pull type near-infrared BODIPY photosensitizers. *Journal of Materials Chemistry C*, *10*(24), 9344–9355. https://doi.org/10.1039/D2TC01526A

22. Kaneza, N., Zhang, J., Liu, H., Archana, P. S., Shan, Z., Vasiliu, M., … Pan, S. (2016). Electrochemical and Spectroscopic Properties of Boron Dipyrromethene–Thiophene–Triphenylamine-Based Dyes for Dye-Sensitized Solar Cells. *The Journal of Physical Chemistry C*, *120*(17), 9068–9080. https://doi.org/10.1021/acs.jpcc.6b01611

23. Ojha, M., Banerjee, M., Ray, S., Singh, A. K., Anoop, A., & Singh, N. D. P. (2022). Switching photorelease to singlet oxygen generation by oxygen functionalization of phenothiazine photocages. *Chemical Communications*, *58*(16), 2754–2757. https://doi.org/10.1039/D1CC06950K

24. Duvva, N., Eom, Y. K., Reddy, G., Schanze, K. S., & Giribabu, L. (2020). Bulky Phenanthroimidazole–Phenothiazine D−π–A Based

Organic Sensitizers for Application in Efficient Dye-Sensitized Solar Cells. *ACS Applied Energy Materials*, *3*(7), 6758–6767. https://doi.org/10.1021/acsaem.0c00892

25. Sharma, R., Thomas, M. B., Misra, R., & D'Souza, F. (2019). Strong Ground- and Excited-State Charge Transfer in C3-Symmetric Truxene-Derived Phenothiazine-Tetracyanobutadine and Expanded Conjugates. *Angewandte Chemie*, *131*(13), 4394–4399. https://doi.org/10.1002/ange.201814388

26. Bejan, A., Shova, S., Damaceanu, M.-D., Simionescu, B. C., & Marin, L. (2016). Structure-Directed Functional Properties of Phenothiazine Brominated Dyes: Morphology and Photophysical and Electrochemical Properties. *Crystal Growth & Design*, *16*(7), 3716–3730. https://doi.org/10.1021/acs.cgd.6b00212

27. Gangadhar, P. S., Reddy, G., Prasanthkumar, S., & Giribabu, L. (2021). Phenothiazine functional materials for organic optoelectronic applications. *Physical Chemistry Chemical Physics*, *23*(28), 14969–14996. https://doi.org/10.1039/D1CP01185E

28. Hart, A. S., K. C., C. B., Subbaiyan, N. K., Karr, P. A., & D'Souza, F. (2012). Phenothiazine-Sensitized Organic Solar Cells: Effect of Dye Anchor Group Positioning on the Cell Performance. *ACS Applied Materials & Interfaces*, *4*(11), 5813–5820. https://doi.org/10.1021/am3014407

29. Salunke, J., Guo, X., Lin, Z., Vale, J. R., Candeias, N. R., Nyman, M., … Vivo, P. (2019). Phenothiazine-Based Hole-Transporting Materials toward Eco-friendly Perovskite Solar Cells. *ACS Applied Energy Materials*, *2*(5), 3021–3027. https://doi.org/10.1021/acsaem.9b00408

30. Hua, Y., Chang, S., Huang, D., Zhou, X., Zhu, X., Zhao, J., … Wong, W.-K. (2013). Significant Improvement of Dye-Sensitized Solar Cell Performance Using Simple Phenothiazine-Based Dyes. *Chemistry of Materials*, *25*(10), 2146–2153. https://doi.org/10.1021/cm400800h

31. Ojha, M., Banerjee, M., Ray, S., Singh, A. K., Anoop, A., & Singh, N. D. P. (2022). Switching photorelease to singlet oxygen generation by oxygen functionalization of phenothiazine photocages. *Chemical Communications*, *58*(16), 2754–2757. https://doi.org/10.1039/D1CC06950K

32. Christensen, J. A., Phelan, B. T., Chaudhuri, S., Acharya, A., Batista, V. S., & Wasielewski, M. R. (2018). Phenothiazine Radical Cation Excited States as Super-oxidants for Energy-Demanding Reactions. *Journal of the American Chemical Society*, *140*(15), 5290–5299. https://doi.org/10.1021/jacs.8b01778

33. Zhou, J., Mao, L., Wu, M.-X., Peng, Z., Yang, Y., Zhou, M., … Yang, H.-B. (2022). Extended phenothiazines: synthesis, photophysical and redox properties, and efficient photocatalytic oxidative coupling of amines. *Chemical Science*, *13*(18), 5252–5260. https://doi.org/10.1039/D2SC01086K

34. Rout, Y., Ekbote, A., & Misra, R. (2021). Recent development on the synthesis, properties and applications of luminescent oxidized phenothiazine derivatives. *Journal of Materials Chemistry C*, *9*(24), 7508–7531. https://doi.org/10.1039/D1TC00695A

35. Huang, P., Manju, Kazim, S., Lezama, L., Misra, R., & Ahmad, S. (2021). Tailoring of a Phenothiazine Core for Electrical Conductivity and Thermal Stability: Hole-Selective Layers in Perovskite Solar Cells. *ACS Applied Materials & Interfaces*, *13*(28), 33311–33320. https://doi.org/10.1021/acsami.1c08470

36. Kim, G., Yeom, H. R., Cho, S., Seo, J. H., Kim, J. Y., & Yang, C. (2012). Easily Attainable Phenothiazine-Based Polymers for Polymer Solar Cells: Advantage of Insertion of S,S-dioxides into its Polymer for Inverted Structure Solar Cells. *Macromolecules*, *45*(4), 1847–1857. https://doi.org/10.1021/ma202661b

37. Cong, Z., Han, M., Fan, Y., Fan, Y., Chang, K., Xiao, L., … Li, Z. (2022). Ultralong blue room-temperature phosphorescence by

cycloalkyl engineering. *Materials Chemistry Frontiers*, *6*(12), 1606–1614. https://doi.org/10.1039/D2QM00284A

38. Ren, J., Tian, Y., Wang, Y., Yang, J., Fang, M., & Li, Z. (2022). The influence of π–π stacking on the room temperature phosphorescence of phenothiazine 5,5-dioxide derivatives. *Journal of Materials Chemistry C*. https://doi.org/10.1039/D2TC01537D

39. Xiang, S., Huang, Z., Sun, S., Lv, X., Fan, L., Ye, S., … Wang, L. (2018). Highly efficient non-doped OLEDs using aggregation-induced delayed fluorescence materials based on 10-phenyl-10H-phenothiazine 5,5-dioxide derivatives. *Journal of Materials Chemistry C*, *6*(42), 11436–11443. https://doi.org/10.1039/C8TC03648A

40. Gautam, P., Dhokale, B., Mobin, S. M., & Misra, R. (2012). Ferrocenyl BODIPYs: synthesis, structure and properties. *RSC Advances*, *2*(32), 12105–12107. https://doi.org/10.1039/C2RA21964F

41. Yin, X., Li, Y., Zhu, Y., Jing, X., Li, Y., & Zhu, D. (2010). A highly sensitive viscosity probe based on ferrocene-BODIPY dyads. *Dalton Transactions*, *39*(41), 9929–9935. https://doi.org/10.1039/C0DT00309C

42. Buene, A. F., & Almenningen, D. M. (2021). Phenothiazine and phenoxazine sensitizers for dye-sensitized solar cells – an investigative review of two complete dye classes. *Journal of Materials Chemistry C*, *9*(36), 11974–11994. https://doi.org/10.1039/D1TC03207K

Chapter 7

β-Pyrrole Functionalized Push–Pull BODIPYs: Synthesis, Photophysical, Electrochemical, Thermal and Computational Studies

7.1. Introduction

The design and synthesis of organic π-conjugated push–pull systems are of interest due to their application in optoelectronic devices, fluorescent switches and bioimaging.[1–7] The push–pull materials have excellent electronic and optical properties that can be perturbed by altering the strength of the appropriate donor/acceptor unit or the π-linker.[8–10] The electron-rich N, O, and S containing heterocyclic entities were incorporated into the push–pull systems for tuning their optical and redox properties.[11] Boron dipyrromethene dyes are among the most extensively studied organic fluorophores due to their easy synthetic modifications and high photochemical stability. The BODIPY dyes exhibit properties such as strong absorption throughout visible region, high molar extinction coefficient, high fluorescence quantum yield and excellent thermal stability.[12] These properties make them suitable dye for a wide range of applications, such as in fluorescent switches, optoelectronic materials, chemosensors, nonlinear optics (NLOs), photovoltaic devices, fluorescent labelling and photodynamic therapy.[13–24] The photophysical and redox properties of the BODIPYs can be tuned significantly *via* functionalizing at the pyrrolic and *meso*- positions of the BODIPY core.[25–29] Generally, the BODIPY exhibits an electronic absorption band in 500–530 nm range with a high molar extinction coefficient and strong fluorescence quantum yields.[30] The BODIPY dyes are redox-active molecule and exhibits good reversibility of the oxidation and reduction waves at low potential.[31]

Carbazole is a good electron donor moiety which exhibits an electronic absorption band in 300–400 nm range and is widely used in optoelectronic applications.[32–34] The phenothiazine exhibits a non-planar, butterfly-shaped structure containing electron-rich heteroatoms (S and N) and excellent electrochemical stability.[35–38] The 10*H*-phenothiazine is a colourless molecule and exhibits an absorption maxima at 316 nm in CH_2Cl_2.[39–42] The sulfur atom in the phenothiazine unit is in the sulfide state (+2). There has been limited study into the oxygen functionalization of the sulfur atom (sulfides, sulfoxides, and sulfones) in the thiazine ring of the phenothiazine.[43]

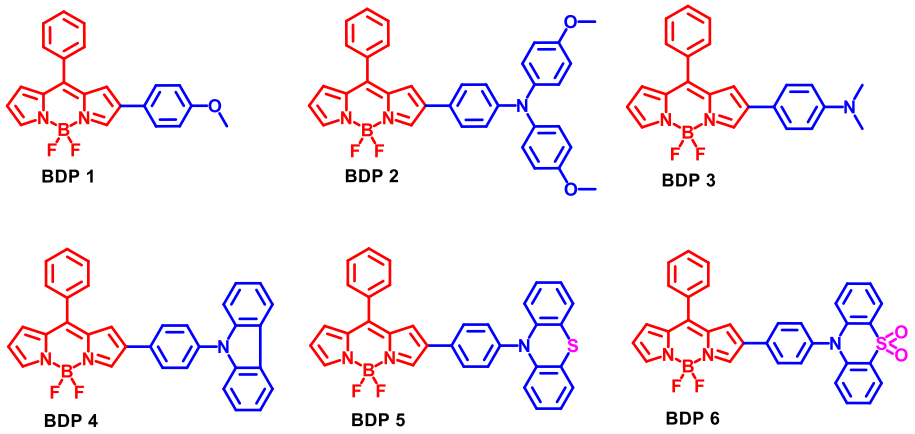

Chart 7.1. Molecular structures of the investigated push–pull BODIPYs **BDP 1–6**.

Herein, we have synthesized the push–pull BODIPYs **BDP 1–6** *via* Suzuki cross-coupling reaction with different donor groups and by increasing the oxidation state of the sulfur atom in the thiazine ring as shown in Chart 7.1. In the push–pull BODIPYs **BDP 1–6,** the BODIPY act as an acceptor unit, whereas anisole, *N*,*N*-dimethylaniline, *N*,*N*-dimethyl anisole, *N*-phenyl carbazole, *N*-phenyl phenothiazine and *N*-phenyl phenothiazine-5,5-dioxide act as donor groups. We explored the effect of varying the electron donor units on the photophysical, electrochemical, thermal, and theoretical studies of the BODIPY. The computational studies show that the HOMOs are delocalized over donor and BODIPY unit, whereas the LUMOs are localized on the acceptor BODIPY core. The phenothiazine substituted BODIPY **BDP 5** exhibits

a low HOMO–LUMO gap compared to the phenothiazine-5,5-dioxide functionalized BODIPY **BDP 6** due to the strong donor–acceptor interaction.

7.2. Results and discussion

The synthetic procedure of the push–pull BODIPYs **BDP 1–6** is shown in Scheme 7.1. The *β*-mono bromo BODIPY **1** was synthesized as per the reported procedure.[44] The push–pull BODIPYs **BDP 1–6** were synthesized *via* Palladium-catalyzed Suzuki cross-coupling reaction and increasing the oxidation state of the sulfur atom in the thiazine ring by using *m*-CPBA in good yields (Scheme 7.1). The *β*-mono bromo BODIPY **1** reacts with boronate ester of anisole **2** and boronate ester of *N*,*N*-dimethyl anisole **3** using a catalytic amount of $Pd(PPh_3)_4$ and Toluene: EtOH: H_2O (6:3:1) solvent at 80 ℃ for 12 h which resulted in the push–pull BODIPYs **BDP 1** and **2** in 75% and 63% yields, respectively. Similarly, the BODIPY **1** reacts with boronate ester of *N*,*N*-dimethylaniline **4**, boronate ester of *N*-phenyl carbazole **5**, and boronate ester of *N*-phenyl phenothiazine **6** using Toluene: EtOH: H_2O (6:3:1) solvent in the presence of $Pd(PPh_3)_4$ at 80 ℃ for 12 h which resulted the BODIPYs **BDP 3**, **4,** and **5** in 72%, 76%, and 80% yields, respectively. The push–pull BODIPY **BDP 5** was further modified by increasing the oxidation state of the sulfur atom in the thiazine ring, using *m*-CPBA as an oxidizing agent. The phenothiazine substituted BODIPY **BDP 5** reacts with *m*-chloroperbenzoic acid (*m*-CPBA) (3.0 equivalents) using dichloromethane (DCM) solvent at room temperature for 1 h, resulting in phenothiazine 5,5-dioxide functionalized BODIPY **BDP 6** in 80% yield (Scheme 7.1).

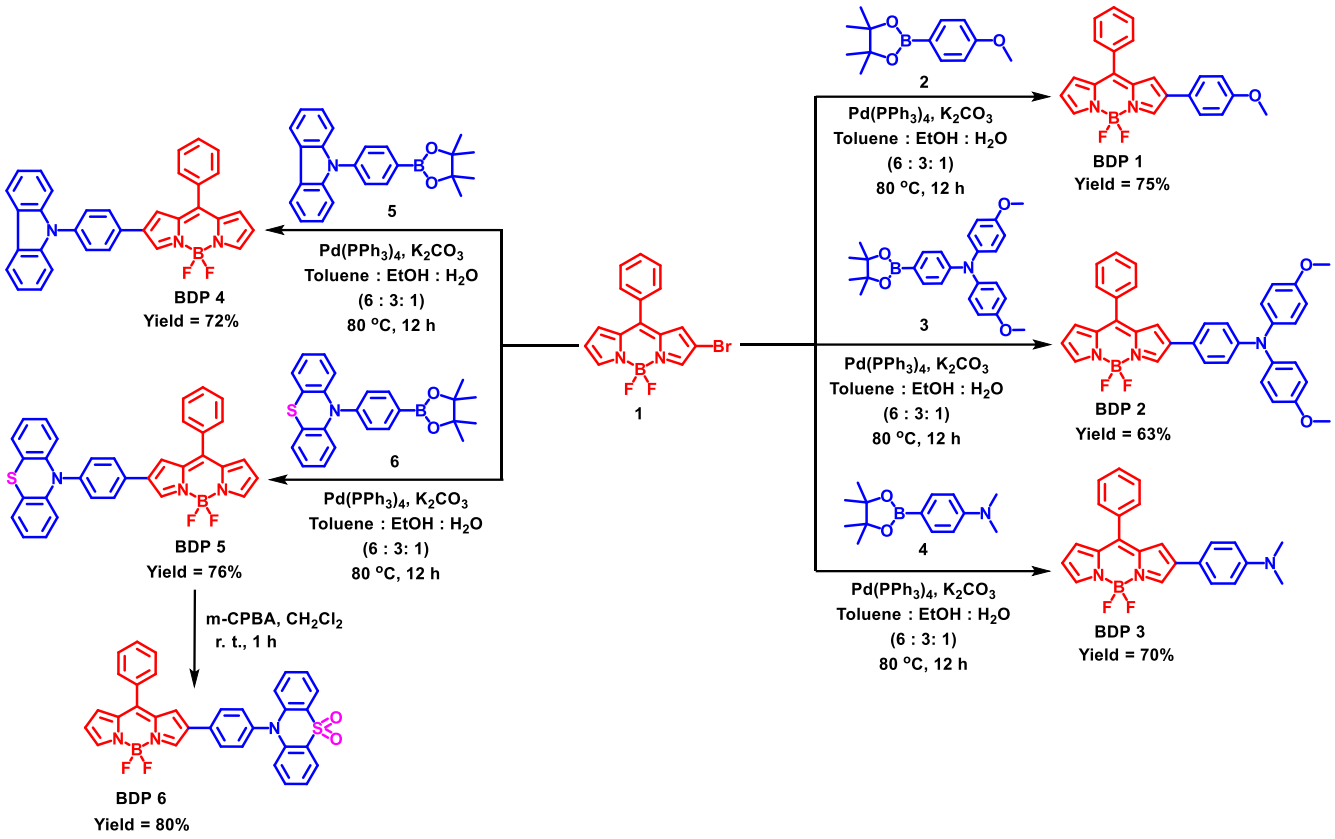

Scheme 7.1. Synthetic route of the push–pull BODIPYs **BDP 1–6**.

The push–pull BODIPYs **BDP 1–6** were purified by column chromatography (silica gel size = 100–200 mesh) using Hexane: DCM as a solvent. The BODIPYs **BDP 1–6** are readily soluble in organic solvent acetone, chloroform, dichloromethane, acetonitrile, and tetrahydrofuran. The ^{1}H NMR, ^{13}C NMR, ^{11}B NMR and HRMS techniques were used to characterize the molecular structures of the push–pull BODIPYs **BDP 1–6**.

7.3. Photophysical properties

The electronic absorption spectra of the push–pull BODIPYs **BDP 1–6** were recorded in dry dichloromethane (DCM) solvent at room temperature which are depicted in Figure 7.1, and the data are tabulated in Table 7.1.

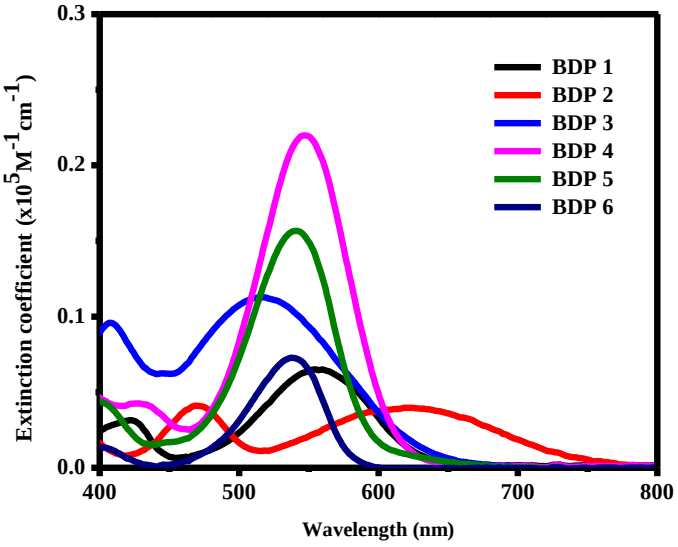

Figure 7.1. Electronic absorption spectra of the push–pull BODIPYs **BDP 1–6** in dry DCM (10^{-5} M).

Generally, the BODIPY dyes exhibit an intense electronic absorption band around 500–530 nm range. The push–pull BODIPYs **BDP 1–6** exhibit two intense absorption bands at 350–480 nm range corresponding to the $S_0 \rightarrow S_2$ ($\pi \rightarrow \pi^*$) transition and an absorption band from 510–650 nm attributed to the $S_0 \rightarrow S_1$ ($\pi \rightarrow \pi^*$) transition in the UV-visible spectra (Figure 7.1). The anisole and *N*,*N*-dimethyl anisole functionalized push–pull BODIPYs **BDP 1** and **2** exhibit absorption band at 419 nm, 559 nm and 469 nm, 628 nm, respectively, which corresponds to the π–π^* transition. The *N*,*N*-dimethylaniline and *N*-phenyl carbazole substituted BODIPYs **BDP 3** and **4** exhibit an intense absorption band at 409 nm, 521 nm, and 431 nm, 548 nm, respectively, corresponding to the π–π^* transition. The phenothiazine and phenothiazine 5,5-dioxide functionalized BODIPYs **BDP 5** and **6** exhibit absorption bands at 400 nm, 545 nm and 395 nm, 538 nm respectively, attributed to π–π^* transition (Figure 7.1). The electronic absorption band of the push–pull BODIPY **BDP 2** exhibits a bathochromic shift compared to **BDP 1**, **3**, **4**, **5,** and **6** due to the strong donor ability of the 4-methoxy-*N*-(4-methoxyphenyl)-*N*-phenylaniline unit. The push–pull BODIPYs **BDP 1–5** are non-fluorescent in nature, whereas phenothiazine 5,5-dioxide functionalized BODIPY **BDP 6** is a

fluorescent molecule. The optical bandgap of the push–pull BODIPYs **BDP1–6** estimated from the onset wavelength of the UV-visible absorption spectra follow the order **BDP 6> BDP 5> BDP 4> BDP 1> BDP 3> BDP 2**. The optical band gap trend shows that increasing the number of oxygen atoms increases the optical band gap, resulting in a hypsochromic shift in electronic absorption spectra. The photophysical result concludes that the push–pull BODIPY **BDP 2** (4-methoxy-*N*-(4-methoxyphenyl)-*N*-phenylaniline) exhibits a red shift and low optical band gap compared to rest of the **BDPs**. The photophysical results are also explained by theoretical calculations.

Table 7.1. Photophysical, electrochemical and thermal stability data of the push–pull BODIPYs **BDP 1–6**.

Photophysical data[a]				**Electrochemical data[b]**		**Thermal stability[c]**
Compound	**$\lambda_{(S_0 \rightarrow S_1)}$ (nm)**	**ε (M^{-1} cm^{-1})**	**Optical band gap (eV)**	**E_{ox} (V)**	**E_{red} (V)**	**T_d (°C)**
BDP 1	559	6490	1.70	1.21 1.46	–0.73	300
BDP 2	628	3930	1.20	0.58 1.16	–0.72	308
BDP 3	521`	1190	1.68	0.56 0.82	–0.73	287
BDP 4	543	2190	1.92	1.10 1.41	–0.80	160
BDP 5	545	1567	1.90	0.61 1.20	–0.69	275
BDP 6	534	8970	1.96	1.39 1.61	–0.70	144

[a] Absorbance recorded in dry DCM at 10^{-5} M conc. λ_{abs}: absorption wavelength. ε: extinction coefficient. **[b]** Electrochemical analysis was estimated by differential pulse voltammetry in 0.1 M solution of

Bu_4NPF_6 in DCM at 100 mV s^{-1} scan rate *versus* Ag/AgCl at 25 °C. E_{oxi} and E_{red} values are based on DPV analysis. [c] Decomposition temperatures for 5% weight loss at a heating rate of 10 °C min^{-1}, under a nitrogen atmosphere.

7.4. Electrochemical properties

The cyclic voltammetry (CV) and differential pulse voltammetry (DPV) were used to study the redox properties of the push–pull BODIPYs **BDP 1–6**. All the measurements were recorded in dry dichloromethane (DCM) solvent at room temperature using 0.1 M tetrabutylammonium hexafluorophosphate (Bu_4NPF_6) as a supporting electrolyte. The representative CV and DPV plots of the BODIPYs **BDP 1–6** are depicted in Figure 7.2 and the redox potentials of the push–pull BODIPYs **BDP 1–6** are tabulated in Table 7.1.

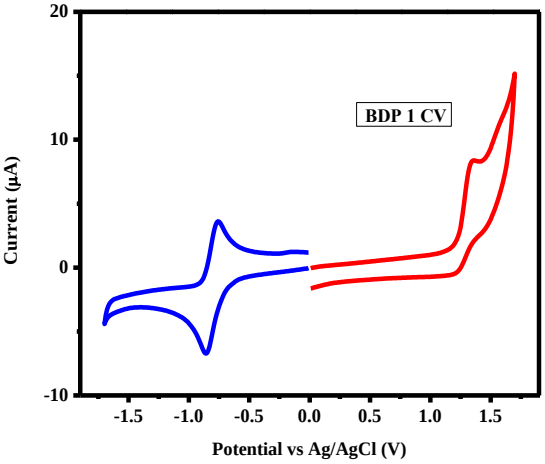
BDP 1 CV
Current (µA)
Potential vs Ag/AgCl (V)

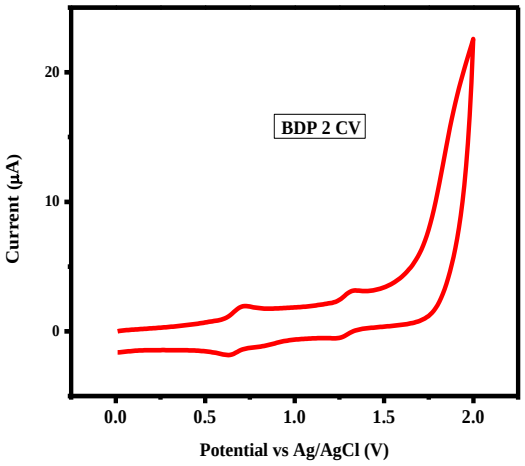
BDP 2 CV
Current (µA)
Potential vs Ag/AgCl (V)

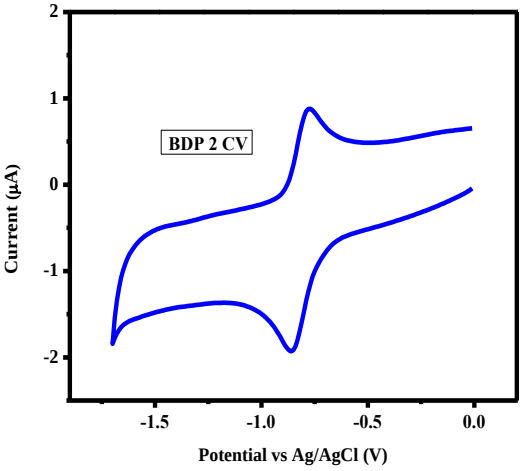
BDP 2 CV
Current (µA)
Potential vs Ag/AgCl (V)

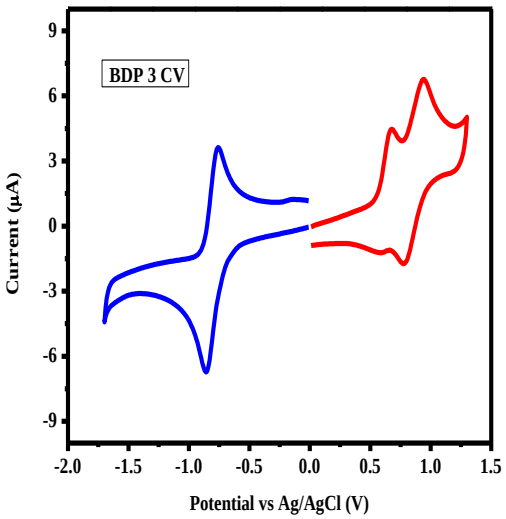
BDP 3 CV
Current (µA)
Potential vs Ag/AgCl (V)

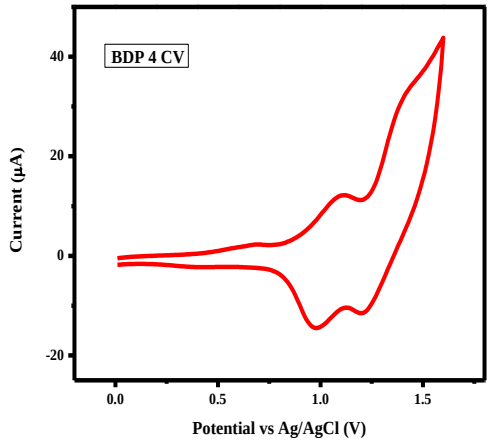
BDP 4 CV
Current (µA)
Potential vs Ag/AgCl (V)

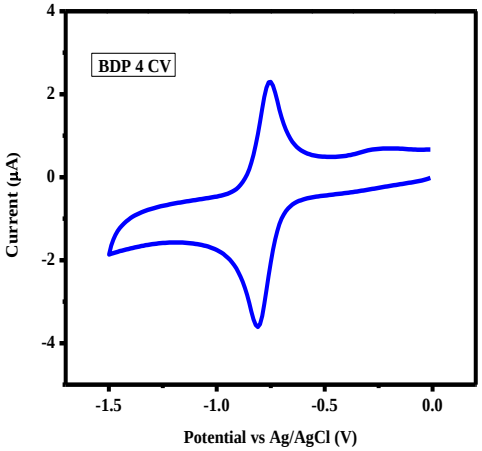
BDP 4 CV
Current (µA)
Potential vs Ag/AgCl (V)

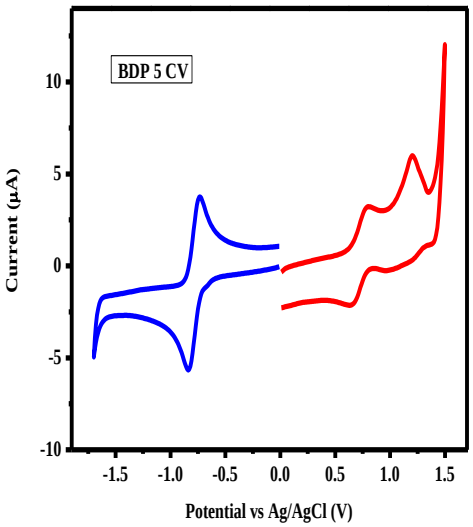
BDP 5 CV
Current (µA)
Potential vs Ag/AgCl (V)

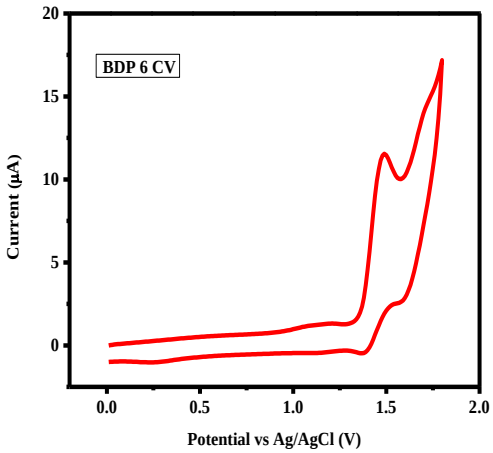
BDP 6 CV
Current (µA)
Potential vs Ag/AgCl (V)

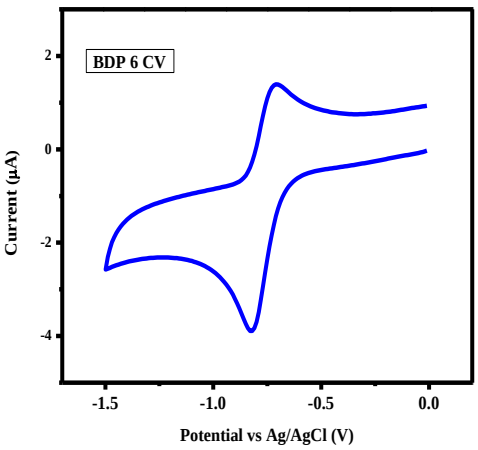
BDP 6 CV
Current (µA)
Potential vs Ag/AgCl (V)

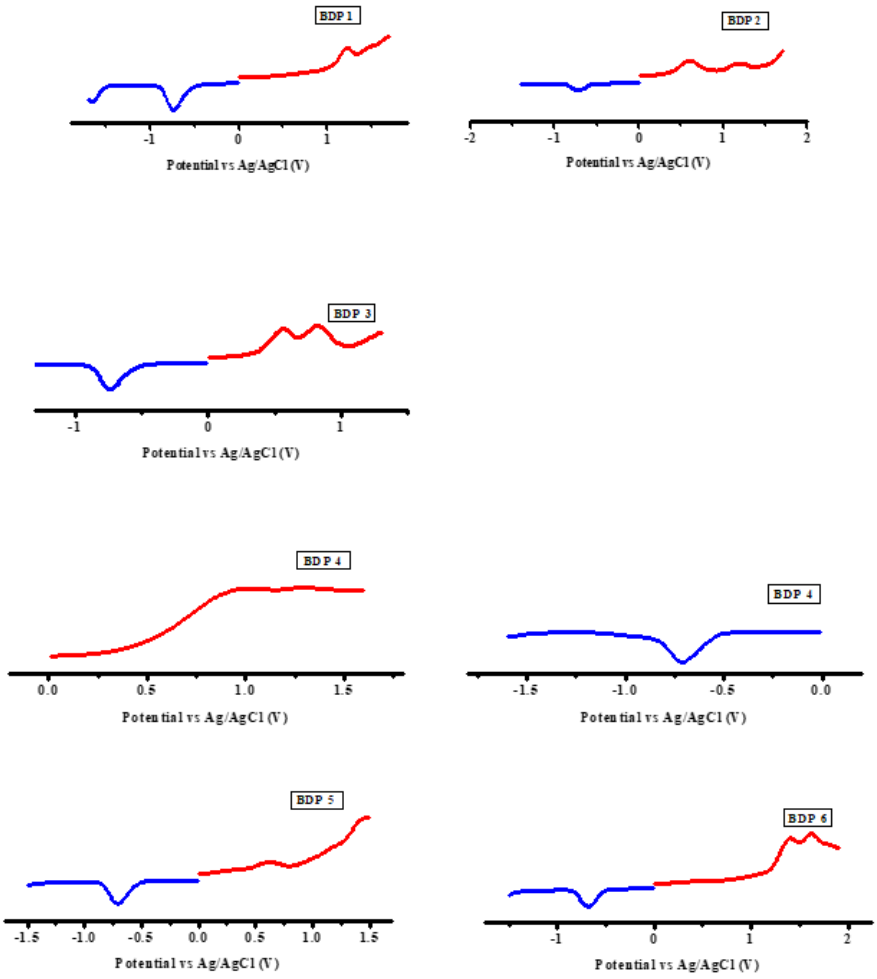

Figure 7.2. CV and DPV plots of the push–pull BODIPYs **BDP 1–6** using 0.1 M solution of Bu_4NPF_6 in DCM solvent at 100 mV s^{-1} scan rate *versus* Ag/AgCl at 25 °C.

The phenothiazine unit exhibits a single reversible oxidation wave at low potential.[45] The BODIPY unit exhibits a single oxidation wave and a single reduction wave due to the formation of a mono π-radical cation and a mono π-radical anion.[46] The push–pull BODIPYs **BDP 1–6** exhibit two oxidation waves and one reduction wave at low potential due to the presence of redox-active entities. The anisole and *N*,*N*-dimethyl anisole substituted push–pull BODIPYs **BDP 1** and **2** exhibit two oxidation at +1.21, +1.46 V and +0.58, +1.16 V, and a single reduction potential at –0.73 V; –0.72 V, respectively (Table 7.1). The

electrochemical analysis suggests that the **BDP 2** exhibit easy oxidation compared to anisole functionalized BODIPY **BDP 1** due to the strong donor ability of *N*,*N*-dimethyl anisole group. The *N*,*N*-dimethylaniline and *N*-phenyl carbazole substituted BODIPYs **BDP 3** and **BDP 4** exhibit oxidation at +0.56, +0.82 V and +1.10, +1.41 V, and reduction at –0.73 V; –0.80 V, respectively (Table 7.1). The redox potential values of the **BDP 3** and **4** indicates that the *N*,*N*-dimethylaniline exhibits easier oxidation compared to the *N*-phenyl carbazole. The phenothiazine and phenothiazine 5,5-dioxide functionalized BODIPYs **BDP 5** and **BDP 6** exhibit oxidation at +0.61 V; +1.20 V, and +1.39 V; +1.61 V, and reduction at –0.69 V; –0.70 V, respectively (Table 7.1). The electrochemical analysis data suggest that the phenothiazine substituted BODIPY **BDP 5** shows easier oxidation and reduction compared to phenothiazine 5,5-dioxide functionalized BODIPY **BDP 6** due to the strong donor ability of the phenothiazine unit. The push–pull BODIPYs **BDP 1–6** exhibit the first oxidation wave at +0.56 to +1.39 V range, attributed to oxidation of the donor moieties, and the second oxidation wave at higher potential ranging from +0.82 to +1.61 V, due to the formation of mono-radical cation of BODIPY unit. The BODIPYs **BDP 1–6** exhibit a single reduction wave at –0.69 V to –0.80 V range, attributed to the formation of the mono-radical anion of BODIPY unit. The redox properties of the push–pull BODIPYs **BDP 1–6** suggests that the strong donor groups show easier oxidation at low potential and the oxidation process strongly depends on the donor ability of the molecule. The HOMO and LUMO energy levels of the push–pull BODIPYs **BDP 1–6** were estimated by using the first onset potential of oxidation and reduction waves. The evaluated HOMO energy levels of the push–pull BODIPYs **BDP 1, BDP 2** and **BDP 3** at –5.65 eV, –5.02 eV and –5.00 eV, and LUMO energy levels at –3.71 eV, –3.72 eV and –3.71 eV respectively. The HOMO and LUMO energy levels of the push–pull BODIPYs **BDP 4**, **BDP 5** and **BDP 6** are estimated at –5.54 eV, –5.05 eV, and –5.83 eV and –3.64 eV, –3.75 eV and –3.74 eV respectively. The estimated electrochemical band gap (E_{gap}) of the push–pull BODIPYs **BDPs 1–6** are 1.94 eV, 1.30 eV, 1.29 eV, 1.90 eV, 1.30 eV

and 2.09 eV respectively. The phenothiazine 5,5-dioxide functionalized BODIPY **BDP 6** exhibits large electrochemical band gap compared to **BDPs 1–5**, which is in good agreement with the theoretical HOMO–LUMO gap. The electrochemically estimated HOMO and LUMO energy levels of the push–pull BODIPYs **BDP 1–6** indicate that the variation of donor units significantly affects the HOMO energy level compared to the LUMO energy levels. The HOMO–LUMO gap calculated from electrochemical analysis shows good agreement with the theoretical HOMO–LUMO gap calculated from DFT calculation.

7.5. Thermal Properties

Thermal stability is an essential characterization of the push–pull materials for optoelectronic application. The thermal properties of the push–pull BODIPYs **BDP 1–6** were measured by thermogravimetric analysis (TGA) at a heating rate of 10 °C min^{-1} and monitoring the weight loss against temperature under the nitrogen atmosphere.

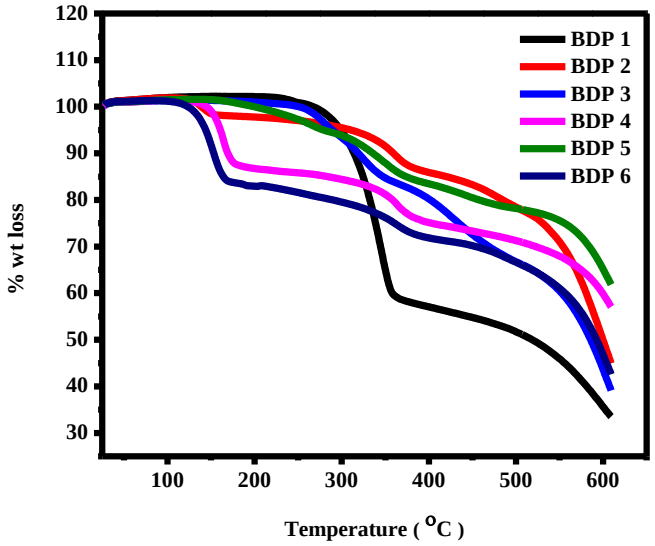

Figure 7.3. Thermogravimetric analysis (TGA) of the push–pull BODIPYs **BDP 1–6**, measured at a heating rate of 10 °C min^{-1} under a nitrogen atmosphere.

The π-conjugated push–pull BODIPYs **BDP 1–6** exhibit good thermal stability, and the corresponding thermograms are shown in Figure 7.3. The thermal stability data of the push–pull BODIPYs **BDP 1–6** data are summarized in Table 7.1. The decomposition temperatures for the BODIPYs **BDP 1–6** at 5% weight loss were found to be at 300 ℃, 308 ℃, 287 ℃, 160 ℃, 275 ℃ and 144 ℃, respectively.

The *N*,*N*-dimethyl anisole functionalized BODIPY **BDP 2** exhibits the highest thermal stability compared to the rest of the **BDPs** and the incorporation of oxygen atom decreases the thermal stability. The push–pull BODIPYs **BDP 1–6** follows the order **BDP 2**> **BDP 1**> **BDP 3**> **BDP 5**> **BDP 4**> **BDP 6**.

7.6. Theoretical calculations

To understand the geometry and electronic properties of the push–pull BODIPYs **BDP 1–6**, the density functional theory (DFT) and time-dependent DFT calculations were performed at the B3LYP/6-31G (d, p) and CAM-B3LYP/6-31G (d, p) level, respectively in Gaussian 09W program. The energy level diagram and frontier molecular orbitals (FMOs) of the push–pull BODIPYs **BDP 1–6** are shown in Figure 7.4.

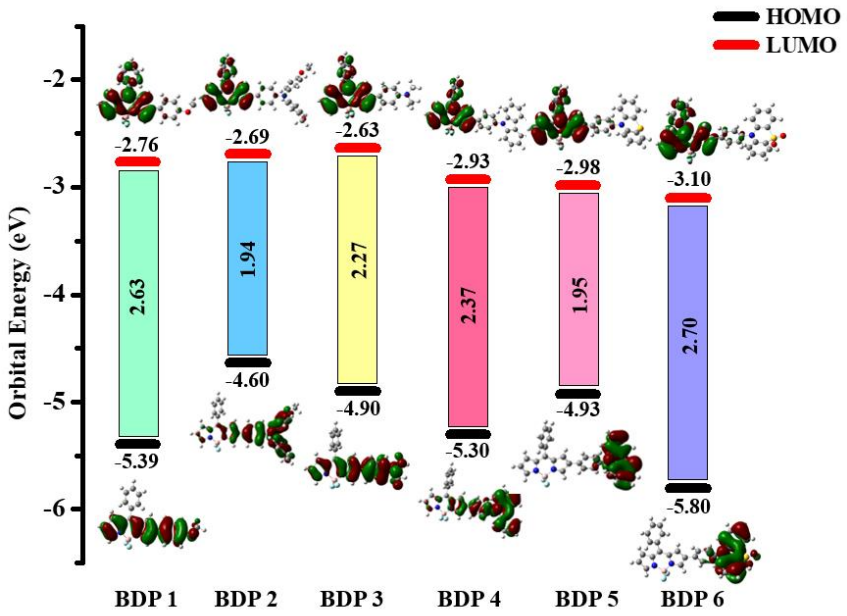

Figure 7.4. Energy level diagram and frontier molecular orbitals of the

push–pull BODIPYs **BDP 1–6** estimated from DFT calculation (B3LYP/6-31G (d, p) level).

The optimized molecular structures of the push–pull BODIPYs **BDP 1–4** shows that the highest molecular orbitals (HOMOs) are delocalized over both the donor and BODIPY unit, whereas the HOMOs of the phenothiazine and phenothiazine 5,5-dioxide functionalized BODIPYs **BDP 5** and **BDP 6** are localized on donor unit (Figure 7.4). The lowest occupied molecular orbitals (LUMOs) of the push–pull BODIPYs **BDP 1–6** are cantered on the acceptor BODIPY unit.

The computationally estimated HOMO energy levels of the push–pull BODIPYs **BDP 1–6** are –5.39 eV, –4.60 eV, –4.90 eV, –5.30 eV, –4.93 eV, and –5.80 eV, and the LUMO energy levels are –2.76 eV, –2.69 eV, –2.63 eV, –2.93 eV, –2.98 eV and –3.10 eV, respectively (Figure 7.4). The HOMO–LUMO gap of the **BDP 1–6** are 2.63, 1.94, 2.27, 2.37, 1.95 eV, and 2.70 eV, respectively (Figure 7.4) and follow the order **BDP 6> BDP 1> BDP 4> BDP 3> BDP 5> BDP 2**. The phenothiazine-5,5-dioxide functionalized BODIPY **BDP 6** exhibits a large HOMO–LUMO gap compared to phenothiazine substituted **BDP 5** due to the low donor ability of the phenothiazine-5,5-dioxide unit and weak donor–acceptor interaction (Figure 7.4). The optical band gap calculated from the onset of the electronic absorption spectra were found in good agreement with the theoretically estimated HOMO–LUMO gap.

The time-dependent DFT calculations were carried out to study the electronic properties of the optimized push–pull BODIPYs **BDP 1–6** at the CAM-B3LYP/6-31G (d, p) level in dichloromethane solvent. The polarized continuum model (PCM) was used to analyze the solvent effect in TD-DFT calculation. The TD-DFT results of the push–pull BODIPYs **BDP 1–6** were closely matched with the experimentally recorded absorption spectra. The push–pull BODIPYs **BDP 1–3** show an absorption band in the shorter wavelength at 349 nm, 382 nm, and 371 nm, respectively, originating from HOMO–1 → LUMO energy level, which are attributed to the π–π* transition. The transition in the

longer wavelength region observed for BODIPYs **BDP 1–3**, at 456 nm, 492 nm, and 491 nm, respectively, originates from HOMO → LUMO energy level, corresponds to the π–π* transition (Figure 7.5 and Table 7.2). The push–pull BODIPYs **BDP 4–5** show absorption band in the shorter wavelength at 345 nm and 330 nm, respectively originating from HOMO–3 → LUMO energy level, whereas the **BDP 6** exhibits absorption band at 328 nm, originates from HOMO–2 → LUMO energy level, which are attributed to π–π* transition. The transition in the longer wavelength region observed for **BDP 4–6**, at 445 nm, 439 nm, and 437 nm, originating predominantly from HOMO–1 → LUMO, HOMO–2 → LUMO, and HOMO–1 → LUMO energy level, respectively which can be associated with the π–π* transition (Figure 7.5 and Table 7.2).

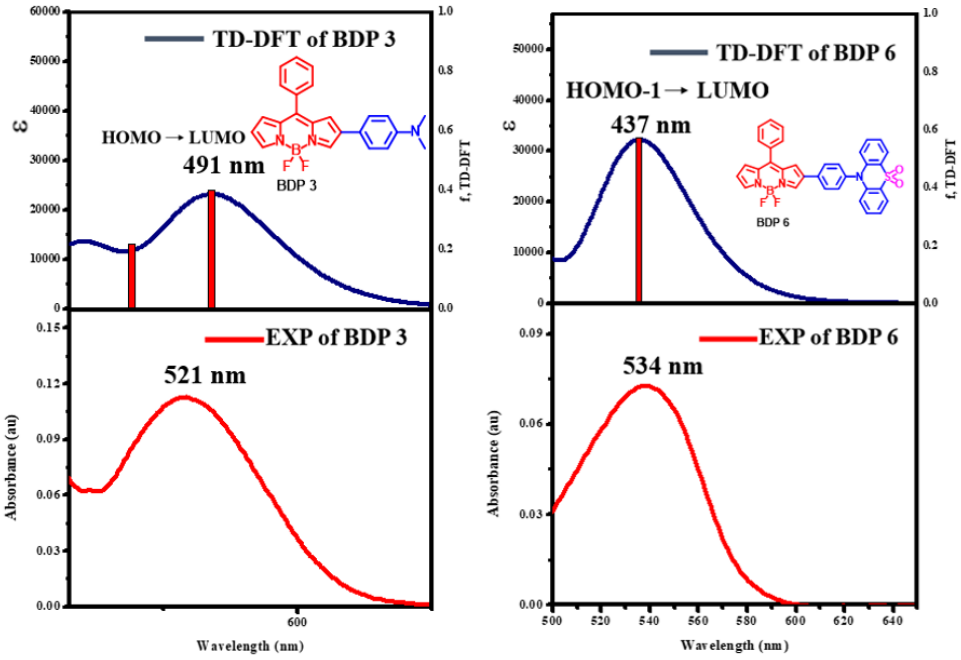

Figure 7.5. UV-vis absorption spectra of the push–pull BODIPYs **BDP 3** and **BDP 6**. Experimental (bottom) and TD-DFT predicted (top) in DCM solvent.

The transitions with composition, oscillatory strength, and assignments are tabulated in supporting information (Table 7.2). The theoretically calculated electronic absorption wavelength values were found in good agreement with the experimental data and can be affected

by various factors, including solvent effect, temperature, and dipole moment.

Table 7.2. Calculated electronic transitions of the push–pull BODIPYs **BDP 1–6**.

Compound	Wavelength (nm)	Composition	f[a]	Assignment
BDP 1	349	HOMO-1→LUMO (0.66)	0.21	π–π*
	456	HOMO→LUMO (0.67)	0.64	π–π*
BDP 2	382	HOMO-1→LUMO (0.54)	0.28	π–π*
	492	HOMO→LUMO (0.59)	0.63	π–π*
BDP 3	371	HOMO-1→LUMO (0.64)	0.30	π–π*
	491	HOMO→LUMO (0.65)	0.56	π–π*
BDP 4	345	HOMO-3→LUMO (0.46)	0.12	π–π*
	445	HOMO-1→LUMO (0.51)	0.78	π–π*
BDP 5	330	HOMO-3→LUMO (0.66)	0.17	π–π*
	439	HOMO-2→LUMO (0.69)	0.78	π–π*
BDP 6	328	HOMO-2→LUMO (0.66)	0.16	π–π*
	437	HOMO-1→LUMO (0.69)	0.79	π–π*

f[a] oscillator strength

7.7. Experimental section

General methods

All the chemicals were used as received unless otherwise indicated. All oxygen or moisture sensitive reactions were performed under inert atmosphere. All the chemicals were purchased from commercial sources and used without further purification. ^{1}H NMR (500 MHz) and ^{13}C NMR (126 MHz) spectra were recorded on the Bruker Avance (III) 500 MHz, using $CDCl_3$ as solvent and the chemical shifts were reported in parts per million (ppm) with TMS (0 ppm) and $CDCl_3$ (77.00 ppm) as standards. Tetramethylsilane (TMS) was used as reference for recording ^{1}H (of residual proton; δ = 7.26 ppm), and ^{13}C (of residual proton; δ = 77.0 ppm) spectra in $CDCl_3$. UV-visible absorption spectra were recorded on a PerkinElmer Lambda 35

instrument. All the measurements were carried out at 25 ℃. HRMS was recorded with an Agilent 6545A Q-TOF mass spectrometer and on a Bruker-Daltonics micrOTOF-Q II mass spectrometer. Cyclic voltammograms (CVs) were recorded on a PalmSens 4 electrochemical analyzer using Glassy carbon as a working electrode, Pt wire as the counter electrode, and Ag/AgCl as the reference electrode. Thermogravimetric analysis was performed on the Mettler Toledo thermal analysis system.

Synthesis and characterization of BDP 1: *β*-mono bromo BODIPY **1** (0.1 g, 0.28 mmol), boronate ester of anisole **2** (0.74 g, 0.31 mmol), $Pd(PPh_3)_4$ (0.016 g, 0.01 mmol), and potassium carbonate (0.131 g, 0.95 mmol) was dissolved in Toluene/ethanol/water (6/3/1 v/v/v) and heated to reflux for 12 h under a nitrogen atmosphere. The reaction mixture was cooled to room temperature and poured into water. The organic layer was extracted with dichloromethane, and the combined organic layers were washed with saturated brine solution and water and dried over anhydrous sodium sulphate. After filtration and solvent evaporation, the residue was purified by silica-gel column chromatography using hexane/dichloromethane (50/50 v/v) as the eluent. A dark purple solid of **BDP 1** was obtained in 75% yield (0.81 g) (m.p. 173 ℃). **^{1}H NMR (500 MHz, $CDCl_3$) δ** 8.25 (s, 1H), 7.93 (s, 1H), 7.66 – 7.53 (m, 5H), 7.46 (d, *J* = 8.7 Hz, 2H), 7.01 (s, 1H), 6.91 (d, *J* = 8.7 Hz, 3H), 6.54 (d, *J* = 2.5 Hz, 1H), 3.83 (s, 3H). **^{13}C NMR (126 MHz, $CDCl_3$) δ** 159.4, 146.6, 143.7, 142.4, 135.9, 135.1, 134.4, 134.0, 131.1, 130.8, 130.6, 128.6, 126.8, 125.3, 125.0, 118.3, 114.5, 55.5; **^{11}B NMR ($CDCl_3$, 128 MHz, ppm) δ** 0.25 (t, $J_{B\text{-}F}$ = 23 Hz); **HRMS (ESI-TOF)** m/z calculated for $C_{22}H_{17}BF_2N_2O$ = 375.1479 $[M + H]^+$, measured 375.1501 $[M + H]^+$.

Synthesis and characterization of BDP 2: *β*-mono bromo BODIPY **1** (0.1 g, 0.28 mmol), boronate ester of *N*,*N*-dimethyl anisole **3** (0.137 g, 0.31 mmol), $Pd(PPh_3)_4$ (0.016 g, 0.01 mmol), and potassium carbonate (0.131 g, 0.95 mmol) was dissolved in Toluene/ethanol/water (6/3/1 v/v/v) and heated to reflux for 12 h under a nitrogen atmosphere. The reaction mixture was cooled to room temperature and poured into water.

The organic layer was extracted with dichloromethane and the combined organic layers were washed with saturated brine solution and water and dried over anhydrous sodium sulphate. After filtration and solvent evaporation, the residue was purified by silica-gel column chromatography using hexane/dichloromethane (60/40 v/v) as the eluent. A dark blue solid of **BDP 2** was obtained in 63% yield (0.103 g) (m.p. 176 °C). **^{1}H NMR (500 MHz, $CDCl_3$) δ** 8.27 (s, 1H), 7.93 (s, 1H), 7.66 – 7.54 (m, 5H), 7.34 (d, *J* = 8.7 Hz, 2H), 7.13 – 7.05 (m, 4H), 7.00 (s, 1H), 6.92 (t, *J* = 6.0 Hz, 3H), 6.86 (m, 4H), 6.55 (m, 1H), 3.82 (s, 6H). **^{13}C NMR (126 MHz, $CDCl_3$) δ** 156.0, 148.4, 146.1, 143.1, 142.7, 140.6, 135.9, 133.9, 130.6, 130.5, 128.5, 126.6, 126.1, 124.3, 120.5, 118.0, 114.7, 55.5; **^{11}B NMR ($CDCl_3$, 128 MHz, ppm) δ** 0.25 (t, $J_{B\text{-}F}$ = 23 Hz); **HRMS (ESI-TOF)** m/z calculated for $C_{35}H_{28}BF_2N_3O_2$ = 594.2141 $[M + Na]^+$, measured 594.2157 $[M + Na]^+$.

Synthesis and characterization of BDP 3: *β*-mono bromo BODIPY **1** (0.1 g, 0.28 mmol), boronate ester of *N*,*N*-dimethylaniline **4** (0.78 g, 0.31 mmol), $Pd(PPh_3)_4$ (0.016 g, 0.01 mmol), and potassium carbonate (0.131 g, 0.95 mmol) was dissolved in Toluene/ethanol/water (6/3/1 v/v/v) and heated to reflux for 12 h under a nitrogen atmosphere. The reaction mixture was cooled to room temperature and poured into water. The organic layer was extracted with dichloromethane and the combined organic layers were washed with saturated brine solution and water and dried over anhydrous sodium sulphate. After filtration and solvent evaporation, the residue was purified by silica-gel column chromatography using hexane/dichloromethane (30/70 v/v) as the eluent. A light brown solid of **BDP 3** was obtained in 70% yield (0.111 g) (m.p. 180–185 °C). **^{1}H NMR (500 MHz, $CDCl_3$) δ** 8.32 (s, 1H), 7.80 – 7.39 (m, 7H), 7.29 (d, *J* = 1.3 Hz, 1H), 6.72 (m, 3H), 6.45 – 6.21 (m, 2H), 2.97 (s, 6H). **^{13}C NMR (126 MHz, $CDCl_3$) δ** 155.5, 149.8, 148.8, 139.7, 138.1, 137.6, 134.7, 130.8, 129.9, 128.6, 127.6, 126.7, 123.7, 122.1, 121.9, 112.6, 111.9, 77.2, 76.7, 40.4; **^{11}B NMR ($CDCl_3$, 128 MHz, ppm) δ** 0.25 (t, $J_{B\text{-}F}$ = 23 Hz); **HRMS (ESI-TOF)** m/z calculated for $C_{23}H_{20}BF_2N_3$ = 388.1795 $[M + H]^+$, measured 388.1623 $[M + H]^+$.

Synthesis and characterization of BDP 4: *β*-mono bromo BODIPY **1** (0.1 g, 0.28 mmol), boronate ester of *N*-phenyl carbazole **5** (0.117 g, 0.31 mmol), $Pd(PPh_3)_4$ (0.016 g, 0.01 mmol), and potassium carbonate (0.131 g, 0.95 mmol) was dissolved in Toluene/ethanol/water (6/3/1 v/v/v) and heated to reflux for 12 h under a nitrogen atmosphere. The reaction mixture was cooled to room temperature and poured into water. The organic layer was extracted with dichloromethane and the combined organic layers were washed with saturated brine solution and water and dried over anhydrous sodium sulphate. After filtration and solvent evaporation, the residue was purified by silica-gel column chromatography using hexane/dichloromethane (50/50 v/v) as the eluent. A light pink solid of **BDP 4** was obtained in 72% yield (0.105 g) (m.p. 180–182 °C). **^{1}H NMR (500 MHz, $CDCl_3$) δ** 8.38 (s, 1H), 8.17 (d, *J* = 4 Hz, 2H), 8.04 (s, 1H), 7.77 (d, *J* = 4 Hz, 2H), 7.69 – 7.60 (m, 7H), 7.43 – 7.42 (m, 4H), 7.33 – 7.30 (m, 2H), 7.21 (s, 1H), 7.03 (s, 1H), 6.63 (s, 1H). **^{13}C NMR (126 MHz, $CDCl_3$) δ** 147.3, 144.9, 141.6, 140.8, 137.0, 135.7, 135.5, 133.9, 132.1, 131.9, 131.0, 130.6, 128.7, 127.6, 126.9, 126.1, 125.8, 123.5, 120.4, 120.1, 119.0, 109.8; **^{11}B NMR ($CDCl_3$, 128 MHz, ppm) δ** 0.35 (t, $J_{B\text{-}F}$ = 25 Hz); **HRMS (ESI-TOF)** m/z calculated for $C_{33}H_{22}BF_2N_3$ = 509.1875 $[M]^+$, measured 509.1881 $[M]^+$.

Synthesis and characterization of BDP 5: *β*-mono bromo BODIPY **1** (0.1 g, 0.28 mmol), boronate ester of *N*-phenyl phenothiazine **6** (0.127 g, 0.31 mmol), $Pd(PPh_3)_4$ (0.016 g, 0.01 mmol), and potassium carbonate (0.131 g, 0.95 mmol) was dissolved in Toluene/ethanol/water (6/3/1 v/v/v) and heated to reflux for 12 h under a nitrogen atmosphere. The reaction mixture was cooled to room temperature and poured into water. The organic layer was extracted with dichloromethane and the combined organic layers were washed with saturated brine solution and water and dried over anhydrous sodium sulphate. After filtration and solvent evaporation, the residue was purified by silica-gel column chromatography using hexane/dichloromethane (50/50 v/v) as the eluent. A light purple solid of **BDP 5** was obtained in 76% yield (0.118

g) (m.p. 236 °C). **^{1}H NMR (500 MHz, $CDCl_3$) δ** 8.32 (s, 1H), 8.01 (s, 1H), 7.73 (d, *J* = 8.4 Hz, 2H), 7.67 – 7.54 (m, 5H), 7.38 (d, *J* = 8.4 Hz, 2H), 7.15 (s, 1H), 7.08 – 6.95 (m, 3H), 6.85 (m, 4H), 6.60 (d, *J* = 2.7 Hz, 1H), 6.28 (m, 2H). **^{13}C NMR (126 MHz, $CDCl_3$) δ** 147.4, 145.0, 144.2, 141.6, 140.5, 135.7, 135.5, 133.8, 133.2, 132.8, 132.3, 131.0, 130.6, 128.7, 127.7, 127.0, 125.9, 122.8, 120.9, 119.1, 116.5; **^{11}B NMR ($CDCl_3$, 128 MHz, ppm) δ** 0.13 (t, $J_{B\text{-}F}$ = 23 Hz); **HRMS (ESI-TOF)** m/z calculated for $C_{33}H_{22}BF_2N_3S$ = 541.1596 $[M]^+$, measured 541.1604 $[M]^+$.

Synthesis and characterization of BDP 6: In a 50 mL round bottomed flask m-Chloroperbenzoic acid (0.95 g, 0.55 mmol) was added to **BDP 5** (0.1 g, 0.18 mmol) in DCM (20 ml) at room temperature for 1h. Upon the completion of the reaction, the mixture was purified by silica gel column chromatography with CH_2Cl_2 to get the desired **BDP 6** as pink solid. Yield 0.84 g (80%) (m.p. 305–310 °C). **^{1}H NMR (500 MHz, $CDCl_3$) δ** 8.33 (s, 1H), 8.17 (m, 2H), 8.02 (m, 2H), 7.83 (d, *J* = 8.3 Hz, 2H), 7.69 – 7.56 (m, 5H), 7.44 – 7.35 (m, 4H), 7.23 (s, 1H), 7.19 (s, 1H), 7.02 (d, *J* = 4.1 Hz, 1H), 6.67 (d, *J* = 8.7 Hz, 2H), 6.63 (d, *J* = 3.0 Hz, 1H). **^{13}C NMR (126 MHz, $CDCl_3$) δ** 170.3, 145.8, 140.9, 137.8, 134.8, 134.5, 134.0, 133.7, 133.1, 132.9, 132.8, 131.1, 130.6, 130.4, 130.0, 128.8, 128.3, 126.0, 123.6, 122.8, 122.2, 117.3; **^{11}B NMR ($CDCl_3$, 128 MHz, ppm) δ** 0.19 (t, $J_{B\text{-}F}$ = 22 Hz); **HRMS (ESI-TOF)** m/z calculated for $C_{33}H_{22}BF_2N_3O_2S$ = 573.1494 $[M]^+$, measured 573.1524 $[M]^+$.

7.8. Conclusion

The push–pull BODIPYs **BDP 1–6** were synthesized *via* Pd-catalyzed Suzuki cross-coupling and by increasing the oxidation state of the sulfur atom in the triazine ring. The *N*,*N*-di-*p*-anisylaminophenyl functionalized BODIPY **BDP 2** shows bathochromic shift in absorption spectra and high thermal stability compared to rest of these push–pull BODIPYs. The redox properties demonstrate that the phenothiazine functionalized BODIPY **BDP 5** exhibits easy oxidation at low potential compared to phenothiazine 5,5-dioxide substituted BODIPY **BDP 6** due

to the strong electron donor ability of the phenothiazine unit. The theoretically estimated HOMOs of the push–pull BODIPYs **BDP 1–4**, are delocalized over whole molecule, whereas in **BDP 5** and **BDP 6**, it localized on the donor phenothiazine and phenothiazine 5,5-dioxide unit. The LUMOs are centered on the acceptor BODIPY unit in all cases. The phenothiazine 5,5-dioxide functionalized BODIPY **BDP 6** exhibits a large HOMO–LUMO gap compared to phenothiazine substituted BODIPY **BDP 5** due to increase in the oxidation state of the sulfur atom, which decreases the donor ability of the phenothiazine unit. This research suggests that the synthesis of the push–pull chromophores by varying the electron donor groups and altering the oxidation state of a sulfur atom are the key factor in tuning the HOMO–LUMO gap which is useful for the development of optoelectronic materials.

7.9. References

1. Boens, N., Leen, V., & Dehaen, W. (2012). Fluorescent indicators based on BODIPY. *Chemical Society Reviews*, *41*(3), 1130–1172. https://doi.org/10.1039/C1CS15132K

2. Qin, Y., Liu, X., Jia, P.-P., Xu, L., & Yang, H.-B. (2020). BODIPY-based macrocycles. *Chemical Society Reviews*, *49*(16), 5678–5703. https://doi.org/10.1039/C9CS00797K

3. Bassan, E., Gualandi, A., Cozzi, P. G., & Ceroni, P. (2021). Design of BODIPY dyes as triplet photosensitizers: electronic properties tailored for solar energy conversion, photoredox catalysis and photodynamic therapy. *Chemical Science*, *12*(19), 6607–6628. https://doi.org/10.1039/D1SC00732G

4. Liao, J., Xu, Y., Zhao, H., Wang, Y., Zhang, W., Peng, F., … Yang, X. (2015). Synthesis, optical, electrochemical properties and photovoltaic performance of novel panchromatic meso-thiophene BODIPY dyes with a variety of electron-donating groups at the 3,5-positions. *RSC Advances*, *5*(105), 86453–86462. https://doi.org/10.1039/C5RA15389A

5. Sun, Z.-B., Guo, M., & Zhao, C.-H. (2016). Synthesis and Properties of Benzothieno[b]-Fused BODIPY Dyes. *The Journal of Organic Chemistry*, *81*(1), 229–237. https://doi.org/10.1021/acs.joc.5b02531

6. Belmonte-Vázquez, J. L., Avellanal-Zaballa, E., Enríquez-Palacios, E., Cerdán, L., Esnal, I., Bañuelos, J., … Peña-Cabrera, E. (2019). Synthetic Approach to Readily Accessible Benzofuran-Fused Borondipyrromethenes as Red-Emitting Laser Dyes. *The Journal of Organic Chemistry*, *84*(5), 2523–2541. https://doi.org/10.1021/acs.joc.8b02933

7. Poddar, M., Sharma, V., Mobin, S. M., & Misra, R. (2018). 1,8-Naphthalimide-Substituted BODIPY Dyads: Synthesis, Structure, Properties, and Live-Cell Imaging. *Chemistry – An Asian Journal*, *13*(19), 2881–2890. https://doi.org/10.1002/asia.201800816

8. Rout, Y., Gautam, P., & Misra, R. (2017). Unsymmetrical and Symmetrical Push–Pull Phenothiazines. *The Journal of Organic Chemistry*, *82*(13), 6840–6845. https://doi.org/10.1021/acs.joc.7b00991

9. Gautam, P., Misra, R., Thomas, M. B., & D'Souza, F. (2017). Ultrafast Charge-Separation in Triphenylamine-BODIPY-Derived Triads Carrying Centrally Positioned, Highly Electron-Deficient, Dicyanoquinodimethane or Tetracyanobutadiene Electron-Acceptors. *Chemistry – A European Journal*, *23*(38), 9192–9200. https://doi.org/10.1002/chem.201701604

10. Wang, D., Guo, X., Wu, H., Wu, Q., Wang, H., Zhang, X., … Jiao, L. (2020). Visible Light Excitation of BODIPYs Enables Dehydrogenative Enamination at Their α-Positions with Aliphatic Amines. *The Journal of Organic Chemistry*, *85*(13), 8360–8370. https://doi.org/10.1021/acs.joc.0c00620

11. Rout, Y., Montanari, C., Pasciucco, E., Misra, R., & Carlotti, B. (2021). Tuning the Fluorescence and the Intramolecular Charge Transfer of Phenothiazine Dipolar and Quadrupolar Derivatives by

Oxygen Functionalization. *Journal of the American Chemical Society*, *143*(26), 9933–9943. https://doi.org/10.1021/jacs.1c04173

12. Ulrich, G., Goeb, S., De Nicola, A., Retailleau, P., & Ziessel, R. (2011). Chemistry at Boron: Synthesis and Properties of Red to Near-IR Fluorescent Dyes Based on Boron-Substituted Diisoindolomethene Frameworks. *The Journal of Organic Chemistry*, *76*(11), 4489–4505. https://doi.org/10.1021/jo200246q

13. Filatov, M. A., Karuthedath, S., Polestshuk, P. M., Callaghan, S., Flanagan, K. J., Telitchko, M., … Senge, M. O. (2018). Control of triplet state generation in heavy atom-free BODIPY–anthracene dyads by media polarity and structural factors. *Physical Chemistry Chemical Physics*, *20*(12), 8016–8031. https://doi.org/10.1039/C7CP08472B

14. Gong, Q., Cheng, K., Wu, Q., Li, W., Yu, C., Jiao, L., & Hao, E. (2021). One-Pot Access to Ethylene-Bridged BODIPY Dimers and Trimers through Single-Electron Transfer Chemistry. *The Journal of Organic Chemistry*, *86*(21), 15761–15767. https://doi.org/10.1021/acs.joc.1c01824

15. Hayashi, Y., Yamaguchi, S., Cha, W. Y., Kim, D., & Shinokubo, H. (2011). Synthesis of Directly Connected BODIPY Oligomers through Suzuki–Miyaura Coupling. *Organic Letters*, *13*(12), 2992–2995. https://doi.org/10.1021/ol200799u

16. Lu, P., Chung, K.-Y., Stafford, A., Kiker, M., Kafle, K., & Page, Z. A. (2021). Boron dipyrromethene (BODIPY) in polymer chemistry. *Polymer Chemistry*, *12*(3), 327–348. https://doi.org/10.1039/D0PY01513J

17. Misra, R., Jadhav, T., Dhokale, B., Gautam, P., Sharma, R., Maragani, R., & Mobin, S. M. (2014). Carbazole-BODIPY conjugates: design, synthesis, structure and properties. *Dalton Transactions*, *43*(34), 13076–13086. https://doi.org/10.1039/C4DT00983E

18. Saravanan, V., Ganesan, S., & Rajakumar, P. (2020). Synthesis and DSSC application of BODIPY decorated triazole bridged and

benzene nucleus cored conjugated dendrimers. *RSC Advances*, *10*(31), 18390–18399. https://doi.org/10.1039/D0RA01672A

19. Sutradhar, T., & Misra, A. (2020). The role of π-linkers and electron acceptors in tuning the nonlinear optical properties of BODIPY-based zwitterionic molecules. *RSC Advances*, *10*(66), 40300–40309. https://doi.org/10.1039/D0RA02193H

20. Zatsikha, Y. V., Didukh, N. O., Swedin, R. K., Yakubovskyi, V. P., Blesener, T. S., Healy, A. T., … Kovtun, Y. P. (2019). Preparation of Viscosity-Sensitive Isoxazoline/Isoxazolyl-Based Molecular Rotors and Directly Linked BODIPY–Fulleroisoxazoline from the Stable meso-(Nitrile Oxide)-Substituted BODIPY. *Organic Letters*, *21*(14), 5713–5718. https://doi.org/10.1021/acs.orglett.9b02082

21. Bandi, V., Das, S. K., Awuah, S. G., You, Y., & D'Souza, F. (2014). Thieno-Pyrrole-Fused 4,4-Difluoro-4-bora-3a,4a-diaza-s-indacene–Fullerene Dyads: Utilization of Near-Infrared Sensitizers for Ultrafast Charge Separation in Donor–Acceptor Systems. *Journal of the American Chemical Society*, *136*(21), 7571–7574. https://doi.org/10.1021/ja503015f

22. Kaur, N., Steerteghem, N. V., Singla, P., Kaur, P., Clays, K., & Singh, K. (2017). Second-order nonlinear polarizability of ferrocene–BODIPY donor–acceptor adducts. Quantifying charge redistribution in the excited state. *Dalton Transactions*, *46*(4), 1124–1133. https://doi.org/10.1039/C6DT04455G

23. Wang, H., Zhao, W., Liu, X., Wang, S., & Wang, Y. (2020). BODIPY-Based Fluorescent Surfactant for Cell Membrane Imaging and Photodynamic Therapy. *ACS Applied Bio Materials*, *3*(1), 593–601. https://doi.org/10.1021/acsabm.9b00977

24. Zou, J., Yin, Z., Ding, K., Tang, Q., Li, J., Si, W., … Dong, X. (2017). BODIPY Derivatives for Photodynamic Therapy: Influence of Configuration versus Heavy Atom Effect. *ACS Applied Materials &*

Interfaces, *9*(38), 32475–32481. https://doi.org/10.1021/acsami.7b07569

25. Misra, R., Dhokale, B., Jadhav, T., & Mobin, S. M. (2013). Donor–acceptor meso-alkynylated ferrocenyl BODIPYs: synthesis, structure, and properties. *Dalton Transactions*, *42*(37), 13658–13666. https://doi.org/10.1039/C3DT51374B

26. Shinde, J., Thomas, M. B., Poddar, M., Misra, R., & D'Souza, F. (2021). Does Location of BF2-Chelated Dipyrromethene (BODIPY) Ring Functionalization Affect Spectral and Electron Transfer Properties? Studies on α-, β-, and Meso-Functionalized BODIPY-Derived Donor–Acceptor Dyads and Triads. *The Journal of Physical Chemistry C*, *125*(43), 23911–23921. https://doi.org/10.1021/acs.jpcc.1c06704

27. Popere, B. C., Della Pelle, A. M., & Thayumanavan, S. (2011). BODIPY-Based Donor–Acceptor π-Conjugated Alternating Copolymers. *Macromolecules*, *44*(12), 4767–4776. https://doi.org/10.1021/ma200839q

28. Dhokale, B., Gautam, P., Mobin, S. M., & Misra, R. (2013). Donor–acceptor, ferrocenyl substituted BODIPYs with marvelous supramolecular interactions. *Dalton Transactions*, *42*(5), 1512–1518. https://doi.org/10.1039/C2DT31632C

29. Lu, H., Mack, J., Yang, Y., & Shen, Z. (2014). Structural modification strategies for the rational design of red/NIR region BODIPYs. *Chemical Society Reviews*, *43*(13), 4778–4823. https://doi.org/10.1039/C4CS00030G

30. Reddy, G., Duvva, N., Seetharaman, S., D'Souza, F., & Giribabu, L. (2018). Photoinduced energy transfer in carbazole–BODIPY dyads. *Physical Chemistry Chemical Physics*, *20*(43), 27418–27428. https://doi.org/10.1039/C8CP05509B

31. Popere, B. C., Della Pelle, A. M., & Thayumanavan, S. (2011). BODIPY-Based Donor–Acceptor π-Conjugated Alternating

Copolymers. *Macromolecules*, *44*(12), 4767–4776. https://doi.org/10.1021/ma200839q

32. Matteucci, E., Baschieri, A., Sambri, L., Monti, F., Pavoni, E., Bandini, E., & Armaroli, N. (2019). Carbazole-Terpyridine Donor-Acceptor Dyads with Rigid π-Conjugated Bridges. *ChemPlusChem*, *84*(9), 1353–1365. https://doi.org/10.1002/cplu.201900213

33. Reddy, G., Duvva, N., Seetharaman, S., D'Souza, F., & Giribabu, L. (2018). Photoinduced energy transfer in carbazole–BODIPY dyads. *Physical Chemistry Chemical Physics*, *20*(43), 27418–27428. https://doi.org/10.1039/C8CP05509B

34. Chen, S., Wang, L., Zhang, J., Hao, Z., Huang, H., & Deng, G.-J. (2017). Modular Synthesis of Carbazole-Based Conjugated Molecules through a One-Pot Annulation/Dehydrogenation Sequence. *The Journal of Organic Chemistry*, *82*(20), 11182–11191. https://doi.org/10.1021/acs.joc.7b02305

35. Hart, A. S., K. C., C. B., Subbaiyan, N. K., Karr, P. A., & D'Souza, F. (2012). Phenothiazine-Sensitized Organic Solar Cells: Effect of Dye Anchor Group Positioning on the Cell Performance. *ACS Applied Materials & Interfaces*, *4*(11), 5813–5820. https://doi.org/10.1021/am3014407

36. Buene, A. F., & Almenningen, D. M. (2021). Phenothiazine and phenoxazine sensitizers for dye-sensitized solar cells – an investigative review of two complete dye classes. *Journal of Materials Chemistry C*, *9*(36), 11974–11994. https://doi.org/10.1039/D1TC03207K

37. Gangadhar, P. S., Reddy, G., Prasanthkumar, S., & Giribabu, L. (2021). Phenothiazine functional materials for organic optoelectronic applications. *Physical Chemistry Chemical Physics*, *23*(28), 14969–14996. https://doi.org/10.1039/D1CP01185E

38. Sinha, A., & Ravikanth, M. (2022). Phenothiazine-Embedded Hexaphyrins. *Organic Letters*, *24*(6), 1335–1340. https://doi.org/10.1021/acs.orglett.1c04374

39. Sun, D., Rosokha, S. V., & Kochi, J. K. (2004). Donor−Acceptor (Electronic) Coupling in the Precursor Complex to Organic Electron Transfer: Intermolecular and Intramolecular Self-Exchange between Phenothiazine Redox Centers. *Journal of the American Chemical Society*, *126*(5), 1388–1401. https://doi.org/10.1021/ja038746v

40. Rout, Y., Misra, R., Singhal, R., Biswas, S., & Sharma, G. D. (2018). Phenothiazine-based small-molecule organic solar cells with power conversion efficiency over 7% and open circuit voltage of about 1.0 V using solvent vapor annealing. *Physical Chemistry Chemical Physics*, *20*(9), 6321–6329. https://doi.org/10.1039/C7CP08308D

41. Huang, Z.-S., Meier, H., & Cao, D. (2016). Phenothiazine-based dyes for efficient dye-sensitized solar cells. *Journal of Materials Chemistry C*, *4*(13), 2404–2426. https://doi.org/10.1039/C5TC04418A

42. Krämer, C. S., & Müller, T. J. J. (2003). Synthesis and Electronic Properties of Alkynylated Phenothiazines. *European Journal of Organic Chemistry*, *2003*(18), 3534–3548. https://doi.org/10.1002/ejoc.200300250

43. Rout, Y., Ekbote, A., & Misra, R. (2021). Recent development on the synthesis, properties and applications of luminescent oxidized phenothiazine derivatives. *Journal of Materials Chemistry C*, *9*(24), 7508–7531. https://doi.org/10.1039/D1TC00695A

44. Dhokale, B., Gautam, P., Mobin, S. M., & Misra, R. (2013). Donor–acceptor, ferrocenyl substituted BODIPYs with marvelous supramolecular interactions. *Dalton Transactions*, *42*(5), 1512–1518. https://doi.org/10.1039/C2DT31632C

45. Müller, T. J. J. (1999). First synthesis and electronic properties of ring-alkynylated phenothiazines. *Tetrahedron Letters*, *40*(36), 6563–6566. https://doi.org/10.1016/S0040-4039(99)01402-1

46. Gautam, P., Dhokale, B., Mobin, S. M., & Misra, R. (2012). Ferrocenyl BODIPYs: synthesis, structure and properties. *RSC Advances*, *2*(32), 12105–12107. https://doi.org/10.1039/C2RA21964F

47. Rahman, A., Praveen Kumar, P. P., Yadav, P., Goswami, T., Shanavas, A., Ghosh, H. N., & Neelakandan, P. P. (2022). Gold–BODIPY Nanoparticles with Luminescence and Photosensitization Properties for Photodynamic Therapy and Cell Imaging. *ACS Applied Nano Materials*, *5*(5), 6532–6542. https://doi.org/10.1021/acsanm.2c00616

48. Khan, F., Ekbote, A., & Misra, R. (2019). Reversible mechanochromism and aggregation induced enhanced emission in phenothiazine substituted tetraphenylethylene. *New Journal of Chemistry*, *43*(41), 16156–16163. https://doi.org/10.1039/C9NJ03290H

49. Poddar, M., Cesaretti, A., Ferraguzzi, E., Carlotti, B., & Misra, R. (2020). Singlet and Triplet Excited-State Dynamics of 3,7-Bis(arylethynyl)phenothiazines: Intramolecular Charge Transfer and Reverse Intersystem Crossing. *The Journal of Physical Chemistry C*, *124*(33), 17864–17878. https://doi.org/10.1021/acs.jpcc.0c01786

Chapter 8

Conclusions and Future Scope

8.1. Conclusions

In recent years, donor–acceptor or push–pull chromophores based on BODIPY have acquired a substantial amount of attention from the scientific community. The nature of the D–A interaction is determined by the donor's ability to donate electrons, the acceptor's ability to accept electrons, and the structure of the spacer connecting them. One of the powerful acceptors are the BODIPY fluorophores.[1] They have a high fluorescence quantum yield, strong absorption, high photostability and adjustable redox properties.[2–5] The BODIPY based chromophores exhibit a good photochemical stability and excellent solubility in wide range of solvents.[6] The BODIPYs generally exhibit a strong absorption band around 500–550 nm range corresponding to $S_0 \rightarrow S_1$ (π–π^*) transition and a shoulder peak at lower wavelength region due to a vibrational transition. The BODIPY also has a weak absorption band around 350–380 nm range, which corresponds to the $S_0 \rightarrow S_2$ (π–π^*) transition. The BODIPYs commonly emit a narrow spectrum between 530–560 nm range.[7] The photonic properties of the BODIPYs can be modified by varying the type of the donor, acceptor and spacer substituents. BODIPYs can be engaged at the α, β-pyrrolic and *meso*-positions. We functionalized β-pyrrolic and *meso* positions of BODIPYs with strong electron donor or acceptor units *via* variable spacers and evaluated various sites of BODIPY for enhanced electronic communication, as well as investigated efficient D–A systems. Tuning of optical and electronic properties of the donor–acceptor BODIPY dyes have been investigated to improve the efficiency of a wide range of applications including organic light emitting diodes, photodynamic therapy, bioimaging, nonlinear optics, dye sensitized solar cells and single molecule switches.[8, 9] In this regard, we have designed, and synthesized variety of donor and acceptor substituted β-

pyrrolic and *meso*-functionalized donor–acceptor BODIPYs and investigated their photophysical, electrochemical, thermal and computational properties.

In chapter 3, the design and synthesis of push–pull BODIPYs **1**–**10**, were reported *via* Pd-catalyzed Suzuki, Heck, Sonogashira cross-coupling, and [2+2] cycloaddition-retroelectrocyclization reactions with good yields. The UV-visible absorption spectra of cyclohexa-2,5-diene-1,4-ylidene-expanded TCBD functionalized BODIPYs exhibit intramolecular charge transfer (ICT) band in the longer wavelength region as compared to TCBD substituted BODIPYs due to strong donor–acceptor interactions. The electrochemical studies of push–pull BODIPYs **4**, **5**, **9** and **10**, demonstrate that the cyclohexa-2,5-diene-1,4-ylidene-expanded TCBD unit acts as a strong electron acceptor and exhibit multiple reduction wave at low potential as compared to TCBD unit. The theoretically predicted HOMOs of BODIPYs **1–10**, are delocalized over the donor phenothiazine and carbazole unit, whereas the LUMOs are localized over acceptor BODIPY, TCBD, and cyclohexa-2,5-diene-1,4-ylidene-expanded TCBD unit. These findings suggest that the introduction of strong acceptor cyclohexa-2,5-diene-1,4-ylidene-expanded TCBD decreases the HOMO–LUMO gap more as compared to the TCBD unit which resulted in a bathochromic shift in UV-vis spectra. This research work opens new avenue to explore the design and synthesis of push–pull chromophores with low HOMO–LUMO gap for various optoelectronic application.

In chapter 4, a set of push–pull BODIPYs **3**–**5** and **7**–**9**, were synthesized *via* Pd-catalyzed Sonogashira cross-coupling followed by [2+2] cycloaddition-retroelectrocyclization reaction in good yields. The photophysical results show that the ICT band of cyclohexa-2,5-diene-1,4-ylidene-expanded TCBD functionalized BODIPYs **5** and **9**, exhibit a bathochromic shift compared to TCBD functionalized BODIPYs **4** and **8**, because of strong–donor interaction. The redox properties of TCBD and cyclohexa-2,5-diene-1,4-ylidene-expanded TCBD substituted BODIPYs **4**, **5**, **8** and **9**, display multiple reduction waves at low

potential due to the formation of mono and di-radical anion on TCBD unit. The redox properties reveals that the cyclohexa-2,5-diene-1,4-ylidene-expanded TCBD unit act as strong acceptor compared to the TCBD unit. The *N*,*N*-dimethylaniline substituted donor–acceptor BODIPY **3** exhibits the highest thermal stability as compared to BODIPYs **4, 5, 7, 8,** and **9**. The computational calculations revel that the incorporation of cyclohexa-2,5-diene-1,4-ylidene-expanded TCBD unit decreases the HOMO–LUMO gap more compared to TCBD due to strong donor–acceptor interactions. The research reports a new avenue to design π-conjugated donor–acceptor chromophores with low HOMO–LUMO gap for optoelectronic applications.

In chapter 5, a set of donor–acceptor **BODIPYs 1**–**4** were designed and synthesized *via* palladium-catalyzed Sonogashira cross-coupling and subsequent [2+2] cycloaddition-retroelectrocyclization reactions in good yields. The photophysical properties reveal that the **BODIPY 4** exhibits a strong ICT band at a longer wavelength region compared to **BODIPYs 1–3**, due to strong donor–acceptor interaction. The redox properties of push–pull **BODIPYs 1–4** exhibits multiple reduction waves due to presence of multiple-redox active entities. The **BODIPYs 3** and **4** exhibit multiple reduction waves at low potential due to presence of strong acceptor TCBD and cyclohexa-2,5-diene-1,4-ylidene-expanded TCBD units. The phenyl incorporated *N*,*N*-dimethylaniline functionalized push–pull **BODIPY 2** exhibits the highest thermal stability as compared to **BODIPYs 1, 3** and **4**. The theoretical results reveal that the incorporation of phenyl spacer, TCBD, and cyclohexa-2,5-diene-1,4-ylidene-expanded TCBD unit perturbs the HOMO–LUMO energy gap. The donor–acceptor **BODIPYs 1–4** shows that the HOMOs are delocalized over both donor *N*,*N*-dimethylaniline and acceptor BODIPY unit, whereas the LUMOs are localized on acceptors TCBD and cyclohexa-2,5-diene-1,4-ylidene-expanded TCBD unit. The **BODIPY 4** exhibits low HOMO–LUMO gap compared to **BODIPY 3** due to strong accepting nature of cyclohexa-2,5-diene-1,4-ylidene-expanded TCBD unit. This research provides an important route

for synthesizing a donor–acceptor chromophores with low HOMO–LUMO gap for different optoelectronic applications.

In chapter 6, we reported a set of push–pull chromophores **BPTZ 1–8**, which were synthesized *via* palladium-catalyzed Suzuki cross-coupling reaction and modulate the oxidation state of the sulfur atom on the phenothiazine unit by two oxygen functionalization. The photophysical study reveals that the phenothiazine substituted BODIPYs **BPTZ 1**–**4** exhibits a bathochromic (red) shift compared to phenothiazine-5,5-dioxide substituted BODIPYs **BPTZ 5**–**8** due to the good donor ability of phenothiazine unit and strong donor-acceptor interaction. The electrochemical properties of the phenothiazine-5,5-dioxide substituted BODIPYs **BPTZ 5–8** exhibit reduced electron donating ability relative to the phenothiazine substituted BODIPYs **BPTZ 1–4**. DFT and TD-DFT calculations provided a broad understanding of the electronic structures and absorption spectra of the push–pull chromophores **BPTZ 1–8**, and show that upon modulating the oxidation state of the sulfur atom on phenothiazine unit increases the HOMO–LUMO gap, resulted a blue shift in the absorption spectra. These findings suggest that oxygen functionalization is an effective strategy to synthesize new push–pull BODIPYs with low HOMO–LUMO gap for various optoelectronic applications.

In chapter 7, the push–pull BODIPYs **BDP 1–6** were synthesized *via* Pd-catalyzed Suzuki cross-coupling and by increasing the oxidation state of the sulfur atom in the triazine ring. The *N*,*N*-dimethyl anisole functionalized BODIPY **BDP 2** shows bathochromic shift in absorption spectra and high thermal stability compared to rest of these push–pull BODIPYs. The redox properties demonstrate that the phenothiazine functionalized BODIPY **BDP 5** exhibits easy oxidation at low potential compared to phenothiazine 5,5-dioxide substituted BODIPY **BDP 6** due to the strong electron donor ability of the phenothiazine unit. The *N*,*N*-dimethyl anisole functionalized BODIPY **BDP 2** exhibits the highest thermal stability compared to the rest of the **BDPs** and the incorporation of oxygen atom decreases the thermal stability. The theoretically

estimated HOMOs of the push–pull BODIPYs **BDP 1–4**, are delocalized over whole molecule, whereas in **BDP 5** and **BDP 6**, it localized on the donor phenothiazine and phenothiazine 5,5-dioxide unit. The LUMOs are cantered on the acceptor BODIPY unit in all cases. The phenothiazine 5,5-dioxide functionalized BODIPY **BDP 6** exhibits a large HOMO–LUMO gap compared to phenothiazine substituted BODIPY **BDP 5** due to increase in the oxidation state of the sulfur atom, which decreases the donor ability of the phenothiazine unit. This research suggests that the synthesis of the push–pull chromophores by varying the electron donor groups and altering the oxidation state of a sulfur atom are the key factor in tuning the HOMO–LUMO gap which is useful for the development of optoelectronic materials. [10]

8.2. Future scope

The thesis highlights an important strategy for design and synthesis of donor–acceptor *β*-pyrrolic and *meso*-functionalized BODIPY based molecules with tunable photonic properties and low HOMO–LUMO gap. The HOMO–LUMO gap of the donor–acceptor functionalized BODIPY dyes can be modified by (a) varying the number of donor/acceptor units, (b) enhancing the conjugation length and (c) changing the π-linker. The variation in the donor/acceptor strength perturbs the HOMO–LUMO gap to greater extent. The incorporation of strong acceptor tetracyanobutadiene (TCBD) and cyclohexa-2,5-diene-1,4-diylidene-expanded TCBD units at the *β*-pyrrolic and *meso*-position of the BODIPY resulted in the significant tuning of the photophysical, electrochemical and HOMO–LUMO gap. The incorporation of strong electron acceptor cyclohexa-2,5-diene-1,4-diylidene-expanded TCBD unit resulted in a red shift of the absorption compared to TCBD unit due to strong intramolecular charge-transfer (ICT) interactions. The *β*-pyrrolic and *meso*-substituted BODIPYs with broad absorption spectra in the visible region could be promising candidate for various applications such as in bioimaging, photodynamic therapy, sensors, laser, organic field-effect transistor, nonlinear optics and dye sensitized solar cells.

8.3. References

1. Gautam, P., Dhokale, B., Mobin, S. M., & Misra, R. (2012). Ferrocenyl BODIPYs: synthesis, structure and properties. *RSC Advances*, *2*(32), 12105–12107. https://doi.org/10.1039/C2RA21964F

2. Qin, Y., Liu, X., Jia, P.-P., Xu, L., & Yang, H.-B. (2020). BODIPY-based macrocycles. *Chemical Society Reviews*, *49*(16), 5678–5703. https://doi.org/10.1039/C9CS00797K

3. Shen, B., & Qian, Y. (2016). A novel triphenylamine-BODIPY dendron: click synthesis, near-infrared emission and a multi-channel chemodosimeter for Hg2+ and Fe3+. *Journal of Materials Chemistry B*, *4*(47), 7549–7559. https://doi.org/10.1039/C6TB02469F

4. Sansalone, L., Tang, S., Garcia-Amorós, J., Zhang, Y., Nonell, S., Baker, J. D., … Raymo, F. M. (2018). A Photoactivatable Far-Red/Near-Infrared BODIPY To Monitor Cellular Dynamics in Vivo. *ACS Sensors*, *3*(7), 1347–1353. https://doi.org/10.1021/acssensors.8b00262

5. Shinde, J., Thomas, M. B., Poddar, M., Misra, R., & D'Souza, F. (2021). Does Location of BF2-Chelated Dipyrromethene (BODIPY) Ring Functionalization Affect Spectral and Electron Transfer Properties? Studies on α-, β-, and Meso-Functionalized BODIPY-Derived Donor–Acceptor Dyads and Triads. *The Journal of Physical Chemistry C*, *125*(43), 23911–23921. https://doi.org/10.1021/acs.jpcc.1c06704

6. Bassan, E., Gualandi, A., Cozzi, P. G., & Ceroni, P. (2021). Design of BODIPY dyes as triplet photosensitizers: electronic properties tailored for solar energy conversion, photoredox catalysis and photodynamic therapy. *Chemical Science*, *12*(19), 6607–6628. https://doi.org/10.1039/D1SC00732G

7. Boens, N., Leen, V., & Dehaen, W. (2012). Fluorescent indicators based on BODIPY. *Chemical Society Reviews*, *41*(3), 1130–1172. https://doi.org/10.1039/C1CS15132K

8. Lakshmi, V., Rao, M. R., & Ravikanth, M. (2015). Halogenated boron-dipyrromethenes: synthesis, properties and applications. *Organic & Biomolecular Chemistry*, *13*(9), 2501–2517. https://doi.org/10.1039/C4OB02293A

9. Shah, M. F., Mirloup, A., Chowdhury, T. H., Sutter, A., Hanbazazah, A. S., Ahmed, A., … Islam, A. (2020). Cross-conjugated BODIPY pigment for highly efficient dye sensitized solar cells. *Sustainable Energy & Fuels*, *4*(4), 1908–1914. https://doi.org/10.1039/C9SE01090D

10. **Yadav, I. S.**, & Misra, R., (2023). *β*-Pyrrole Functionalized Push–Pull BODIPYs: Synthesis, Photophysical, Electrochemical, Thermal and Computational Studies. *Journal of Porphyrins and Phthalocyanines*, 27, 887–895. https://doi.org/10.1142/S1088424623501018